MOLECULAR STRUCTURES OF NATURAL POLYMERS: CUTIN, SUBERIN, AND MELANIN

by

SHIYING TIAN

A dissertation submitted to the Graduate Faculty in Chemistry in partial fulfillment of the requirements for the degree of Doctor of Philosophy, The City University of New York

2005

INFORMATION TO USERS

The quality of this reproduction is dependent upon the quality of the copy submitted. Broken or indistinct print, colored or poor quality illustrations and photographs, print bleed-through, substandard margins, and improper alignment can adversely affect reproduction.

In the unlikely event that the author did not send a complete manuscript and there are missing pages, these will be noted. Also, if unauthorized copyright material had to be removed, a note will indicate the deletion.

ProQuest Information and Learning Company
300 North Zeeb Road
P.O. Box 1346
Ann Arbor, MI 48106-1346

This manuscript has been read and accepted for the Graduate Faculty in Chemistry in satisfaction of the dissertation requirement for the degree of Doctor of Philosophy.

1/25/05
Date

Ruth E. Stark
Prof. Ruth E. Stark
Chair of Examining Committee

1/26/05
Date

Gerald Koeppl
Prof. Gerald Koeppl
Executive Officer

Prof. James D. Batteas

Prof. Steve Greenbaum

Supervisory Committee

The City University of New York

Abstract

MOLECULAR STRUCTURES OF NATURAL POLYMERS: CUTIN, SUBERIN, AND MELANIN

by

Shiying Tian

Advisor: Professor Ruth E. Stark

Natural polymers play an important role in the nature. Studies on molecular structures of natural polymers can help to understand their biological functions. This work seeks to understand the molecular structures of three natural polymers: lime fruit cutin, potato suberin, and *C. neoformans* fungal melanin. Due to the intractability of these materials, strategies of solid state NMR, isotopic labeling were employed in these studies. Partial degradation strategy was also employed in the study of lime fruit cutin and poato suberin.

Lime cutin was degraded with KOH and HF. Six monomers, 4 dimers, 5 trimers, and a tetramer were isolated from the degradation products by TLC, HPTLC, and HPLC. Structures of these isolated compounds were elucidated from NMR and MS data. Dimers of the two most abundant monomers in lime cutin, 10,16-dihydroxyhexadecanoic acid and 10-oxo-16-hydroxyhexadecanoic acid, with different combinations were separated and identified. Trimers separated and identified in our studies mainly consist of these two most abundant monomers. Other monomers and their oligomers were also separated and identified. A modified KOH degradation method was developed in order to enhance oligomeric

compositions and sizes in the products. A separation protocol was also developed to improve isolation efficiency of target compounds. KOH degradation method was also applied to potato suberin, trends of retention time in liquid chromatography were linked to structural features of the compounds.

Cross-Polarization (CP) magic-angle spinning (MAS) ^{13}C NMR reveals function groups of esters, aliphatic chain, and polysaccharide in lime cutin and potato suberin with different relative amounts. High-Resolution (HR) MAS NMR reveals more structural details of lime cutin, which are consistent with the degradation results. Polysaccharide moieties of potato suberin were evidenced in HRMAS NMR spectra.

The incorporation of labeled precursors into the melanin products is demonstrated by the NMR data. Melanins derived from different precursors have generally similar aliphatic and aromatic spectroscopic features, but structural differences are also suggested by their NMR spectra. A polysaccharide moiety found in [1-^{13}C] D-mannose melanin suggests close association or covalent binding of melanin to the fungal cell wall.

ACKNOWLEDGMENTS

I would like to express my sincere gratitude to my mentor, Professor Ruth E. Stark, who gave me the wonderful opportunity to be involved in the field of molecular structural studies on natural polymers and guided me patiently in my every growth step.

I would like to extend my thanks to Dr. Hsin Wang, who introduced me to NMR instrumentation and experiment setup.

I thank all my committee members, Professor James D. Batteas and Professor Steve Greenbaum, for their sound advice and strong supports.

I would like to give my special thanks to our collaborators, Professor Arturo Casadevall and Javier Garcia-Rivera, for their kind contribution of melanin samples.

I also want to give my thanks to my wife, Xiaoping Xi, and my daughter, Yiran Tian. It is their love and strong support that enables me to concentrate on my research.

Table of Contents

List of Tables

List of Figures

Chapter 1. The Natural Polymers Cutin, Suberin, and Melanin

1.1 Significance

1.1.1 Cutin

Most epidermal cells of the aerial parts of higher plants such as leaves, fruits, and nonwoody stems are covered by a continuous extracellular membrane of soluble and polymerized lipids called the cuticle (Fig. 1.1). Its structure and composition vary largely among plants, organs and growth stages, but it is basically composed of a cutin matrix with waxes embedded in (intracuticular) and deposited on the surface (epicuticular) of the matrix.[2] The cutin polymer consists largely of esterified hydroxylated fatty acids and hydroxylated epoxy acids with typical chain lengths of 16 - 18 carbon atoms.[3,4]

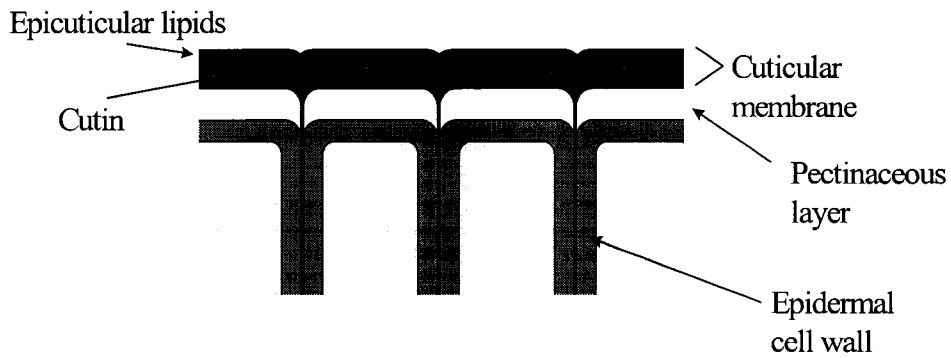

Figure 1.1. Schematic drawing of cutin in an epidermal cell.[1]

Plant cuticle is a unique biopolymer because of its physical, chemical, mechanical and morphological properties. Vascular plants have been protected by this complex biopolymer since they managed to establish themselves on dry land around 400 million years ago. The main function of the cuticle is to minimize water

loss.[5,6] Other important roles played by the cuticle are limiting the loss of substances from plant internal tissues and protection of the plant from physical, chemical and biological attack.[5]

The rheology of the plant cuticle and cutin is of particular interest. It is known that diffusion and sorption across polymers are influenced by the mechanical properties of the polymer itself. Some factors that affect these properties are the polymer density, the presence of fillers and plasticizers in the polymer matrix, and the temperature. Two important physiological processes are impacted by these properties. One is the use of foliar applied chemicals, which could modify the permeability of the biopolymer. The other physiological issue is fruit cracking as a consequence of insufficient flexibility of the cutin. Cuticle cracking is a persistent and widespread problem in some greenhouse-grown fruits, causing degradation of fruit appearance and subsequent serious economic losses.[7] Water absorbed by the cutin acts as a plasticizer, promoting molecular flexibility and softening the polymer network. One can hypothesize that water disrupts hydrogen-bonded cross-links between chains and also diminishes chain–chain methylene hydrophobic interactions.[8,9]

Isolated plant cuticles and cutins from several species show a significantly elevated specific heat[10-12] compared with other plant materials. The specific heat value of cutin was around 2–2.5 J K^{-1} g^{-1}, whereas cellulose, the main component of plant cell wall, has a specific heat of 1.5 J K^{-1} g^{-1}. Although the cuticular material contributes only as a minor mass fraction to whole leaves and fruits, it could play an

important role as a thermoregulator in the course of the biophysical interaction between the plant and the environment.

The integrity of the cutin polymer is crucial to the function of the cuticle as a barrier to solutes, either directly as a barrier or indirectly as a matrix for the deposition of waxes. Cutin not only has an impact on the interaction of the plant with its environment, but it also prevents organ fusion early in development. Cutin monomers seem to serve as potential messengers in plant–pathogen interactions, and they may play a role in the plant's defense response.[13]

All of these properties must stem ultimately from the molecular structures of cutins. Thus studies of the monomers and the connectivities among monomers have the potential to provide key information for understanding and improvement of the functions of cutins.

1.1.2 Suberin

Suberin is an extracellular matrix polymer that is deposited together with suberin-associated waxes at distinct locations during plant growth that are species-specific (Figure 1.2). It has long been hypothesized that suberized cells act as preformed, as well as wound-induced, antimicrobial barriers,[1,14,15] and this hypothesis is supported by recent evidence showing that *Erwinia carotovora* and *Fusarium sambucinum* infection is greatly enhanced when suberization is inhibited.[16] The primary role of suberized cells appears to be water retention. Suberin is constitutively present in the secondary growth periderm of aerial tissues and in several underground tissues, e.g. epidermis, hypodermis, peridermis and the

Casparian strips of the root endodermis. It may be deposited in bundle sheets, the chalazae and absicission zone during seed development, and in secretory organs as well as fibers.[17] Suberin is also deposited in response to wounding and pathogenic attack as a barrier against water and solute loss and as protection against opportunistic pathogen invasion. Despite functional, structural, and chemical similarities of suberin to cutin, suberin is characterized by a different composition and a specific location inside of the primary cell wall close to the plasma membrane. The latter feature is diagnostic for suberin.

Suberin is comprised of a phenolic (aromatic or lignin-like) domain that may be attached to the cell wall[18] and an aliphatic (lipid, hydrophobic) domain which is probably attached to the phenolic domain. Soluble waxes are embedded within the suberin matrix and provide resistance to water vapor loss.

As for cutins, studies of the molecular structures of suberins (monomers and the connectivities among monomers) will provide key information toward an explanation of the functions of suberin. Biosynthetic pathways for its formation may be deduced from the structure of the polymeric materials obtained from isotope-labeled precursors. [18,19]

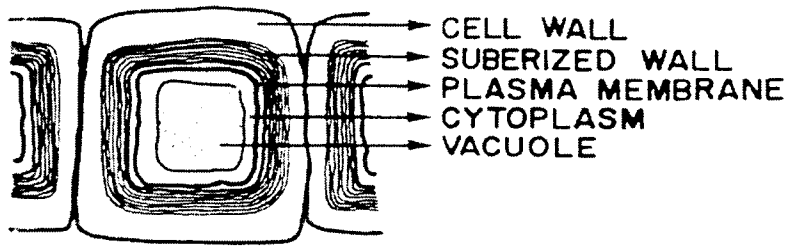

Figure 1.2. Schematic drawing of suberin.[1]

1.1.3 Melanin

Many of the dark pigments in nature are melanins (Figure 1.3) and lignins.[20] Melanins are found in all biological kingdoms and are believed to be composed of polymerized phenolic or indolic compounds that are highly resistant to degradation.[21] There are two types of melanins: eumelanins and pheomelanins. Eumelanins are black and brown and contain carbon and nitrogen. Pheomelanins are red and brown and contain carbon, nitrogen and sulfur. The melanized fungus *Cryptococcus neoformans* (described below) contains eumelanins.

Melanin has a clear role in camouflage and sexual display.[22] It can act as a sunscreen but is not a very effective one. It can also scavenge active chemical species, but this, too, is not done very effectively. It produces active radicals that can damage DNA. It binds to therapeutic drugs in ways that are either beneficial or deleterious.[23,24] Melanin is envisaged as an energy transducer with the properties of an amorphous semiconductor;[25] it can absorb many different types of energy and dissipate them in the form of heat. However, if the energy input is too great, the output can be expressed in the form of activated chemical species that can damage cellular macromolecules resulting in cell death, mutations, and cancer. The protective aspect of melanin in dark skin is seen as resulting from its high concentration and its confinement to ellipsoidal and densely packed organelles that can effectively shield the nucleus. In light skin, its radical nature is seen as potentially participating in the carcinogenic process, particularly when overwhelmed by intense episodes of sunburn. In plant pathogenic fungi, melanins appear to provide rigidity to cell walls, which in twin permits high turgor pressures

needed to penetrate plant cells. Melanins are also used for host defense in insects, where a phenoloxidase system in the hemolymph can be activated by foreign substances to synthesize melanin that can coat intruders.[26] Melanins are immunologically active and possess anti-inflammatory properties. Information on the molecular structure of melanin may be used for rational development of drugs that inhibit the process of polymerization.

Cryptococcus neoformans is an opportunistic fungal pathogen that causes life-threatening infections in 6 – 8% of patients with AIDS.[27] Cryptococcal infections in immunosuppressed patients are difficult to teat effectively, because antifungal therapy is often unable to eradicate the infection. C. neoformans has a phenoloxidase enzyme (laccase) which can catalyze the synthesis of fungal melanin from a variety of catechol precursors.[28] In turn, fungal melanin has been shown to pretect C. neoformans against oxidants, amphotericin B, and macrophages in vitro.[29] The ability of C. neoformans to melanize in vitro has been associated with virulence, but melanin synthesis in vivo has not been demonstrated. Establishing whether melanization occurs in vivo is important for understanding the relationship of phenoloxidase activity, pigment production, and virulence. To date, this has not been possible, because stains for melanin are not specific for this compound.[30] Molecular structural characteristics of fungal melanin may help diagnosis of melanization occurring in vivo.

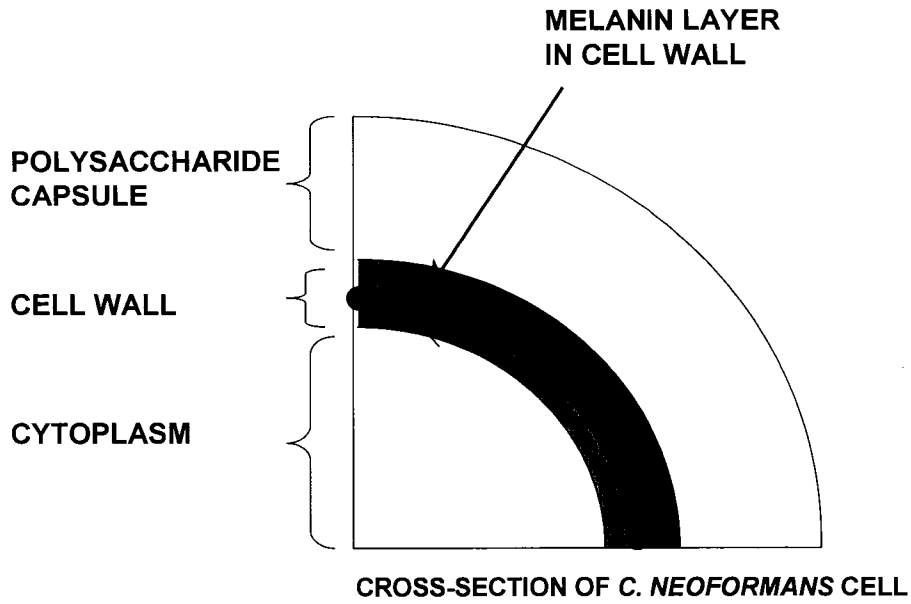

Figure 1.3. Schematic drawing of fungal melanin.
(Casadevall, A. and Stark, R. E., NIH Gant Proposal)

1.2 Prior Studies of Molecular Structure

1.2.1 Cutin

Cutin is the major constituent (between 40% and 80% by weight) of the cuticle and, from a chemical point of view, is defined as a polymeric network of oxygenated C_{16} and C_{18} fatty acids linked by ester bonds. Cutins are crosslinked polymers, therefore they are insoluble in all solvents. This fact has hampered investigation of their covalent structure and domain architecture. To meet this challenge, strategies of partial depolymerization using enzymatic or chemical reagents and spectroscopic examination of solvent-swelled intact cutin and insoluble residues from partial depolymerization were recently developed.[31-33]

Cutin can be depolymerized through cleavage of the ester bonds by alkaline hydrolysis, transesterification or enzymatic hydrolysis.[3,32] These chemical methods yield monomers and/or their derivatives depending on the reagent used. Cutin consists of C_{16} and C_{18} families of monomers (Figure 1.4).[1] The major component of the former is dihydroxypalmitic acid in which one hydroxyl group is at the ω-carbon and the other is at the C-10, C-9, C-8 or C-7 positions. A mixture of positional isomers with one dominant isomer is often found. Much smaller amounts of palmitic acid and 16-hydroxypalmitic acid are also found. The major components of the C_{18} family of cutin acids are 18-hydroxyoctadecenoic acid, 9,10-epoxy-18-hydroxyoctadecanoic acid, and 9,10,18-trihydroxyoctadecanoic acid together with their unsaturated analogs. In some cases, cutin monomers that could be derived from further oxidation or reduction of the above components are also found.

In lime fruit cutin, two monomers, 10-oxo-16-hydroxyhexadecanoic acid and 10,16-dihydroxyhexadecanoic acid, account for 98% of the total weight of the obtained monomers[34]. The chemical evidence that the polymer is held together mainly by primary alcohol ester linkages is consistent with its observed susceptibility to cutinases, which also show preference for hydrolysis of primary alcohol esters. A pentamer representing the cross-link regions of the polymer has been isolated by degradation using enzymes that are specific for the hydrolysis of primary alcohol esters.[35] Dimers consisting of the two most abundant monomers and a dimer consisting of two 10,16-dihydroxyhexadecanoic acid units were reported.[33] A tetramer based on C_{16} fatty acids and hydroxyfatty acids linked by secondary ester bonds was also identified after mild chemical degradation.[33] Information on

the molecular structure and chemical reactivity of cutin was extracted from the comparison of the NMR spectra of intact cutin, soluble monomers and oligomers, and insoluble residues.

Since the soluble products obtained after depolymerization may not always represent the architecture of the intact polymer, the recent use of nondestructive techniques has produced more useful and complementary information. Solid-state NMR analysis on isolated cuticles and cutin is one approach to the structure of intact cutin. Most studies indicate that cutin is a moderately amorphous and flexible network with motional constraints at specific cross-linked sites.[36] Less than half of the methylenes are in a molecular domain categorized as rigid, with about 59% in a molecular domain of less rigid character.[36,37] More recently, 2D NMR spectroscopy of solvent-swollen samples has been used to investigate the changes produced by partial depolymerization, using enzymatic or chemical reagents, of the intact polyesters.[31] These studies confirmed the general structural features deduced from indirect and classical chemical studies: the cutin polyester is held together mostly by primary alcohol ester linkages, with about half of the secondary hydroxyl groups involved in ester cross-links.[38] New structural studies focused on Fourier-transform infrared (FT-IR) spectroscopic analysis of isolated plant cuticles and cutin have also been performed.[13,39] This latter noninvasive tool can be used to check the purity of cuticle isolation and chemical characteristics of the isolates after partial depolymerization.[40] X-ray diffraction analysis has also been carried out. Isolated tomato fruit cutin has been studied extensively with this technique, suggesting a model of cutin comprised of an amorphous structure that acts as molecular sieve

with two major hydrophobic interplanar spacings around 1.0 and 0.45 nm. These distances are large enough to accommodate molecules of low molecular weight.[39]

Molecular dynamics (MD) calculations have been applied to obtain an initial structure based on the molecular characteristics described above. It is known that MD calculations can provide detailed information that helps to rationalize macroscopically observed behavior from a microscopic standpoint. MD simulations suggested that cutin is a moderately flexible network with motional constraints mainly located at the cross-link sites of ester functional groups.[41] The molecular modeling yields a picture of cutin agreeing with their amorphous and hydrophobic characteristics.

Extensive studies on the biosynthetic pathway of cutin assembly from monomers have been conducted.[32,42] The biosynthesis of the C_{18} family of monomers has been more thoroughly studied than that of the C_{16} family monomers, revealing that oxygenated octadecanoates are derived from oleic acid (and also from linoleic acid) by ω-hydroxylation and epoxidation of the double bond followed by the hydroxylation of the epoxide.[32,42] The oxygenated octadecanoates are then hydrolyzed to the diol 9,10-dihydroxyoctadecanoic acid by an epoxide hydrolase.[43,44] Enantioselectivity studies of the epoxidation reaction showed that the epoxides (9*R*,10*S*) and (9*S*,10*R*) were produced in a 9:1 ratio.[45]

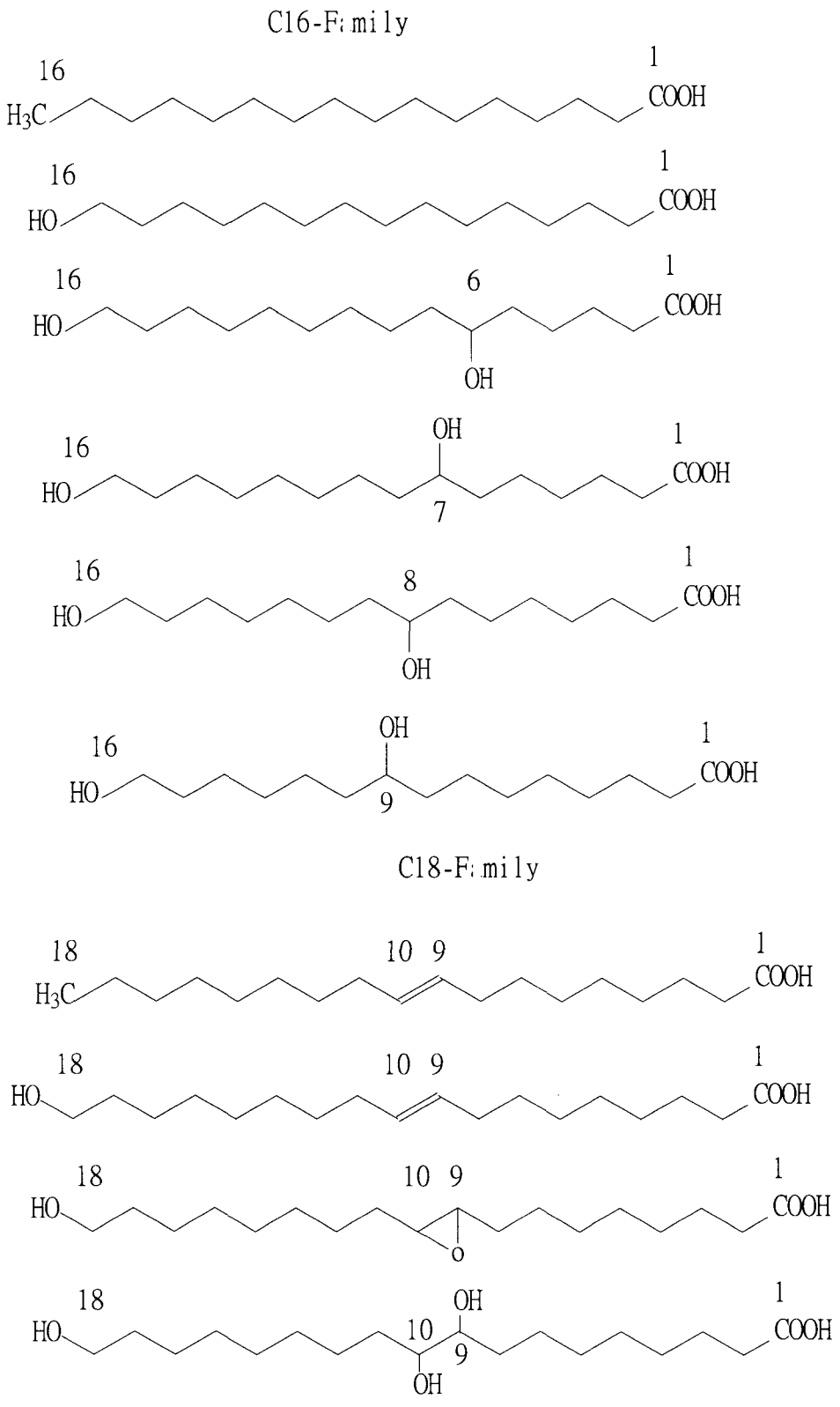

Figure 1.4. The major monomers found in cutin.[46]

1.2.2 Suberin

The suberin biopolymer contains poly(aliphatic) and poly(phenolic) domains (SPAD and SPPD). Both the SPAD and the SPPD have their own unique chemical composition and are hypothesized exist as distinct entities within suberized cells [18]. They do, however, appear to be covalently linked together, presumably at the inner surface of the cell wall.[47-50] The SPAD of suberized tissues is assembled from a series of specific, and in some cases unique, aliphatic components (Figure 1.5). The main aliphatic structural components of the SPAD include 1-alkanols, ω-hydroxyalkanoic acids, α,ω-dioic acids, mid- chain epoxide- and di- and tri-hydroxy-substituted octadecanoates, and glycerol.[51,52] In addition, hydroxycinnamic acids such as *p*-coumaric, caffeic, and especially ferulic acids, as well as ferulic acid esters of long-chain alcohols (Figure 1.6), have been identified in hydrolysates and extracts, respectively, from suberized tissues.[52]

The principal analytical tools used to identify SPAD components are (*i*) organic solvent extraction to isolate nonpolymerized wax components, (*ii*) hydrolysis (including BF_3–MeOH transesterification, reduction with $LiAlH_4$, and alkaline hydrolysis with $NaOCH_3$ or NaOH) to isolate esterified components, and (*iii*) subsequent gas chromatography of their TMS-, methyl-, or acetyl-derivatives. The yield and spectrum of aliphatics is dependent on hydrolysis conditions, with complete removal achieved only by very harsh treatment.[49] The proportion of the individual aliphatic components differs widely from species to species. For example, in potato (*Solanum tuberosum*) suberin, α, ω-dioic acids (33% of monomers) and ω-hydroxyalkanoic acids (32% of monomers) predominate in the

SPAD, whereas epoxides and mid-chain hydroxylated fatty acids are present in only trace amounts. By contrast, epoxides (31% of monomers) and ω-hydroxyalkanoic acids (41% of monomers) predominate in cork (*Quercus. suber*).[51]

The first attempts to define the SPPD of suberized tissues relied on alkaline nitrobenzene oxidation (NBO), a degradative technique that results in cleavage of phenylpropanoid side chains and yields benzaldehyde, benzoate, and acetophenone derivatives with aromatic substitution patterns representative of the phenylpropanoids in the intact tissue. But the presence of *p*-hydroxybenzaldehyde, vanillin, and syringin in NBO hydrolysates can be equally indicative of hydroxycinnamic acids or monolignols or even other phenolics such as tyramine, as all yield similar substituted benzaldehydes upon hydrolysis.[53] The presence of substituted benzaldehydes in the hydrolysate was taken as evidence of lignin. A new picture of the SPPD began to emerge when more selective lignin degradation techniques such as thioacidolysis, which cleaves only 8-*O*-4' ethers of monolignols (Figure 1.7), was applied to suberized tissues.[54,55] For example, thioacidolytic analysis of suberized potato tissues yielded approximately 10% of the monomers released from lignified tissues. Since thioacidolysis only degrades between 20 and 40% of lignin to monomers, this result suggests that potato SPPD contains much less "lignin" than lignified tissues. Comparisons between methylated and nonmethylated samples further revealed that the monolignols in the SPPD are more highly cross-linked than those in wood or wheat straw lignins.[55] No evidence for *p*-hydroxy-substituted phenolics was found with thioacidolysis, despite the abundance of this monosubstituted phenolic in NBO hydrolysates.[54] A significant proportion of

the *p*-hydroxybenzaldehyde units released via NBO were derived from tyramine, presumably present as feruloyltyramine units in the SPPD.[53,56] NMR studies, in which the metabolic fate of specific carbon atoms in the phenylpropanoid side chain was tracked using 1-[^{13}C]-L-Phe, 2-[^{13}C]-L-Phe, and 3-[^{13}C]-L-Phe, demonstrated that hydroxycinnamic acids were major components of the potato SPPD, and supported the conclusion that they were covalently cross-linked via bonds other than esters.[57] Subsequently, it was shown that suberized tissues contain a significant amount of both hydroxycinnamic acids and monolignols.[58]

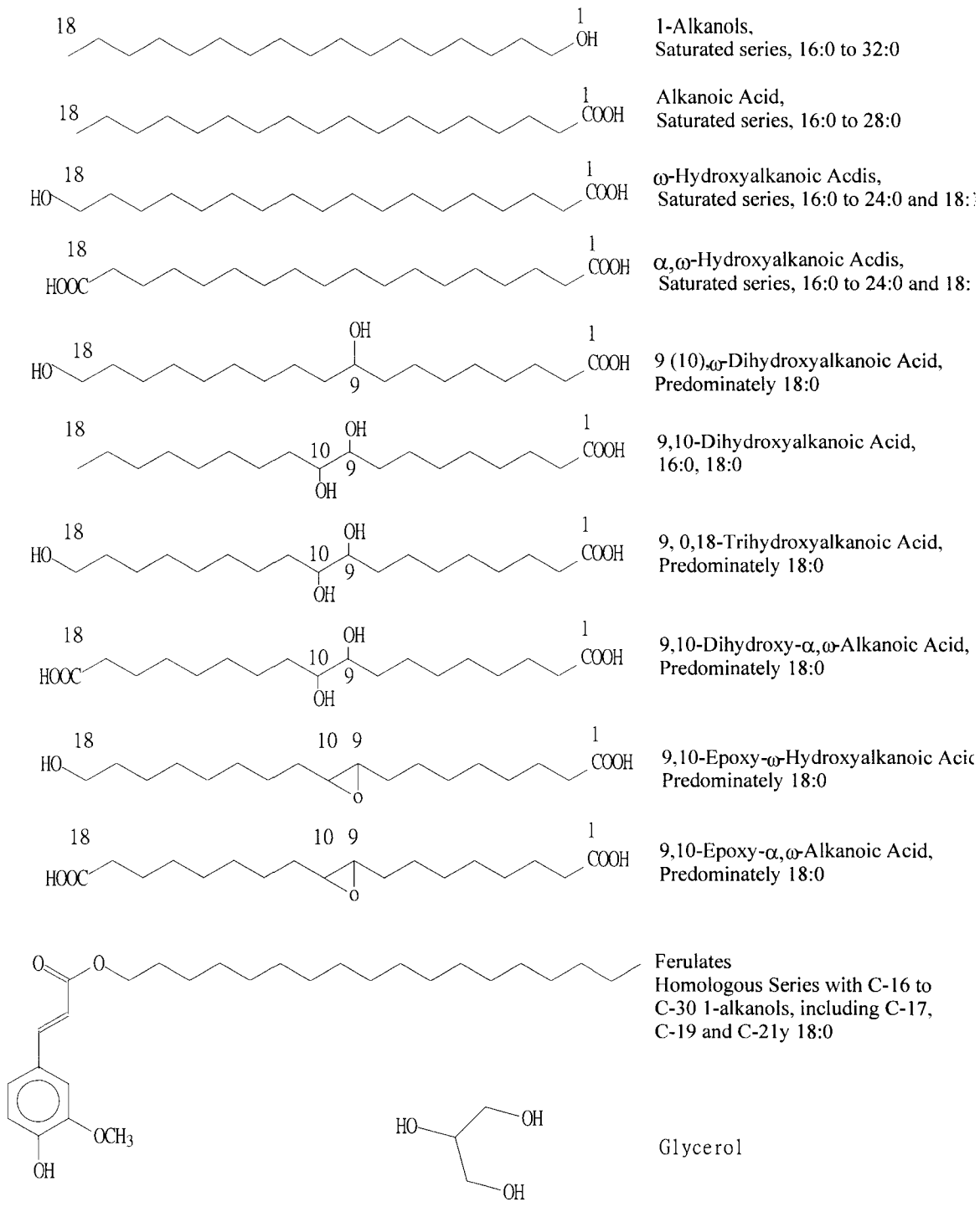

Figure 1.5 Aliphatic precursors of suberized tissues.

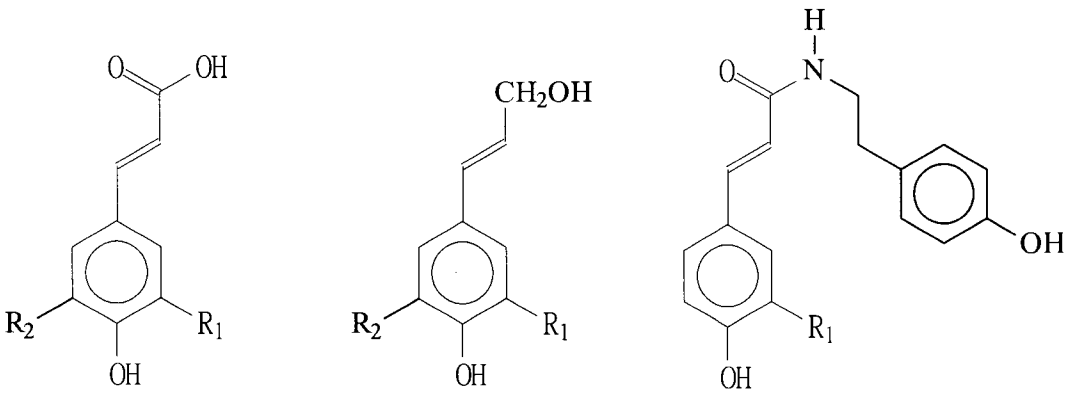

R_1=R_2=H, *p*-Coumaric Acid
R_1=OH, R_2=H, Caffeic Acid
R_1=OCH_3, R_2=H, Ferulic Acid
R_1=R_2=OCH_3, Sinapic Acid

R_1=R_2=H, *p*-Coumaryl Alcohol
R_1=OH, R_2=H, Coniferyl Alcohol
R_1=R_2=OCH_3, Sinapyl Alcohol

R_1=H, *p*-Coumaroyltyramine
R_1=OCH_3, Feruloyltyramine

Figure 1.6. Phenolic precursors of suberized tissues.

1.2.3 Melanin

Several research groups have used CPMAS ^{13}C and ^{15}N solid-state NMR in conjunction with established chemical shift trends to tentatively identify functional groups in synthetic and natural eumelanins from animal or fungal sources.[59-63].Although signals from carboxylic acids, aromatics, and uncyclized aliphatic chains have been found in all of these materials, their relative spectral intensities vary widely due to diverse sample sources and the possible presence of proteinaceous contaminants.[62] Broad line widths have been attributed to the structural heterogeneity of each biopolymer as well as the presence of paramagnetic centers. [64] Narrower ^{13}C resonances were obtained for human hair melanin than those for sepia melanin because free radical concentration in human hair melanin is only observed as one-tenth of that in sepia melanin. Human hair melanin has much higher proportion of aliphatic components.[65] Alternatively, solution-state NMR has

been used for more than two decades to characterize melanins and soil organic matter dissolved in strong base.[61,66-69] As with chemical degradation methods, an incomplete or distorted picture of the original material may result from this procedure, and in practice, the ^{13}C and ^{1}H spectra have often displayed disappointing resolution attributed to high viscosity, unpaired electron density, and chemical heterogeneity.

1.3 Open Questions to be addressed

1.3.1 Cutin and Suberin

Whereas the details about the chemical composition, biosynthesis, and macromolecular assembly and structure of suberin and cutin are slowly coming to light, it is clear that a lot remains to be learned regarding the types of inter-unit linkages, and perhaps more critically, the details of their macromolecular assembly. Development of new depolymerization methods, which can produce bigger oligomers present in higher proportions among the products, can potentially reveal more information on the connectivities among monomers. The linkage information is very important to the properties, and consequently to the physiological functions, of the materials.

Although more connectivity information of monomers can be extracted from better-controlled depolymerization methods, some of the connectivity information can still be lost because of limitations in the specificities, completeness, and other unknown factors of the depolymerization. In solid-state ^{13}C NMR studies, many peaks overlap and become indistinguishable because of line broadening. Thus we

can't get all the information on the structure of cutin and suberin even if this information may be present in the spectra. A technique called high-resolution magic-angle spinning (HRMAS) has been applied to plant polymers by our group in the past few years. This technique combines many advantages of both solid-state NMR and solution NMR. Swelling the materials in organic solvents (the best solvent is dimethyl sulfoxide (DMSO)), allows molecular motion and partial averaging of dipolar interactions, so that MAS then produces well-resolved ^{1}H and ^{13}C NMR spectra. With enhanced resolution, 2D NMR experiments such as TOCSY, HMQC, and HMBC can be applied to suberin and cutin. The results from this latter method agree very well with those from the degraded material, but the new information is extracted from intact materials, excluding possible misleading information from further reactions of the likely products of chemical or enzymatic depolymerization. Three- dimensional or even four-dimensional HRMAS NMR on natural or selectively labeled suberin and cutin may provide more definitive information on the three dimensional structures of the materials, which are macromolecular assemblies. As a complementary method, HRMAS NMR may provide some information on the molecular organization of cutin and suberin that neither degradation nor CPMAS NMR of powdered samples can provide. By comparing the results for depolymerized, intact CPMAS NMR, and HRMAS NMR, new structural insights may be derived. The comparison could also be used to evaluate the efficiencies and specificities of the depolymerization methods.

Although there is no doubt that phenolic moieties exist in suberin, covalent bonding between phenolic and aliphatic monomers has never been verified. With

appropriate depolymerization methods and HPLC separation, fragments consisting of phenolic and aliphatic monomers could be separated and identified. Covalent bonds between aliphatic and phenolic moieties or polysaccharides would support strong binding between suberin or cutin and other cell layers. This information could allow us to design and test hypotheses regarding the functions of different cell layers and their relationships.

1.3.2 Melanin

High-resolution ^{13}C and ^{15}N solid-state NMR provide tantalizing first looks at the structural features of such intractable materials, but they are limited by uncertainties in both the numerical values and interpretations of the chemical shifts. The combination of ^{13}C biosynthetic labeling, CPMAS NMR, and sample swelling [70] can identify key functional groups in *C. neoformans* melanin and suggests a general strategy for more comprehensive elucidation of the molecular structure of this enigmatic polymer. Using of different labeled precursors, including those containing ^{15}N, will enhance signals of other regions of melanin that display weak signals in natural abundance spectra. Moreover, 3D experiments can further spread spectra out and distinguish those nuclei with very close chemical shifts. Molecular structural characteristics obtained from NMR studies of isolated fungal melanins may result in a resolution for diagnosis of melanization occurring in vivo, especially providing diagnostic NMR information for detection of melanization with in vivo magnetic resonance imaging (MRI).

Chapter 2. Introduction

2.1 Introduction to Nuclear Magnetic Resonance

2.1.1 Basic Introduction to NMR

Nuclear magnetic resonance (NMR) is a phenomenon that occurs when the nuclei of certain atoms are equilibrated in a static magnetic field and exposed to a second oscillating magnetic field. NMR involves the magnetic energy levels of nuclei when they are placed in a magnetic field, and the transitions occur in the radiowave region of the spectrum. Although the first experiments were carried out in 1945, useful chemical applications became possible only after the discovery of the chemical shift effect in 1949. The first commercial NMR spectrometer appeared in 1953, and the subject developed very rapidly thereafter.

Some nuclei experience this phenomenon, and others do not, depending on whether they possess a property called spin. Spin is a fundamental property of nature like electrical charge or mass. Spin comes in multiples of 1/2 and can be positive or negative. Protons, electrons, and neutrons possess spin. Individual unpaired electrons, protons, and neutrons each possess a spin of 1/2. Two or more particles with spins having opposite sign can pair up to eliminate the observable manifestations of spin. In nuclear magnetic resonance, it is unpaired nuclear spins that are of importance. When the proton is placed in an external magnetic field, its spin will have two possible energy levels (Fig. 2.1). These energy states can be characterized by the nuclear spin quantum number, I, and are separated by an amount ΔE, which is field dependent:

$$\Delta E = h\gamma \mathbf{B}_0/2\pi$$

where γ is the magnetogyric ratio and $\mathbf{B}_0$ is the magnitude of the applied static magnetic field. The magnetogyric ratio is the proportionality constant that relates the observed resonance frequency ($h\nu$ = E) for a particular nucleus to the applied field. The NMR observation frequency can be expressed in terms of the magnetogyric ratio and the applied field:

$$\nu = \gamma \mathbf{B}_0/2\pi$$

$$\text{or} \quad \omega = \gamma \mathbf{B}_0.$$

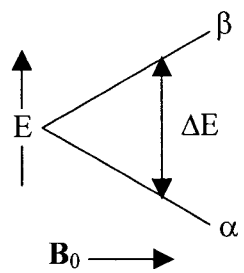

Figure 2.1. Energy level diagram for a spin with I = ½ in a magnetic field $\mathbf{B}_0$.

The two energy states for protons will be populated unequally, with the ratio of the populations being given by the Boltzmann equation:

$$N_\beta / N_\alpha = \exp[-(E_\beta - E_\alpha)/kT],$$

where N_α is the population of the lower state and N_β is the population of the upper state. The population difference is dependent on both the field and the nuclear species under observation.

The total magnetic moment or magnetization, **M**, of the sample is the vector sum of the magnetizations of the individual spins. At equilibrium, the net magnetization vector **M** lies along the direction of the applied magnetic field $\mathbf{B}_o$ which is designated as the $+z$ axis (Fig. 2.2(a)), and is called the equilibrium magnetization

$\mathbf{M_0}$. In this configuration, the z component of magnetization M_z equals $\mathbf{M_0}$. M_z is referred to as the longitudinal magnetization. Although there is a component of the precessing magnetization in the xy plane, the vector sum in the xy plane is zero, [71] and there is no net transverse (M_x or M_y) magnetization at equilibrium because it can be directed in any direction at random.[72] When a magnetic moment, μ, moves in a uniform magnetic field, $\mathbf{B_0}$, a torque is exerted on the magnetic moment which tends to align it perpendicular to the field. However, since this torque can only alter the component of angular momentum perpendicular to $\mathbf{B_0}$ and μ, the net result corresponds to a rotation of the direction of μ in a cone with its axis along $\mathbf{B_0}$ at a frequency $\gamma\mathbf{B_0}/2\pi$ hertz, i.e. the movement of μ traces out a cone about $\mathbf{B_0}$ (Fig. 2.2(b)). This motion is known as Larmor precession.

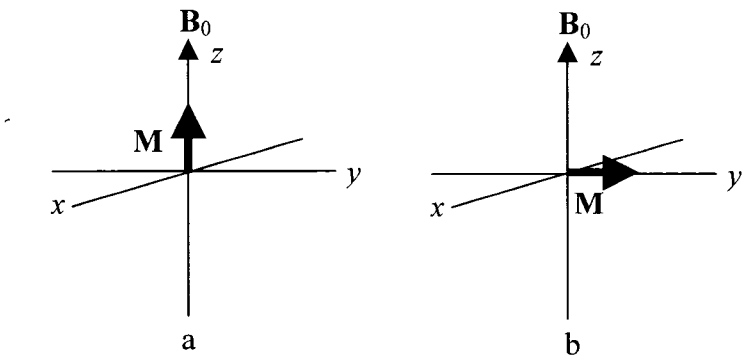

Figure 2.2. The behavior of the bulk magnetization, **M**, (a) at equilibrium, and (b) after perturbation by a pulse.

If a second magnetic field, $\mathbf{B_1}$, is applied perpendicular to $\mathbf{B_0}$ and oscillates at the same frequency as the precession, **M** will move toward the xy plane. The $\mathbf{B_1}$ field is applied as a pulse of duration t_p, typically tens of microseconds. The magnetization will flip toward the xy plane, traversing an angle $\theta = \gamma\mathbf{B_1}t_p$. When t_p is appropriate,

the magnetization will flip into the *xy* plane, thus M_z=0. After this perturbation, the system will return to equilibrium. The spin-lattice relaxation time (T_1) is the time required to reduce the difference between the longitudinal magnetization (M_z) and its equilibrium value by a factor of *e*.

If the net magnetization is placed in the *xy* plane as described above, it will rotate about the *z* axis after the $\mathbf{B}_1$ pulse has ended. In addition to the rotation, the net magnetization starts to dephase because each type of spin is experiencing a slightly different magnetic field and precesses at its own Larmor frequency. The longer the elapsed time, the greater the phase difference. Eventually, the net magnetization in the *xy* plane will be zero. The spin-spin relaxation time, T_2, is the time required to reduce the transverse magnetization by a factor of *e*. T_2 is always less than or equal to T_1.

It is convenient to define a rotating frame of reference, which rotates about the *z* axis at the Larmor frequency. We distinguish this rotating coordinate system from the laboratory system by primes on the *x* and *y* axes, *x'y'*. A magnetization vector rotating at the Larmor frequency in the laboratory frame appears stationary in a frame of reference rotating about the *z* axis. In the rotating frame, relaxation of the M_z magnetization to its equilibrium value looks the same as it does in the laboratory frame. However, a transverse magnetization vector rotating about the *z* axis at the same frequency as the rotating frame will appear stationary in the rotating frame. A magnetization vector traveling faster than the rotating frame rotates clockwise about the *z* axis. A magnetization vector traveling slower than the rotating frame rotates counter-clockwise about the *z* axis.

The phenomenon of the chemical shift arises because of shielding (screening) of the nuclei from the external magnetic field by the electrons. Since the shielding effect is caused by the electronic environment, values of σ will vary with the position of the nucleus in the molecule. Factors that affect electron density will also affect σ. Chemical shift differences are usually reported in parts per million (ppm). These are obtained from measurements in Hz divided by ν_0, the operating frequency of the spectrometer. In such dimensionless units, chemical shift differences are invariant to the spectrometer conditions, and may therefore be interpreted as molecular characteristics.

For a given compound the appearance of the spectrum is governed by intramolecular chemical shift differences, i. e. differences in resonance frequency for different nuclei of the same molecule. The intensity of absorption is strictly proportional to the concentration of the nuclei giving rise to the absorption. This property is of great importance for structure determination. The proportionality of intensity to concentration for NMR is valid for comparisons between different concentrations of impurities, isomer ratios, etc. It is also a straightforward matter to obtain absolute concentrations for a given chemical in solution if standard concentrations can be prepared.

Spin-spin coupling refers to the magnetic interactions between individual spins through the intervening bonding electrons, so that the nuclear spins are connected indirectly. The spin-spin coupling is field independent and is usually smaller than other forms of magnetic interactions, typically ~ 12 Hz for geminal protons, 2-9 Hz for protons separated by three bonds, and as much as 150 Hz for ^{13}C-^{1}H pairs.[73] Its

magnitude is reflected by a spin-spin coupling constant, and the coupling constant depends on chemical environment. Spin-spin coupling is only effective between nuclei in the same molecule.

In contrast to the spin-spin coupling, dipole-dipole coupling involves magnetic interactions through space instead of through chemical bonds. Because dipole-dipole coupling is proportional to the magnetogyric ratio and inversely proportional to the third power of the distance between the nuclei, it is dominant for ^{1}H, ^{19}F, and possibly ^{31}P; it decreases rapidly in magnitude as the internuclear distance increases. Theoretical analysis shows that the dipole-dipole coupling has a dependence of $(3\cos^2\theta - 1)$ on the angle between the internuclear vector and the direction of the external field $\mathbf{B}_0$.

2.1.2 Solution-State NMR

In solution-state NMR, rapid Brownian motion of molecules averages the dipole-dipole coupling to zero because the angle varies with time and the expression $(3\cos^2\theta - 1)$ vanishes. But spin-spin coupling remains in solution-state NMR. An important method for detecting spin-spin coupling and thus through-bond connectivity is 2D homonuclear chemical shift correlation spectroscopy (COSY). The cross peaks in a 2D COSY spectrum correlate the chemical shifts of two protons and indicate the presence of scalar coupling between them. The basic COSY pulse sequence (Fig. 2.3) is simply

$$90° - t_1 - 90° - \text{Acquire } (t_2)$$

where t_1 is an incremented delay. The first 90° pulse makes the magnetization precess in the *xy* plane at a frequency ν_1 which depends on its shift, δ, and on each of the couplings with which the nucleus is involved. The second 90° pulse mediates the magnetization transfer among the transitions of a coupled system. Transfer may occur between transitions of the same nucleus, in which case the appropriate 2D peaks fall on the diagonal of a square plot. Off-diagonal peaks show that the resonances at the relevant shift positions on the two axes are coupled through chemical bonds.

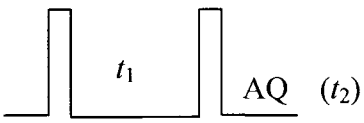

Figure 2.3. The basic COSY pulse sequence.

Heteronuclear multiple-quantum correlation (HMQC) represents a class of pulse sequences for 'reverse correlation', i. e. heteronuclear correlation with detection of protons. HMQC shows all the correlations of ^{1}H and X nuclei, like ^{13}C, connected directly through one bond. A simple but effective version of this sequence is shown in Fig. 2.4. The delay Δ_1 is set equal to $1/(2J_{CH})$ and so can be tuned for one-bond or long-range couplings. Multiple-quantum correlation will transfer the polarization from X nuclei to protons. If an X nucleus has more than one proton, the effect of the relatively small homonuclear coupling during the short delays Δ_1 may be neglected. During t_1, dephasing caused by any J_{HX} coupling is refocused by the 180° proton

pulse. However, the effect of any J_{HH} coupling is not refocused, since both coupled nuclei are influenced by the 180° pulse.

Heteronuclear multiple-bond correlation (HMBC) is a sensitive method for the determination of long-range (two- and three-bond) ^{1}H-heteronuclear connectivity. This is also a through-bond interaction. One of the commonly used versions of the pulse sequence for HMBC is a modification of HMQC (Figure 2.5). The first 90° (^{13}C) pulse serves as a low-pass J filter, suppressing one-bond correlations in the two-dimensional spectrum and passing long-range correlations with smaller J. This pulse creates heteronuclear multiple-quantum coherence for protons directly coupled to a ^{13}C nucleus, which is then removed from the two-dimensional spectrum by alternating the phase of the ^{13}C pulse along the $\pm x$ axis without changing the receiver phase. The second 90° (^{13}C) pulse creates ^{1}H-^{13}C multiple-quantum coherence for the long-range connectivities. The 180° proton pulse effectively removes the effect of the proton shifts from the t_1 modulation frequency by interchanging the zero- and double-quantum components. Thus, after the final 90° (^{13}C) pulse, the ^{1}H signals that originate from ^{1}H-^{13}C multiple-quantum coherence are modulated by ^{13}C chemical shifts and homonuclear proton couplings.

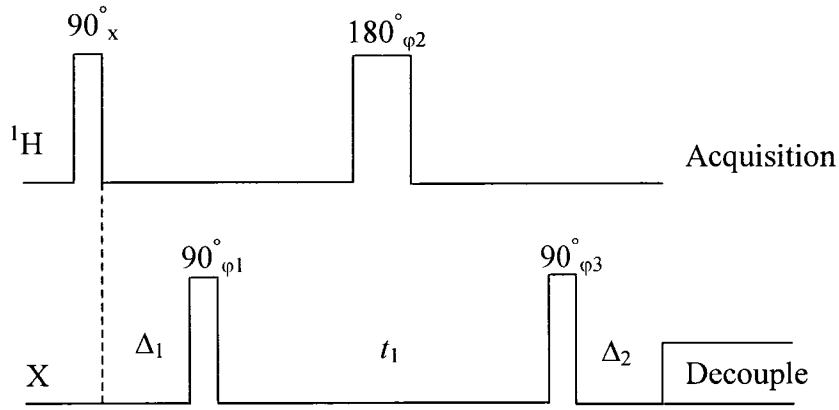

Figure 2.4. Pulse sequence for HMQC.

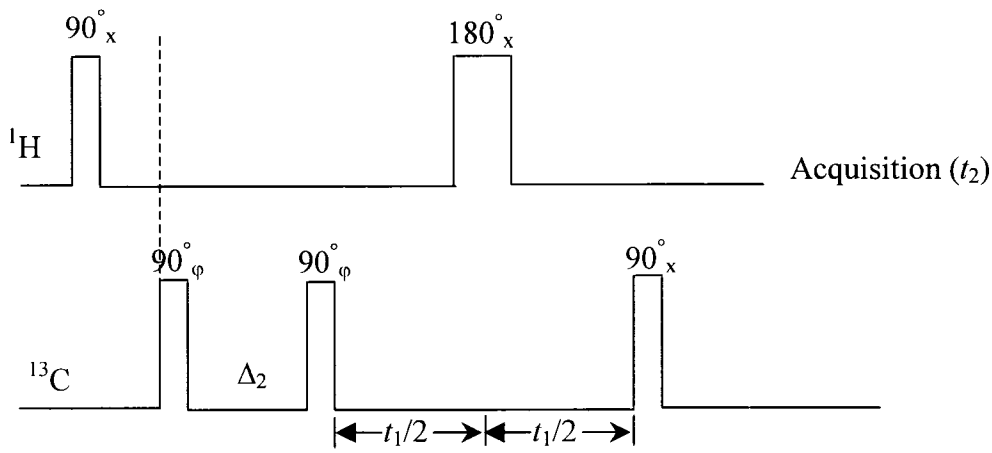

Figure 2.5. Pulse sequence for HMBC

The nuclear Overhauser effect (NOE) is defined as the change in the integrated NMR absorption intensity of a nuclear spin when the NMR absorption of another spin is saturated. Consider a two-spin system IS which is not J-coupled. Transition probabilities (W) per unit time between states are defined as in Fig. 2.6. The equilibrium populations of each level are governed by the Boltzmann distribution. If irradiation of S is continued for a long enough time (~ 10 μs), a new population

distribution gradually develops as relaxation occurs through W_2 and W_0. W_2 increases the intensity of the I transitions by attempting to establish a Boltzmann distribution between levels 1 and 4, whereas W_0 decreases the I intensity by equilibrating levels 2 and 3. The resulting net change in the intensity of I as a result of the competition between W_2 and W_0 is the nuclear Overhauser effect. An increase in intensity is usually defined as a positive NOE, and a decrease in intensity is a negative NOE.

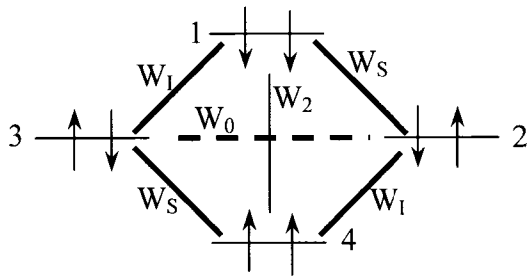

Figure 2.6. Spin states and transition probabilities for a two- spin system IS.

If the irradiation of the S spin is continuous, this is called a steady-state NOE. If the irradiation of the S spin is conducted by applying a selective 180° pulse to one of the resonances, the result is to invert, within a few milliseconds, the populations of the levels associated with the S spin. W_0 and W_2 begin to redistribute this non-equilibrium population, and the NOE at I starts to build up. Because the irradiation is not continuous, both spins will have relaxed back to their original population distribution within a few T_1s. This is referred to as a transient NOE, and it will reach its maximum after about one T_1 and then decline.

Two-dimensional nuclear Overhauser effect spectroscopy (NOESY) applied to protons is one of the most important techniques available in biological spectroscopy,

since under the correct conditions a complete set of short-range (< 5 Å) through-space connectivities can be obtained for a macromolecule. The pulse sequence for NOESY is shown in Figure 2.7. The non-selective pulse pair, 90° – t_1 - 90°, generates oscillations of population at a frequency ω_1. τ is a mixing time during which the NOEs develop, and the third 90° pulse reads the state of the system to measure the size of the NOEs.

For a spin on resonance with a zero precession frequency in the rotating frame, the first 90° pulse puts the magnetization in the *xy* plane. During t_1 there is no precession, so that after the second 90° pulse the magnetization is lined up along the $-z$ axis. During τ, transient NOEs will develop from it in the usual way, and these will be detected by the final 90° pulse.

A spin having a precession frequency in the rotating frame will precess by an amount that depends on both its shift and the time t_1. Therefore, the effectiveness of the second pulse in generating a net 180° pulse depends on shift and t_1; the pulse will act only on that component of the vector that is in the *yz* plane. The crosspeaks in a 2D spectrum will consist of responses corresponding to the size of the transient NOE that has built up during τ. It is possible, by analysis of how the cross peak intensity varies with τ, to extract approximate distance information from such spectra.

^{1}H-^{1}H NOE responses are largest in the slow-tumbling extreme. NOESY tends not to be used in studies of rapidly tumbling molecules except where frequency selectivity is a severe problem or where many NOE connections are sought.

NOESY is the usual method of choice for large molecules (e.g. proteins and nucleic acids) in the slow-tumbling regime.

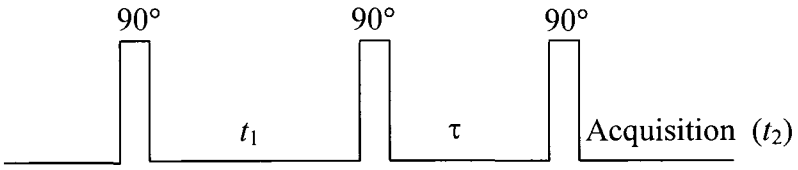

Figure 2.7. NOESY pulse sequence.

2.1.3 Solid-State NMR

In solids the molecules are generally rotating slowly, so that dipolar interactions are not averaged to zero. Thus the many possible overlapping 'powder patterns' make the solid-state NMR spectra much broader than those in solution-state NMR. In order to average dipole-dipole coupling, a technique called magic-angle spinning (MAS) can be used. If a solid sample spins rapidly enough at 54.7° to $\mathbf{B}_0$, the geometric factor $(3\cos^2\theta - 1)$ becomes zero. Under these conditions, the dipolar interaction is averaged to zero, and so dipolar broadening is eliminated, giving much higher resolution. The technique applies to both homonuclear and heteronuclear cases. But the rate of spinning required to average the dipolar interactions completely has to be greater than the static linewidth expressed in Hz. This can be several tens of kHz, and such speeds are difficult to achieve in practice. At spinning speeds lower than the static bandwidth, the dipolar coupling may not be averaged totally, but the resolution can be improved.

Low signal-to-noise is the first difficulty faced in solid-state NMR of dilute spins such as ^{13}C. Spectral broadening due to dipolar interactions with protons is another difficulty in the way of getting satisfactory solid-state spectra. A third problem is the fact that spin-lattice relaxation times can be very long, so that signal averaging methods, which can improve signal-to-noise by obtaining more transients, are not very efficient. This sensitivity problem can be overcome with a technique called cross polarization (CP), which can enhance the signal of dilute spins by deriving additional magnetization from the abundant spins I such as ^{1}H. Not only will the effective spin-lattice relaxation time be reduced to that of abundant spins I, which is typically much shorter, but the signal of the dilute spins S can also be enhanced by the order of γ_I/γ_S. Fig. 2.8 shows the pulse sequence used to achieve CP. The first step is to apply a 90° pulse on the proton channel and to spin-lock the ^{1}H magnetization in the *y* direction of the rotating frame. At this point the r.f. in the ^{13}C channel is switched on, and the amplitude of the magnetic field $\mathbf{B}_1c$ is adjusted so that the Hartmann-Hahn condition is fulfilled: $\gamma_H B_{1H} = \gamma_C B_{1C}$. This condition implies that in their respective rotating frames of reference the protons and carbons precess at equal rates and that the effective energies are comparable, thus allowing a rapid transfer of magnetization. The combination of MAS and CP can help to obtain a well-resolved and highly sensitive solid spectrum.

Since a maximum signal will be observed only when the Hartmann-Hahn condition is satisfied, the disadvantage of this CP pulse sequence is that only one kind of carbon's Hartmann-Hahn condition can be matched at one time. When we apply the power level to match one carbon's Hartmann-Hahn condition, the other

carbons may be mismatched, for instance if the sample has significant molecular motion or if dipolar interactions are partially averaged by MAS. To match all the carbons, a technique called Variable Amplitude CP (VACP) was developed. The power level can be varied in an up/down style as shown in Figure 2.9a; this is called variable-amplitude cross-polarization (VACP). [74] To get a better result, a ramped amplitude of the power called Ramped Amplitude CP (RAMP-CP) was later introduced (Figure 2.9b). [75] In RAMP-CP, all the carbons will be matched and the S/N of all the carbons will increase.

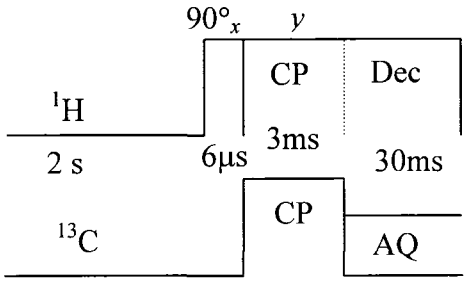

Figure 2.8. The cross polarization pulse sequence, showing approximate times for each step.

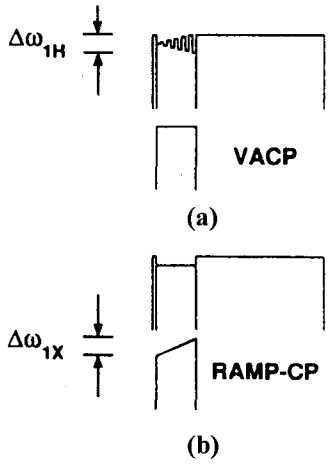

Figure 2.9. Cross-polarization Pulse Sequences: (a) VACP; (b) RAMP-CP.

2.1.3.1 Separation of Protonated Carbons from Nonprotonated Carbons

The standard CPMAS experiment is not well suited for selective decoupling, off-resonance decoupling, or other techniques that distinguish between different carbon types. To do this we have to modify the pulse sequence for standard CPMAS. We insert a time delay between the contact time and the acquisition, during which we turn off the proton field. All carbon spins will dephase under the influence of the proton dipolar field, but those with attached protons will dephase very quickly compared to those without protons. After a relatively short time (40 ~ 100 μs) the proton field is reapplied to decouple the heteronuclear dipolar interactions during the acquisition of the carbon free-induction decay, which will now come from only the nonprotonated carbons that were not completely dephased during the delay time.[76] Highly mobile protonated carbons, which also diphase slowly, may also be retained in the spectrum. Subtraction of the delayed-decoupling spectrum from the

standard CPMAS spectrum yields the spectrum of the carbons with protons, assuming that signal intensities from nonprotonated carbons are invariant. By arraying the delay time, we can obtain the maximum suppression of the signals from protonated carbons.

2.1.3.2 Carbon-Carbon Spin Diffusion

Cross-Polarization Phase-Sensitive NOESY (CPNOESYPS) is a 3-pulse 2D exchange correlation sequence similar to the high-resolution NOESY experiment in solution-state NMR. [77] CPNOESYPS can be run as a direct polarization experiment or the first 90° pulse can be replaced by a cross-polarization pulse element. Figure 2.10 is a diagram of this sequence. For CPNOESY, cross peaks occur between resonances that share mutual through-space dipolar coupling or interact through weak spin diffusion. The experiment can be very informative regarding molecular structure, because the maximum distance that can be probed for ^{13}C-^{13}C pairs is approximately 7 Å.

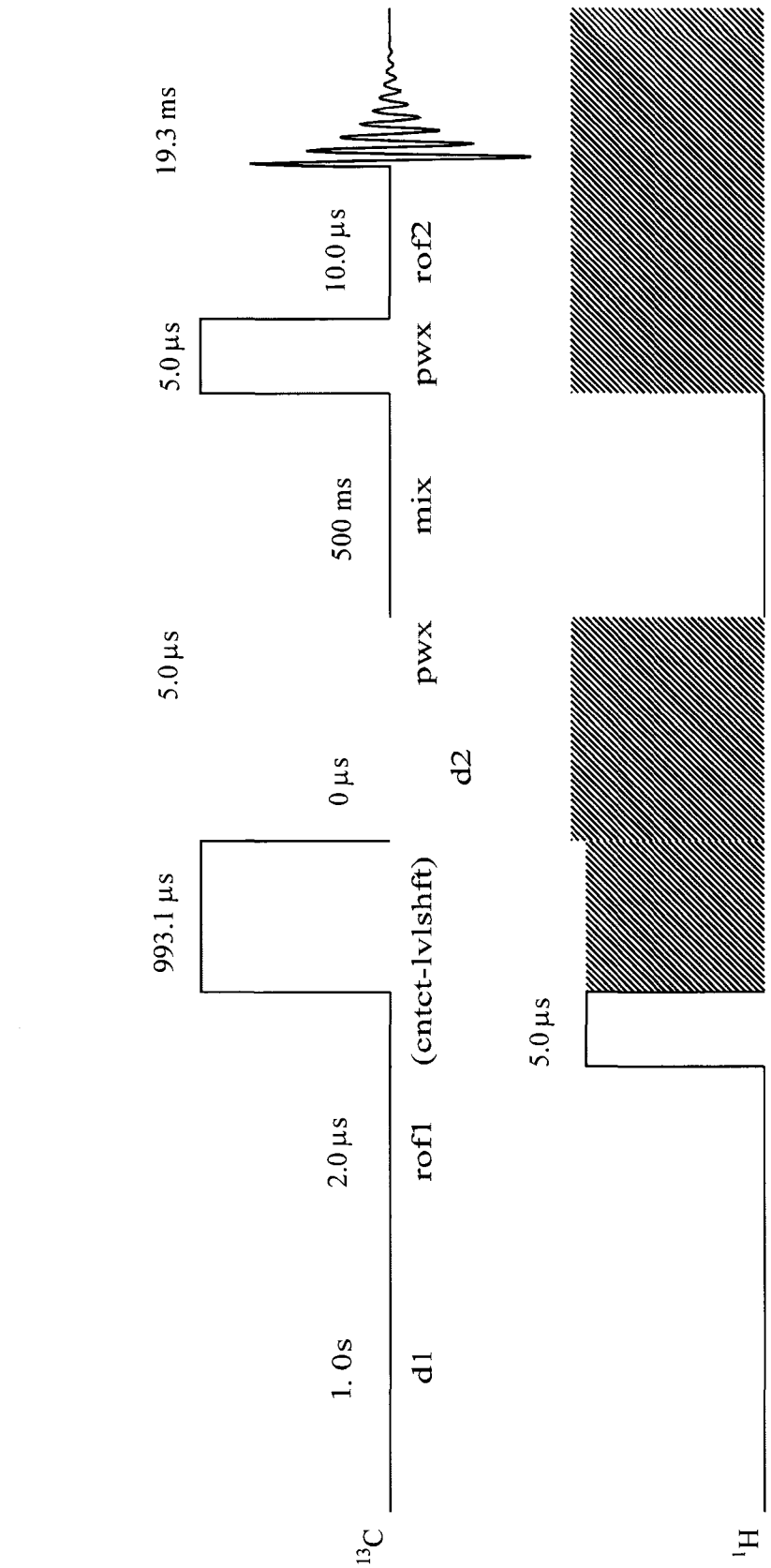

Figure 2.10. Pulse sequence of CPNOESYPS with cross-polarization.

2.1.3.3 Distinguishing Mobile and Immobile Carbons

Good-quality solid-state MAS ^{13}C NMR spectra are obtainable for some samples using direct polarization with MAS and decoupling of protons. If the proton decoupling power is high enough (≥ 50 kHz), both scalar and dipolar coupling will be removed (DPMASDD). The decoupling power can also be selected so that it removes only scalar decoupling without affecting the dipolar coupling (~ 5 kHz) (DPMASSD). Under this latter circumstance, the signals from immobile (or rigid) carbons will quickly dephase and only signals from mobile carbons can be observed.[36]

2.1.4 High-Resolution Magic-Angle Spinning (HRMAS) NMR

HRMAS NMR combines high-resolution NMR experiments with dipolar-reducing sample rotation of viscous or gel-like samples. If a solid sample can be swelled with a solvent, the mobility of the sample will increase, and the anisotropic interactions will be averaged to some extent. Under static or traditional *z*-axis spinning conditions, the spectral resolution for such static samples is still much lower than what is achieved for solution samples. The excess broadening under static conditions is due to a combination of residual dipolar interactions and variations in the bulk magnetic susceptibility. MAS can efficiently average these left-over components of the solid-state line width, and it thus produces NMR spectra that display resolution approaching that of liquid samples.

Since the ^{1}Hresolution is more like that in solution state than solid-state NMR, multidimensional techniques using HRMAS NMR such as HMQC, HMBC, and NOESY can also be conducted on a swelled sample. Three-dimensional

experiments such as NOESY-HSQC can be used in HRMAS. Figure 2.11 shows a pulse sequence for NOESY-HSQC. Overlapping or difficult-to-assign peaks in NOESY can be resolved in NOESY-HSQC because the spectrum is spread in one more dimension.

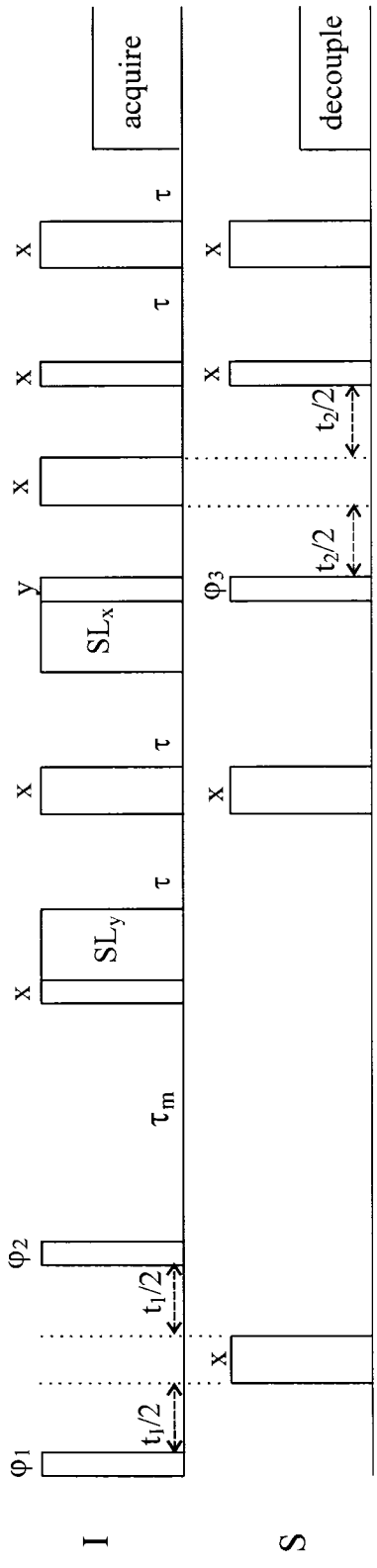

Figure 2.11. Pulse sequence of a 3D NOESY-HSQC experiment. The phase cycling is $\varphi_1 = 2(x), 2(-x)$; $\varphi_2 = 4(x), 4(-x)$; $\varphi_3 = x, -x$; and receiver = $x, -x, -x, x, -x, x, x, -x$. The spin-lock purge pulses (SL) are applied for 1 – 2 ms.

2.2 Introduction to Chromatography

2.2.1 Principles of Chromatography

Chromatography is an analytical technique that resolves a chemical mixture into its components by passing it through a medium that retards each compound to a varying degree; an instrument capable of accomplishing this is called a chromatograph. The retarding system can be a surface adsorbant, such as silica, alumina, cellulose, or charcoal, capable of reversibly adsorbing the compounds. The earliest use of this technique, by the Russian botanist Mikhail Tsvett (c.1903), involved the separation of highly colored compounds, hence the name *chromatography*.

For traditional chromatography, a liquid sample is applied to a narrow cross section or zone of a column, which is filled with a particular packing or support material. A solvent is pumped through the column, sweeping the sample from the inlet to the outlet and through a detector. It is the differential interaction of the various components in the sample with the stationary phase of the packing material and the solvent that effects the separation. This is shown in Figure 2.12, where a mixture of the molecules A and C has been injected into a narrow zone at the inlet of the column. While moving with the solvent (mobile phase), A and C become slightly separated because C shows a greater affinity for the stationary phase and moves more slowly than A. Eventually A elutes, distinct from and followed by C; this separation is the goal of chromatography.

A chromatogram is a two-dimensional plot of molecules eluting from a column; absorbance or some other characteristic property is plotted against elution time or volume, as diagrammed in Figure 2.13 for the molecules shown in the preceding figure.

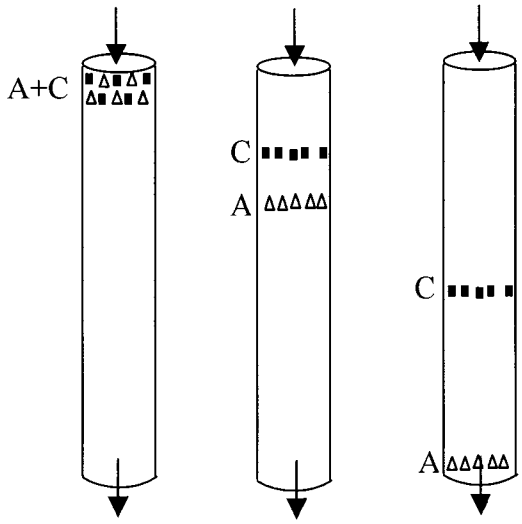

Figure 2.12. Chromatographic process

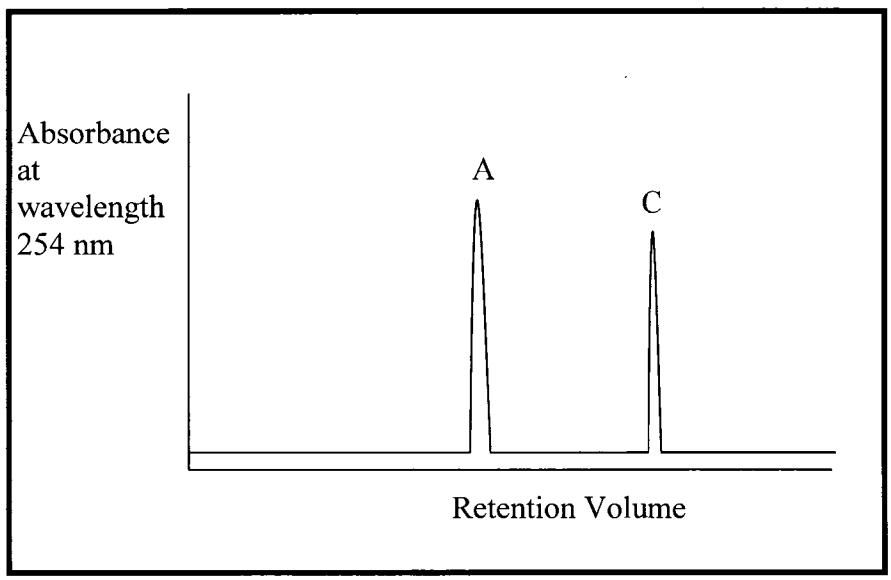

Figure 2.13. Chromatogram of the separation diagrammed in Figure 2.12.

2.2.2 Column Chromatography

In column chromatography the adsorbent is packed into a column and a solution of the mixture is added at the top. An appropriate solvent is passed through the column, thus washing or eluting the compounds down the column. For instance, a polar substance that is adsorbed very tightly to the surface will be retarded efficiently by the column, whereas a nonpolar substance will elute (dissolve in the solvent) very rapidly. By varying the nature of the solid adsorbent and the eluting solvent, even very similar substances can be resolved.

2.2.3 Thin-Layer Chromatography (TLC and HPTLC)

A TLC plate is a sheet of glass, metal, or plastic that is coated with a thin layer of a solid adsorbent (usually silica or alumina). A plate with fine adsorbent particles is referred to as high-performance TLC (HPTLC). A small amount of the mixture to be analyzed is spotted near the bottom of this plate. The TLC plate is then placed in a shallow pool of a solvent in a developing chamber so that only the very bottom of the plate is immersed in the liquid. This liquid, or the eluent, is the mobile phase, which rises slowly up the TLC plate by capillary action.

As the solvent moves past the spot that was applied, an equilibrium is established for each component of the mixture between the molecules adsorbed on the solid and the molecules in solution. In principle, the components will differ in solubility and in the strength of their adsorption to the adsorbent, and some components will be carried farther up the plate than others in a given unit time. When the solvent has reached the top of the plate, the plate is removed from the developing chamber and

dried; then the separated components of the mixture are visualized. If the compounds are colored, visualization is straightforward. Usually the compounds are not colored, so a UV lamp is used to visualize the plates.

2.2.4 High Performance Liquid Chromatography (HPLC) [78]

HPLC is one mode of chromatography, the most widely used analytical technique. HPLC utilizes a liquid mobile phase to separate the components of a mixture. These components (or analytes) are first dissolved in a solvent and then forced to flow through a chromatographic column under high pressure (~ 1000 – 6000 psi). In the column, the mixture is resolved into its components. The degree of resolution is important, and is dependent upon the extent of interaction between the solute components and the stationary phase. The stationary phase is defined as the immobile packing material in the column. The interaction of the solute with mobile and stationary phases can be manipulated through different choices of both solvents and stationary phases. As a result, HPLC has a high degree of versatility not found in other chromatographic systems and has the ability to easily separate a wide variety of chemical mixtures.

There are two types of HPLC classified by the relative polarity of the stationary phase and mobile phase: normal-phase (NP) and reversed-phase (RP) chromatography. In normal-phase chromatography, the stationary bed is strongly polar in nature (e.g., silica gel), and the mobile phase is nonpolar (such as *n*-hexane or tetrahydrofuran). Polar samples are thus retained on the polar surface of the column packing longer than less polar materials. Reversed-phase chromatography is

the inverse: the stationary bed is nonpolar (hydrophobic) in nature, whereas the mobile phase is a polar liquid such as a mixture of water with methanol or acetonitrile. The more nonpolar the material is, the longer it will be retained.

In general, HPLC involves a dynamic adsorption process. Analyte molecules, while moving through the porous packing bead, tend to interact with the surface adsorption sites. Depending on the HPLC mode, different types of adsorption forces may be involved in the retention process. Hydrophobic (non-specific) interactions are the main ones in reversed-phase separations, but dipole-dipole (polar) interactions are dominant in normal-phase mode. All these interactions are competitive. Analyte molecules compete with the eluent molecules for the adsorption sites. Thus, the stronger the analyte interaction with the surface, and the weaker the eluent interaction, the longer the analyte will be retained on the surface.

HPLC separations are based on surface interactions and thus depend on the types of adsorption sites (surface chemistry). Modern HPLC adsorbents are small rigid porous particles with high surface area. The main adsorbent parameters are: particle size (3 to 10μ); particle size distribution (as narrow as possible, usually within 10% of the mean); pore size (70 to 300 Å); surface area (50 to 250 m^2/g); bonding phase density (number of adsorption sites per surface unit, 1 to 5 per 1 nm^2). Depending on the type of the ligand attached to the surface, the adsorbent could be normal phase (-OH, $-NH_2$), or reversed-phase (C8, C18, Phenyl), and even anion (NH_4^+), or cation ($-COO^-$) exchangers. There are many advantages to using smaller particles, but they may not be essential for all separations. The most important advantages are higher resolution, faster analyses, and increased sample load capacity.

A typical stationary phase for NP chromatography is silica, and the mobile phase is hexane (or heptane) that sometimes contains a small amount of isopropanol to increase the polarity of the solvent. The usual application of NP chromatography is a separation of very hydrophobic compounds that are soluble only in nonpolar organic solvents. These compounds do not show strong interaction with the highly polar stationary phase (silica) and can be eluted from the column relatively rapidly (as opposed to their extremely long elution times from an RP column).

Reversed-phase chromatography (RPC) is the most common HPLC mode. It uses hydrophobic packings such as octadecyl- or octylsilane ligands bonded to silica or neutral polymeric beads. The mobile phase is usually water and a water-miscible organic solvent such as methanol or acetonitrile. There are many variations of RPC in which various mobile-phase additives are used to impart a different selectivity. In both NP and RP chromatography, mixtures of solvents can be used either in isocratic (constant composition) or gradient modes. Gradient solvent systems can often improve resolution and throughput.

HPLC instrumentation includes a pump, injector, column, detector and recorder or data system, connected as shown in Figure 2.14. The heart of the system is the column where separation occurs. Since the stationary phase is composed of micrometer size porous particles, a high-pressure pump is required to move the mobile phase through the column. Detectors are also very important in HPLC. There are many types of detectors. Ultraviolet (UV) absorption and wavelength-selective diode array detectors are the most popular ones. UV detectors are very sensitive and non-destructive, but they cannot detect analytes that lack chromophores. Refractive-

Index (RI) detectors and evaporative light scattering detectors (ELSD) are universal detectors. RI detectors are less sensitive than the other detectors and are incompatible with gradient elution, and ELSD detectors require the boiling points of the analytes be higher than those of the eluents. Mass spectroscopy (MS) detectors are widely used today. MS detectors are the most sensitive, have good selectivities, and yield information on molecular structure (see below).

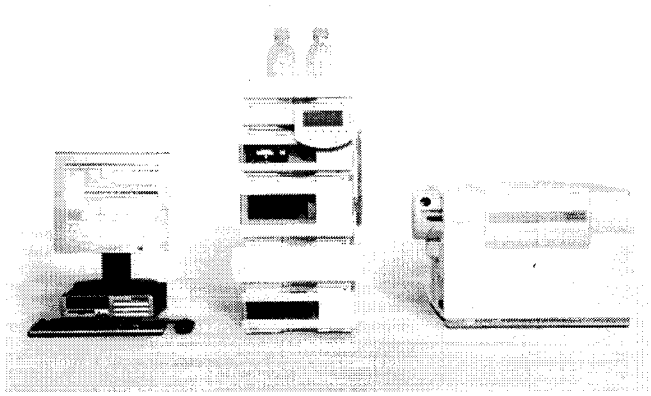

Figure 2.14. Instrumentation of a typical HPLC system (www.agilent.com)

2.2.5 Gel Permeation Chromatography

Gel permeation chromatography (GPC), also known as size exclusion chromatography (SEC), is an accepted technique for characterizing polymers and proteins. It does not rely on chemical differences to effect the separation, but rather it separates polymer molecules on the basis of their size relative to the pores in the packing particles. Its primary use is in measuring molecular weight and molecular weight distributions. The major limitation of conventional GPC using only a concentration detector, such as a refractometer, is that it is unable to distinguish

between the effects of molecular weight and structural differences on molecular size.

The basic principle of SEC separation is that the bigger the molecule, the less likely it is to penetrate into the adsorbent pore space, so, the bigger the molecule the smaller tendency it has to be retained.

2.3 Introduction to Mass Spectroscopy [79]

2.3.1 Basic Principles

Mass spectrometry is an instrumental approach that allows for the mass measurement of molecules. Mass spectrometers use the difference in mass-to-charge ratio (m/e) of ionized atoms or molecules to separate them from each other. Mass spectrometry is therefore useful for size quantitation of atoms or molecules and also for determining chemical and structural information about them. Many molecules also have distinctive fragmentation patterns that provide structural information.

The general operation of a mass spectrometer is: (1) create gas-phase ions; (2) separate the ions in space or time based on their mass-to-charge ratio; (3) measure the quantity of ions of each mass-to-charge ratio (Figure 2.15).

The ion separation power of a mass spectrometer is described by its resolution, which is defined as:

$$R = m / \Delta m$$

where m is the ion mass and Δm is the difference in mass between two resolvable peaks in a mass spectrum. For example, a mass spectrometer with a resolution of 1000 can resolve an ion with m/e of 100.0 from an ion with m/e of 100.1.

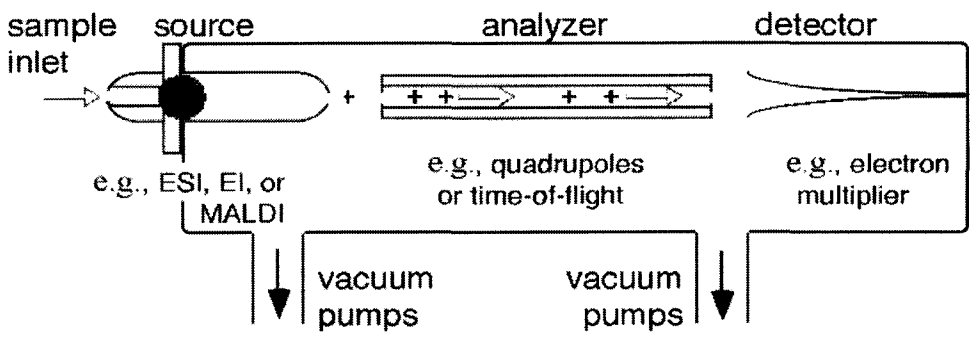

Figure 2.15. Components of a mass spectrometer. (www.masspec.scripps.edu).

Mass spectrometers have become pivotal for a wide range of applications in the analysis of inorganic, organic, and bioorganic chemicals. Examples include dating of geologic samples, drug testing and drug discovery, process monitoring in the petroleum, chemical, and pharmaceutical industries, surface analysis and the structural identification of unknowns. Further, mass spectrometry is being continually improved and has recently made significant advances in its application to molecular biology, where it is now possible to analyze proteins, DNA, and even viruses.

2.3.2 Ionization Methods

Ionization is the act of placing a charge on a neutral molecule. There are many ionization methods applicable to different analytes depending on their different properties.

Electron Ionization (EI) plays an important role in the routine analysis of small molecules (Figure 2.16). The electron ionization technique is straightforward. The sample must be delivered as a gas which is usually accomplished by heating the sample to vaporize it off of the probe. Once in the gas phase, the compound passes into an electron ionization region where it interacts with a beam of electrons of nearly homogeneous energy (70 electron volts), typically causing electron ejection and some degree of fragmentation.

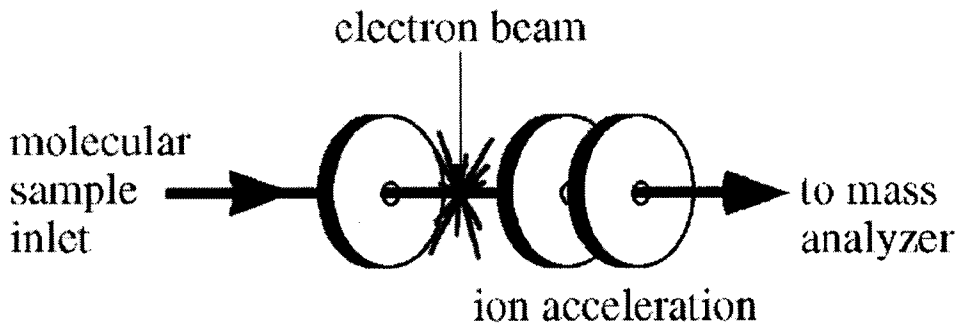

Figure 2.16. Electron ionization spectrometry. (www.masspec.scripps.edu).

Electron ionization is most useful for compounds below a molecular weight of 400 daltons, since larger molecules tend to degrade thermally during vaporization. Whereas electron ionization is one of the most widely used methods of ionization in mass spectrometry, the principal problems associated with it include excessive fragmentation in the ionization source, involatility of large molecules, and thermal decomposition during vaporization. Electron ionization is used principally as a detector for gas chromatography (GC/MS) in a wide variety of applications including synthetic organic chemistry, hydrocarbon analysis, detection of pharmaceutical compounds and drugs of abuse, and environmental studies such as water testing.

Chemical Ionization (CI) is used for samples similar to those analyzed by electron ionization, but it is especially valuable for enhancement of the abundance of the molecular ion. Chemical ionization uses ion-molecule reactions in the gas phase to produce ions from the sample molecule. The chemical ionization process is initiated with a reagent gas such as methane, isobutane, or ammonia, which is initially ionized by electron ionization. A high gas pressure in the ionization source results in the propagation of ion-molecule reactions between the reagent gas ions and reagent gas neutrals. Some of these ions can then react with the analyte molecules to produce ions.

Electrospray Ionization (ESI) generates ions directly from solution (usually an aqueous or aqueous/organic solvent system) by creating a fine spray of highly charged droplets in the presence of a strong electric field (typically 3.5 kV). As the droplet decreases in size, the electric charge density on its surface increases. The mutual repulsion between like charges on this surface becomes so great that it exceeds the forces of surface tension, and ions begin to leave the droplet through what is known as a "Taylor cone" (Figure 2.17). The ions are then directed electrostatically into the mass analyzer. Vaporization of these charged droplets results in the production of singly or multiply-charged gaseous ions. The number of charges retained by an analyte depends on such factors as the composition and pH of the electrosprayed solvent as well as the chemical nature of the sample. For small molecules (< 2000 daltons) ESI typically generates singly or doubly charged ions, whereas for large molecules (> 2000 daltons) the ESI process typically gives rise to a series of multiply-charged species. Because mass spectrometers measure the mass-

to-charge (m/z) ratio, the resultant ESI mass spectrum contains multiple peaks corresponding to the different charged states.

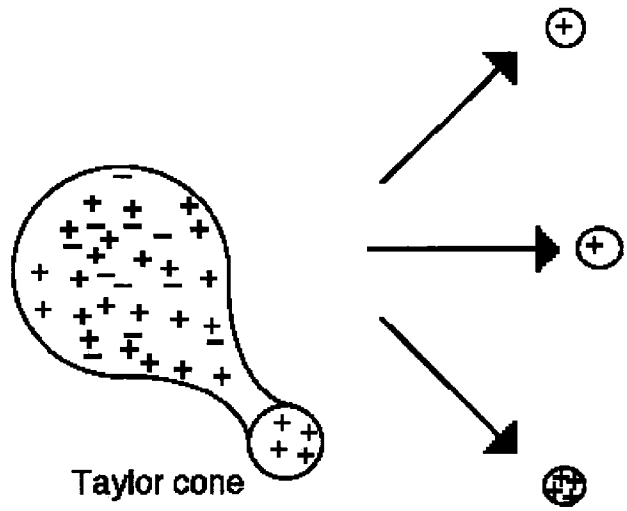

Figure 2.17. Electrospray ionization and the formation of a Taylor cone. (www.masspec.scripps.edu).

ESI allows for very sensitive analysis of small, large and labile molecules such as peptides, proteins, organometallics, oligosaccharides, and polymers. Another advantage of ESI-MS is that because ions are formed directly from solution, it can be used as a convenient mass detector for liquid chromatography (LC). ESI has made liquid chromatography-mass spectrometry (LC-MS) routine, adding a new dimension to the capabilities of liquid chromatography characterization. In fact, using ESI-MS as a detector for liquid chromatography was one of its first obvious applications.

Atmospheric Pressure Chemical Ionization (APCI) is similar to electrospray ionization. Liquid effluent is introduced directly into the atmospheric pressure chemical ionization source. The APCI source contains a heated vaporizer, which facilitates rapid desolvation/vaporization of the droplets. Vaporized sample

molecules are carried through an ion-molecule reaction region at atmospheric pressure. The ionization occurs through a corona discharge, creating reagent ions from the solvent vapor (Figure 2.18). Chemical ionization of sample molecules is very efficient at atmospheric pressure due to their high collision frequency. Proton transfer (protonation MH^+ reactions) occurs in the positive mode, and either electron transfer or proton transfer (proton loss, $[M-H]^-$) in the negative mode. The moderating influence of the solvent clusters on the reagent ions, and of the high gas pressure, reduces fragmentation during ionization and results in primarily molecular ions. APCI is widely used in the pharmaceutical industry to analyze relatively nonpolar, semi-volatile samples of less than 1200 daltons, and it is an especially good ionization source for liquid chromatography.

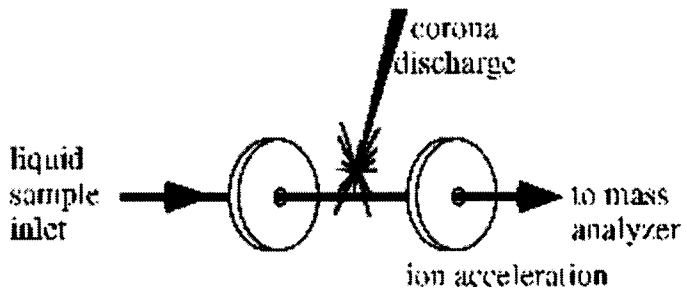

Figure 2.18. Atmospheric Pressure Chemical Ionization (APCI) Mass Spectrometry. (www.masspec.scripps.edu).

Matrix-Assisted Laser Desorption Ionization mass spectrometry (MALDI-MS), first introduced in 1988 by Tanaka and independently by Hillenkamp and Karas, has become a widespread analytical tool for peptides, proteins and most other biomolecules (oligonucleotides, carbohydrates, natural products, and lipids). The efficient and directed energy transfer during a matrix-assisted laser-induced

desorption event provides high ion yields of the intact analyte and allows for the measurement of compounds with high accuracy and sub-picomole sensitivity. MALDI provides for the nondestructive vaporization and ionization of both large and small biomolecules.

Fast Atom Bombardment (FAB) technique is a soft ionization method that typically requires the use of a direct insertion probe for sample introduction and a high-energy beam of xenon atoms or cesium ions to sputter the sample and matrix from the probe's surface.

2.3.3 Ion Analysis[79,80]

Immediately following ionization, gas phase ions enter a region of the mass spectrometer known as the mass analyzer. The mass analyzer is used to separate ions within a selected range of mass-to-charge (m/z) ratios. The analyzer is an important part of the instrument because of the role it plays in the instrument's accuracy and mass range. Ions are typically separated by magnetic fields, electric fields, or by measuring the time it takes an ion to travel a fixed distance.

Quadrupole analyzers are four precisely parallel rods with a direct current (DC) voltage and a superimposed radio-frequency (RF) potential. Quadrupoles have three primary advantages. First, they are tolerant of relatively poor vacuums (~5 x 10^{-5} torr), which make them well-suited to electrospray ionization since the ions are produced under atmospheric pressure conditions. Secondly, quadrupoles are now capable of routinely analyzing up to a m/z of 3000, which is useful because electrospray ionization of proteins and other biomolecules commonly produces a

charge distribution below m/z 3000. Finally, the relatively low cost of quadrupole mass spectrometers makes them attractive as electrospray analyzers.

The physics behind an ion trap analyzer is very similar to a quadrupole analyzer. In an ion trap the ions are trapped in a radio frequency quadrupole field. One method of using an ion trap for mass spectrometry is to generate ions externally with electrospray and then inject them into the trapping volume. The ions are then ejected and detected as the radio frequency field is scanned. Further, it is also possible to isolate one ion species by ejecting all others from the trap. The isolated ions can be fragmented subsequently by collisional activation and the fragments detected to generate a fragmentation spectrum. The primary advantage of quadrupole ion traps is that multiple collision-induced dissociation experiments can be performed without having multiple analyzers. Other important advantages include their compact size and the ability to trap and accumulate ions to increase the signal-to-noise ratio of a measurement.

A time-of-flight (TOF) analyzer is one of the simplest mass analyzing devices and is commonly used with MALDI. Time-of-flight analysis is based on accelerating a set of ions to a detector with the same amount of energy. Because the ions have the same energy, yet a different mass, the ions reach the detector at different times. The smaller ions reach the detector first because of their greater velocity and the larger ions take longer, thus the analyzer is called time-of-flight and the mass is determined at the ions' time of arrival. A TOF analyzer can analyze very high mass ions and has very high sensitivity.

2.3.4 Ion detection

Once an ion passes through a mass analyzer, it will be detected by an ion detector. The detector allows a mass spectrometer to generate a signal current from incident ions by generating secondary electrons, which are further amplified. Alternatively, some detectors operate by inducing a current generated by a moving charge.

Chapter 3. Materials and Methods

3.1 Sample Purification and Preparation

3.1.1 Lime Cutin Polymers and Oligomers

Isolation of Lime Cutin. Limes were purchased locally and washed with distilled water. Skins of 300 limes were peeled into quarters (no smaller) with plastic peeling tools and soaked in distilled water for 30 minutes. Then the skins were shaken at 31°C for 2 days in 3.05 mg/mL *Aspergillus niger* pectinase (31 mg protein/mL, 11.8 units/mg, Sigma P-9179, St. Louis, MO) in a 50 mM pH 4 sodium acetate buffer. Sufficient enzyme solution was added to cover the lime skins, and a stirring bar was added for more mechanical agitation. About 250 mL of solution was needed for 8-10 quartered limes. Parafilm was used to seal the lids of the jars. The shaking speed was set to 150 rpm. Any remaining intact skins were retreated for 1-2 days. The solid "mushy" material was collected in a wire-mesh strainer and cleaned by soaking in distilled water, then collected with a strainer until the washing water was clear. The sheets of cuticle were dried in a SpeedVac centrifugal evaporator for 2 days until their mass was constant.

In order to remove extraneous cellulose (in the cell wall), the dried sheets were treated with 0.4 mg/mL cellulase (activity 64,000 units/g, ICN 150583, Aurora, OH) in 50 mM pH 5.0 acetate buffer at 44 °C for 6 days. This procedure was done in an incubator shaker at 175 rpm, using a stirring bar to enhance mechanical agitation. Upon completion of the treatment, the solid cuticle was collected in a strainer and washed with distilled water as described above.

To remove any remaining pectin, the cuticle was treated with 4.58 mg/mL pectinase in 50 mM pH 4.0 acetate buffer at 31 °C for 16 hours. As described above, the cuticles were shaken and stirred in an incubator at 150 rpm. When the treatment was complete, the solid was collected and dried. Then the cuticles were treated with 0.3 mg/mL hemicellulase (13.8 units/mg, solid powder, Sigma H-7649) in 50 mM pH 5.0 buffer at 45 °C for 8 days with shaking at 175 rpm. The cuticles were dewaxed using successive extractions with three solvents of increasing polarity. Each extraction was run for 2 days; the solvents were methylene chloride (Fisher D-37-20, Pittsburgh, PA), tetrahydrofuran (Fisher T-397-20), and methanol (Fisher AA-34-20) in sequence. The dewaxed material (cutin) was dried under reduced pressure at 80 °C, yielding five grams of cutin in typical preparations. The dry cutin was ground with a Freezer Mill in liquid nitrogen for 8 minutes. The cutin powder was used for NMR analysis or for depolymerization reactions.

Depolymerization of cutin with HF. In order to produce oligomeric fragments, 502 mg of powdered lime fruit cutin was reacted for 0.5 h with anhydrous HF at 0 °C and quenched with diethyl ether in liquid nitrogen (Mort, 1983). After evaporating the ether-HF mixture (120 mg) to dryness, the reaction products were extracted to yield 22 mg of water solubles and 95 mg of chloroform solubles. The unreacted solid residue was reserved for analysis by magic-angle spinning NMR. The chloroform fraction was dried and then extracted with acetonitrile.

Depolymerization of cutin with the traditional KOH method. In order to produce lime cutin oligomers with KOH, 500 mg of cutin was added to 100 mL of 1.5 M KOH solution in methanol. The mixture was stirred at room temperature overnight.

Then the reaction mixture was acidified to pH 5 with concentrated HCl and filtered. The unreacted residue was washed with water to remove the salt and then dried in air for magic-angle spinning NMR. The filtrate was also dried in air and the resulting product mixture was extracted with 30 mL of chloroform/methanol (1:1 v/v) mixture solvent five times until only white salt remained. The extracts were combined and dried under vacuum.

Depolymerization of cutin with a modified KOH method. As shown in Figure 3.1, cutin and KOH were added into a glass extraction thimble. The methanol reaction solvent was added into the 2-neck flask at the bottom of the device. When the condensed methanol drops into the thimble, depolymerization occurs in the thimble. To prevent oligomers from undergoing further depolymerization, the methanol solution is cycled back into the flask once the side chamber is filled. The reaction is quenched by adding HCl from the cylindrical addition funnel to neutralize the solution in the flask. The recycling time is controlled by adjusting the condensation rate of methanol, i.e. by controlling the heater's voltage. After several recycle periods (20 minutes for each cycle), the solution was neutralized and extracted several times with chloroform. The organic layers were combined and washed with distilled water. Then the organic layer was dried over sodium sulfate and filtered. Products were obtained after rotoevaporation of the solvent.

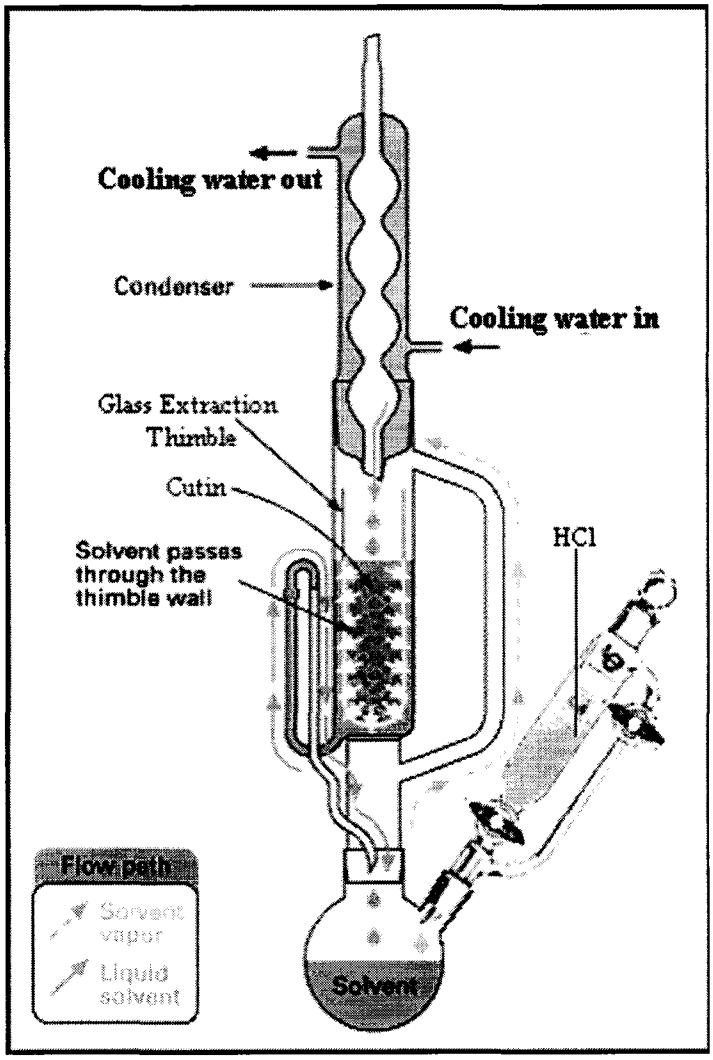

Figure 3.1. Modified Soxhlet extractor used for depolymerization of cutin.

3.1.2 Potato Suberin Polymers

Biosynthesis of the suberin plant polyester occurs following the mechanical wounding of potato tubers. The wounds may be induced by slicing potatoes into disks and allowing the injured tissue to synthesize the protective polymer for a period of 0-14 days. Isotopic labels (^{13}C) may be introduced into suberin by carrying out the wound-healing process in the presence of labeled precursors.

The Russet Burbank (Idaho) variety of potatoes was purchased from a local supermarket. Depending on the geometry of the potato disks used, approximately 200 g of peeled potatoes should yield about 2 g of suberized potato tissue.

Plastic growth chambers were soaked with 25% (v/v) Chlorox bleach. All peelers, knives, forceps, gloves, pipets and filter paper were autoclaved. The potatoes were washed and scrubbed with a brush to remove surface dirt and then soaked in 25% (v/v) bleach solution for 5-10 minutes to sterilize them. Double-processed tissue culture water (Sigma W-3500) was used to rinse the potatoes briefly. The potatoes were then peeled and sliced into disks 4-5 mm thick, about 20 by 30 mm in size. The potato disks were placed on autoclaved filter papers, which were placed in turn on plastic-covered wire mesh in closed growth chamber(s) to allow for air circulation on all sides. The atmosphere was kept humid by placing sterile water in weighing boats underneath the mesh. The potato disks were left to suberize at 25 $\pm$ 0.1 °C in a large refrigerated incubator for 7 days. Some water droplets were observed on the sides of the growth chambers, and the surface of the potatoes darkened noticeably after several days, as expected. No mold was evident.

When the suberization period was complete, the potato disks were removed from the growth chamber. The disks were totally covered by a layer of brown suberized cell walls, which was removed using a small kitchen knife. The suberized cell walls were washed and cleaned thoroughly with running distilled water and a rough (wet) weight of the product was recorded.

To remove extraneous cellulose from unsuberized cell walls, the suberized potatoes were treated with a 2.5% (w/v) solution of *Aspergillus niger* cellulase (ICN 150583, activity 110,000 units/g) at 37° C for 2 days and at 44° C for another 2 days in an incubator shaking at 150 rpm. Upon completion, the solid suberized potato was collected using vacuum filtration and washed with water (100 mL x 3 times). The suberized potato tissues were dried by SpeedVac, and their dry mass was recorded after completion of the cellulase treatment(s).

To remove extraneous pectin, the suberized potato tissues were treated with 1.0 mg/mL *Aspergillus niger* pectinase (Sigma P-9179 @ 31 mg/mL and 11.8 units/mg) at 28 °C for 8 hours and at 31 °C for another 16 hours in an incubator shaking at 150 rpm.

After the enzymatic treatments, the suberized potato tissues were dried in the SpeedVac, just until they were visibly dry. The dry suberized potato tissues were extracted with methylene chloride and methanol-methylene chloride (1:1 v/v) in a Soxhlet extractor for 2 days each. It was important to break up the sample into flakes rather than clumps, so that as much surface area as possible was exposed to the solvents. The suberized potato tissues were air dried in the thimble and then completely dried in the SpeedVac until the mass was constant.

3.1.3 Fungal Melanin

The following preparation was carried out by collaborators at Albert Einstein College of Medicine. *Crypotcoccus neoformans* was grown in a defined minimal medium (15.0 mM glucose, 10.0 mM $MgSO_4$, 29.4 mM KH_2PO_4, 13.0 mM glycine, and 3.0 μM vitamin B_1; pH 5.5) in the presence of 1.0 mM L-dopamine (L-dopa) (Sigma Chemical Co.) for 21 days at 30°C in a rotary shaker at 150 rpm. For isotopically enriched samples, 2,3-$^{13}C_2$(97%),4-^{18}OH(95%)-L-dopa and 1-^{13}C-D-mannose were obtained from Cambridge Isotope Laboratories (Andover, MA). Melanized cells were collected by centrifugation at 3000 rpm for 30 min, washed with phosphate-buffered saline (PBS), and suspended in 1.0 M sorbitol–0.1 M sodium citrate (pH 5.5). Cell wall–lysing enzymes (Sigma Chemical Co.), which contain protease, cellulase and chitinase activities, were added at 10 mg/ml and the suspension was incubated overnight at 30° C to generate protoplasts. The protoplasts were collected by centrifugation, washed with PBS, and incubated in 4.0 M guanidine thiocyanate (denaturant) for 12 h at room temperature with frequent vortexing. A dark particulate material consisting of melanin and cellular debris was collected by centrifugation and washed with PBS. The particulate was then treated with 1.0 mg/ml Proteinase K (Roche Molecular Biochemicals, Indianapolis, IN) (reaction buffer was 10.0 mM Tris, 1.0 mM $CaCl_2$, and 0.5% SDS; pH 7.8) for 4 h at 65° C, washed with PBS, and extracted three times with chloroform. After washing with PBS, the particulate was boiled in 6.0 M HCl for 1 h to hydrolyze cellular contaminants that may still be associated with the melanin. Melanin

particles were collected by centrifugation, washed extensively with PBS, and dialyzed against distilled water for 10 days.

3.2 Oligomer and Monomer Separation and Purification

3.2.1 Column chromatography

Depolymerized cutin and suberin products were prepurified with column chromatography using Silica gel 60 (0.04mm - 0.063 mm). Hexanes, acetone, and methanol were used as eluents of increasing polarity. For some prepurifications, step gradients were employed to get better results. All the solvents were purchased from Fisher Scientific.

3.2.2 Thin Layer Chromatography and Detection

Silica gel 60 plates for thin layer chromatography were purchased from Merck (Gibbstown, NJ). The plates were visualized by spraying with phosphomolybdic acid and heating. Some products or prepurified products were separated and (further) purified by HPTLC. The samples were applied as a line on 10 x 20 cm HPTLC plates, and then placed in a developing chamber with appropriate solvents. Small slices of the plates were cut off and visualized with phosphomolybdic acid, and the rest of the plates were separated into different strips according to the visualized slices. Each strip was scrubbed from the plates and soaked in appropriate solvents. The mixtures were filtered, and the filtrates were rotoevaporated or air dried.

3.2.3 HPLC

Further purification of fractions from TLC or HPTLC separations with higher ratios NMR peak at 4.01 ppm to NMR peaks at 2.28 ppm or molecular ions greater than 700 in MS was achieved using normal-phase (NP) and reversed-phase (RP) HPLC conducted on a Hewlett-Packard Model 1100 instrument equipped with a quaternary solvent delivery system, UV detector, diode array detector, and evaporative light scattering detector (ELSD). Separations were performed with 5 μm analytical and semi-preparative C18 columns, using ELSD and UV detection at 210 nm, a 1-ml/min flow rate, and gradient elution. Isolated compounds were checked for purity by re-injection in two solvent systems. The solvents for NP HPLC were hexanes, acetone, and isopropanol. The solvents for RP HPLC were acetonitrile, methanol, and water. All HPLC grade solvents were purchased from Fisher Scientific. For some separations with ELSD, a splitter was used with a flow rate of 1.4 mL/min; one-seventh of the flow was directed into the ELSD, and six-sevenths of the flow was collected.

Representative ELSD conditions for RP HPLC included a drift tube temperature of 75° C, nitrogen gas flow rate of 1.80 standard liters per minute (SLPM), nitrogen gas pressure of 11.6 psi, and attenuation of 1/2 with a solvent flow rate of 1.0 mL/min for gradient elution with acetonitrile and water (80% - 100 % CH_3CN). Representative ELSD conditions for NP HPLC included a drift tube temperature of 55° C, nitrogen gas flow rate of 1.80 SLPM, nitrogen gas pressure of 11.0 psi, and attenuation of 1/2 with a solvent flow rate of 1.0 mL/min for gradient eluention with acetone and hexanes (7% - 100 % acetone).

3.3 NMR

3.3.1 Solution-State NMR Characterization of Oligomer and Polymer Materials

NMR spectra were acquired on a Varian ^{UNITY}INOVA spectrometer operating at ^{1}H and ^{13}C frequencies of 599.95 and 150.87 MHz, respectively. Soluble samples were dissolved in $CDCl_3$ or CD_3OD to provide a field-frequency lock signal and $CDCl_3$ containing 1% tetramethylsilane (TMS (Aldrich)) to provide an internal chemical shift standard, respectively. One-dimensional ^{1}H spectra were acquired using Varian HCN and nanoprobes. Typical experimental conditions included 16 repetitions, 2.0 s between successive acquisitions, 26,240 time-domain points, and a spectral width of 7200 Hz. Data processing and ^{1}H peak integration were done using VNMR software. ^{13}C chemical shift predictions were made using database software from Advanced Chemistry Development (Toronto, Canada).

Several two-dimensional NMR experiments were used to establish through-bond connectivities within and between monomer units of the oligomer structures. ^{1}H-^{1}H total correlation spectroscopy ('clean' TOCSY)[81] used a spin-lock field of 6.25 kHz and a mixing period of 70 ms in order to allow magnetization transfer throughout each scalar-coupled spin system. Heteronuclear multiple quantum coherence (^{13}C HMQC) spectroscopy[82] was used to identify bonded proton-carbon pairs using a polarization transfer time corresponding to $^{1}J_{CH}$ = 140 Hz. Heteronuclear multiple bond correlation (^{13}C HMBC) spectroscopy[83] was employed to delineate long-range proton-carbon interations, using a polarization transfer time corresponding to $^{3}J_{CH}$ = 10 Hz. In proton-detected HMQC experiments, the GARP sequence[84] was used for

^{13}C decoupling, and pulsed field gradients[85] were used for coherence selection and to minimize spectral artifacts. The HMQC data were typically acquired with spectral widths of 7200 Hz for ^{1}H and 27,150 Hz for ^{13}C, a relaxation delay of 1.0 s between transients, and an array of 2 K x 256 points, zero-filled to 2 K x 1 K points.

3.3.2 Solid-State NMR Characterization of Intact Materials and Residues

The dry solid samples were run on a Varian UNITY*plus* spectrometer operating at a ^{1}H frequency of 300.001 MHz. The experiments were performed on 30-mg samples in a Doty 5-mm XC5 probe spinning at 8.000 ± 0.005 kHz. Spectra were obtained at room temperature. ^{13}C chemical shifts were referenced to hexamethylbenzene (HMB).

3.3.3 High-Resolution Magic-Angle Spinning NMR

MAS ^{1}H spectra of swelled samples were acquired either at 600 MHz (as described above) or on a Bruker 750 MHz wide bore spectrometer operating at a ^{1}H frequency of 750.225 MHz (NY Structural Biology Center, New York, NY). The former experiments were performed with a 4-mm Varian inverse-detection HX nanoprobe equipped with pulsed field gradients, using 1-2 mg of solid sample and magic-angle spinning typically regulated at 2.200 ± 0.001 kHz. The latter experiments were run on a 4-mm HRMAS probe in a 12 μL partially drilled rotor, using about 1 mg of solid sample with about 10 mg of DMSO. The magic-angle spinning speeds were 5.000 ± 0.001 kHz, and the temperature was 50° C.

3.4 Mass Spectrometry

Mass spectral data was acquired on an Agilent Technologies 1100 Series LC/MSD model G1946D instrument using electrospray ionization (Hunter College, CUNY, New York, NY). Ionization was carried out with a drying gas temperature of 175° C, a nebulizer pressure of 40 psi, and a flow rate of 13 L/min. The scanned mass range was between 200 and 1500 amu, with fragmentor values of 250 volts, varying from 60 volts at 50 amu to 125 volts at 1800 amu. The capillary for electrospray experiments was set to 3500 volts. Samples were introduced into the mass spectrometer in a 1:1 mixture of water and acetonitrile containing 0.1% acetic acid and 50 μM ammonium acetate. Data were processed using Agilent Chemstation software.

Chapter 4. Results and Discussion

4.1 Results for Lime Cutin

4.1.1 Solid State ^{13}C NMR

CPMAS solid-state ^{13}C NMR was first used to test the purity of lime cutin prepared by the method described in Chapter 3 (Figure 4.1) [36]. Fairly intense peaks around 30 ppm (assigned to aliphatic methylene groups) are considered to signify reasonable purity if the characteristic cellulose and pectin peaks around 60 - 100 ppm (which should be removed from the material after a series of enzymatic treatments) are much smaller in magnitude.

$T_{1\rho}$ is the spin relaxation time in the rotating reference frame. It is sensitive to much lower frequency motions (~ 50 kHz) than the spin-lattice relaxation time T_1 (~ 75 MHz). The experimental techniques used to obtain the $T_{1\rho}$ relaxation time rely on forced transitory precession or a spin locking pulse. Carbon-13 and proton $T_{1\rho}$ measurements are extremely important because they are sensitive to motions in the mid-kilohertz regime and are thus closely related at least in frequency to mechanical relaxation. For instance, $T_{1\rho}(H)$ can be measured by analyzing the CPMAS ^{13}C signal amplitudes (I) at different contact times. The negative inverse of the slope of a plot of ln(I) vs T_{cp} is $T_{1\rho}(H)$. In our experiment, the plot and results are shown in Figure 4.2 and Table 4.1, respectively. The optimum CP time (when the signal is the strongest) is 800 μs for lime cutin. $T_{1\rho}(H)$ for the carbon at 72 ppm is ~ 9 ms in this preliminary experiment.

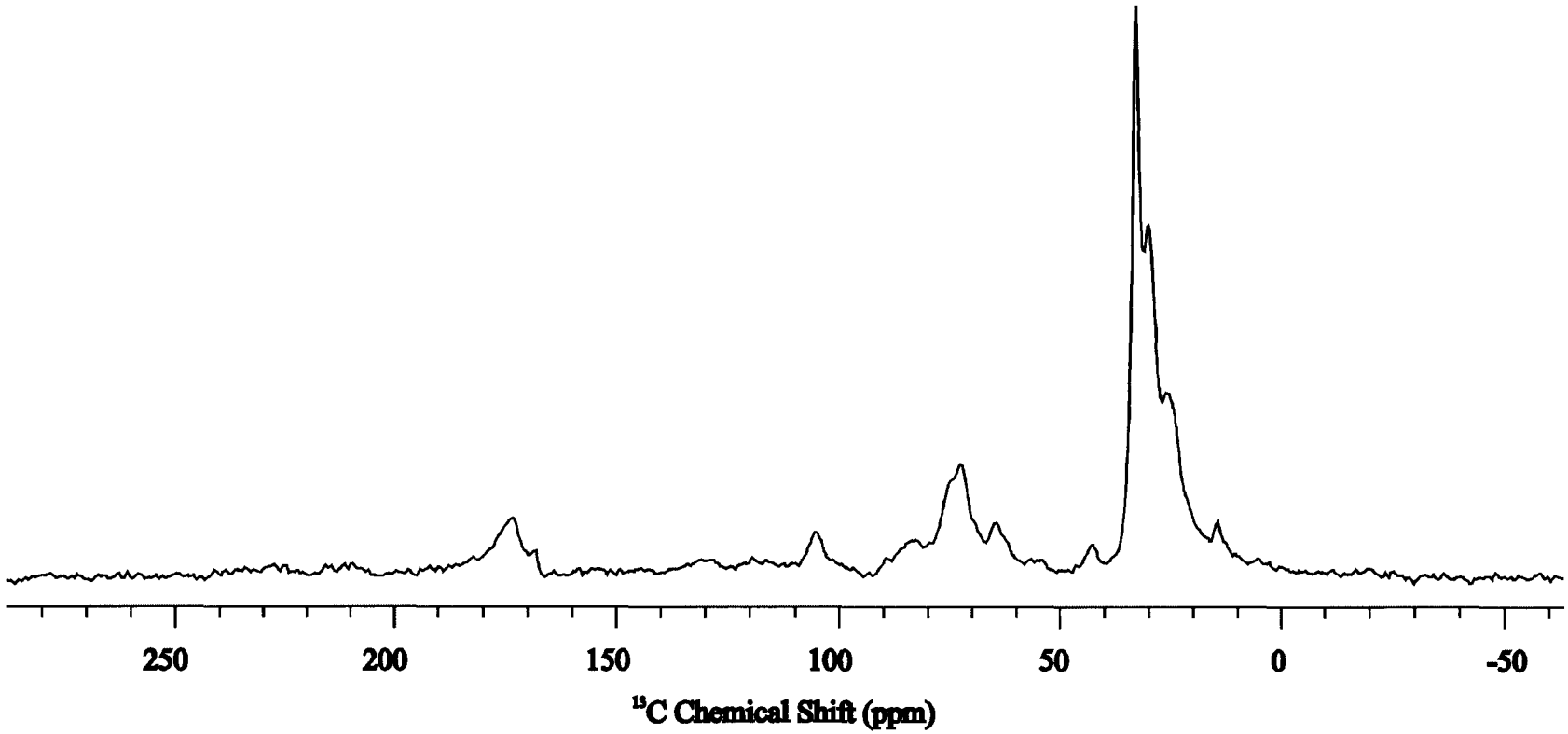

Figure 4.1. Carbon spectrum of lime fruit cutin acquired on a 300 MHz spectrometer with 4000Hz magic-angle spinning. The *y*-axis designates signal intensity (arbitrary units).

Table 4.1. The effect of CP time on the peak intensities of lime cutin

CP time (μs)	200	400	800	1600	3200	6400	12800
Inten. (72ppm)	82.6	88.8	96.3	96.6	85.9	61.7	29.9
Inten. (61ppm)	33.7	35.9	37.9	35.4	33.0	21.7	12.0

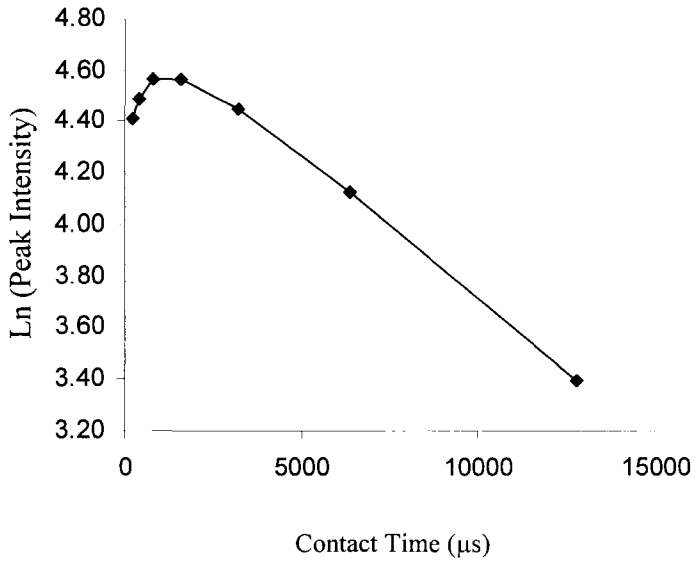

Figure 4.2. Plot of ln(Intensity of peaks) vs contact time.

Separation of protonated carbons from nonprotonated carbons: The standard CPMAS experiment is not well suited to selective decoupling, off-resonance decoupling, or other techniques that distinguish between different carbon types. To do this we have to modify the pulse sequences of the standard CPMAS experiments. A time delay is inserted between the contact time and the acquisition. During this delay time, the proton field is turned off. All carbon spins will dephase under the influence of the proton dipolar field, but those with attached protons will dephase more quickly than those without protons. After a relatively short time (~ 50 μs), the proton field is reapplied to decouple the heteronuclear dipolar interactions during

the acquisition of the carbon free-induction decay, which will now originate from only the nonprotonated carbons which were not completely dephased during the delay time.[76] Subtraction of the delayed-decoupling spectrum from the standard CPMAS spectrum yields the spectrum of the carbons with protons, assuming that signal intensities from nonprotonated carbons are invariant. Figure 4.3 shows the disappearance of the protonated carbons (box 1) after a 40 μs delay before acquisition. Signals from nonprotonated carbons (box 2) remain. The residual signals of CH_2's (box 3) are also expected in this kind of experiment, because molecular motion makes them dephase slowly [86].

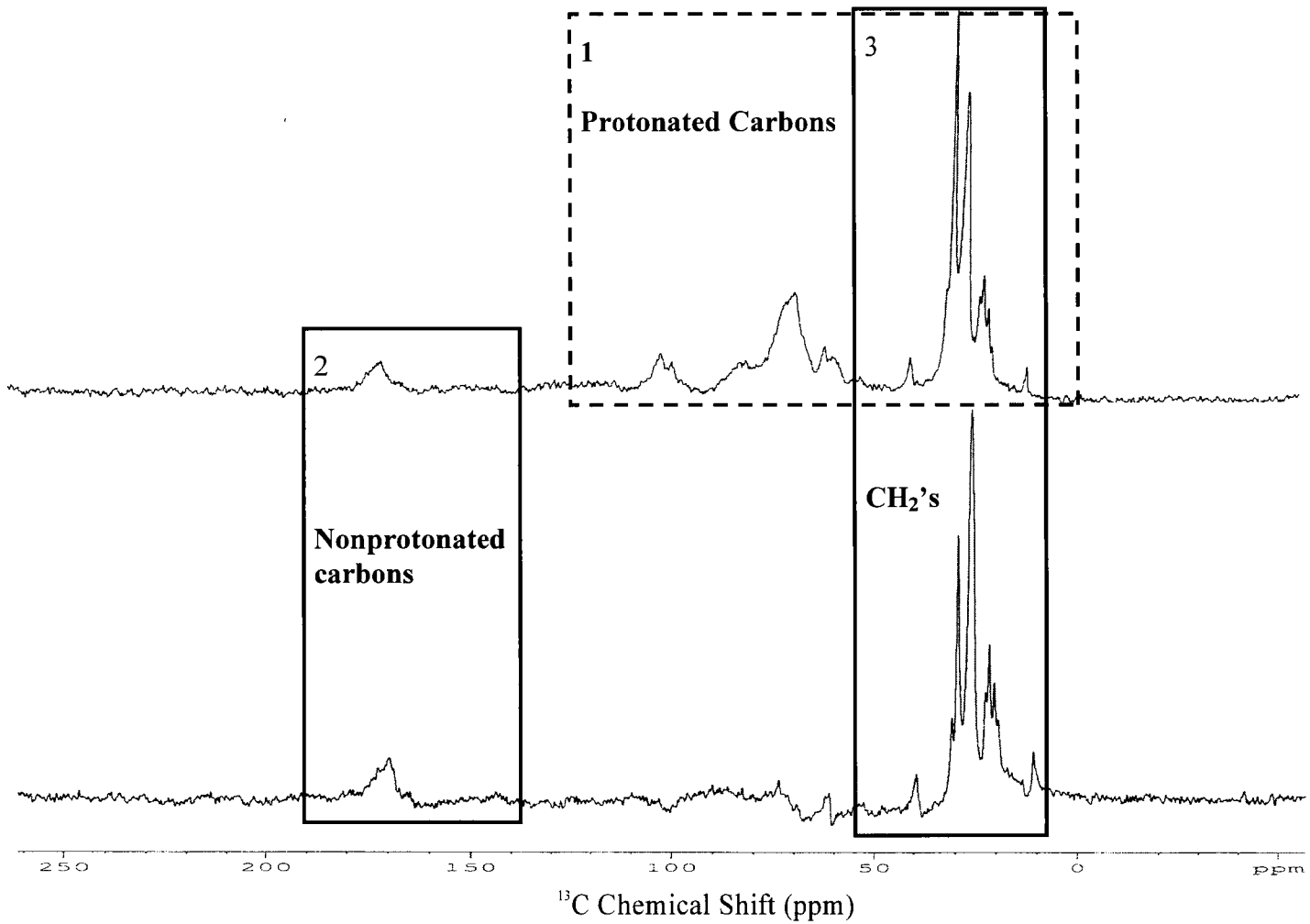

Figure 4.3. CPMAS NMR spectra of lime cutin obtained on a 750 MHz spectrometer (NY Structural Biology Center) at a spinning rate of 10 kHz, line broadening = 50 Hz. Top spectrum: standard CPMAS; bottom spectrum: 40 μs delay between CP and acquisition. Limited signal-to-noise ratio obscures signals from the aromatic carbons.

4.1.2 Degradation Products from Lime Cutin

A modified Soxhlet extractor was used to generate products from KOH depolymerization after a short time (2 hours). Using traditional KOH depolymerization,[31] the components among the soluble products are almost all monomers, which give cutin composition but reveal no information on the polymer's architecture. A reasonable explanation for the predominance of monomeric products is that an oligomer will be depolymerized faster once it is cleaved from the insoluble material, because of its good solubility and greater chance of meeting a reagent molecule. Reducing the depolymerization time may be one solution, but this will result in a far lower yield of the products because of insufficient reaction time. The modified depolymerization method (see Section 3.1.1) is designed to resolve this dilemma.

The bottom spectrum in Figure 4.4 shows a ^{1}H NMR spectrum of one of the mixtures produced with the modified depolymerization method. The solvent recycling time was 15 minutes, and the total reaction time was 2 hours. The ratio of protons at 4.03 ppm (box 1 of Figure 4.4), which is assigned to the methylene group connected to the oxygen of the ester bond, to protons in the region of 1.2 ppm ~ 1.6 ppm (box 2 of Figure 4.4), which are assigned to bulk methylenes, is 1:20 in the mixture as compared with 1:28 in a purified trimer. The peak at 4.03 ppm is a key diagnostic peak for ester linkages of a primary alcohol, whereas the counterpart in a free primary alcohol has a chemical shift of about 3.6 ppm. The chemical shifts of bulk methylene groups remain almost unchanged in ester and alcohol. The ratio of intensities of the peak at 4.03ppm to the peak at 2.28 ppm represents the relative

abundance of CH_2O groups in the sample: the greater the ratio, the more -CH_2O- as compared with other molecular moieties in the sample. Thus, the proportion of oligomers is higher in the mixture. Considering the fact that the mixture may also contain a lot of monomers, this trend in integrals suggests that the new procedure produces oligomers bigger than trimers, which are the biggest oligomers obtained from KOH treatment with the standard setup. One tetramer was separated and identified from products generated by the new procedure (see Section 4.1.2.4).

Mass spectrometry and gel permeation chromatography evidence for the formation of larger oligomers is shown in Figures 4.5 and 4.6, respectively.

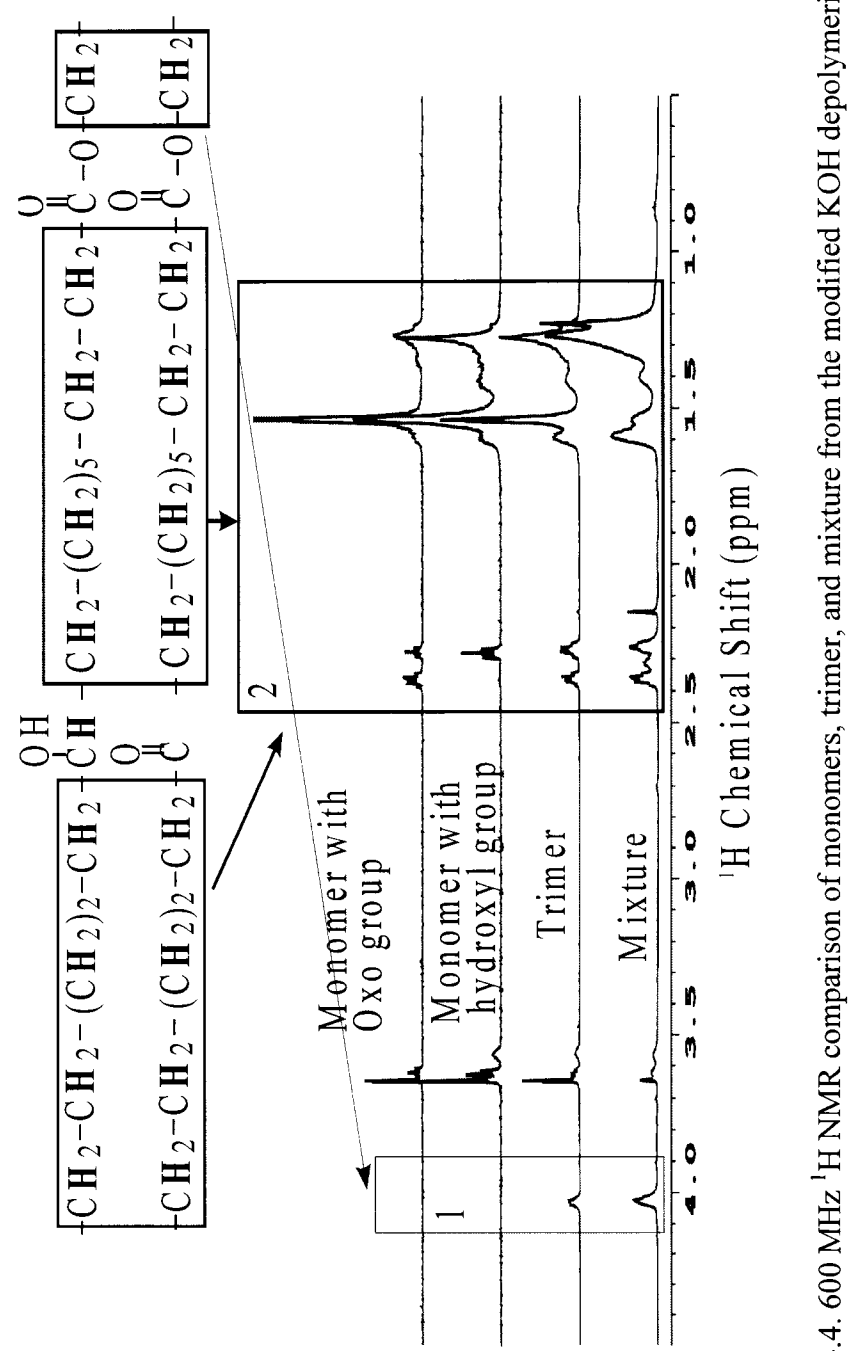

Figure 4.4. 600 MHz ^{1}H NMR comparison of monomers, trimer, and mixture from the modified KOH depolymerization treatment.

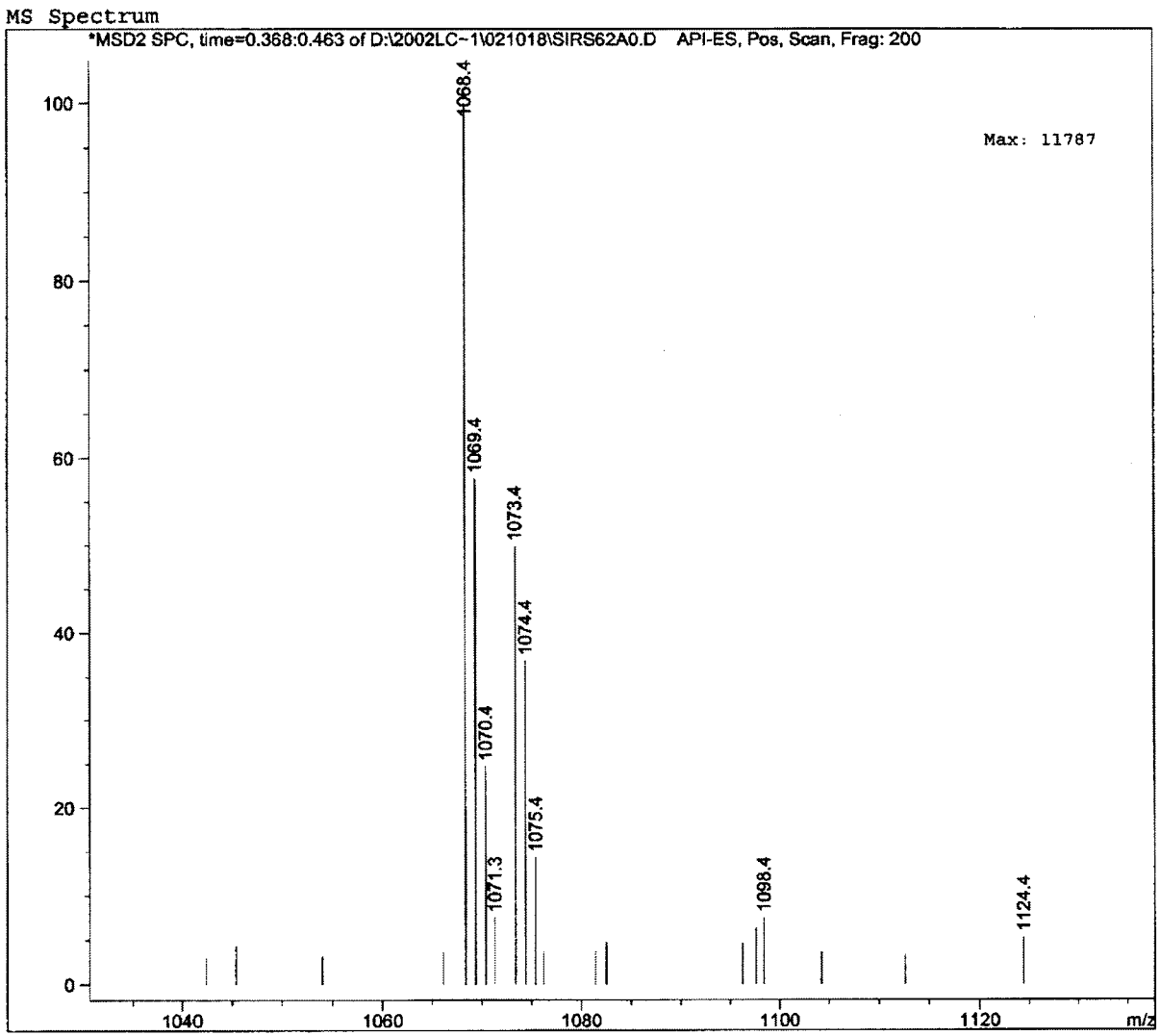

Figure 4.5. Mass Spectrum of a HPLC-pure fraction from HPLC separation of depolymerized products with the modified KOH depolymerization, showing ion intensities vs. mass-to-charge ratios.

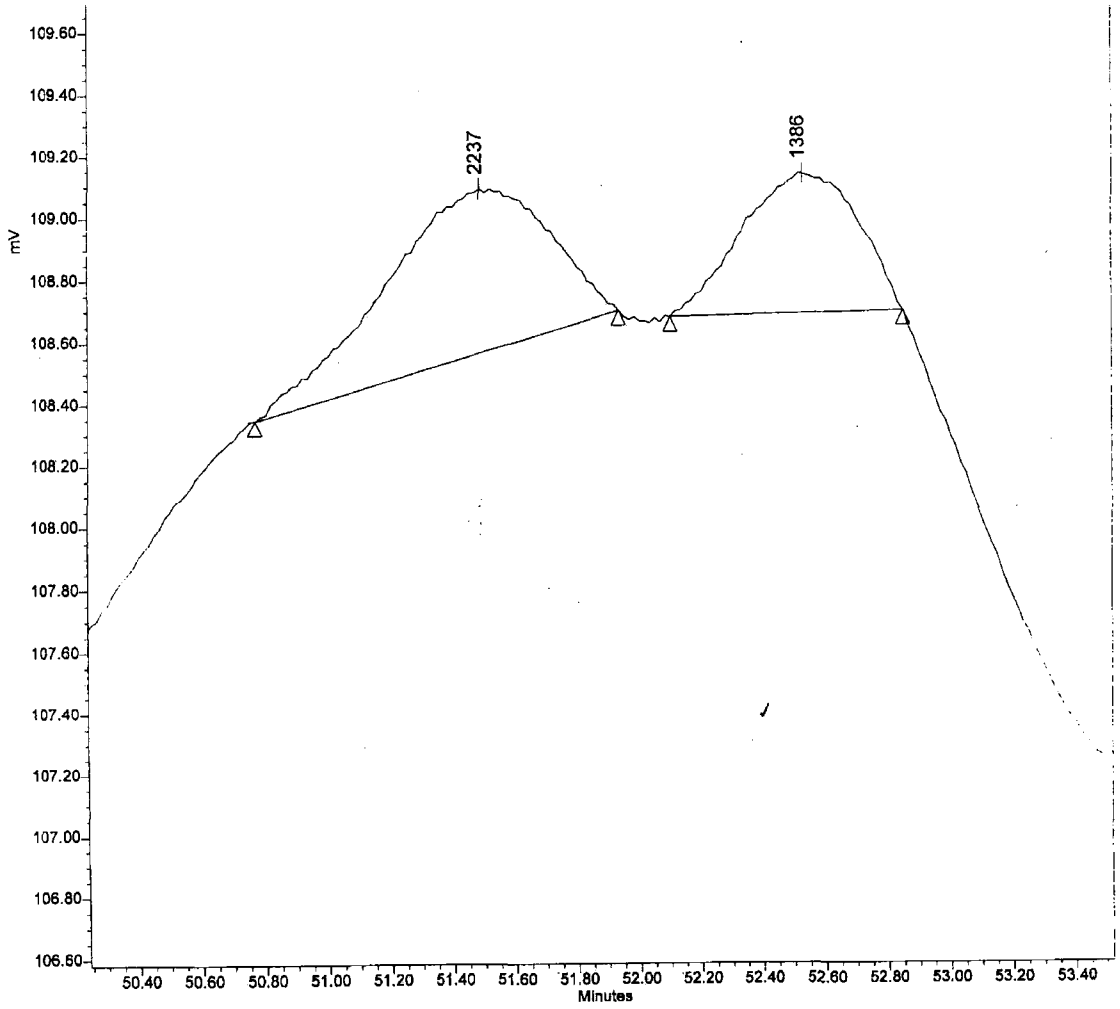

Figure 4.6. GPC evidence for oligomers with high molecular weights (with RI detector, using polystyrene as standards).

Traditional KOH depolymerization reaction of cutin:[31] In a typical traditional KOH depolymerization, three grams of ground cutin were deploymerized in 200 mL of 1M KOH/methanol solution. After depolymerization for 13 minutes, the mixture was filtered. The filtrate was very dark brown and was designated as Filtrate 1. The residue was added to another 200mL of freshly made 1M KOH/methanol solution, and was stirred for another 15 minutes. The resulting filtrate was light brown and

was designated as Filtrate 2. Filtrate 1 and Filtrate 2 were each neutralized to pH 4 ~ 5. After filtering out the KCl salt and drying, the two products were extracted with chloroform (100 mL and 60 mL for 1 and 2, respectively). The two extracted products were named C1 and C2. The yield of crude product from C1 was 1.74 gram (yield 58%), and the yield of crude product from C2 was only 0.07 gram (yield 2%). The two crude products were separated using a silica gel column, HPTLC, and HPLC. Some of the fractions from these separations were analyzed with TLC, HPLC, MS and NMR. The peaks and retention times are almost the same for the two crude products in the silica gel column purification and TLC and HPLC analysis. The functional groups found in NMR of each component were also similar for the two crude products.

The yields of C1 and C2 suggest that the depolymerization occurs mainly during the first 10 minutes of the reaction and is less efficient thereafter. That is, KOH can work rapidly on some part of the material, but cannot work well or may not work at all on the other part of the cutin polymer. We cannot decompose lime cutin completely even with 4M KOH/methanol reflux for a week. For KOH-susceptible cutin materials, the depolymerization may occur uniformly regardless of reaction time, since the products obtained with different reaction times are the same.

Preliminary protocol for separation and purification of products: MS spectra of the crude products and some of the products separated with HPTLC and HPLC showed almost a hundred compounds. Although we can generate a reasonably large amount of crude products, the amounts of most fractions, especially those with oligomers, are very limited, because more than half of the crude product consists of

the several identified monomers. Polarities of larger oligomers (trimers or bigger) with the same constituent monomers are expected to be very similar, and the separation of these oligomers with HPTLC based on their polarities may be impossible. Better chromatography methods like HPLC can sometimes help, but not always. Thus other analytical methods suitable for structural determination of mixtures should also be used. If possible, MS/MS could provide important information on the fragments of each molecule in a mixture, and molecular structures of each component in a mixture could be determined without separation.

Most of the fractions were still mixtures after one separation with HPLC, either in reversed phase or normal phase HPLC. Further separation and purification were needed to obtain pure products. In order to get the most interesting fractions separated first, we utilized ^{1}H NMR spectra to sort our fractions. The fractions with higher ester bond ratios have higher priorities to be separated, because they should consist of bigger oligomers. The rationale for using this criterion was described above.

Figure 4.7 shows the protocol adopted in our separation. The crude depolymerization products were pre-purified with silica gel column chromatography. All of the pre-purified products were mixtures. They were sorted according to their ^{1}H NMR spectra. Then HPLC separation was conducted on each pre-purified product. The fractions from HPLC separations were again sorted based on their ^{1}H NMR spectra, and then the purity of each fraction was tested by injecting the fraction back into HPLC under the same conditions and further checked with HPLC using different solvents. HPLC separation, sorting with ^{1}H

NMR spectra, and purity tests were repeated until a single-peaked fraction was obtained. We call these products HPLC-pure products. The purities of HPLC-pure products were further tested with MS spectra. If a product has only one set of molecular ions in its MS spectrum, we call this an MS-pure product. 2D NMR experiments were conducted on MS-pure products, and their structures were determined by the combination of MS and NMR results.

The prepurification of crude products with a silica gel column may miss some products, because there is always some colorful material left on the column after elution with methanol. Reversed phase chromatography should be a better choice, because very polar components can be eluted easily. In order to separate the very polar components with reversed phase HPLC, a very high proportion of water must be used. Consequently, detection with ELSD will be compromised by the difficulty of achieving evaporation. In practice, no signals could be detected when the eluent contained 40 percent or more of water. Many components absorbed UV radiation too weakly to be detected, even though they could be detected with ELSD. Use of the UV detector on a very concentrated sample yielded many peaks (Figure 4.8), with the best results obtained at a wavelength of 220 nm. Thus, ELSD detection is more sensitive than UV only at 40 percent or less water in the eluent, whereas UV at 220 nm may offer a better alternative at 40 percent or more water. The combination of the two detection methods should give a good representation of the sample. The peak intensities from ELSD are expected to be closer to the real composition of the sample.

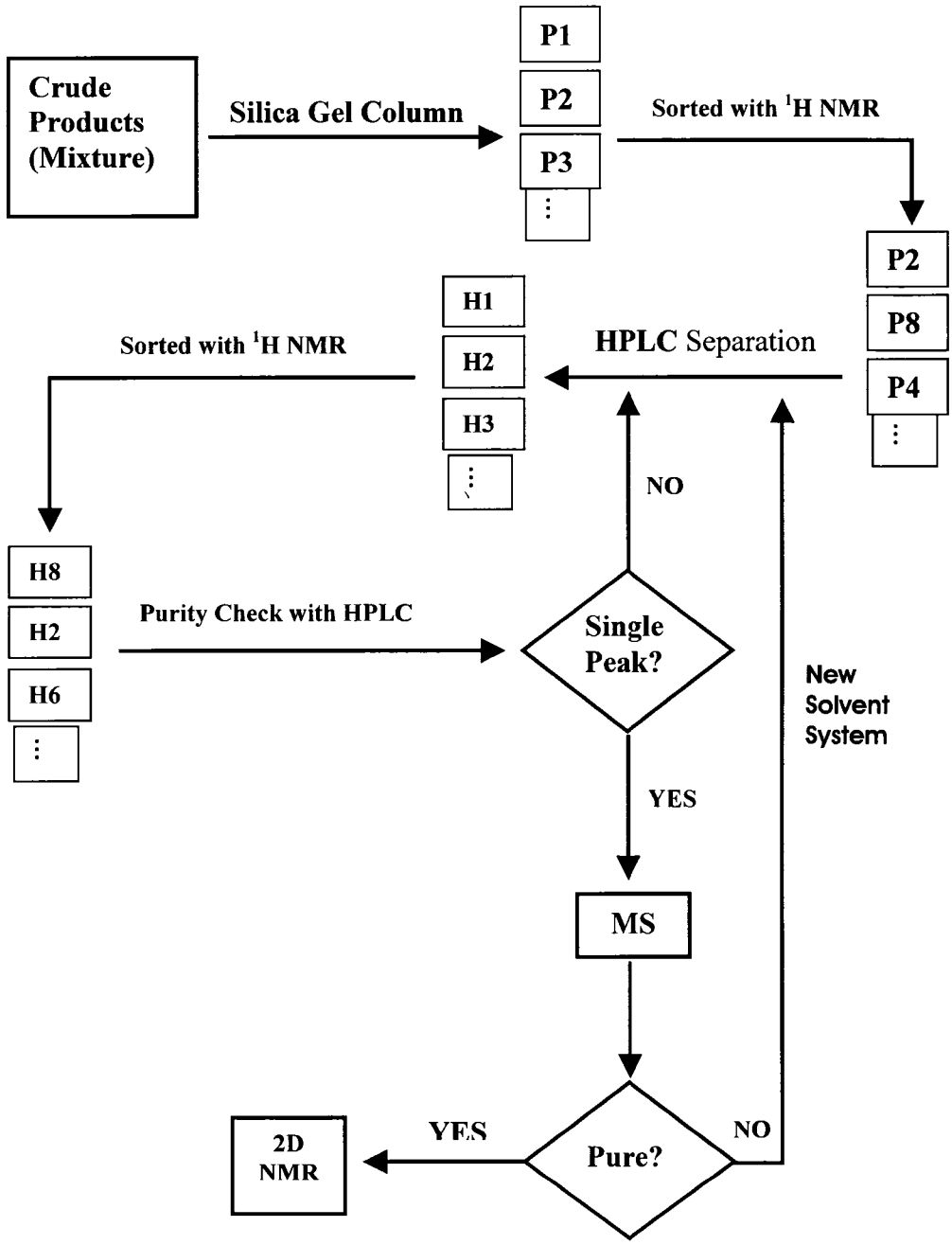

Figure 4.7. Preliminary protocol of separation and purification for lime cutin degradation products.

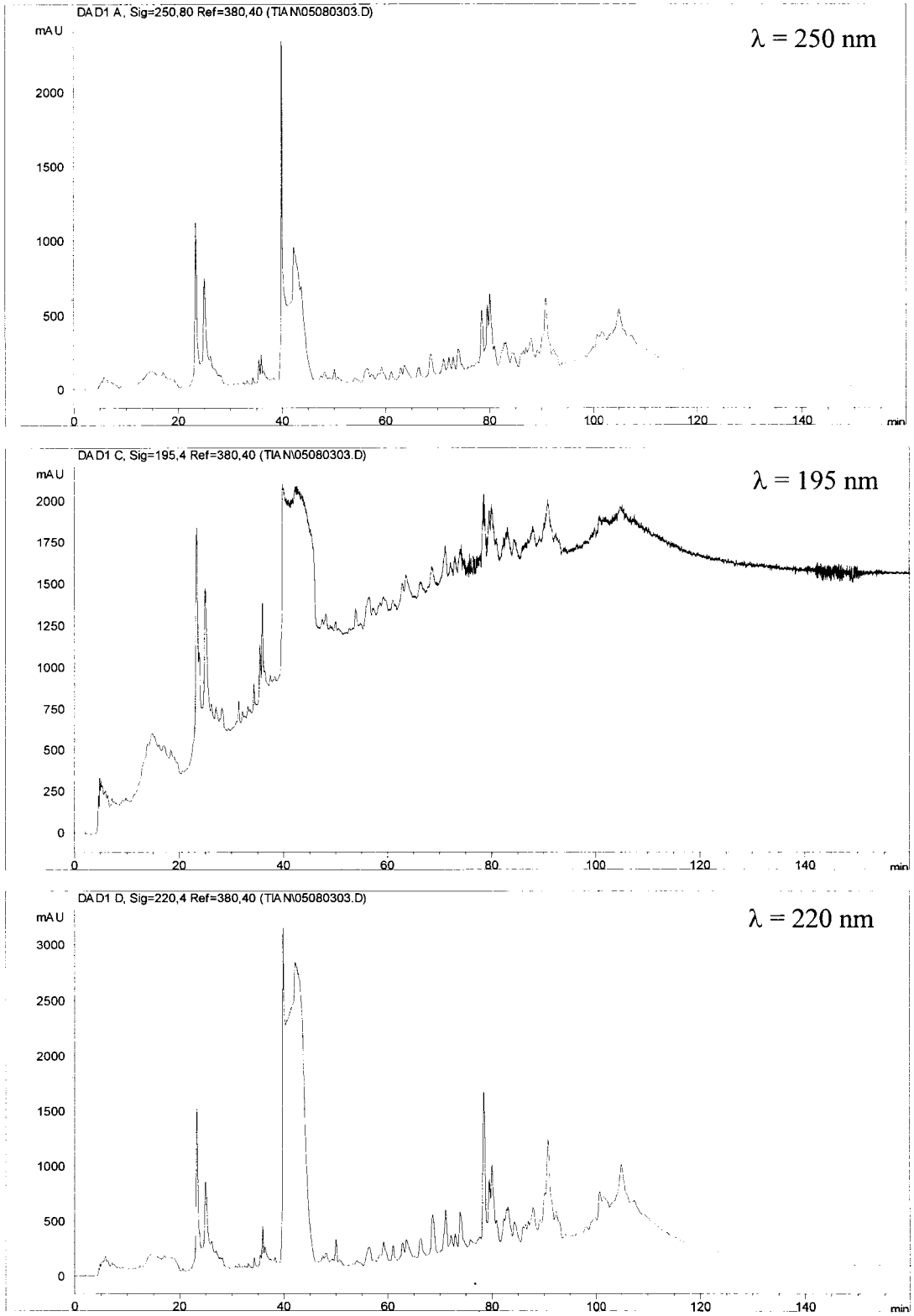

Figure 4.8. Comparison of UV detection for crude products at different wavelengths.

4.1.2.1 Separation and Identification of Monomers in Lime Cutin

Compound 1 is the methyl ester of 10,16-dihydroxyhexadecanoic acid, one of the two most abundant monomers (Figure 4.9) that was separated from the soluble products of KOH treatment of cutin. Proton NMR spectrum (Figure 4.10) shows a diagnostic peak for secondary alcohol at 3.56 ppm. An HMQC correlation between ^{1}H at 3.56 ppm proton and ^{13}C at 71 ppm carbon (in the box of Figure 4.11), which was assigned to the methine group of the secondary alcohol moiety, was observed in the HMQC spectrum. The peak at (3.63 ppm, 63 ppm) in HMQC arises from the terminal primary alcohol group (Figure 4.11). The singlet at 3.64 ppm in the ^{1}H spectrum shows the existence of a methoxyl group (Figure 4.10), and the correlation of this proton with the carbonyl carbon at 174 ppm in the HMBC spectrum demonstrates that the methoxyl group comes from the alcohol moiety of the ester connection in the sample (Figure 4.12). The peak at 2.29 ppm in the proton spectrum (Figure 4.10) was assigned to the methylene protons next to the carbonyl in the carboxylic acid moiety and confirmed by an HMBC connectivity at (2.29, 174 ppm). Although some of the bulk methylenes can't be distinguished, the proposed structure is quite definitive based on the known structures of the monomers. The integration of the protons also supports this structure (Table 4.2). The anomalously high number of bulk methylenes is attributed to the water in the solvent, $CDCl_3$.

Further support for the structure comes from MS. Both 320 m/e ($M+NH_4^+$) and 303 m/e ($M+H^+$) molecular ions, which are normal molecular ions in ESI/MS of similar compounds, were found (Figure 4.13). **Compound 1** has a molecular weight of 302. The peak at m/e 325 was generated from the addition of Na^+, an ion from the

glassware used in the process, to a sample molecule. The fragment at m/e 253 results from the loss of MeO- and H_2O from the molecule. This fragment can lose another H_2O and generate a fragment at m/e 235. Additionally, a fragment at m/e 289 corresponds to loss of MeO- only from the $(M+NH_4^+)$ ion.

Table 4.2. Chemical Shifts and Integrations of **Compound 1**.

Chemical Shift (ppm)	3.65 (s)	3.60 (t)	3.55 (m)	2.28 (t)	1.20~1.70
Integral (Exp.)	3	2	1	2	43
Integration (Theor.)	3	2	1	2	24

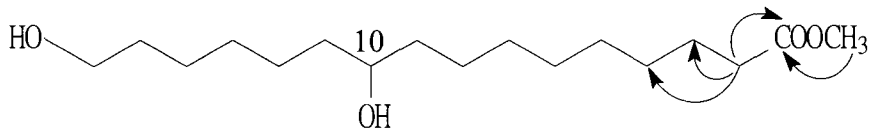

Figure 4.9. Structure and significant multiple-bond correlations of **Compound 1**.

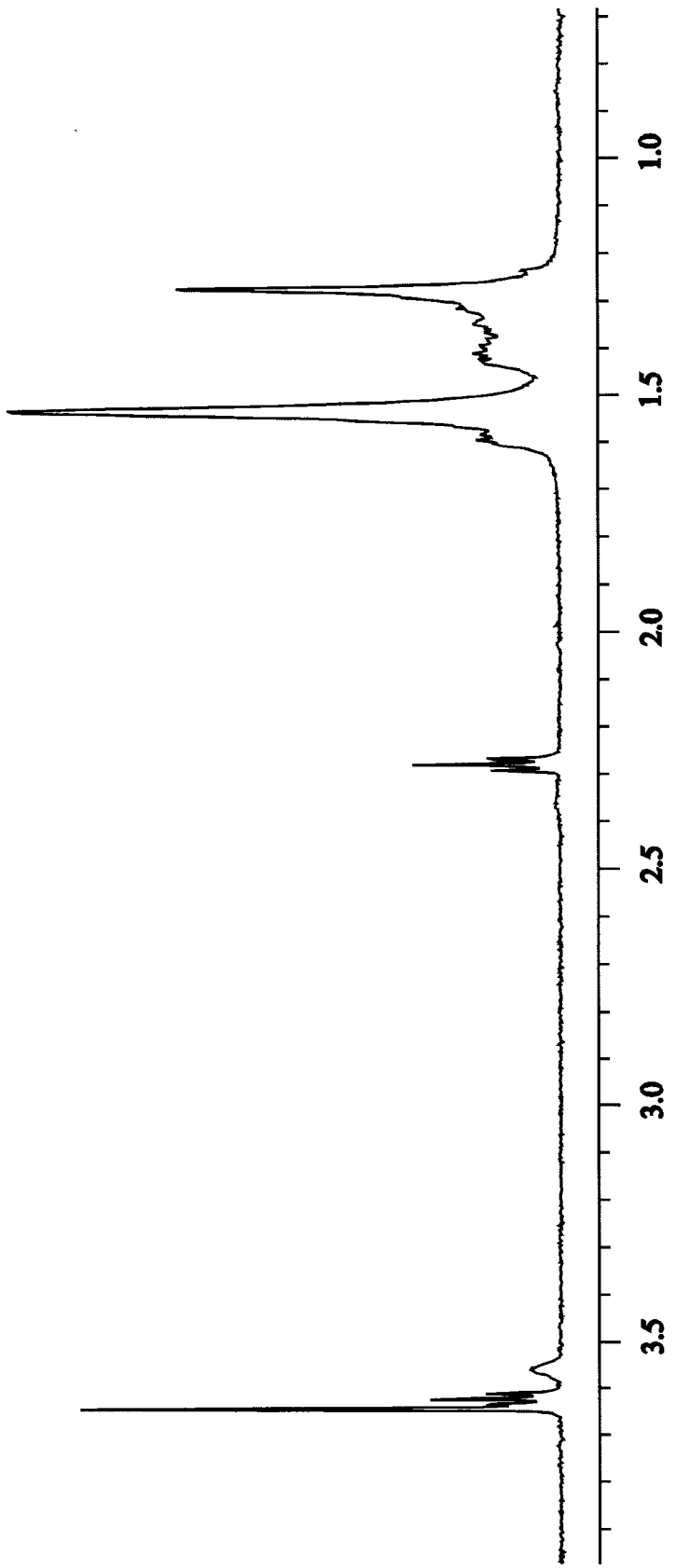

Figure 4.10. ^{1}H 600 MHz NMR spectrum of **Compound 1**.

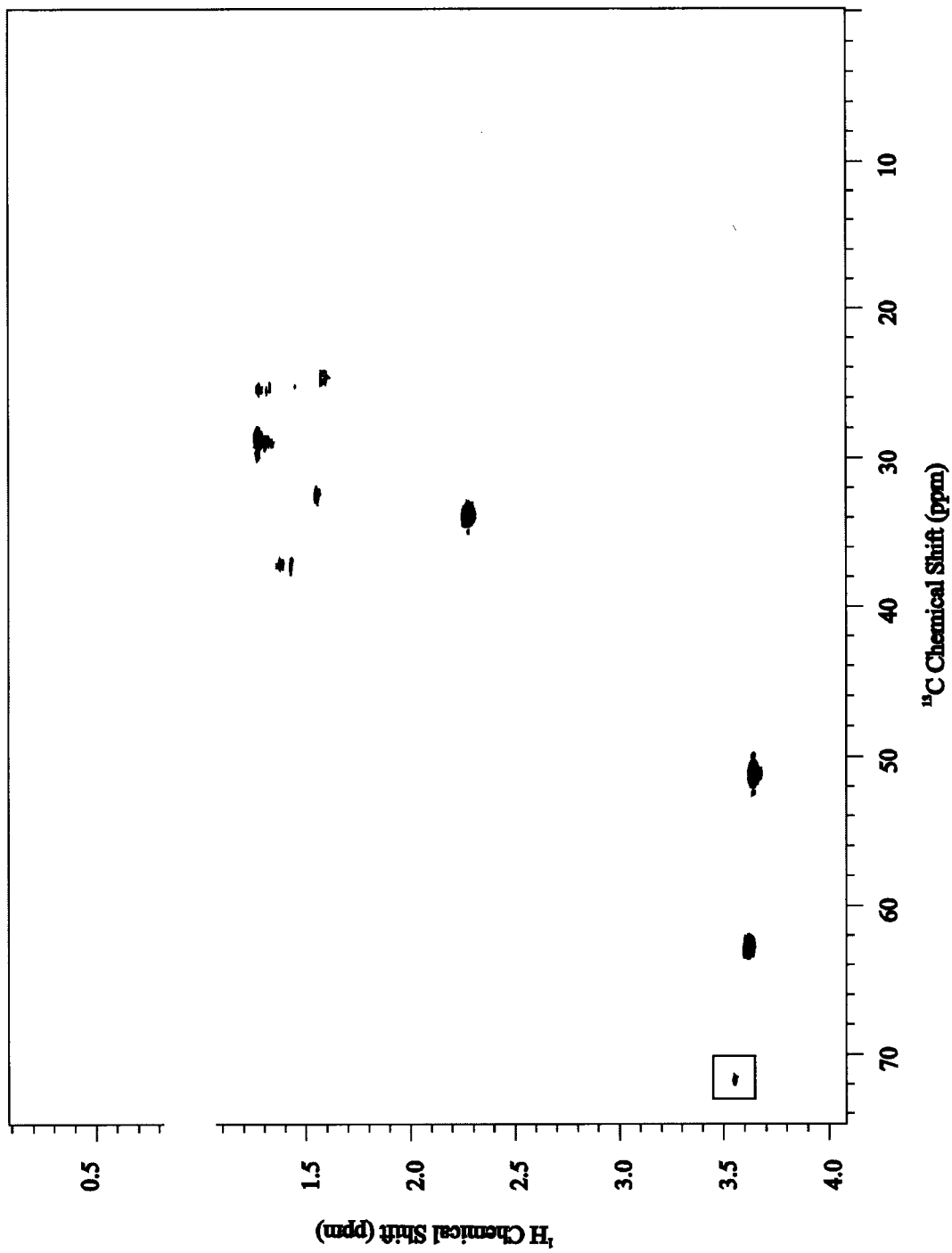

Figure 4.11. Two-dimensional gHMQC spectrum of **Compound 1**.

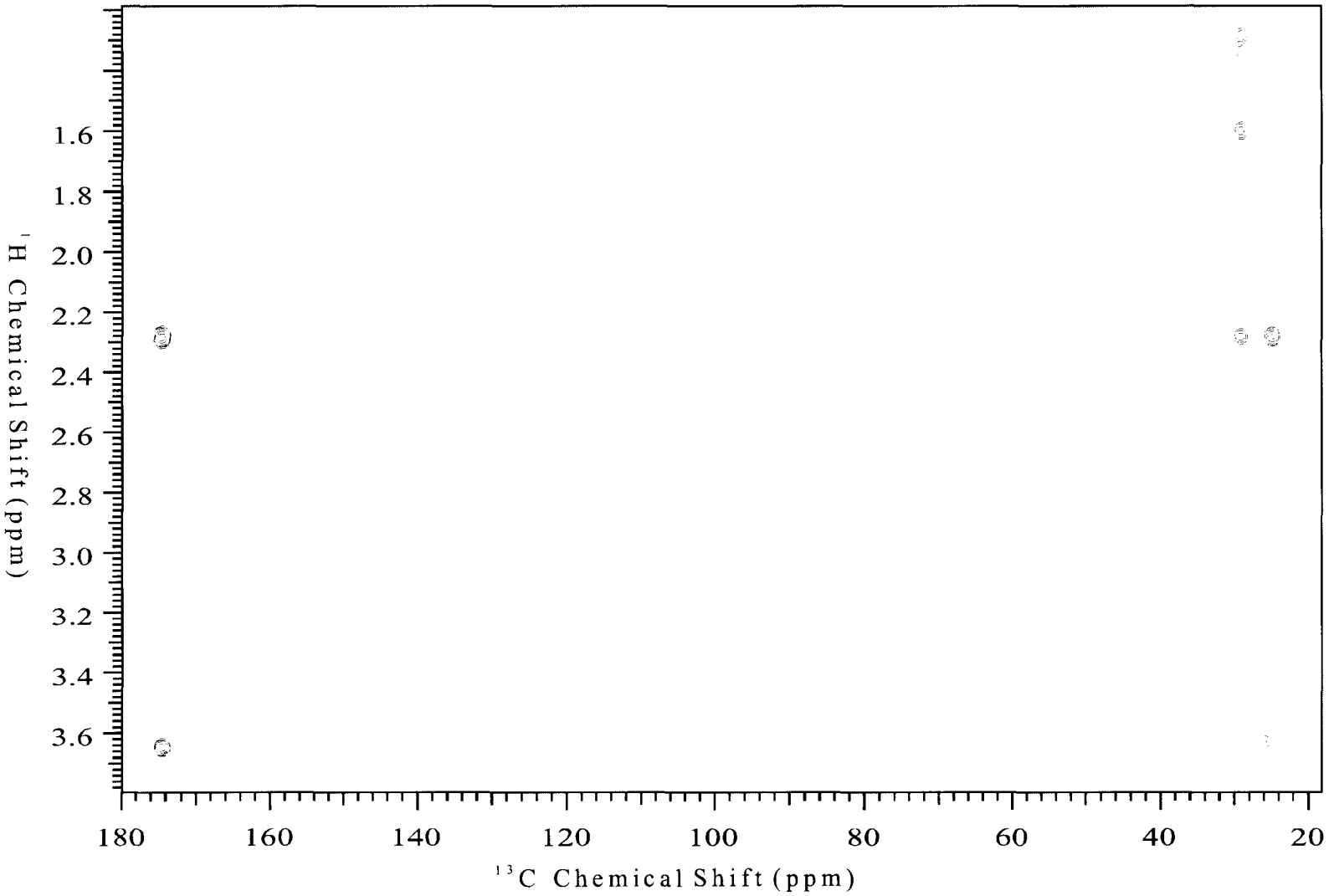

Figure 4.12. Two-dimensional gHMBC spectrum of **Compound 1**.

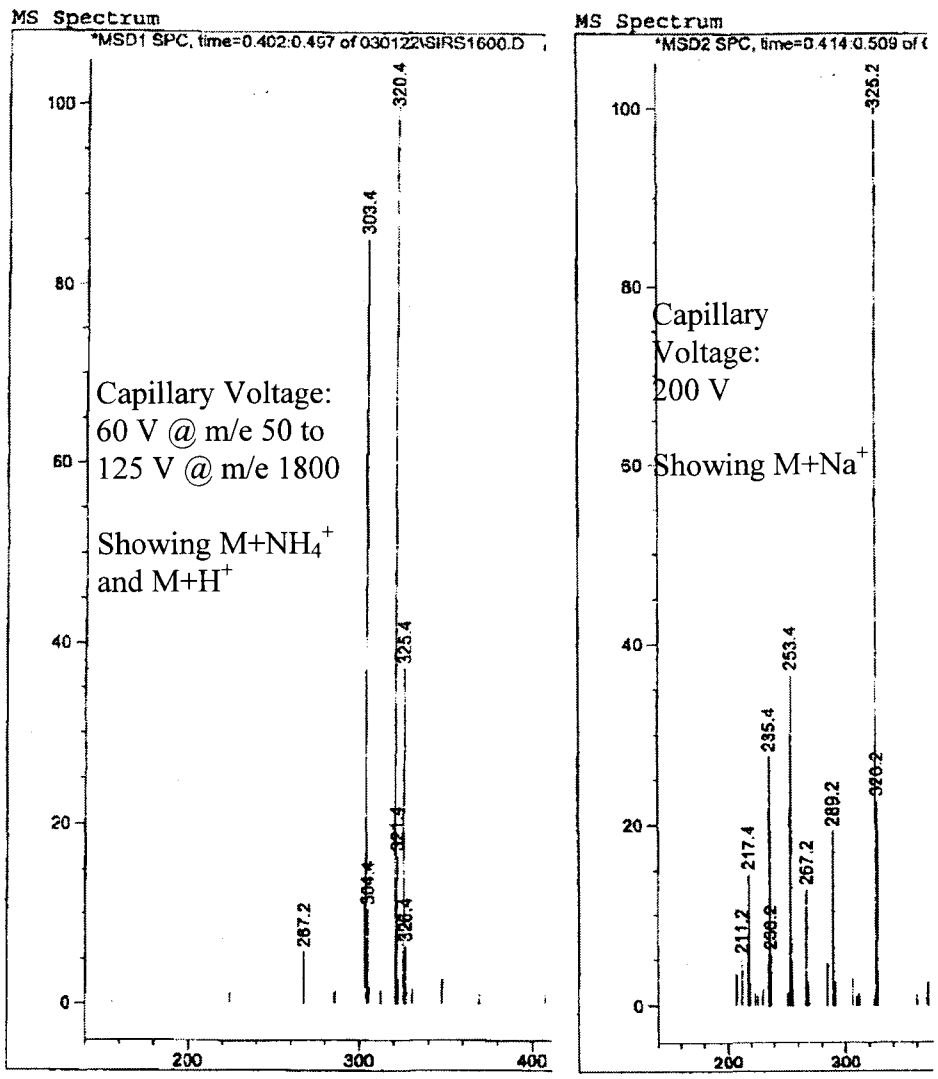

Figure 4.13. Mass spectra of **Compound 1**, showing ion intensity vs. mass-to-charge ratio.

Compound 2 is the methyl ester of the other most abundant monomer of lime cutin (Figure 4.14), 10-oxo-16-hydroxyhexadecanoic acid. It was obtained from the silica gel column separation of the soluble portion of the traditionally KOH-depolymerized cutin. The peak corresponding to the methylene protons next to the ester carbonyl in the carboxylic acid moiety appears at 2.29 ppm (Figure 4.15), the same position as in **Compound 1**. The most significant indicator of the oxo substituent is the HMBC cross peak between the protons at 2.38 ppm and the carbonyl carbon at 211 ppm (Figure 4.16). The integration of the ^{1}H spectrum also supports this structure (Table 4.3). Once again, the extremely high number of bulk methylenes is attributable to the water peak of the solvent, $CDCl_3$.

Further support for the structure comes from MS. In ESI/MS both m/e 318 ($M+NH_4^+$) and m/e 301 ($M+H^+$) molecular ions, which are expected for this compound, were observed (Figure 4.17). The peak at m/e 323 was generated from the addition of Na^+, an ion from the glassware used in the process, to a sample molecule. The fragment at m/e 251 results from loss of MeO- and H_2O from the molecule. A fragment resulting from the loss of a MeO- group from the molecule was also observed at m/e 269. Finally, a fragment from the loss of the terminal methyl group was observed at m/e 285.

Table 4.3. Chemical Shifts and Integration of **Compound 2**.

Chemical Shift (ppm)	3.65 (s)	3.60 (t)	2.38 (t)	2.28 (t)	1.20-1.70
Integral (Exp.)	3	2	4	2	48
Integration (Theor.)	3	2	4	2	20

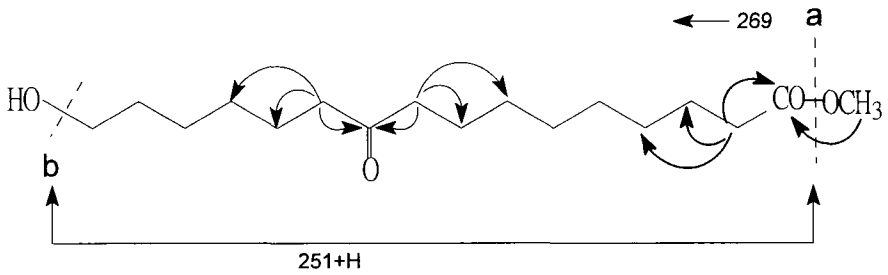

Figure 4.14. Structure and significant multiple-bond correlations of **Compound 2**.

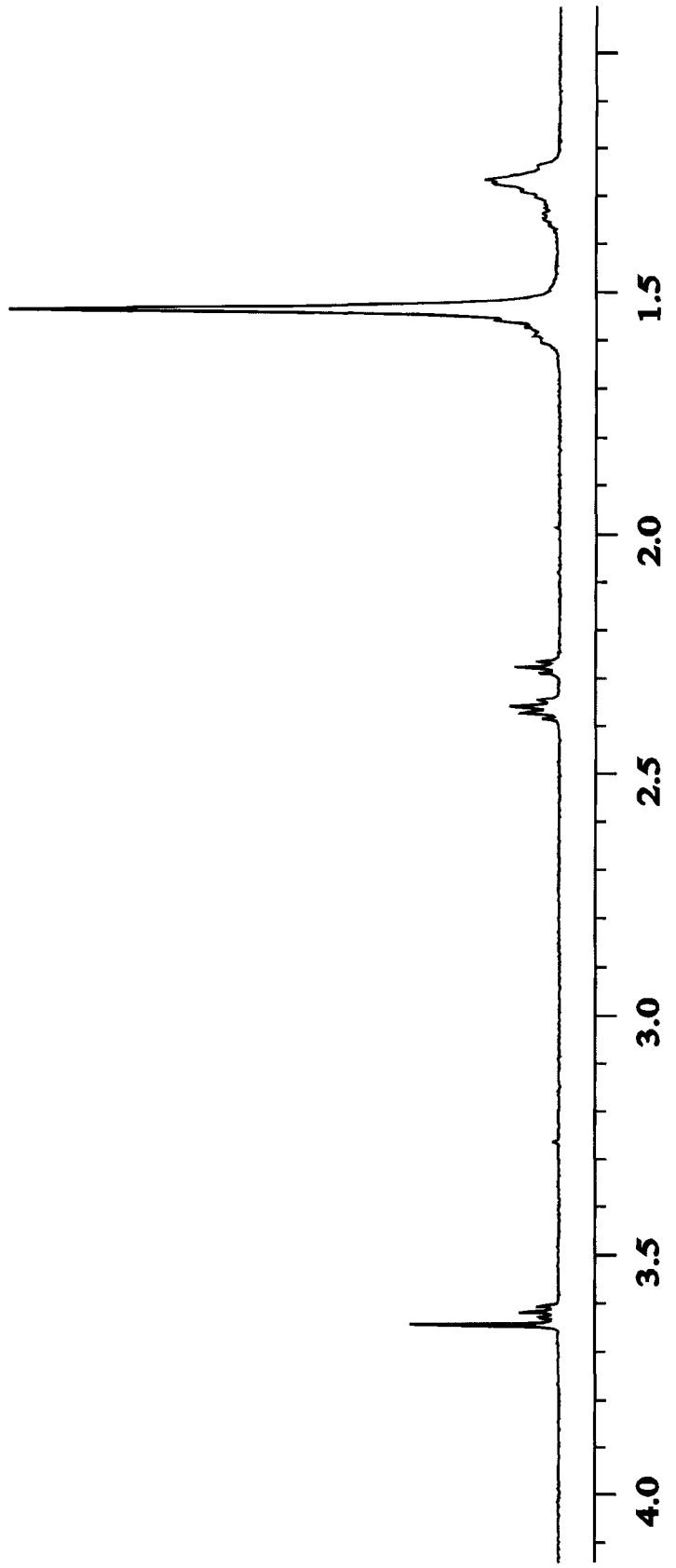

Figure 4.15. ^{1}H 600 MHz NMR spectrum of **Compound 2**.

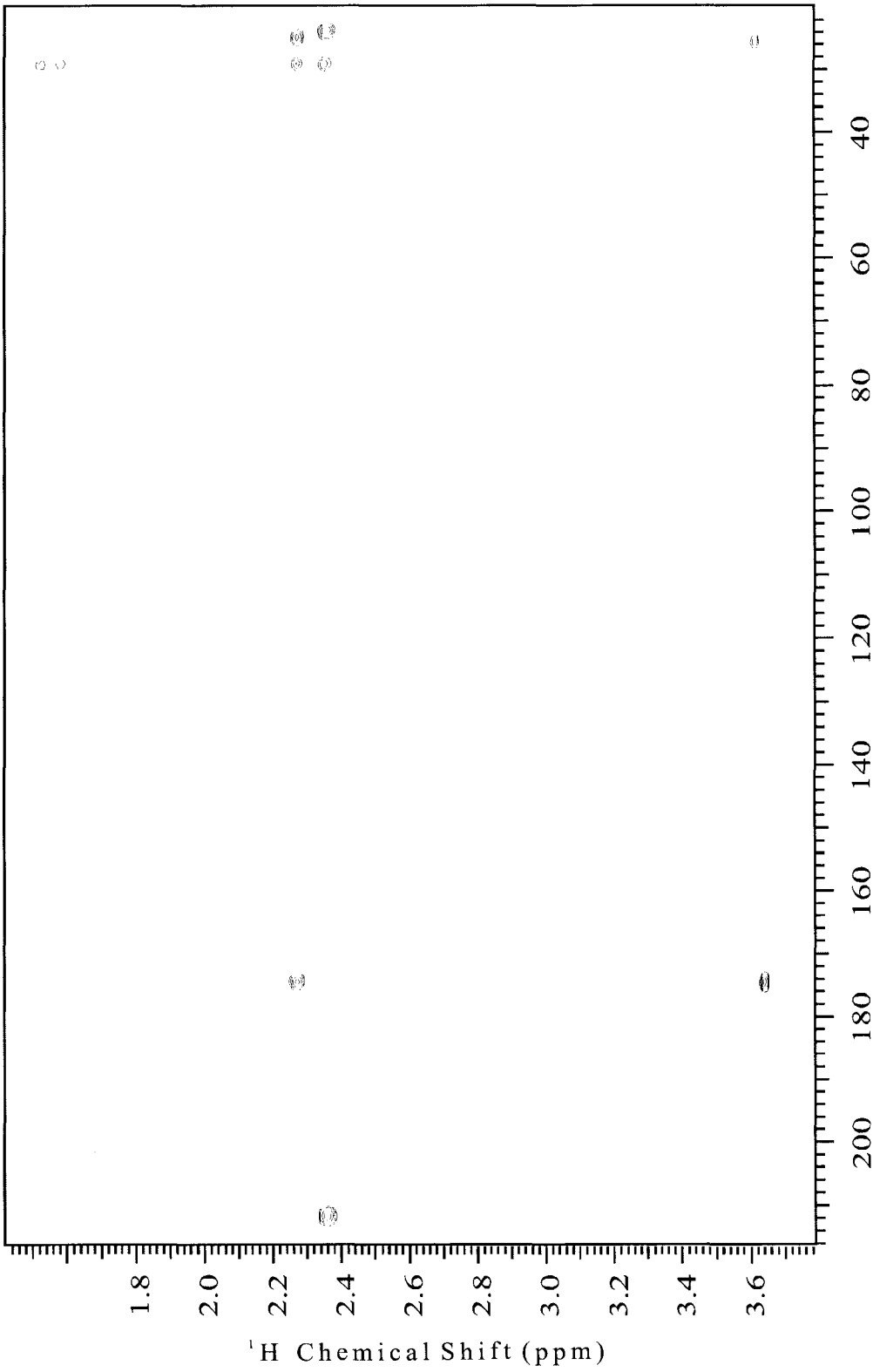

Figure 4.16. Two-dimensional gHMBC spectrum of **Compound 2**, .

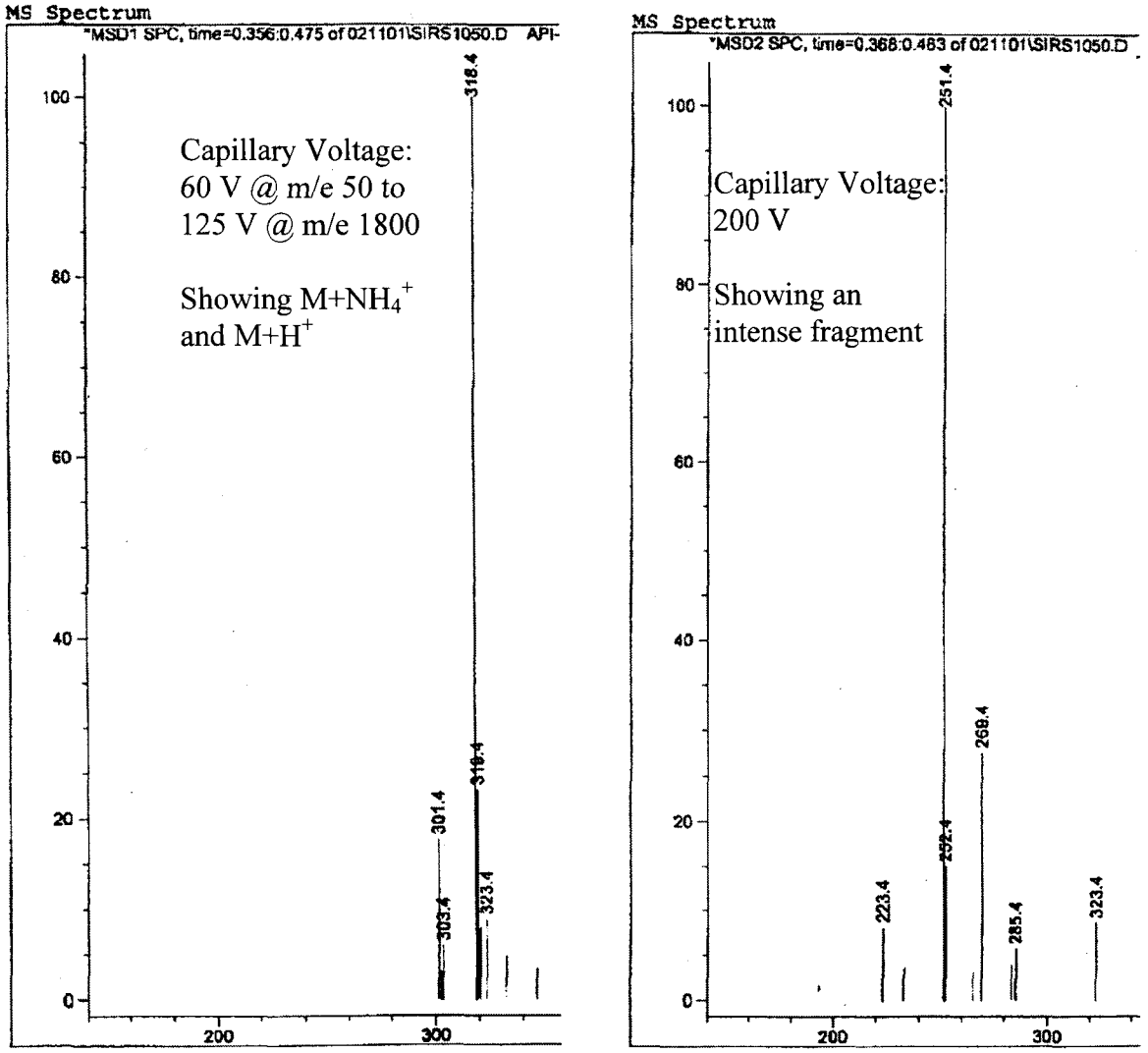

Figure 4.17. Mass spectra of **Compound 2**, showing ion intensity vs. mass-to-charge ratio.

Compound 3 is the methyl ester of a 16-carbon dicarboxylic acid monomer (Figure 4.18). This C_{16} dicarboxylic acid is a rare monomer in lime cutin.[87] Obtained from traditional KOH treatment of lime cutin, it was separated and purified with a silica gel column and HPLC. **Compound 3** was separated first on a silica HPLC column with gradient elution (Table 4.4) (Figure 4.19). Then the collected fractions were further purified on the same column with different gradient eluents (pure hexanes to acetone : hexanes = 1.5 : 98.5) (Figure 4.20). Fraction 5 from the second separation is the monomer of interest.

Table 4.4. Gradient Eluents for Separation of Mixture M314.

Time (min)	0	10	12	15	20
Aceton (%)	0	3	6	6	30
Hexanes (%)	100	97	94	94	70

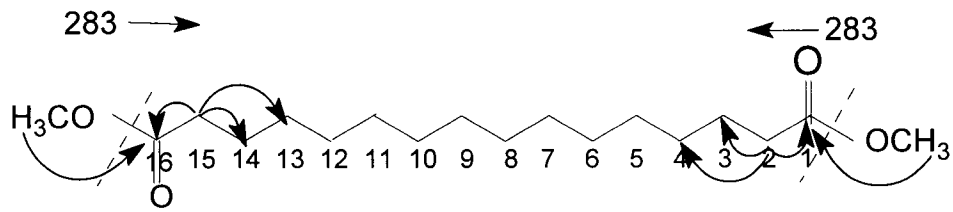

Figure 4.18. Structure and significant 2D gHMBC correlations of **Compound 3**.

In contrast to the previous two monomers, the ^{1}H NMR spectrum of **Compound 3** displays no triplet peak at 3.60 ppm (Figure 4.21), suggesting that it has no free terminal hydroxyl group. The integration of protons (Table 4.5) agrees with the suggested structure. The peak resonating at 0.86 ppm in ^{1}H NMR spectrum has a

weak cross peak in gHMQC (Figure 4.22, highlighted by a box), but it has no connections with the other peaks in gHMBC (Figure 4.23). This observation together with the discrepancy of proton numbers between experimental and theoretical values for bulk methylene groups suggest an unknown impurity. This peak is found in many of our cutin degradation products.

The cross peak at (^{1}H at 3.61 ppm; ^{13}C at 173.9 ppm) in the HMBC spectrum of Figure 4.23 (highlighted by a box) shows a multiple bond connection between methoxyl groups and the carboxyl groups of the ester bonds. This feature further confirms the suggested methyl ester structure.

The main molecular ion ($M+NH_4^+$) at m/e 332 and a small impurity peak at m/e 651 are observed in the lower capillary voltage ESI/MS spectrum (Figure 4.24 (a)). This further confirms the existence of an impurity. Since the amount of the impurity is small, the intensity of impurity peak is low in MS spectrum and causes a small variation from the expected ^{1}H NMR integration (Table 4.5). The peak at m/e 333 in the lower capillary voltage ESI/MS spectrum is the isotopic peak of the main molecular ion; it has intensity about 20 % of the main molecular ion peak, in accordance with the theoretical value. More intense fragment peaks are observed as expected at the higher capillary voltage in ESI/MS. The base peak at m/e 283 in the higher capillary voltage ESI/MS spectrum (Figure 4.24 (b)) is a fragment from cleavage of the molecule at position 'a' (marked in Figure 4.18).

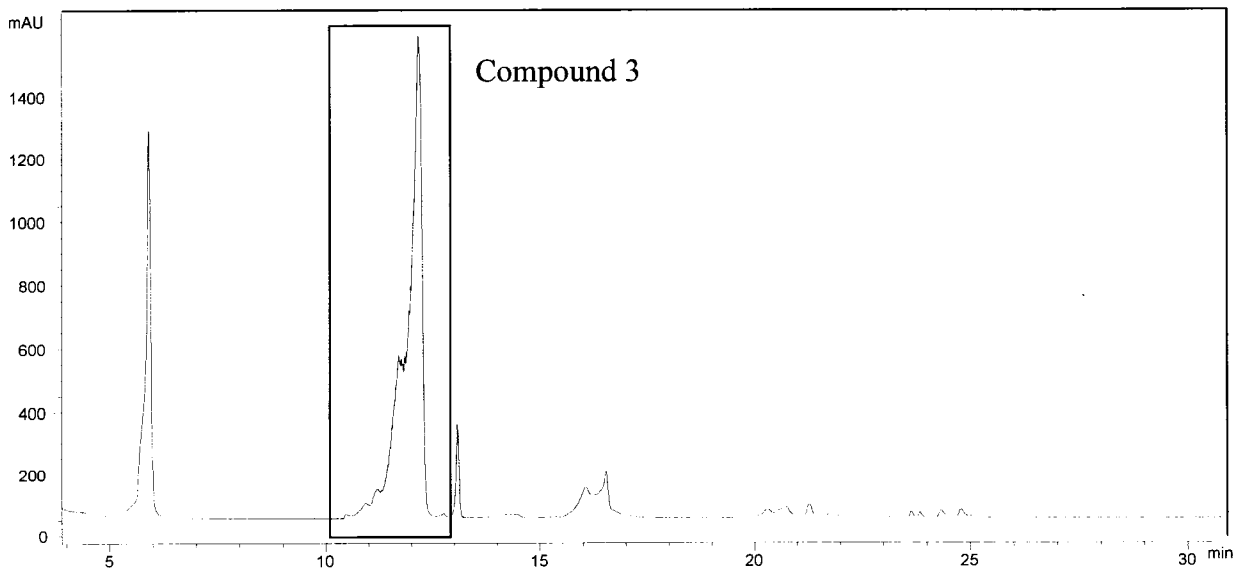

Figure 4.19. HPLC spectrum showing separation of **Compound 3**.

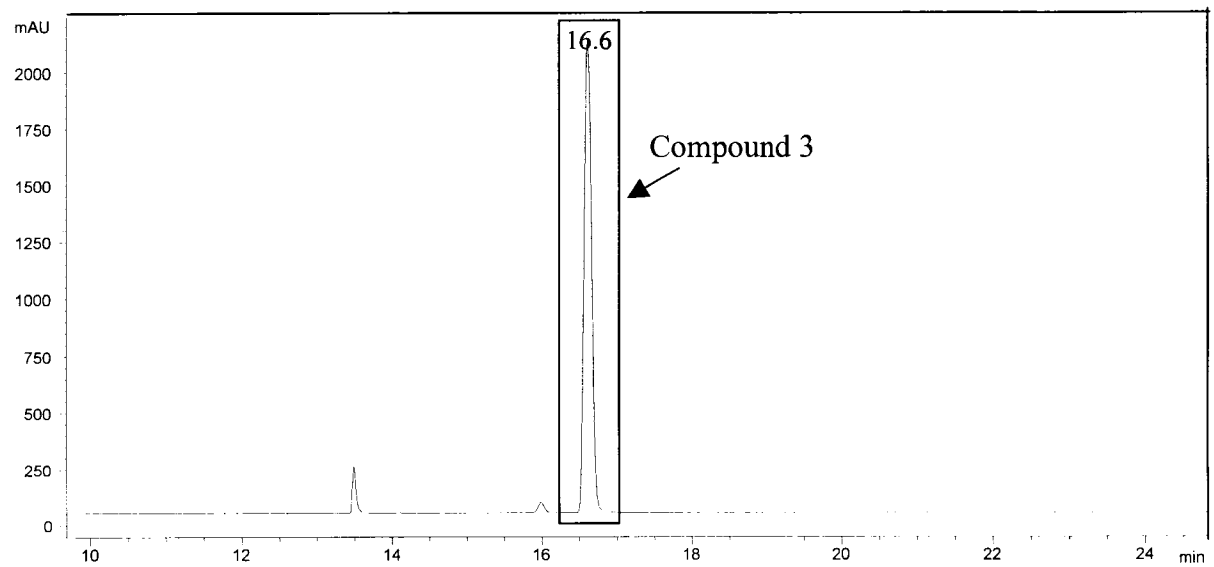

Figure 4.20. Purification of **Compound 3** by HPLC (the first two fractions are not shown).

Table 4.5. Chemical Shifts and Integration of **Compound 3**.

Chemical Shift (ppm)	3.65	2.28	1.60	1.27~1.23	0.86
Integral (Exp.)	6	4	4	28	3
Integration (Theor.)	6	4	4	20	0

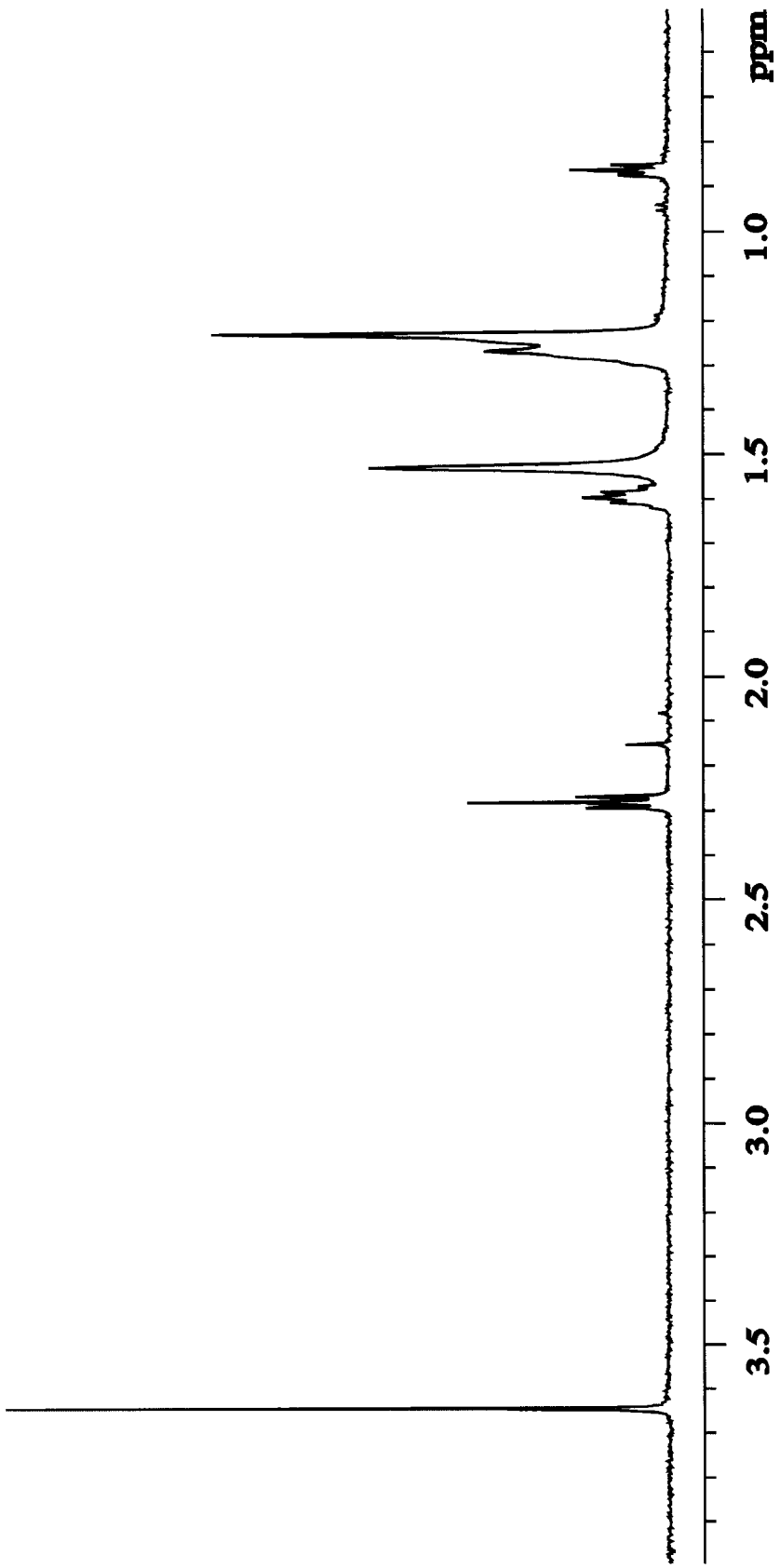

Figure 4.21. 600 MHz ^{1}H NMR spectrum of **Compound 3**.

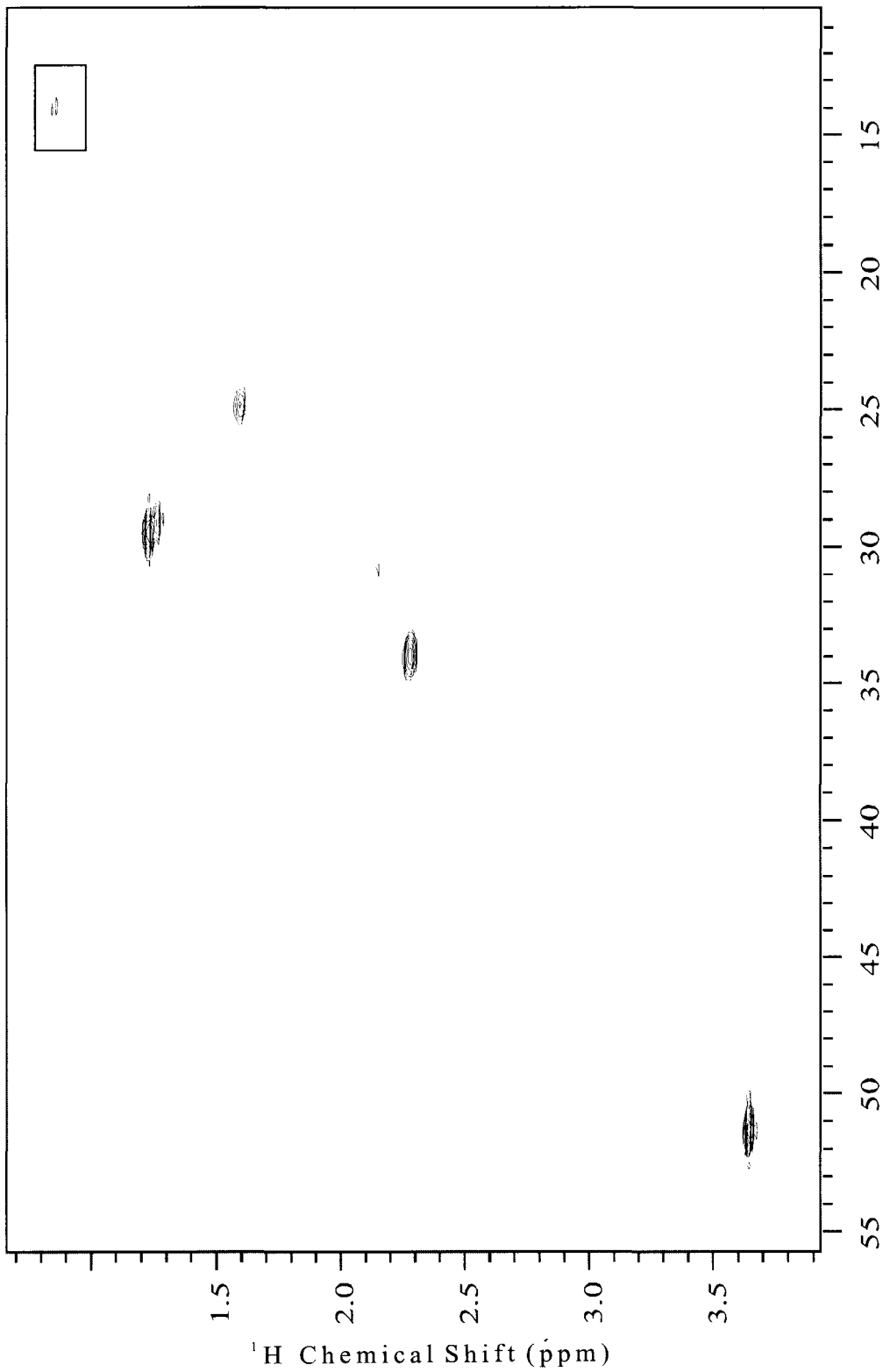

Figure 4.22. Two-dimensional gHMQC spectrum of **Compound 3**.

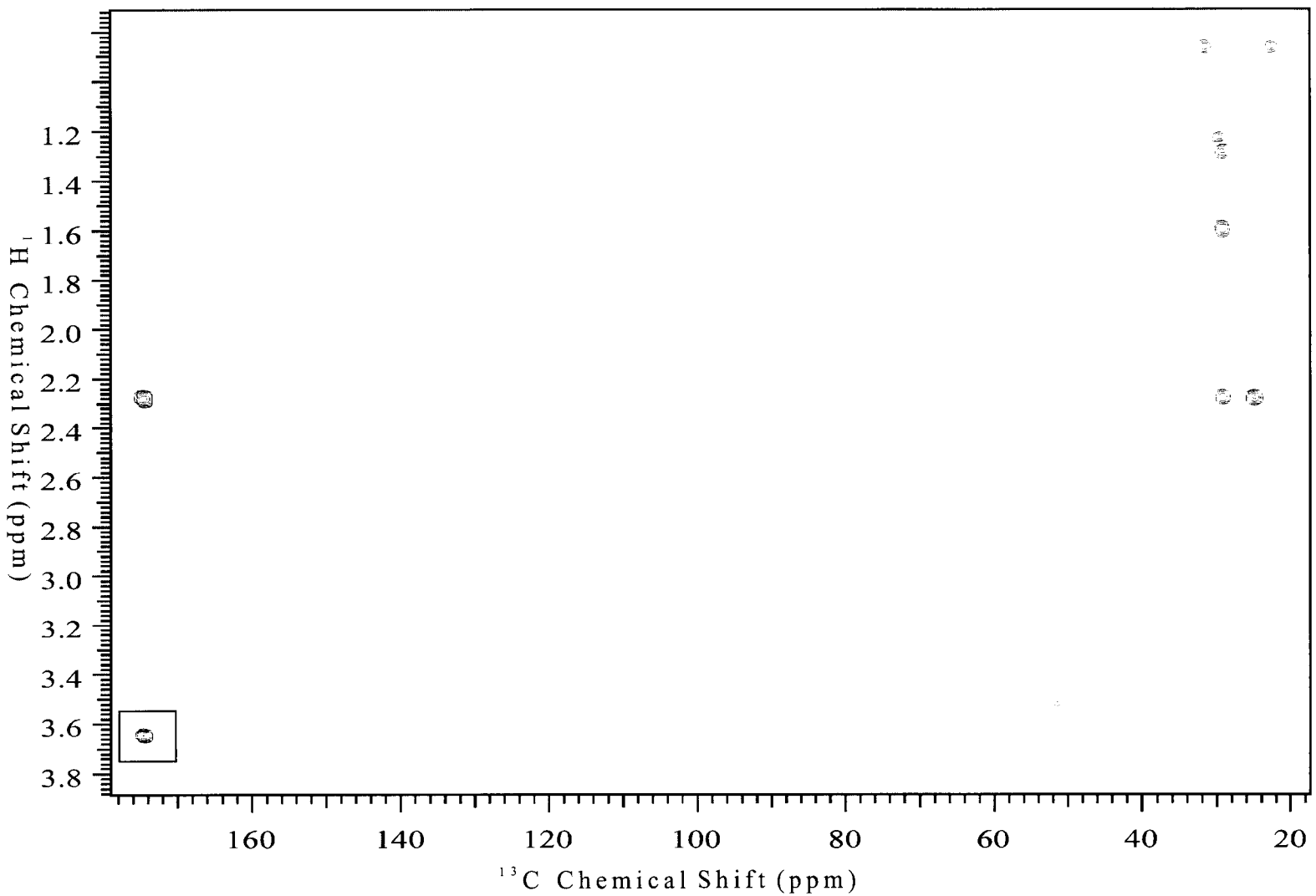

Figure. 4.23. Two-dimensional gHMBC spectrum of **Compound 3**.

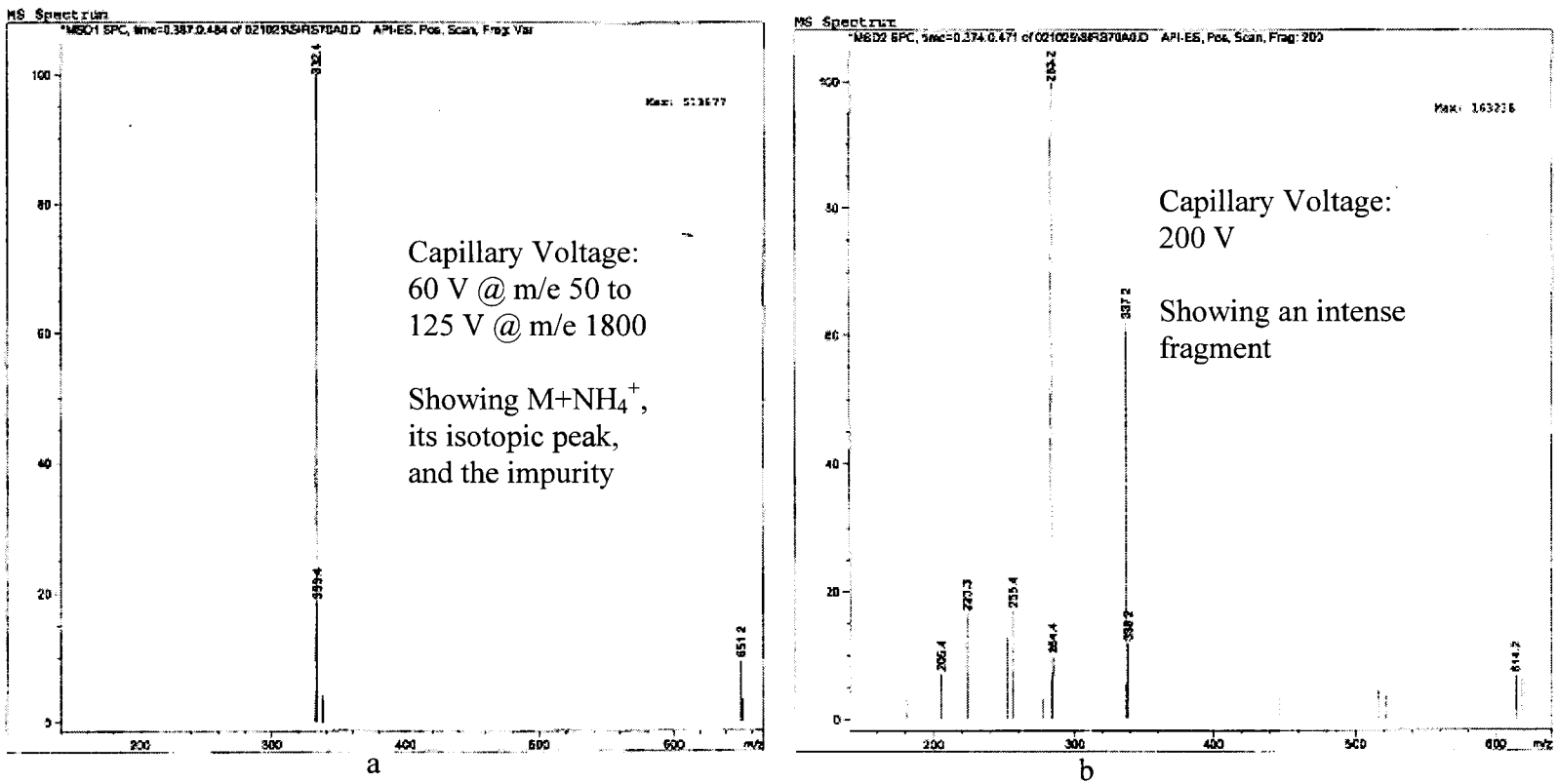

Figure 4.24. Electrospray Ionization Mass Spectra of **Compound 3**, showing ion intensity vs. mass-to-charge ratio.

Three other new monomers containing 18 or 20 carbons, **Compounds 4, 5, and 6**, were found in the depolymerization products of lime cutin (Figure 4.25). These tentative structures were determined from their molecular ions, fragments in their MS spectra, and their polarities in the HPLC separations. Alternative structures with the same molecular ions are possible, but they either have an odd number of carbons (abnormal in natural products) or have too many oxo groups, which contradict the observed polarities. The suggested structures are the most reasonable ones.

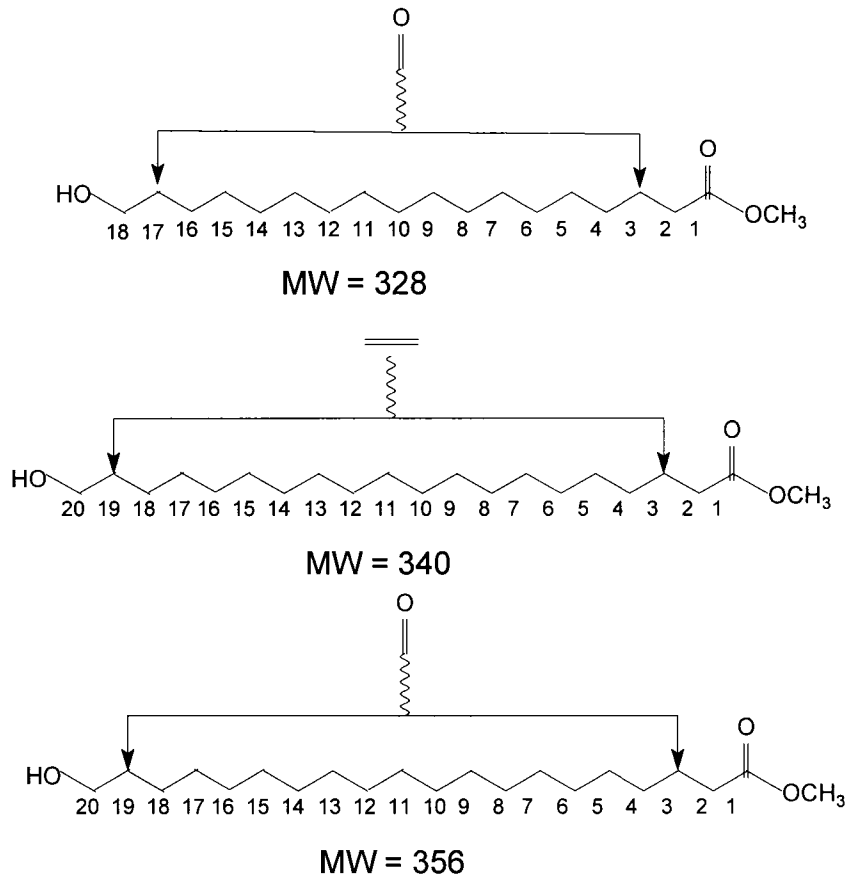

Figure 4.25. Tentative structures of three new monomers from lime fruit cutin. The positions of the midchain functional groups are not determined from the available NMR and MS data.

4.1.2.2 Separation and Identification of Dimers in Lime Cutin

Compound 7 was isolated from HF depolymerization of lime cutin. It was elucidated as a dimer containing two units of 10-oxo-16-hydroxyhexadecanoic acid (Figure 4.26). With the identification of this dimer, all combinations of the two common monomers have now been found.[33,35] Integrations of ^{1}H in the 600 MHz 1D NMR spectrum also support this structure (Figure 4.27). Table 4.6 lists the characteristic peaks and their integrals. More evidence for the structure was obtained from the 600 MHz 2D NMR spectra. Gradient-assisted heteronuclear multiple quantum coherence (gHMQC) gives information on directly bonded protons and carbons. In the gHMQC (Figure 4.28), **Compound 7** shows the following diagnostic correlations: $CH_3\mathbf{CH_2}OC(O)$- (4.11 ppm, 60.12 ppm), -$\mathbf{CH_2}OC(O)$- (4.04 ppm, 63.8 ppm), -$\mathbf{CH_2}C(O)\mathbf{CH_2}$- (2.37 ppm, 42.4 ppm), $HO\mathbf{CH_2}$- (3.67 ppm, 63.1 ppm), and -$\mathbf{CH_2}COO$- (2.27 ppm, 34.2 ppm). Correlations were also seen for the bulk methylene groups. Gradient-assisted heteronuclear multiple-bond (long-range) correlation (gHMBC) gives information on ^{1}H-^{13}C pairs 2 - 3 bonds apart. Cross peaks for the ^{13}C at 173.9 ppm with ^{1}H at 4.04 ppm and ^{1}H at 4.11 ppm have been observed for other cutin oligomers [33,35] and strongly support the proposed structure (Figure 4.29). The other HMBC correlations are marked on the structure of **Compound 7**.

The electrospray MS (ESI-MS) exhibited three types of molecular ions: 583 ($M+H^+$), 600 ($M+NH_4^+$), and 605 ($M+Na^+$) (Figure 4.30). No fragments were obtained even at a voltage of 200 V, so that positions of the oxo groups were deduced on the basis of monomer structures of the component monomers.

Table 4.6. Characteristic Chemical Shifts and Integrals of **Compound 7**.

Chemical Shift (ppm)	4.10	4.03	3.61	2.38	2.28
Integral (Exp.)	2	2	2	7	4
Integration (Theor.)	2	2	2	8	4

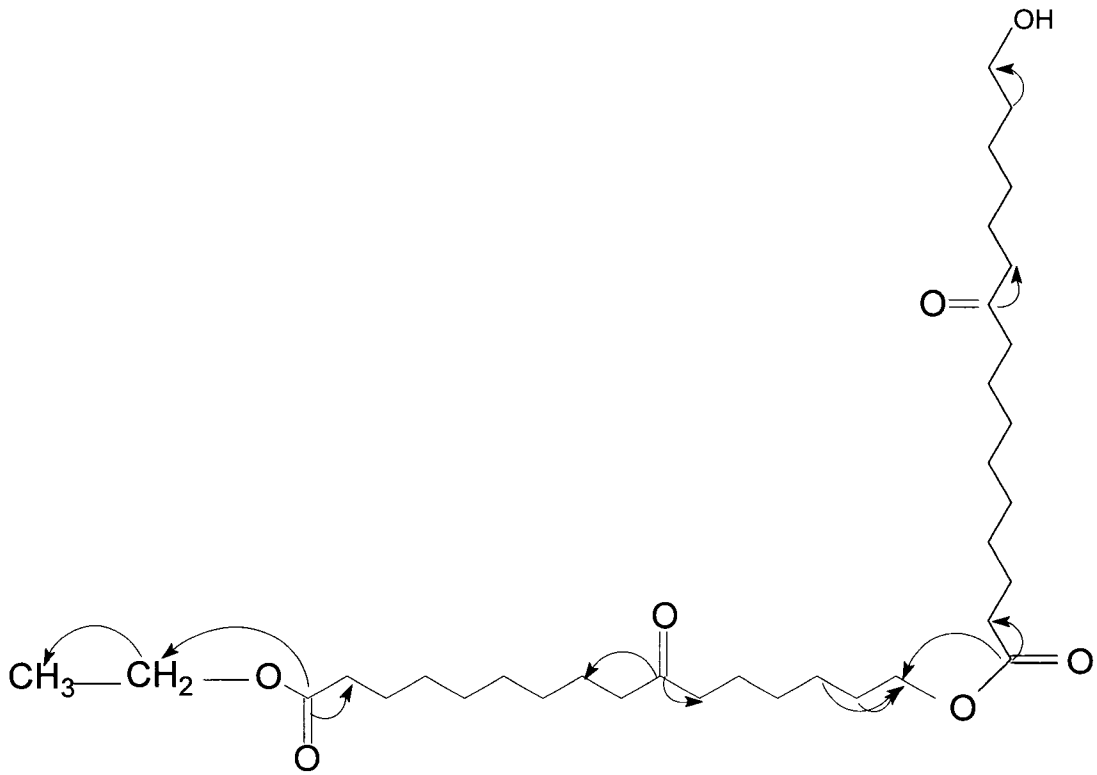

Figure 4.26. Structure of **Compound 7** and significant ^{1}H-^{13}C gHMBC (H to C) correlations.

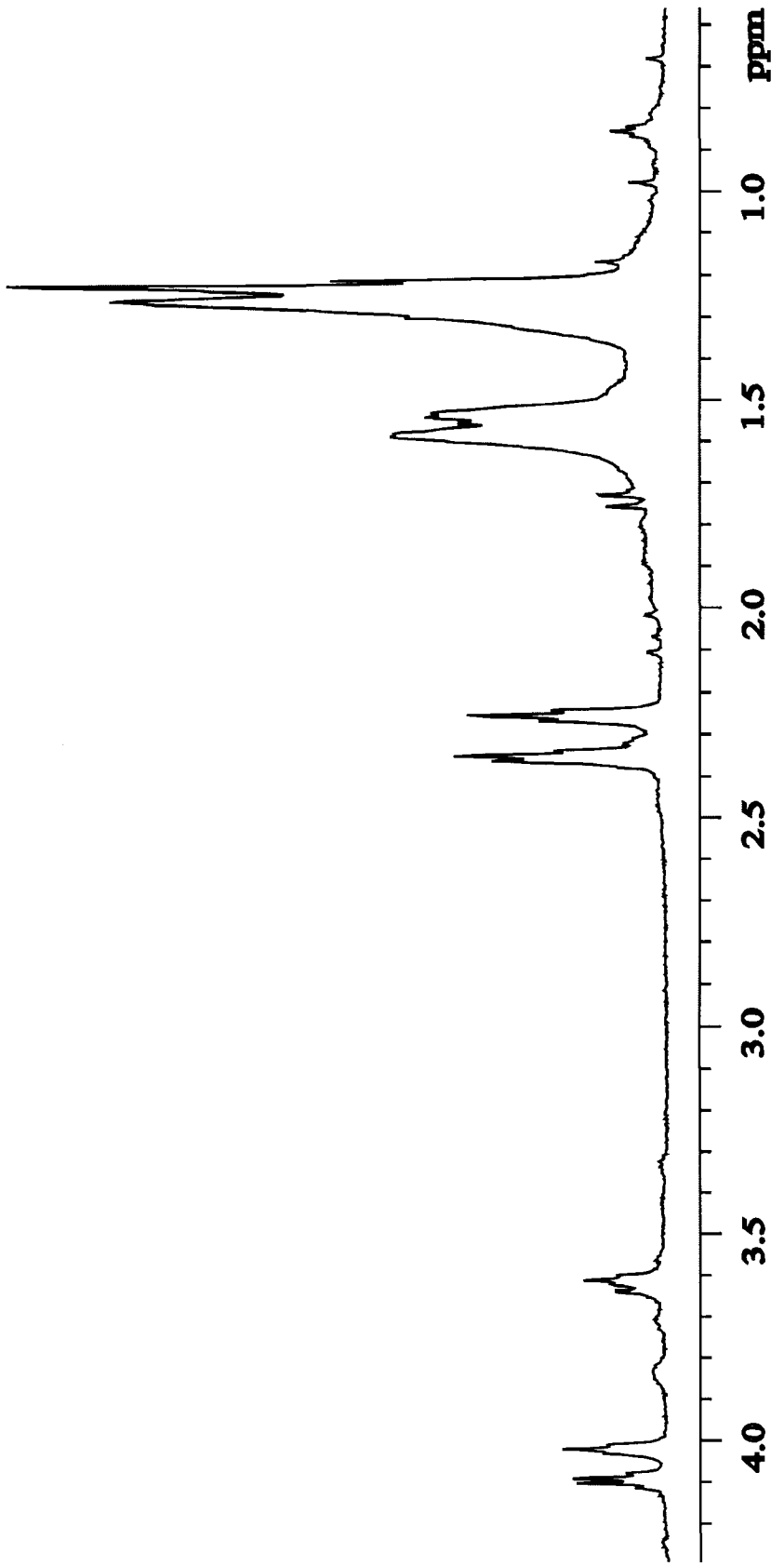

Figure 4.27. Proton NMR spectrum of **Compound 7** acquired with a nanoprobe on a 600 MHz spectrometer.

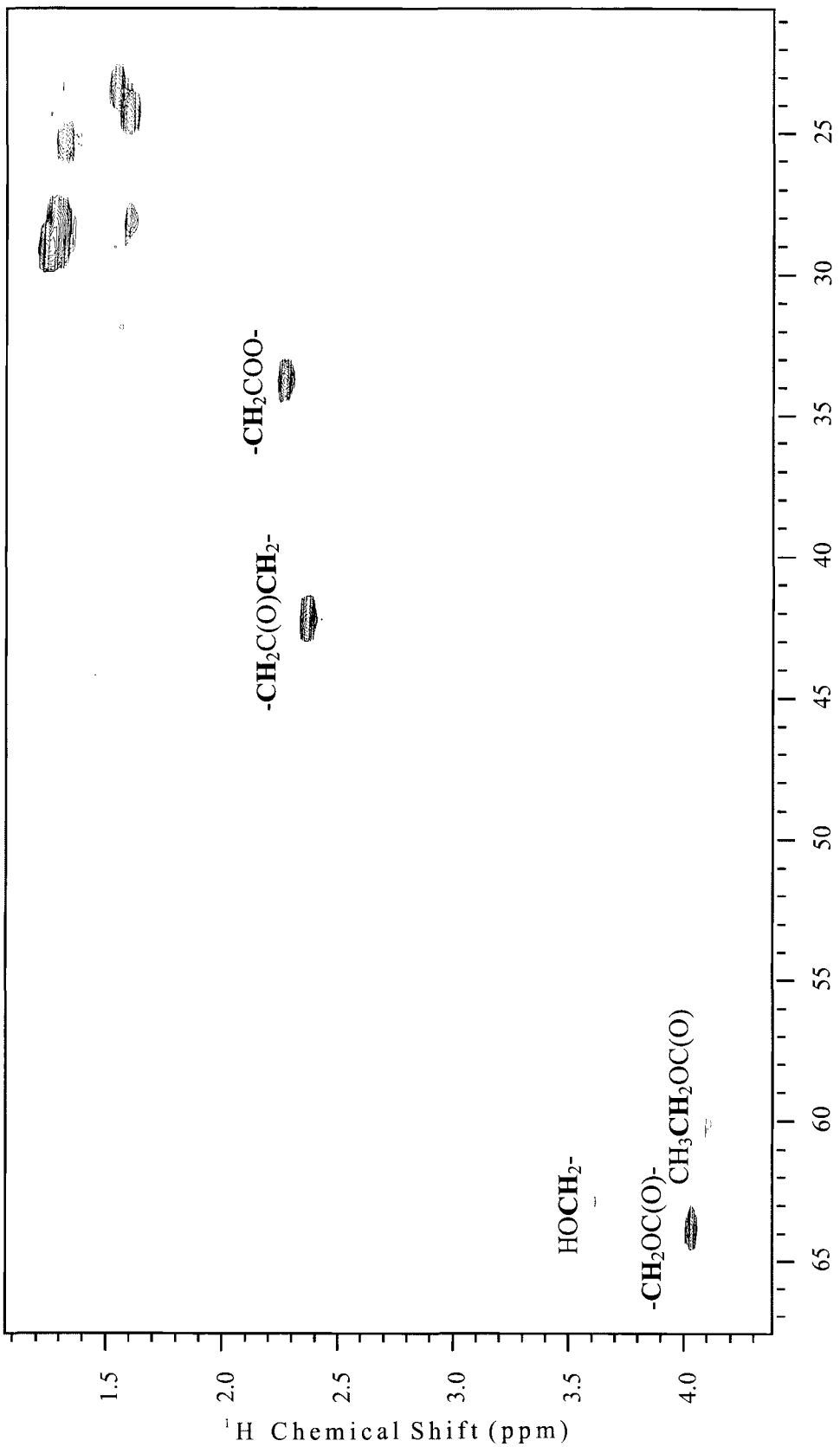

Figure 4.28. One-bond correlation (gHMQCs) NMR spectrum of **Compound 7** acquired with a nanoprobe on a 600 MHz spectrometer.

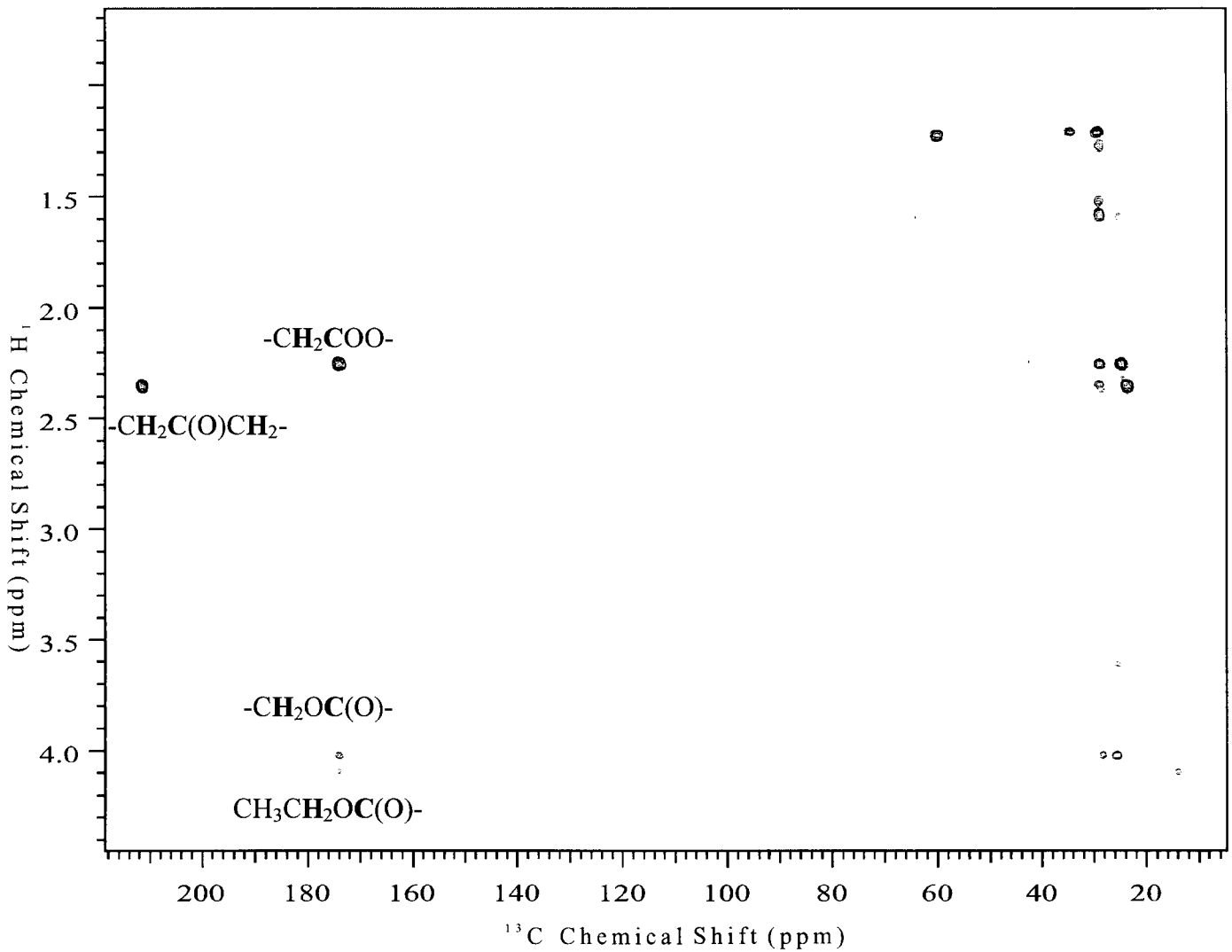

Figure 4.29. Multiple-bond correlation (gHMBCs) NMR spectrum of Compound 7 acquired with nano-probe on 600 MHz Spectrometer.

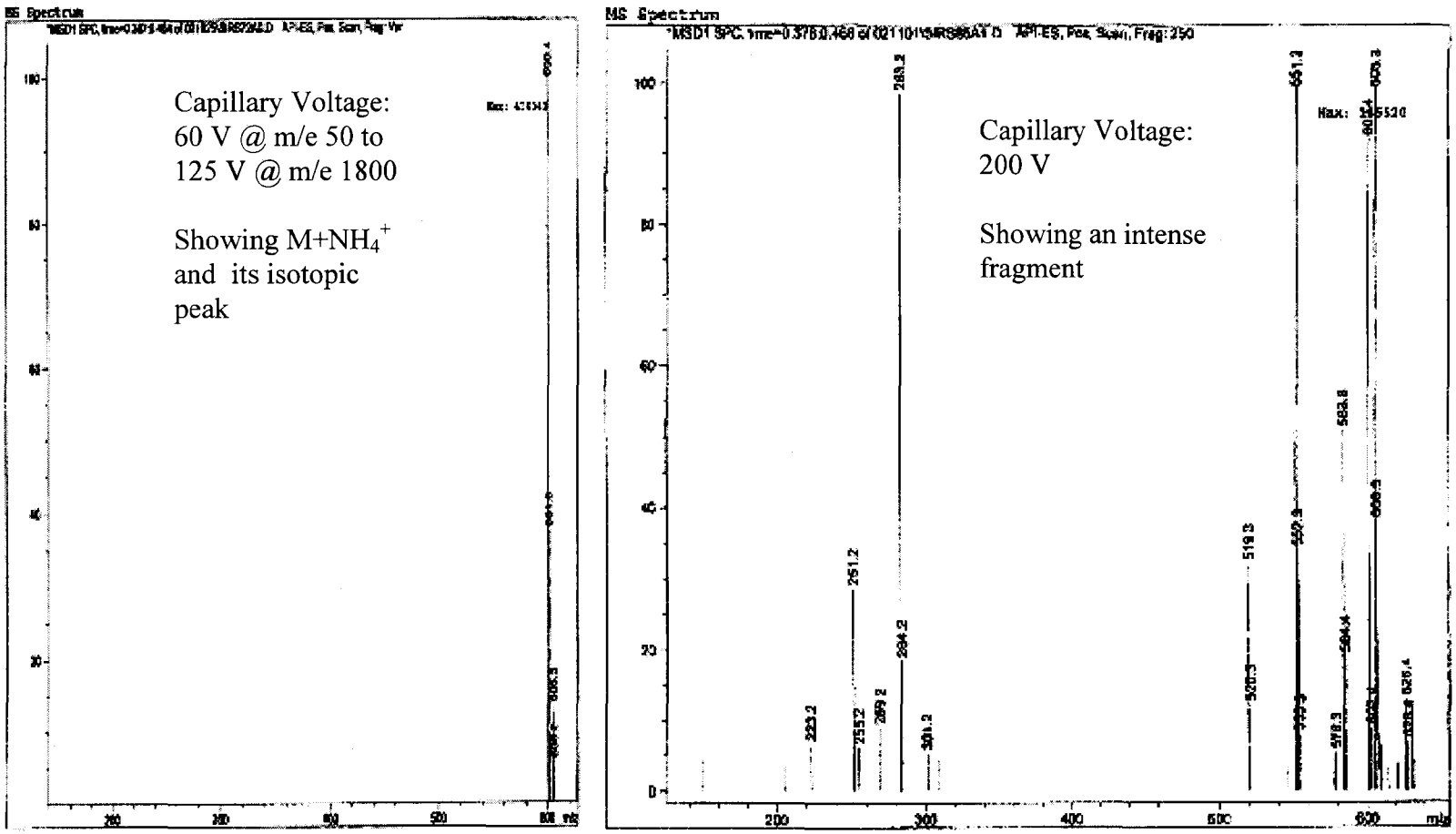

Figure 4.30. ESI/MS of **Compound 7**, showing ion intensity vs. mass-to-charge ratio.

Compound 8 was separated and purified in two ways – reversed phase HPLC and normal phase HPLC. Sample C1_14_30 was separated on a C18 HPLC column using gradient elution with acetonitrile:water = 30:70 to 100% acetonitrile in 60 minutes (Figure 4.31). Fraction 30 was collected between 44.7 and 46.3 minutes with a flow rate of 1.0 mL/min. Sample C1_14_2_10_5_2 was obtained from several steps of separation of C1_14 on a silica gel HPLC column (Figure 4.32). The gradient eluent used for the last step of separation was acetone:hexanes increased from 13:87 to 15:85 in 20 minutes with a flow rate of 1.0 mL/min. Sample C1_14_2_10_5_2 should be purer than C1_14_30 because it was obtained after more separation steps and displays a single peak in the purity test with HPLC (Figure 4.33).

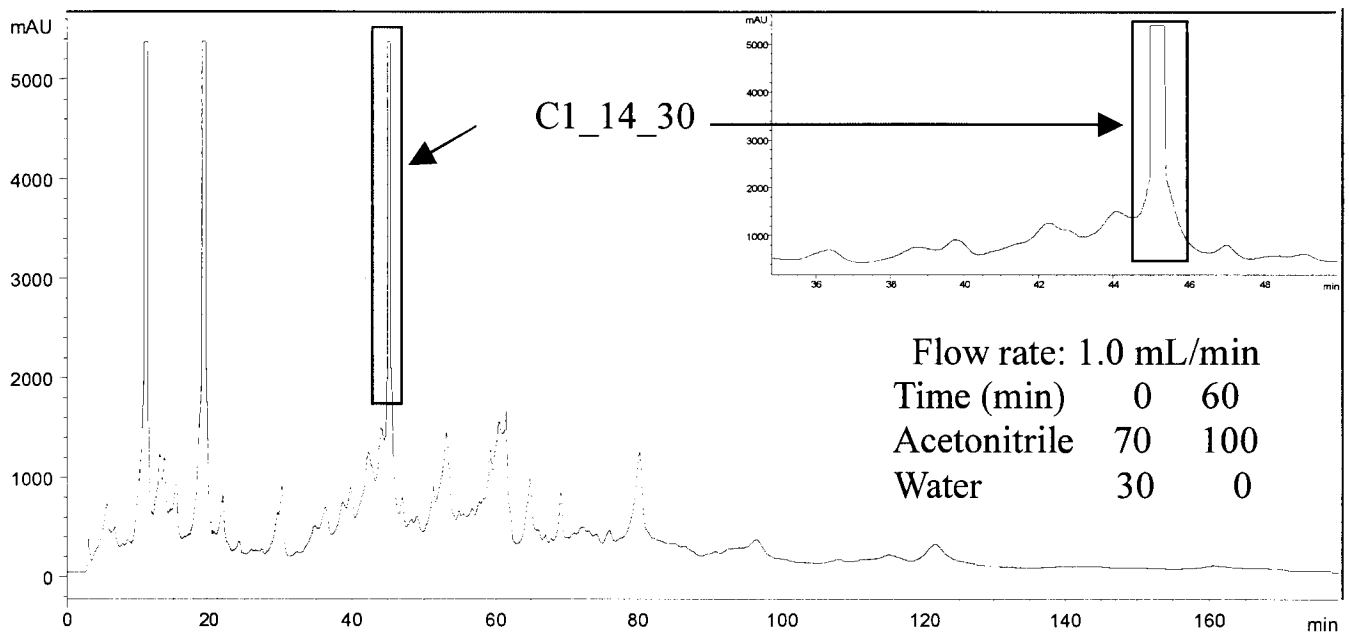

Figure 4.31. HPLC spectrum showing separation of C1_14 on a reversed phase column.

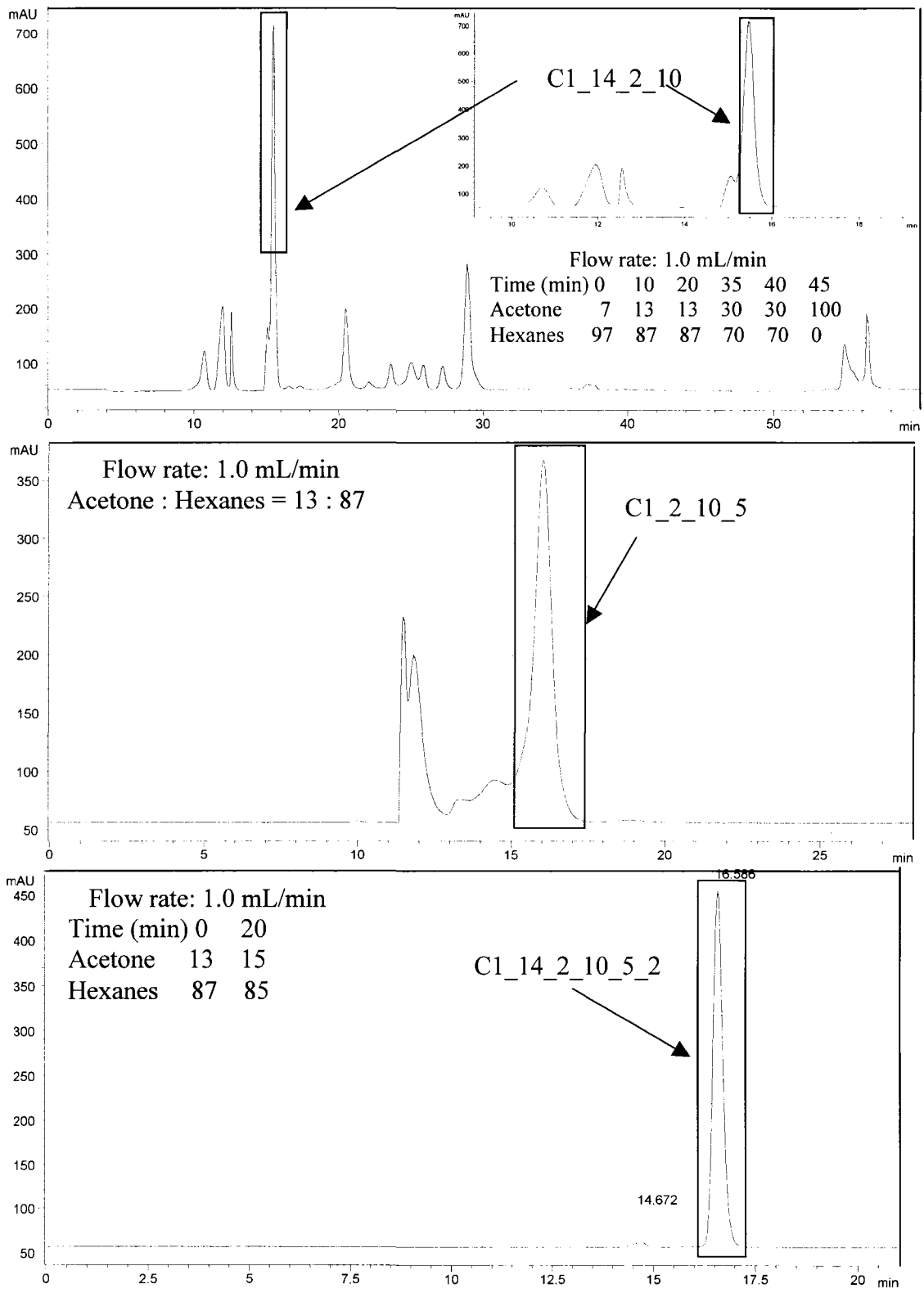

Figure 4.32. HPLC spectra showing separation of C1_14 on a normal phase HPLC column.

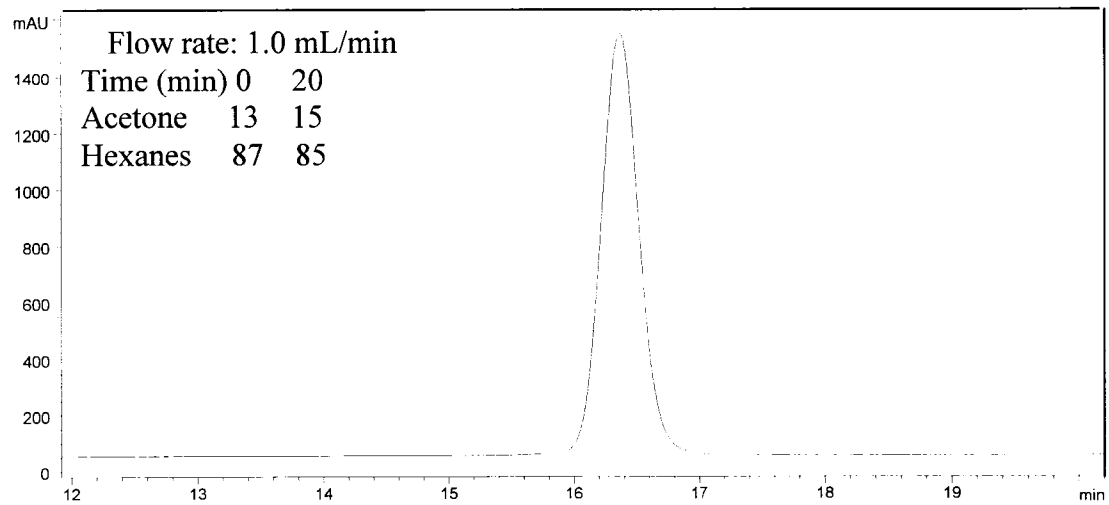

Figure 4.33. Purity test of C1_14_2_10_5_2 with HPLC.

Compound 8 was elucidated as a dimer consisting of a 16-carbon dicarboxylic acid monomer and an oxo-substituted common 16-carbon monomer (Figure 4.34). **Compound 8** has the same molecular weight as **Compound 7**, but the lack of a ^{1}H NMR peak at 3.60 ppm suggests that there is no free primary alcohol functional group in the sample, and the integration of protons in the ^{1}H spectrum (Table 4.7) shows that there are two methoxyl groups in the molecule (Figure 4.35).

The molecular ion ($M+NH_4^+$) and fragments from cleavages 'a' and 'b' were found in ESI MS (Figure 4.36). Cleavage at position 'a' generates a fragment with m/e of 283, whereas cleavage at position 'b' generates a fragment with m/e of 551. The electrospray ionization MS (ESI-MS) exhibited three types of molecular ions: 583 ($M+H^+$), 600 ($M+NH_4^+$), and 605 ($M+Na^+$) (Figure 4.36). The ^{13}C isotopic peak for $M+NH_4^+$ (m/e 601), which has an intensity 38% of that of the molecular ion peak, is consistent with the calculated value of 37.5% for the proposed structure. No fragments from cleavage around the oxo group were obtained even with a capillary

voltage of 200 V. Positions of the oxo groups were assumed based on monomer structures of the component monomers.

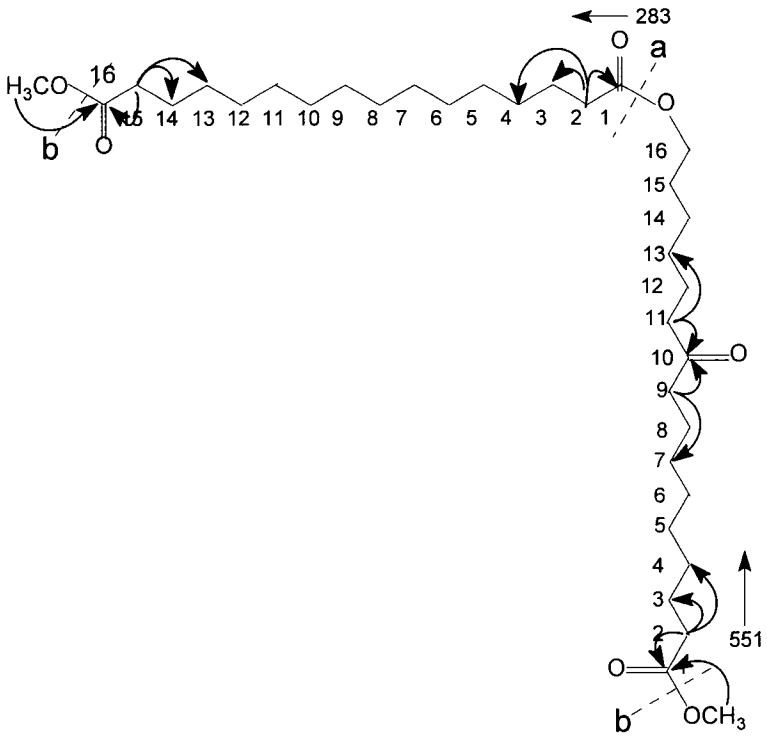

Figure 4.34. Structure and gHMBC correlations of **Compound** 8.

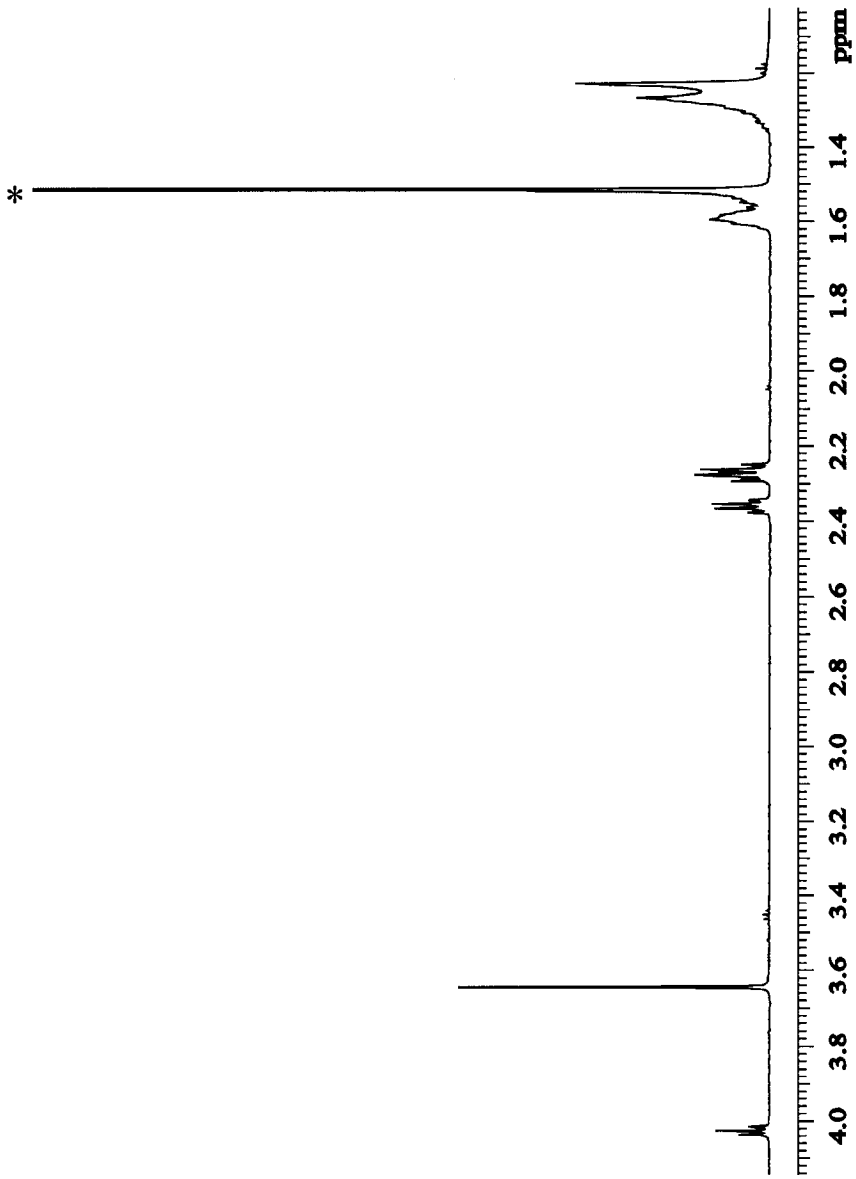

Figure 4.35. 600 MHz ^{1}H NMR spectrum of **Compound 8**.

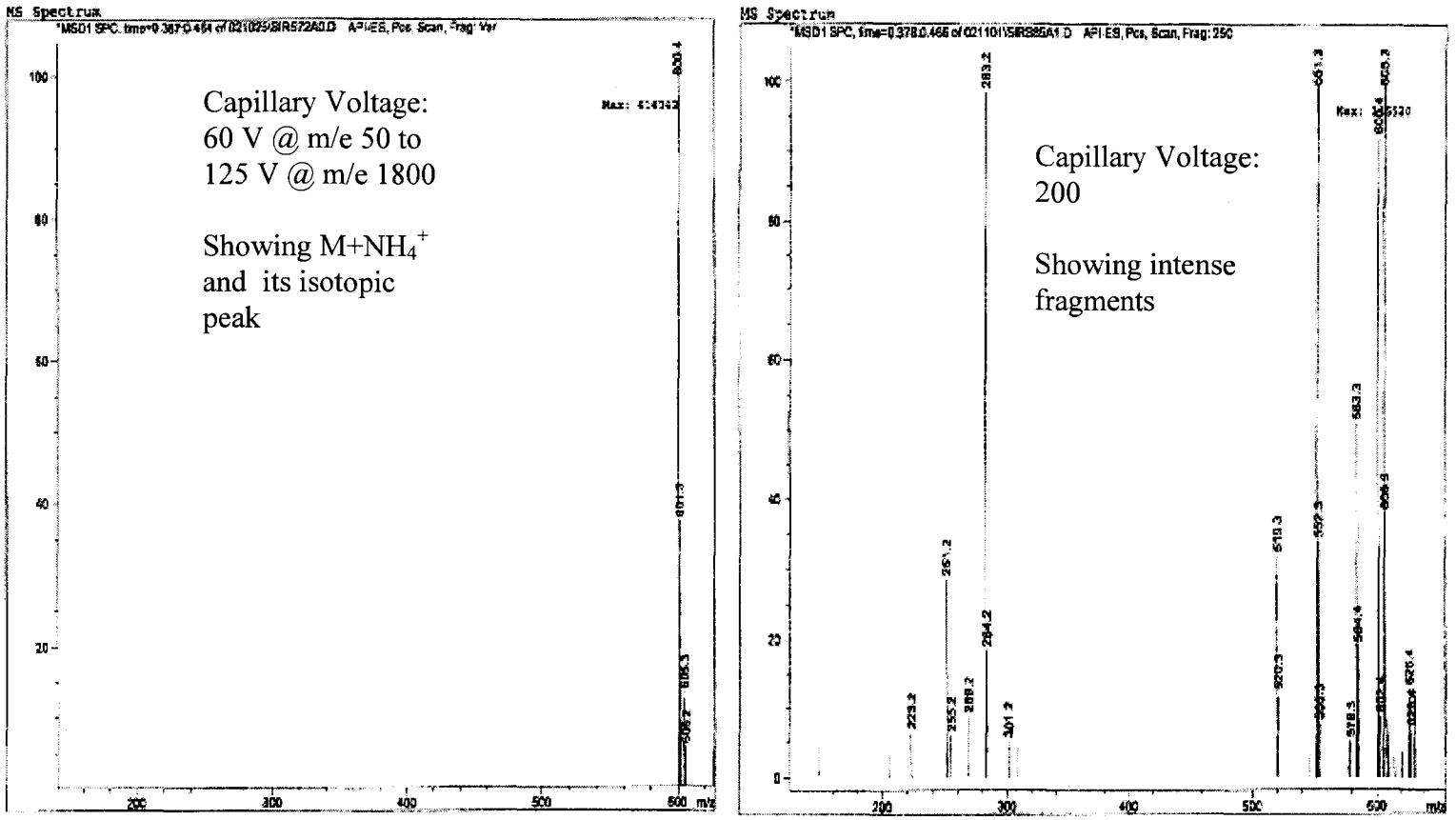

Figure 4.36. ESI- MS of **Compound 8**, showing ion intensity vs. mass-to-charge ratios.

The proton NMR integrals (Table 4.7) agree with this structure. The peak at 1.52 ppm in ^{1}H NMR spectrum (marked with *) (Figure 4.35) comes from water in the solvent, $CDCl_3$. This peak is very close to the sample peak at 1.6 ppm, and it will thus affect the integral of that peak. The disagreements between the calculated values of number of protons and those of found in the experiments may be due to interference from impurities. More evidence for the structure was obtained from its 600 MHz 2D NMR spectra. Gradient-assisted heteronuclear multiple-bond (long-range) correlation (gHMBC) gives information on ^{1}H-^{13}C pairs 2 -3 bonds apart. In its HMBC (Figure 4.37), **Compound 8** shows the following diagnostic correlations: $CH_3OC(O)$- (3.64 ppm, 173.8 ppm), -$CH_2C(O)CH_2$- (2.37 ppm, 211.0 ppm), and -CH_2COO- (2.27 ppm, 173.8 ppm). Correlations for the bulk methylene groups were also seen. The expected cross peak of the ^{13}C at 173.9 ppm with the ^{1}H at 4.04 ppm was missing, possibly because the oxygen atom between the carbonyl carbon and the methylene protons makes the coherence transfer between the carbon and the protons less efficient. This cross peak is usually much weaker than other cross peaks such as -CH_2COO- (2.27 ppm, 173.8 ppm). The other HMBC correlations are marked on the structure of **Compound 8** (Figure 4.34).

Table 4.7. Chemical Shifts and Integrals for **Compound 8**.

Chem Shift (ppm)	4.03	3.65	2.38	2.28	1.60*	1.27~1.23
Integral Found	3	6	5	8	12	42
Calc Integral	2	6	6	6	8	34

* Includes contributions from water at 1.52 ppm.

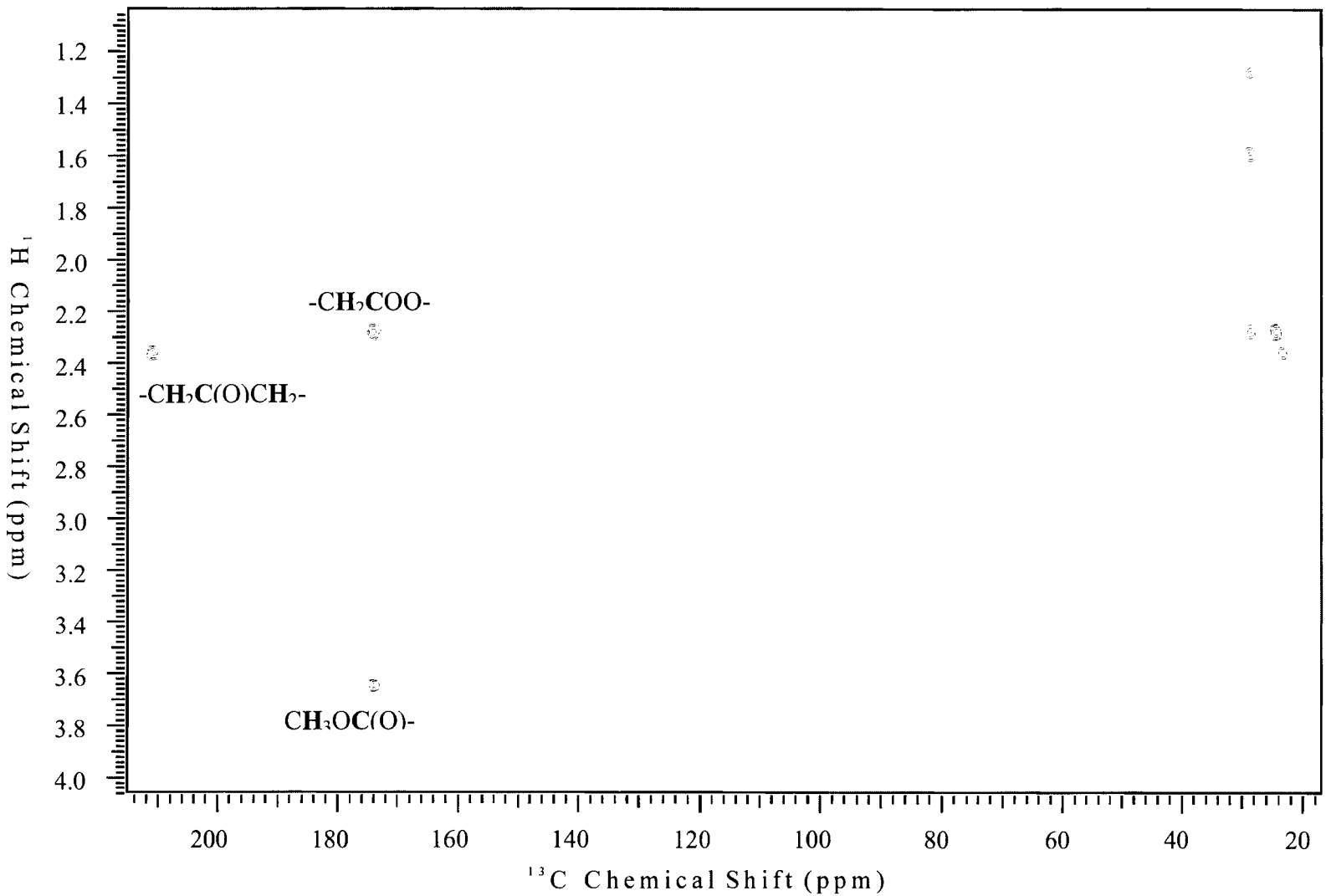

Figure 4.37. gHMBC of **Compound 8**.

Compound 9 was elucidated as a new dimer of two C18 monomers (Figure 4.38). Molecular ions corresponding to ($M+NH_4^+$) and ($M+Na^+$) were observed in ESI-MS at m/e 628 and 633, respectively (Figure 4.39). One monomer lacks mid-chain functional groups, whereas the other one has one oxo group in the chain. The position of the mid-chain oxo group cannot be determined in the absence of MS fragmentation. This compound was found in a mixture. The amount of sample was insufficient for further separation and purification, but its molecular weight, the polarity as deduced from HPLC, and the other isolated compounds all support this provisional structure.

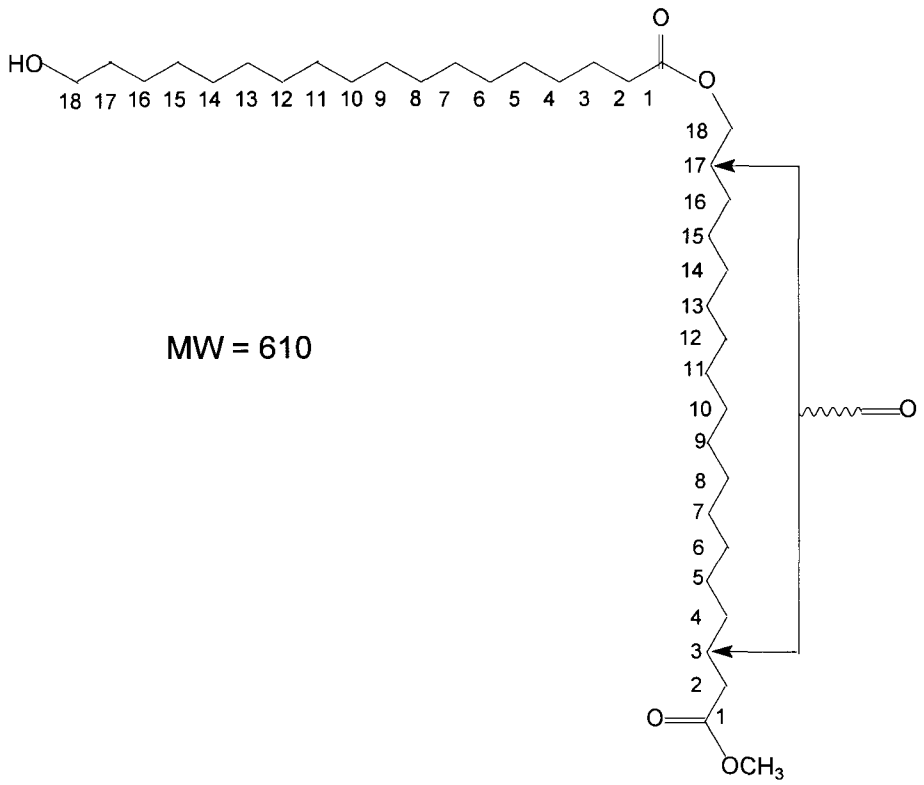

Figure 4.38. Provisional structure of **Compound 9**.

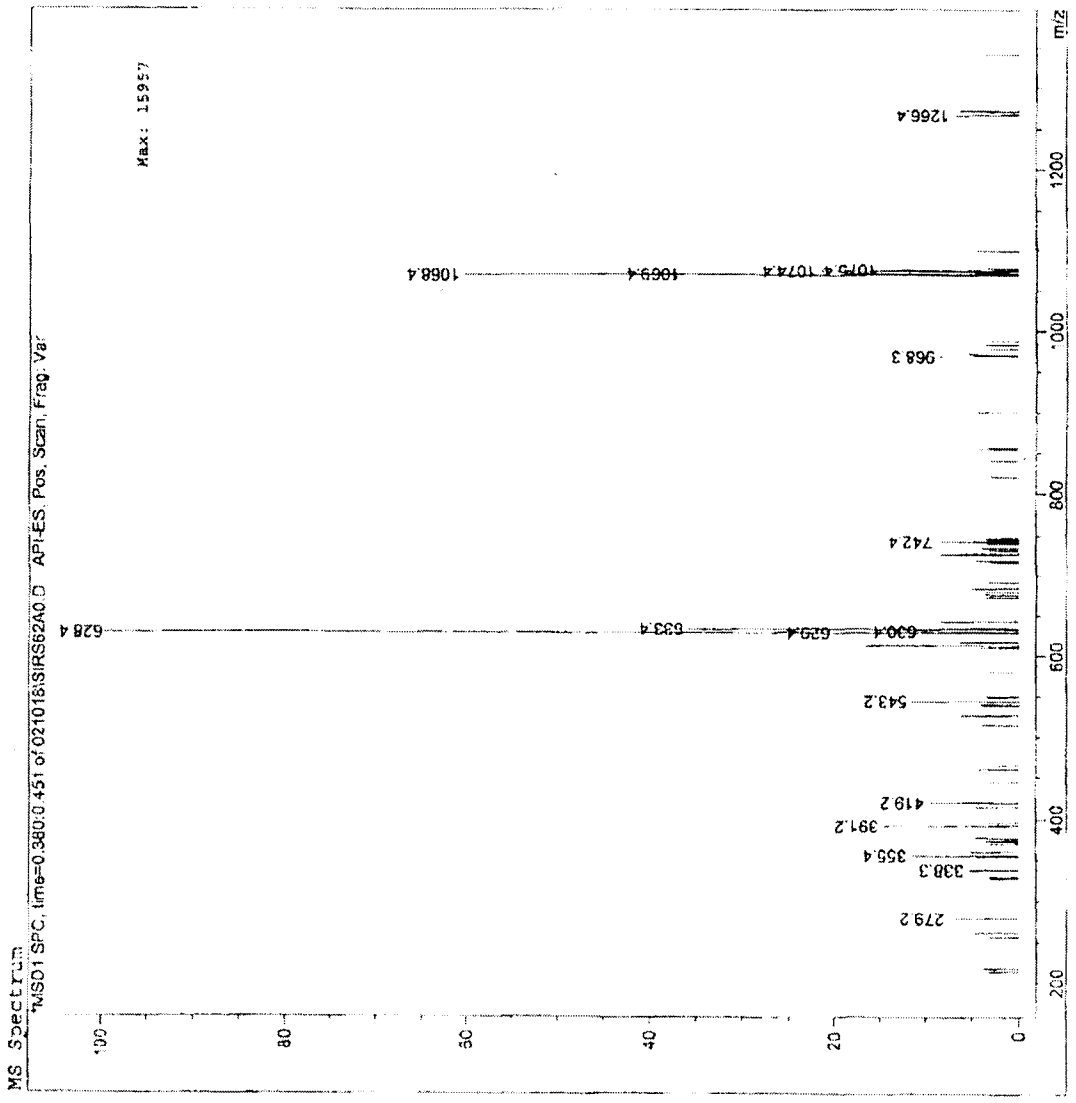

Figure 4.39. ESI/MS of **Compound 9**, showing ion intensities vs. mass-to-charge ratios.

Compound 10 was elucidated as a dimer consisting of a C18 monomer and a C20 monomer (Figure 4.40). Molecular ions corresponding to ($M+NH_4^+$) and ($M+Na^+$) were observed in ESI-MS at m/e 656 and 661, respectively (Figure 4.41). The C20 monomer has no mid-chain functional groups, and the C18 monomer has one oxo group in the chain. The position of the mid-chain oxo group cannot be determined because no fragments were observed in the MS. This sample is pure by MS criteria, but there is not enough sample for NMR measurements, even in a nanotube. The polarity of this compound deduced from the HPLC separation also supports this provisional structure.

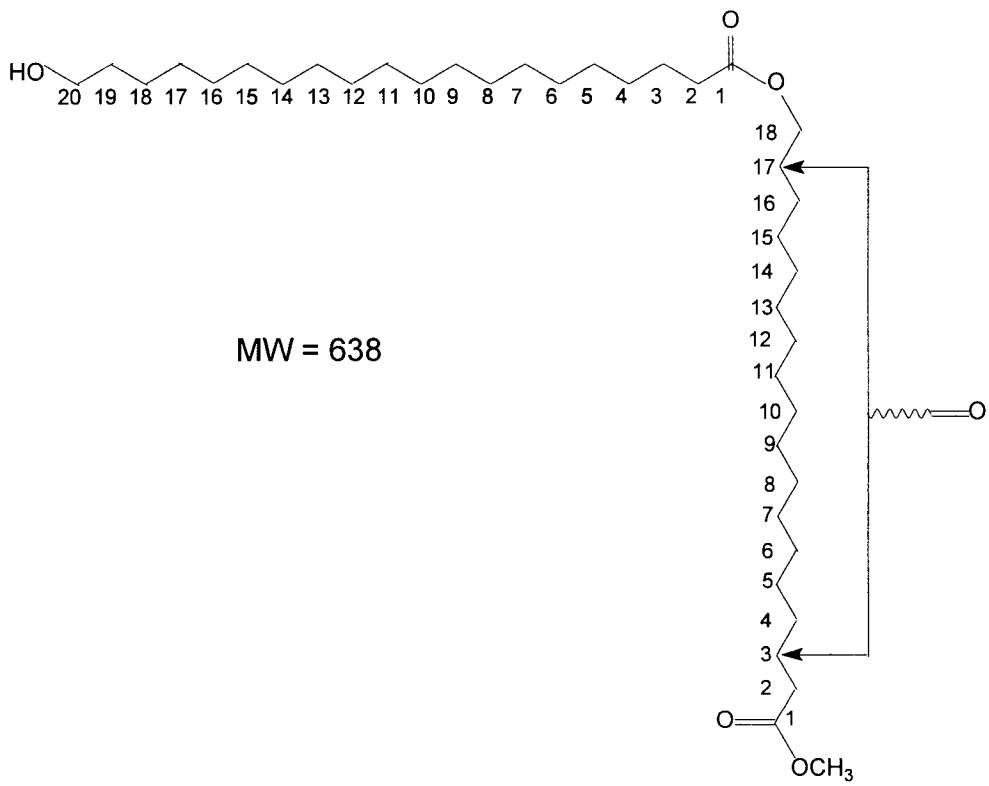

Figure 4.40. Provisional structure of a **Compound 10**.

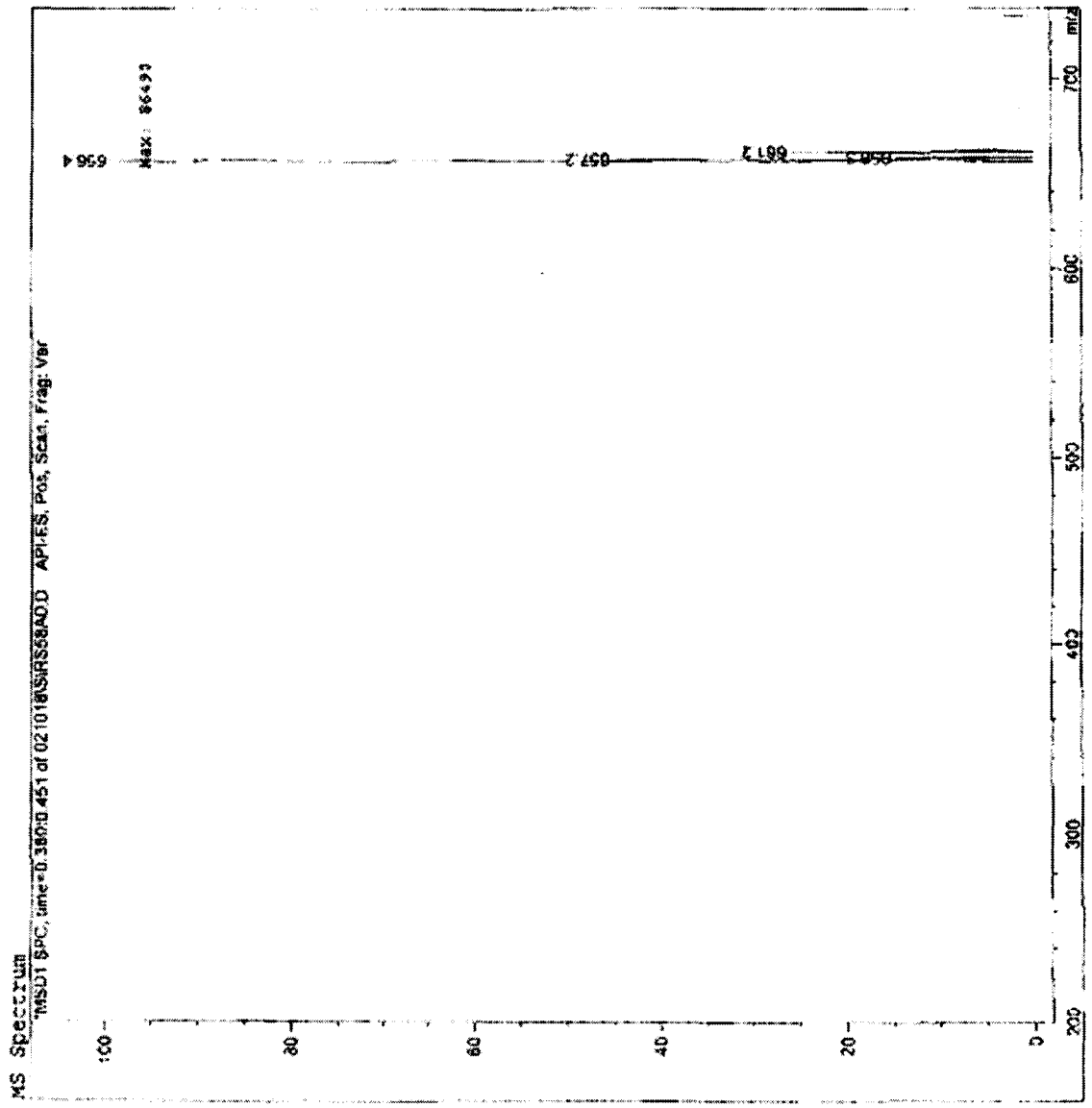

Figure 4.41. ESI/MS of **Compound 10**, showing ion intensities vs. mass-to-charge ratios.

4. 1.2.3 Separation and identification of trimers in lime cutin

Some of the oligomers from KOH or HF treatment of cutin were separated with high performance thin layer chromatography (HPTLC), and the others were obtained from HPLC separation. Five trimers were separated and identified by the HPLC method. The constituents of the trimers were determined with NMR and MS data, but the sequences of the monomers within the trimers remain undetermined because of the lack of fragmentation data from MS. All of the trimers have a methyl ester at the carboxylic acid end and a free alcohol at the other end.

Compound 11 from KOH degradation consists of one unit of 10,16-dihydroxyhexadecanoic acid and two units of 10-oxo-16-hydroxyhexadecanoic acid (Figure 4.42). The positions of the functional groups in the middle of the chain were assumed on the basis of the known monomer structures. Molecular ions corresponding to $M+NH_4^+$ (m/e 856) and $M+Na^+$ (m/e 861) were found in ESI-MS spectrum (Figure 4.43). No $M+H^+$ molecular ion or fragments were found. The ^{13}C isotopic peaks (molecular ions + 1) had intensities 55% of the original peaks, consistent with the determined trimer structure of 49 carbons. A ^1H NMR multiplet at 3.56 ppm was diagnostic for the secondary alcohol group, and a singlet at 3.64 ppm was diagnostic for methyl groups of the terminal ester bonds (Figure 4.44). The proton NMR integrals generally support the determined structure (Table 4.8). The relatively large difference between experimental and theoretical values for the integral of the peak at 3.56 ppm could reflect a greater relative error due to its weak intensity and much broader peak shape. A cross peak is also observed for the secondary alcohol group at (3.56 ppm, 71.9 ppm) in the gHMQC of **Compound 11**

(Figure 4.45). A cross peak between the carbons of the secondary alcohol groups and the protons in the adjacent methylene carbons in the gHMBC spectrum at (1.39 ppm, 71.9 ppm) also provides strong evidence for the existence of a secondary alcohol group in this compound (Figure 4.46). There are no cross peaks involving protons of the secondary alcohol groups observed in the gHMBC spectrum, presumably because there is only a weak signal for the secondary proton. In its gHMQC spectrum, **Compound 11** shows other diagnostic correlations: -**CH_2**OC(O)- (4.03 ppm, 63.8 ppm), -**CH_2**C(O)CH_2- (2.36 ppm, 42.4 ppm), HO**CH_2**- (3.64 ppm, 63.1 ppm), and -**CH_2**COO- (2.26 ppm, 34.2 ppm). Correlations were also seen for the bulk methylene groups. A cross peak for ^{13}C at 173.9 ppm with ^{1}H at 4.03 ppm also supports the elucidated structure. The other HMBC correlations are marked on the proposed structure of **Compound 11** (Figure 4.42).

Table 4.8. Characteristic chemical shifts and integrals for **Compound 11**.

Chem Shift (ppm)	4.03	3.64	3.62	3.56	2.36	2.26
Integral Found	4	3	2	2	6	7
Calc Integral	4	3	2	1	8	6

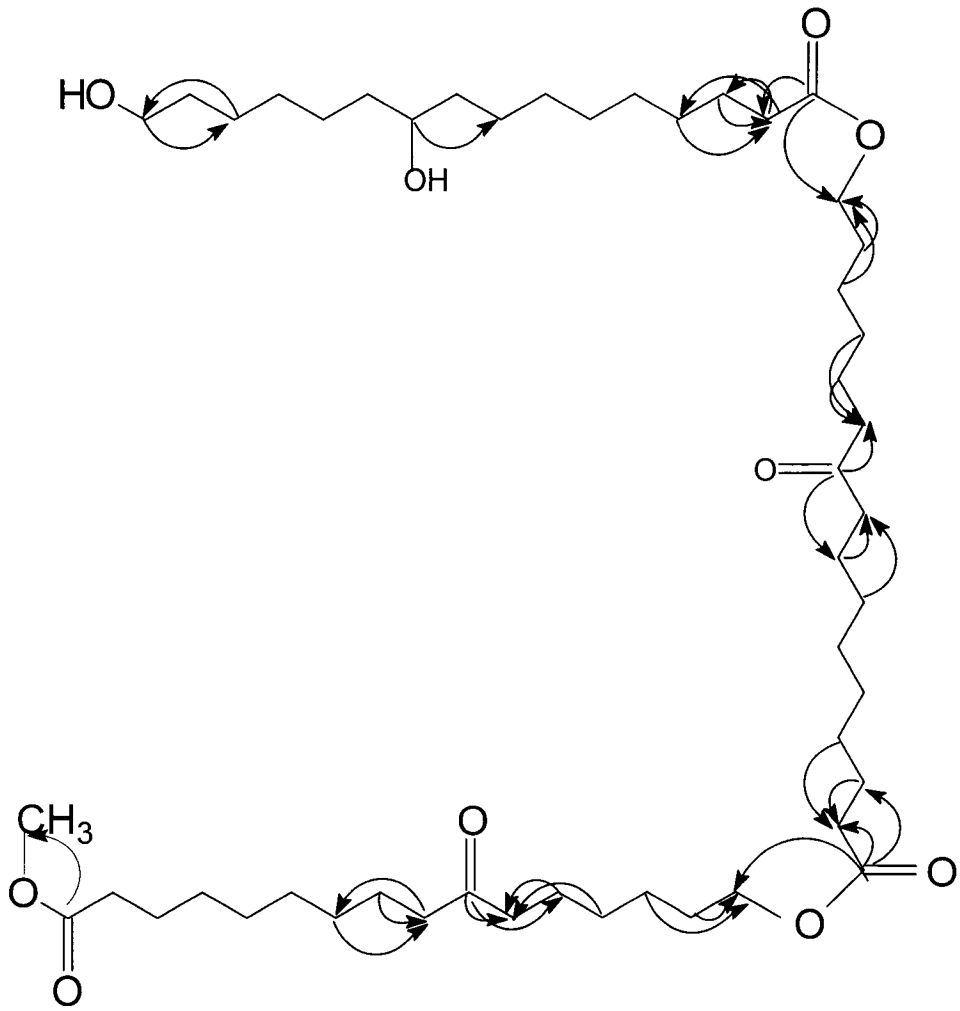

Figure 4.42. Provisional structure of **Compound 11**.

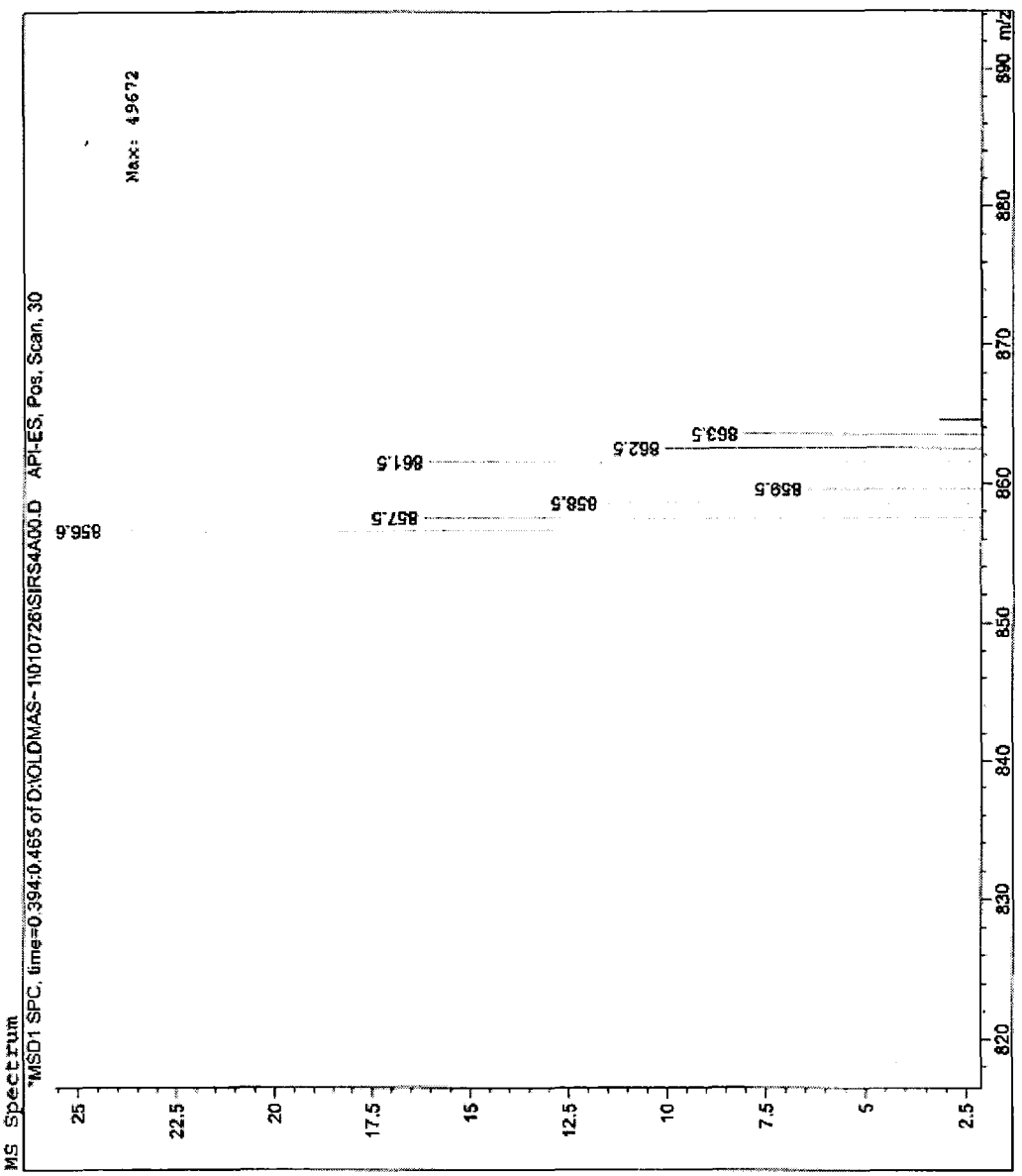

Figure 4.43. ESI/MS spectrum of **Compound 11**, showing ion intensities vs. mass-to-charge ratios.

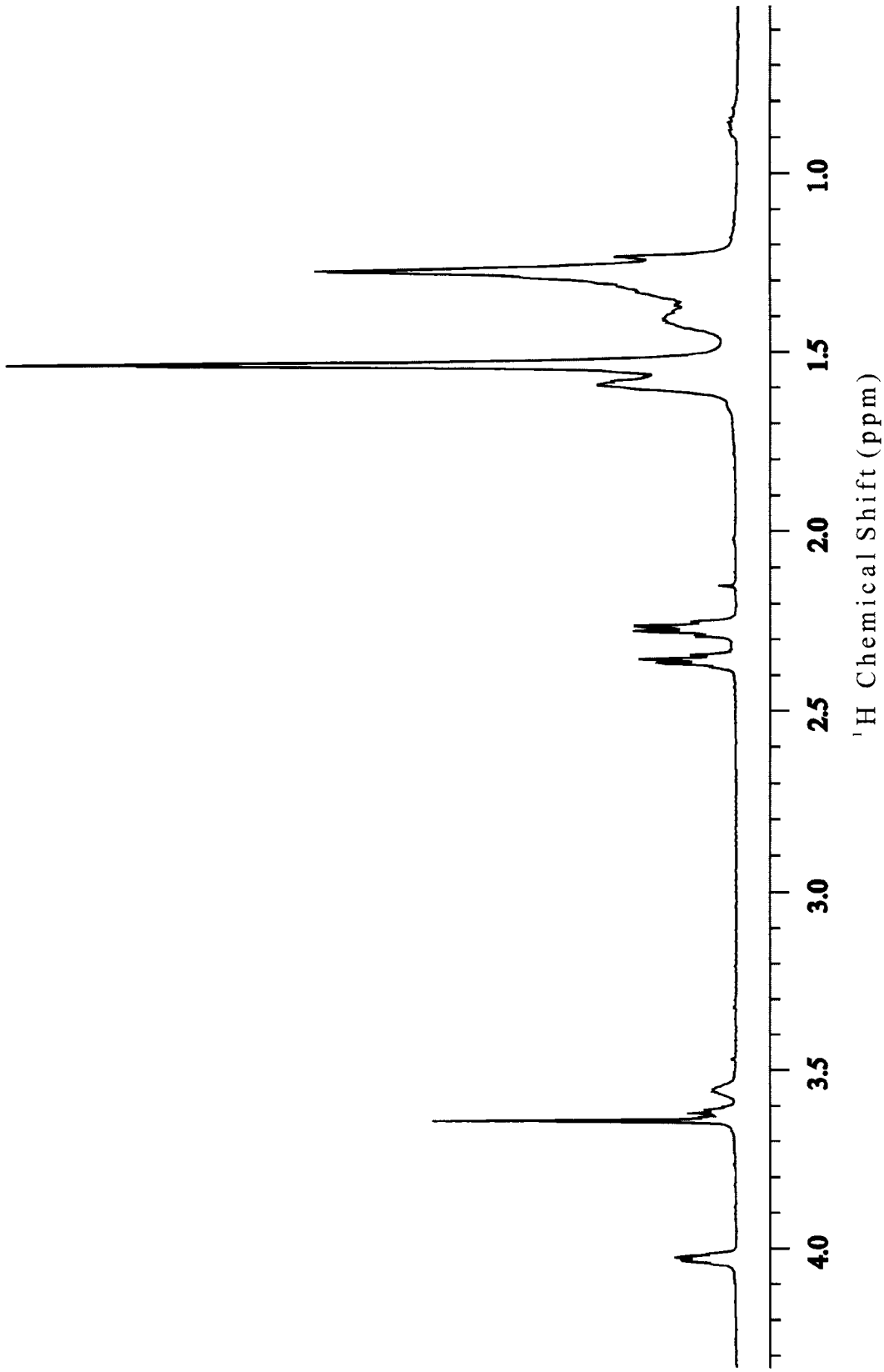

Figure 4.44. 600 MHz ^{1}H NMR spectrum of **Compound 11**.

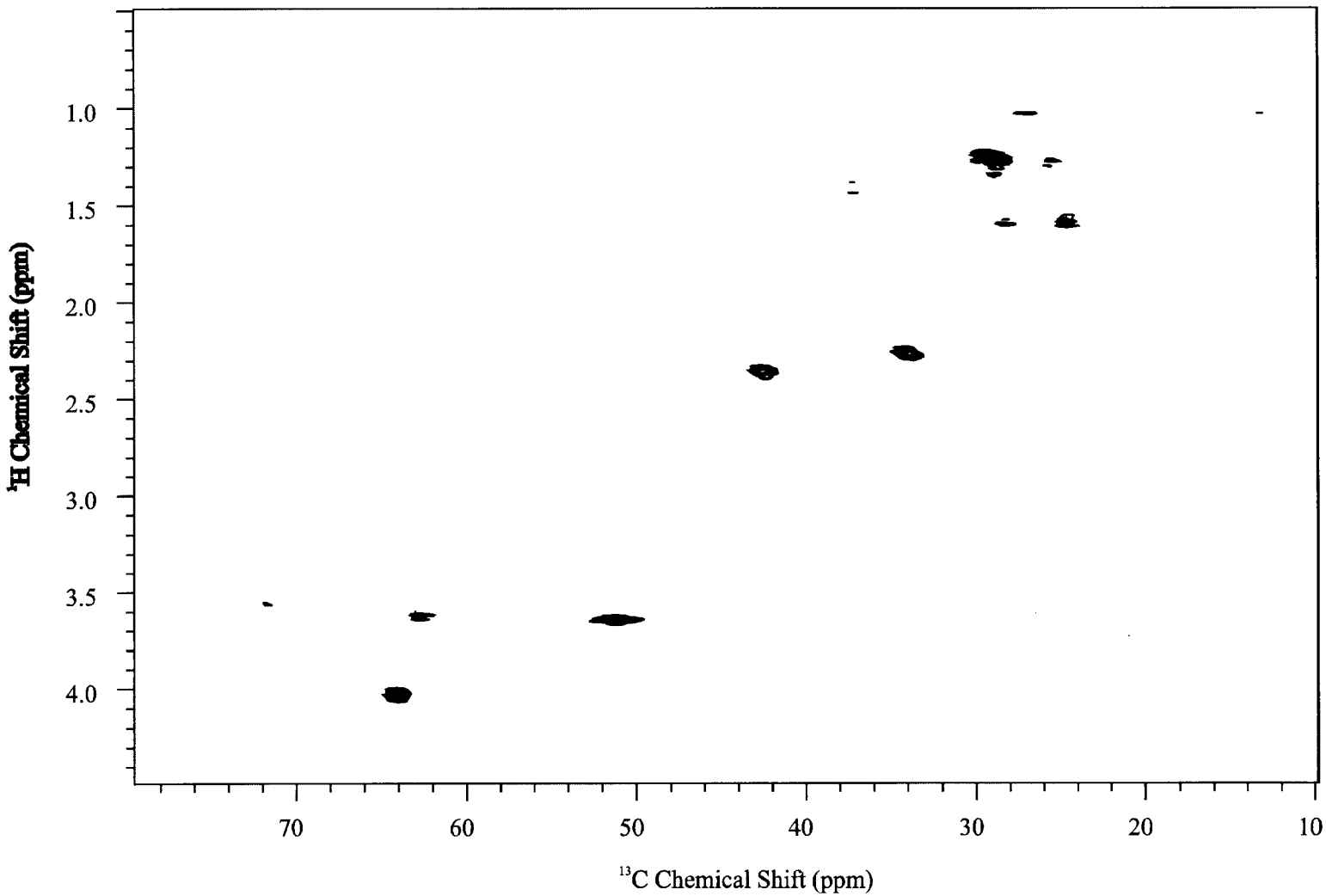

Figure 4.45. gHMQC spectrum of **Compound 11**.

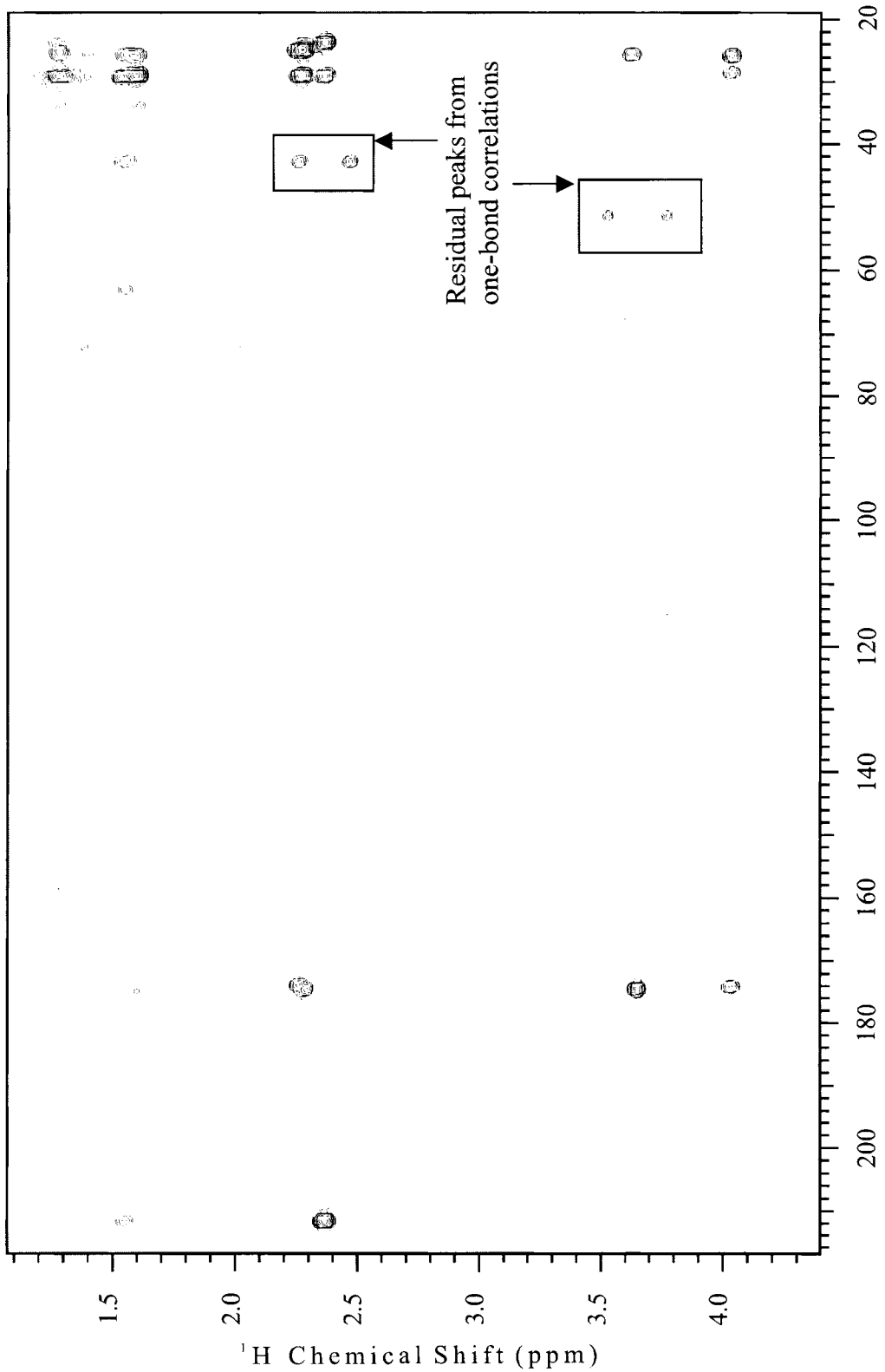

Figure 4.46. gHMBC spectrum of **Compound 11**.

Compound 12 from KOH degradation was elucidated as a trimer consisting of two units of 10,16-dihydroxyhexadecanoic acid and one unit of 10-oxo-16-hydroxyhexadecanoic acid (Figure 4.47). The positions of the functional groups in the middle of the chain were assumed on the basis of the known monomer structures. Molecular ions corresponding to $M+NH_4^+$ (m/e 858) and $M+Na^+$ (m/e 863) were found in ESI-MS spectrum (Figure 4.48). A peak corresponding to $M+H^+$ (m/e 841) was also observed, but no fragments were found (Figure 4.48). The ^{13}C isotopic peak intensity (molecular ions + 1) was about 55 % of the original peaks, consistent with the determined trimer structure containing 49 carbons. 1D (Figure 4.49) and 2D (Figures 4.50 and 4.51) NMR spectra of **Compound 12** are similar to those of **Compound 11**, as expected. The most significant difference is the ^1H NMR integrals for peaks 2.26 ppm and 3.56 ppm (Table 4.9), because **Compound 11** has two mid-chain oxo groups and one mid-chain secondary alcohol groups, whereas **Compound 12** has one mid-chain oxo group and two mid-chain secondary alcohol groups. Diagnostic peaks for secondary alcohol groups and for methyl groups of the terminal ester bonds were observed at 3.56 ppm and 3.64 ppm, respectively, in the 1D ^1H NMR spectrum. The cross peak for secondary alcohol groups at (3.56 ppm, 71.9 ppm) in the gHMQC (Figure 4.50) and the cross peak between the carbons of secondary alcohol groups and the protons on the adjacent methylene carbons at (1.39 ppm, 71.9 ppm) in the gHMBC spectrum (Figure 4.51) confirm the presence of secondary alcohol groups in this compound. There are no cross peaks observed to protons of the secondary alcohol groups observed in gHMBC, as noted previously for **Compound 11**. In gHMQC, **Compound 12** shows other diagnostic correlations:

-**CH$_2$**OC(O)- (4.04 ppm, 63.8 ppm), -**CH$_2$**C(O)**CH$_2$**- (2.36 ppm, 42.4 ppm), HO**CH$_2$**- (3.64 ppm, 63.1 ppm), and -**CH$_2$**COO- (2.26 ppm, 34.2 ppm). Correlations were also seen for the bulk methylene groups. A cross peak for ^{13}C at 173.9 ppm with ^{1}H at 4.04 also supports the structure as elucidated. The other HMBC correlations are marked on the structure of **Compound 12** (Figure 4.47).

Table 4.9. Characteristic chemical shifts and integrals for **Compound 12**.

Chem Shift (ppm)	4.03	3.64	3.62	3.56	2.36	2.26
Integral Found	4	3	2	2	5	8
Calc. Integral	4	3	2	2	4	6

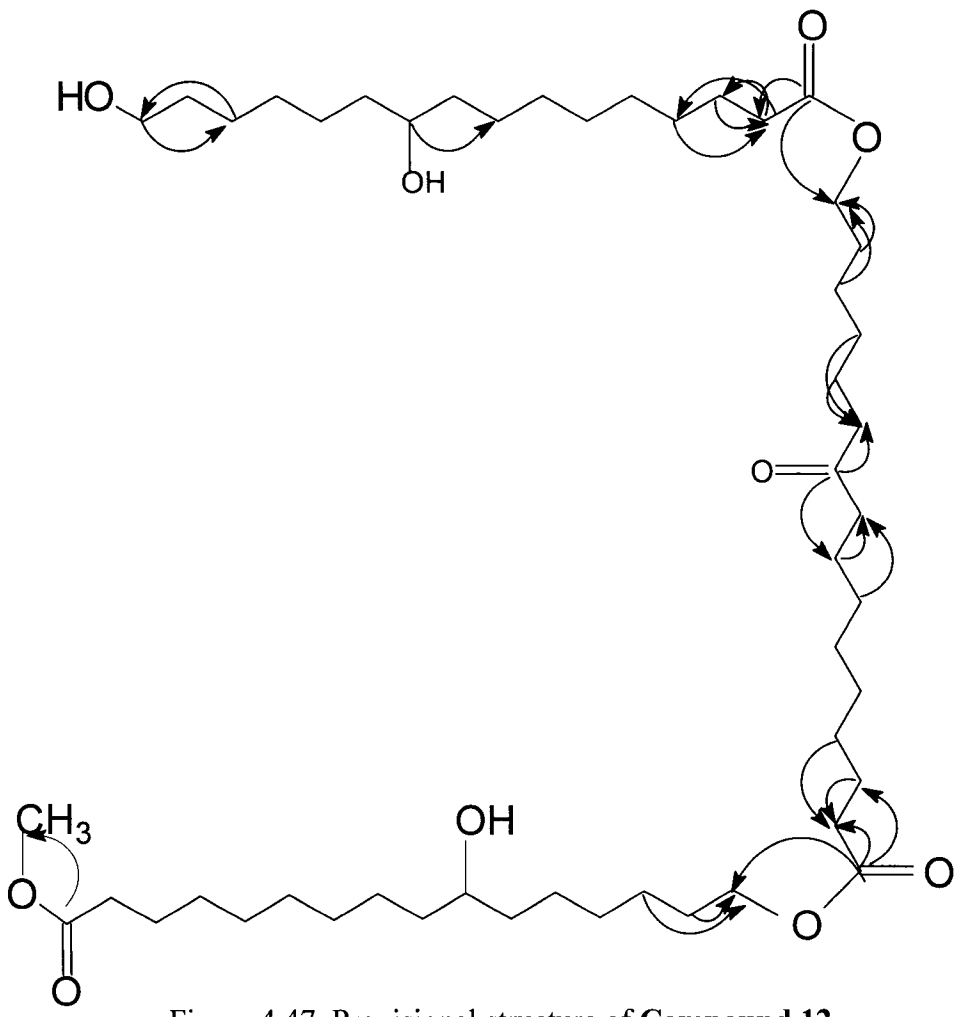

Figure 4.47. Provisional structure of **Compound 12**.

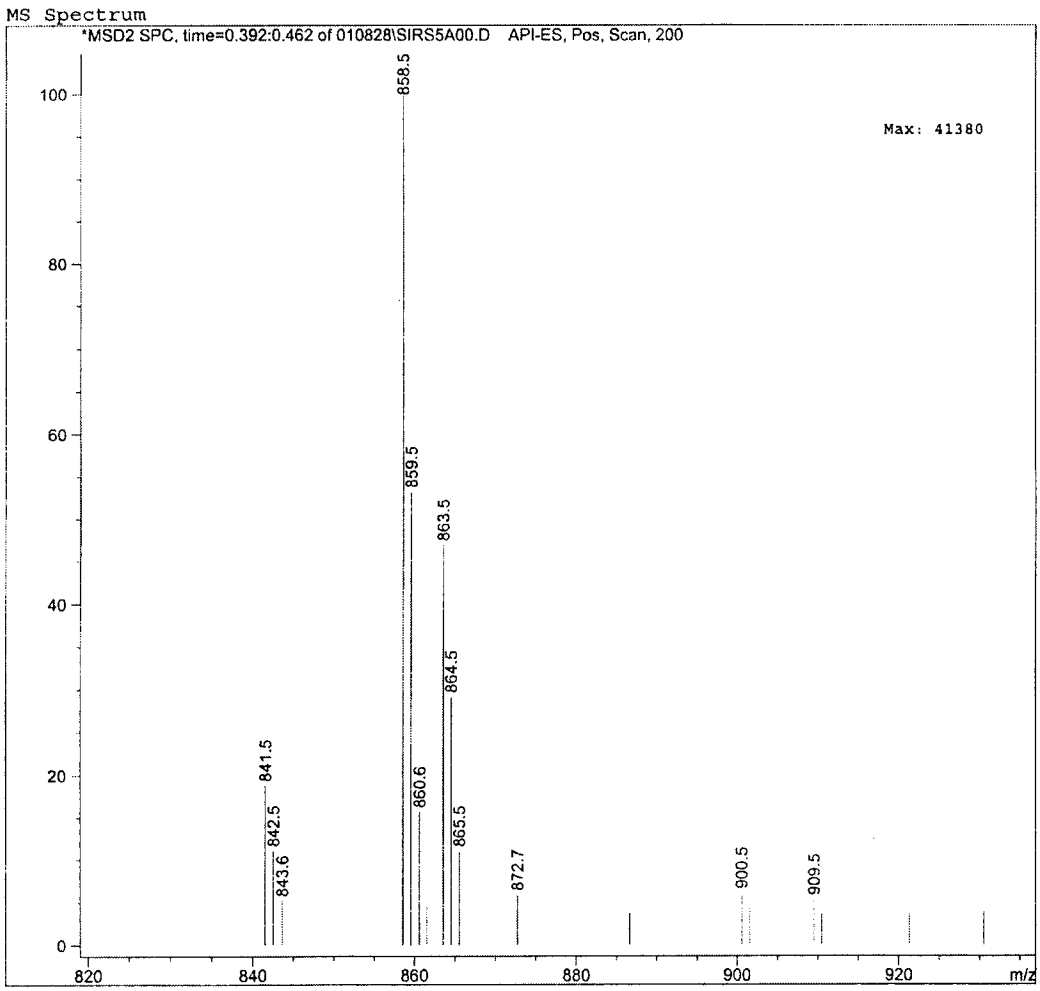

Figure 4.48. ESI/MS spectrum of **Compound 12**, showing ion intensities and mass-to-charge ratios.

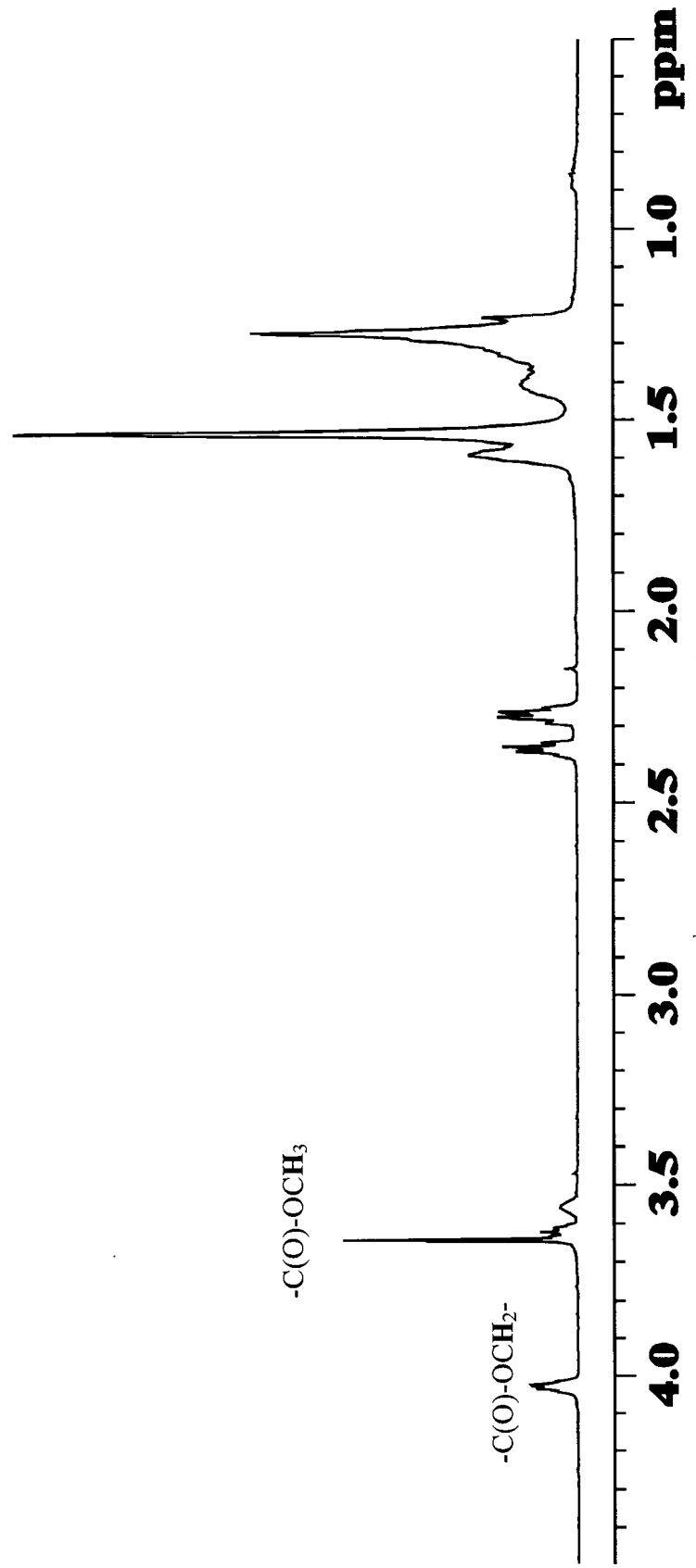

Figure 4.49. 600 MHz ^{1}H NMR spectrum of **Compound 12**.

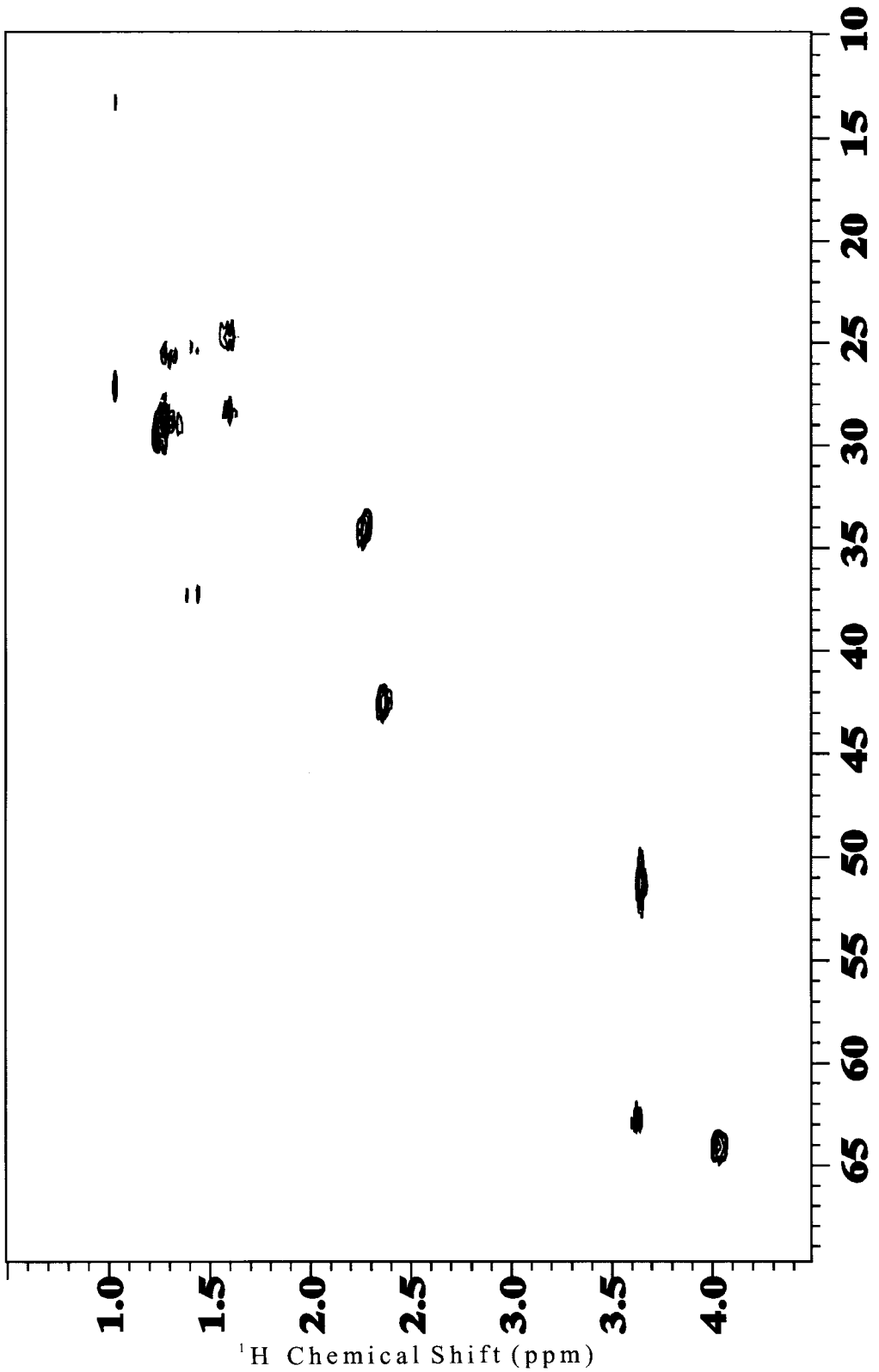

Figure 4.50. gHMQC spectrum of **Compound 12**.

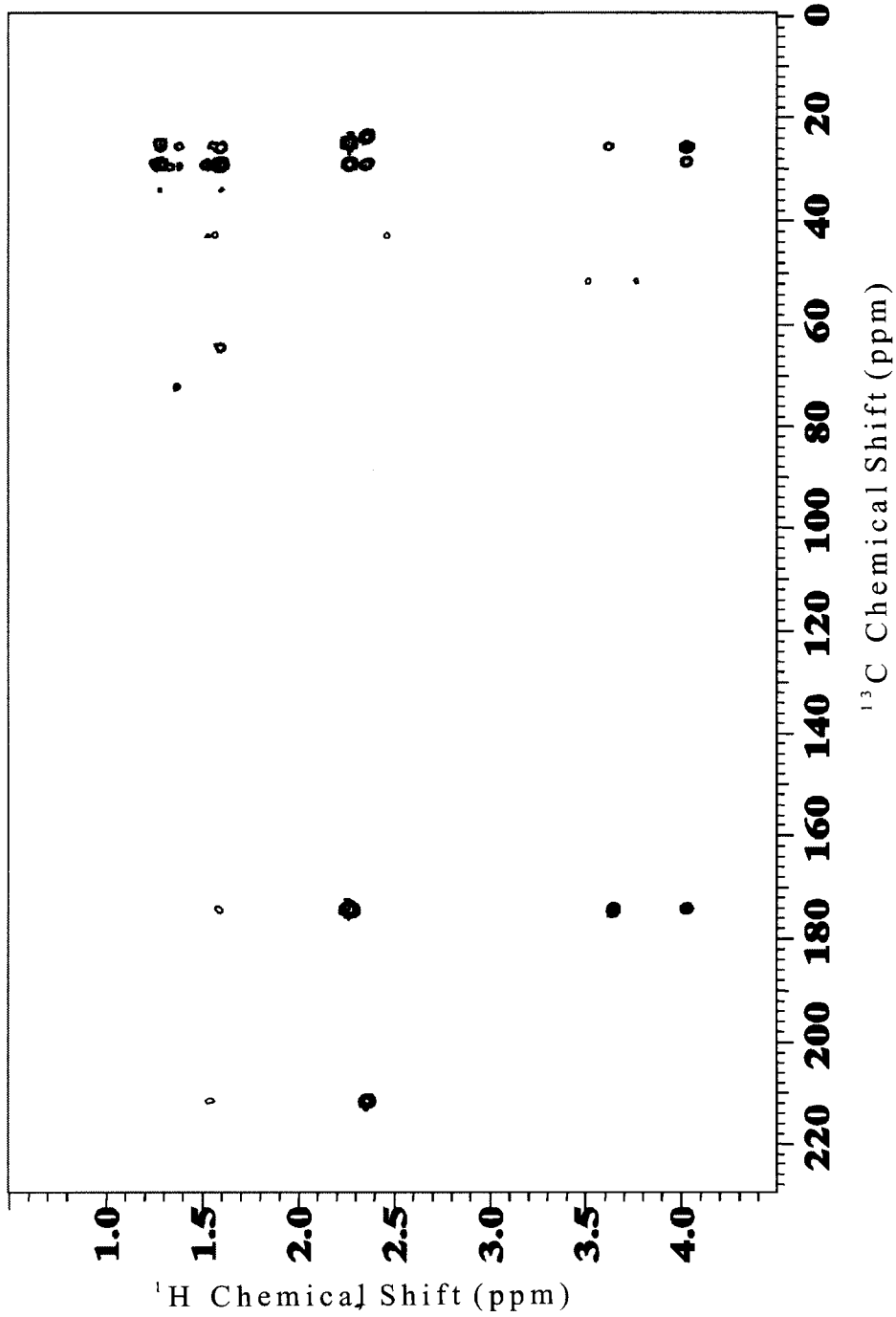

Figure 4.51. gHMBC spectrum of **Compound 12**.

Compound 13 from KOH degradation was elucidated as a new trimer consisting of two units of 10,16-dihydroxyhexadecanoic acid and one unit of 10-oxo-16-hydroxyhexadecanoic acid containing a secondary ester bond linkage between monomers (Figure 4.52). **Compound 13** is a structural isomer of **Compound 12**. Molecular ions corresponding to $M+NH_4^+$ (m/e 858), $M+Na^+$ (m/e 863), and $M+H^+$ (m/e 841) were found in ESI-MS spectrum (Figure 4.53). The ^{13}C isotopic peak intensity (molecular ions + 1) is about 55 % of the original peak, agreeing with the determined trimer structure containing 49 carbons. Fragments were observed from the four cleavages shown in Figure 4.52. The fragment with m/e of 251 is derived from the fragment m/e of 269 after loss of one molecule of H_2O. This loss is common for a terminal-alcohol monomer like many of our dimers and monomers. This sample is not pure: weak peaks corresponding to **Compounds 12** (trimer), a trimer with molecular weight of 838 (**Compound 11**), and perhaps some dimers and monomers are also observed in the ESI/MS spectrum of **Compound 13** (Figure 4.53); molecular ions and fragments of **Compound 12** and **Compound 13** cannot be distinguished. The key NMR peak that supports the structure of **Compound 13** is the CHO resonance occurring at 4.84 ppm in the 1D ^1H NMR spectrum (Figure 4.54), distinguishing **Compound 13** from **Compound 12**. Proton NMR integrals also support the suggested structure, although there are some differences between the experimental and theoretical values (Table 4.10). The discrepancy could be attributed to the impurities evidenced in the ESI/MS spectrum of **Compound 13**. For instance, the trimer impurity has a higher fraction of protons at 2.36 ppm than **Compound 13**, making the integral of this peak higher than it should be (Table

4.10). **Compound 12** has a larger fraction of protons at 4.03 ppm and 2.26 ppm than **Compound 13**, making the integrals of these peaks higher than they should be. Similarly, the anomalously low value for the integral of the peak at 3.64 ppm is likely to arise from the presence of **Compound 12** in the sample. The solvent is $CDCl_3$, which displays a peak from residual HOD at 1.5 ppm. This factor may contribute to the unreasonably high values for proton integrals between 1.00 ppm and 2.00 ppm. A cross peak for the ester bond of a secondary alcohol is observed at (4.84 ppm, 73.8 ppm) in the gHMQC spectrum (Figure 4.55). Moreover, strong evidence for the ester of the secondary alcohol comes from gHMBC cross peaks of the proton at 4.84 ppm with the carbons of the carboxylic acid and methylenes at 173 ppm, 24 and 34 ppm, respectively (Figure 4.56). However, no cross peak for the carbon of the secondary alcohol was observed in the gHMBC spectrum, as expected from **Compound 12.** Other characteristic cross peaks were also found in the 2D spectra of **Compound 13** (Figures 4.55, 4.56), similar to those observed for **Compound 12**.

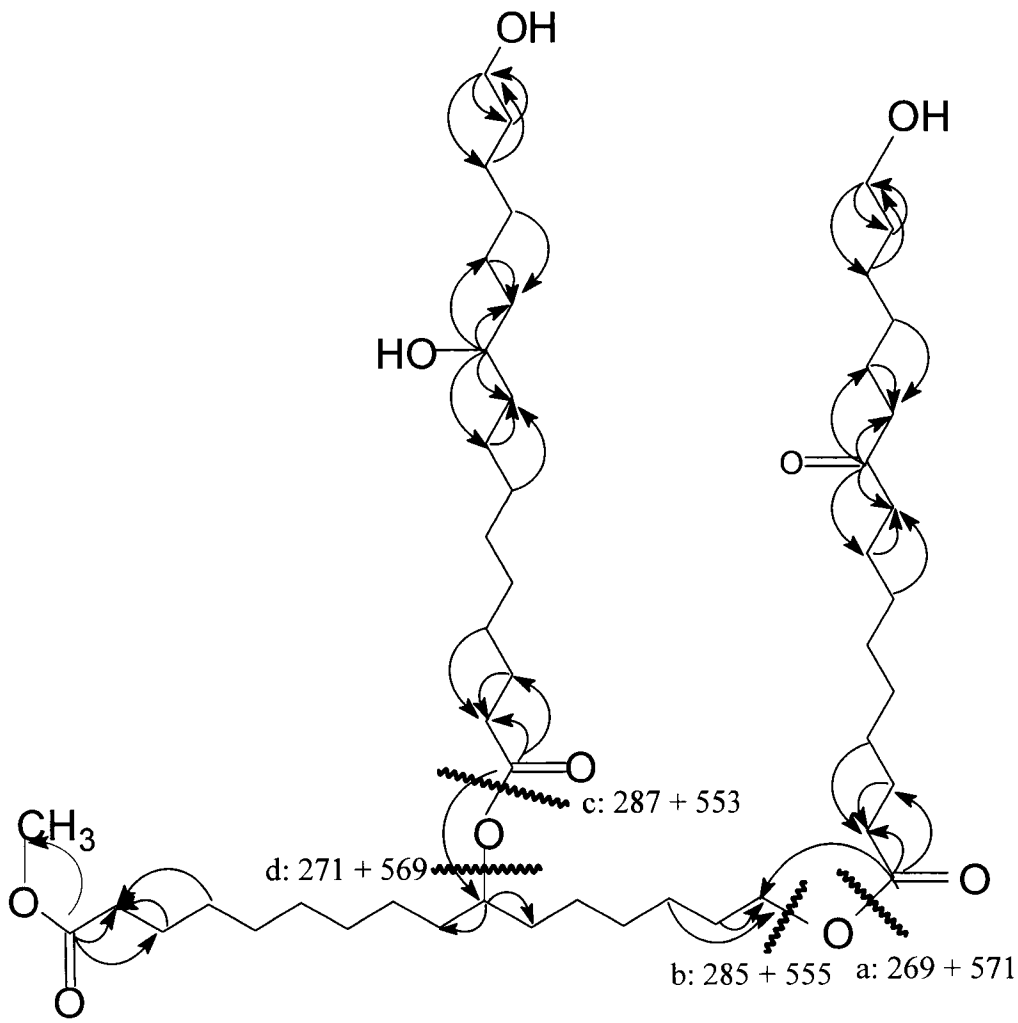

Figure 4.52. Structure, gHMBC correlations, and MS fragmentations of **Compound 13**.

Table 4.10. Proton NMR integrals for **Compound 13**.

Chemical Shift (ppm)	4.84	4.03	3.64	3.60	3.55	2.36	2.26	1.92	1 - 2
Experimental value	1	3.3	2.7	3.4	1.3	5.4	7.2	3.9	83
Calc. value	1	2	3	4	1	4	6	3	68

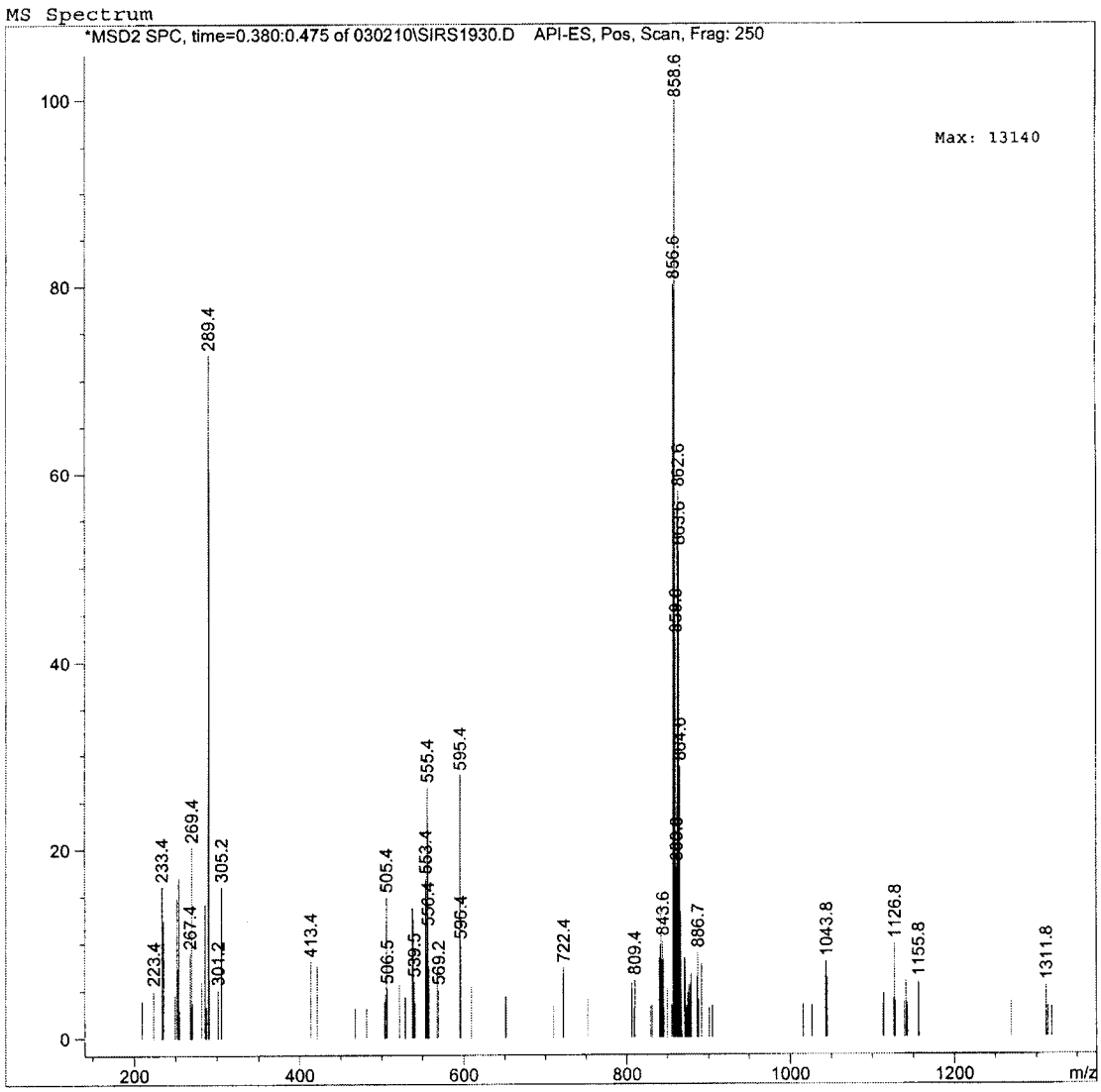

Figure 4.53. ESI/MS spectrum of **Compound 13**, showing ion intensities and mass-to-charge ratios, and evidence of impurities.

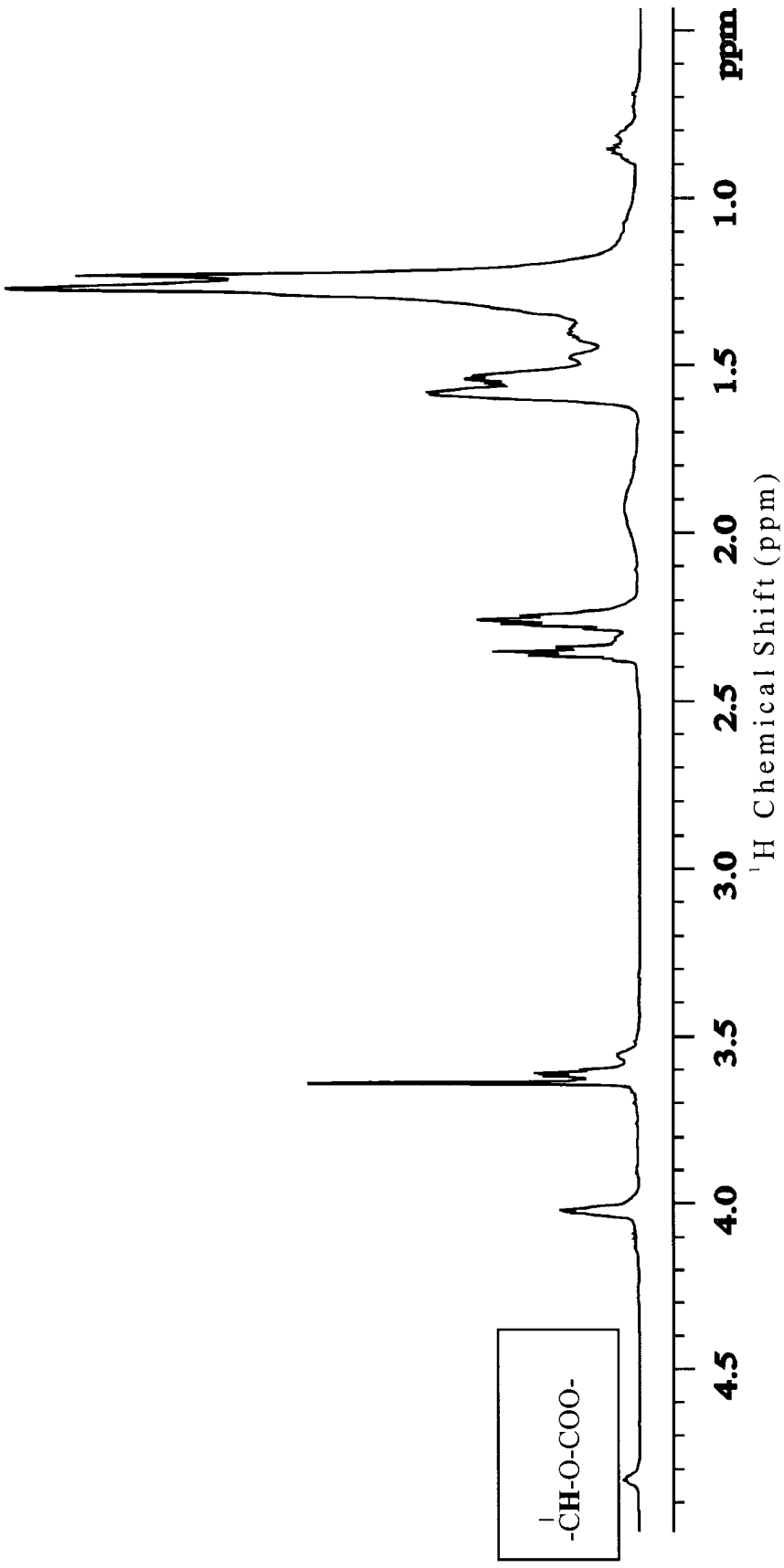

Figure 4.54. 600 MHz ^{1}H NMR spectrum of **Compound 13**.

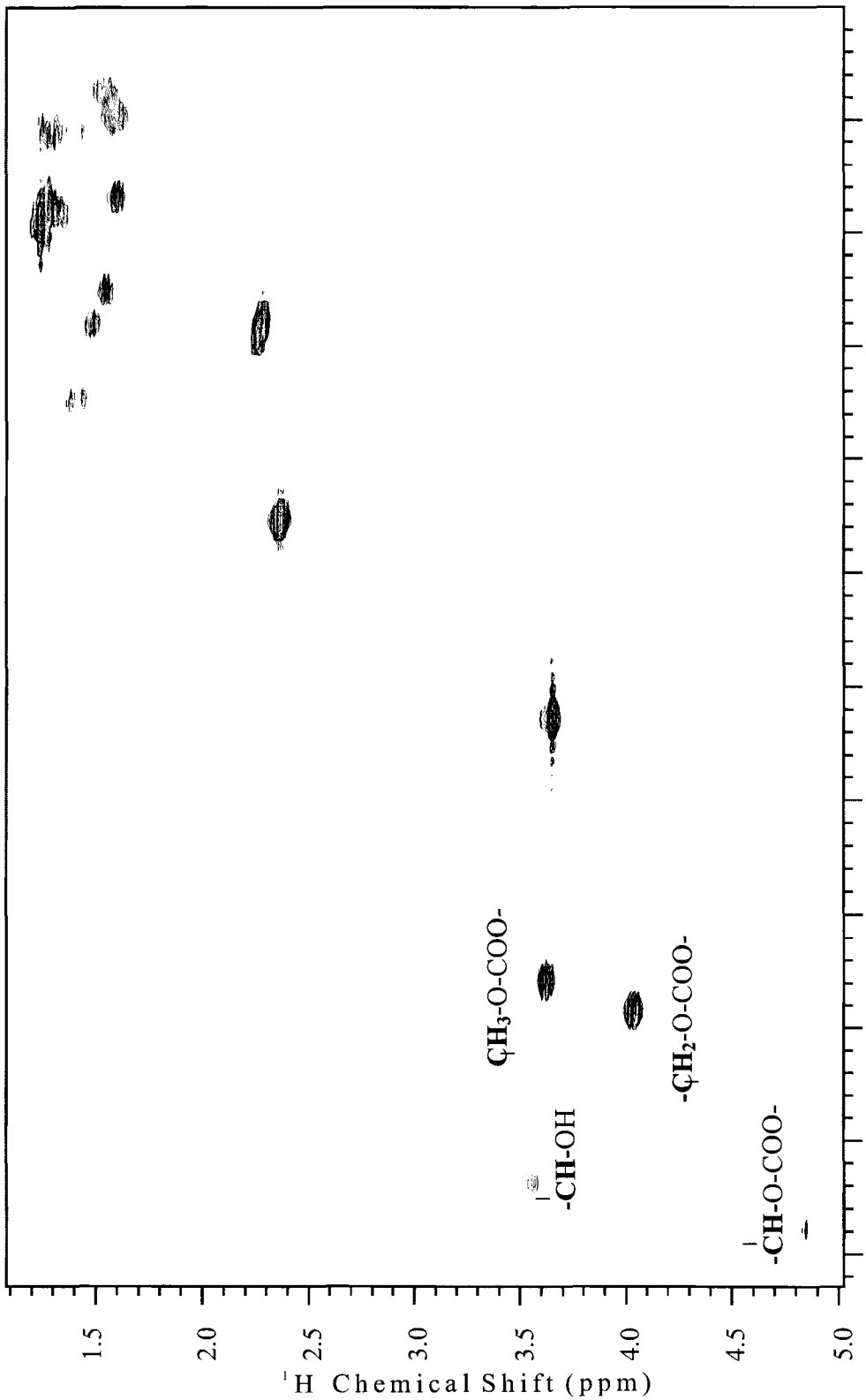

Figure 4.55. gHMQC spectrum of **Compound 13**.

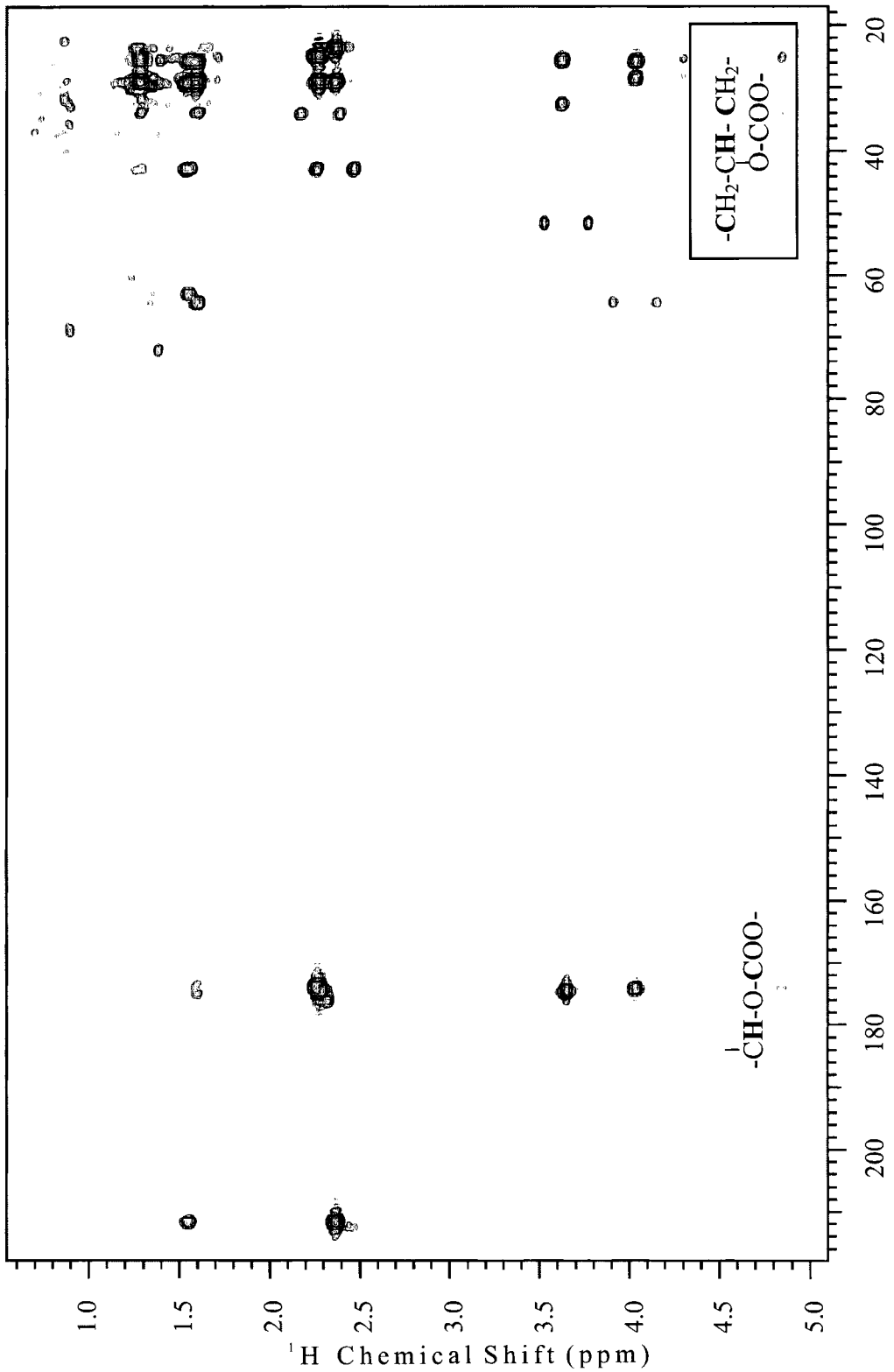

Figure 4.56. gHMBC spectrum of **Compound 13**.

Compound 14 was isolated from HF depolymerization and identified as the ethyl ester of a trimer consisting of three 16-hydroxy-10-oxo-hexadecanoic acid units (Figure 4.57). The positions of the oxo groups were deduced on the basis of the known monomer structures. Molecular ions corresponding to $M+NH_4^+$ (m/e 868) and $M+Na^+$ (m/e 873) were found in the ESI/MS spectrum of **Compound 14** (Figure 4.58). No $M+H^+$ molecular ion or fragments were observed. The ^{13}C isotopic peak intensity (molecular ions + 1) is about 50 % of the original peaks, in agreement with the determined trimer structure containing 50 carbons. Proton NMR integrals also support this structure (Table 4.11 and Figure 4.59). 2D NMR spectra (Figures 4.60 and 4.61) are similar to those of **Compound 7** because of the similarity of their basic structures.

Table 4.11. Characteristic ^1H NMR chemical shifts and integrals for **Compound 14**.

Chem Shift (ppm)	4.10	4.03	3.62	2.36	2.26
Exp. Value	2	4	2	10	6
Calc. Value	2	4	2	12	6

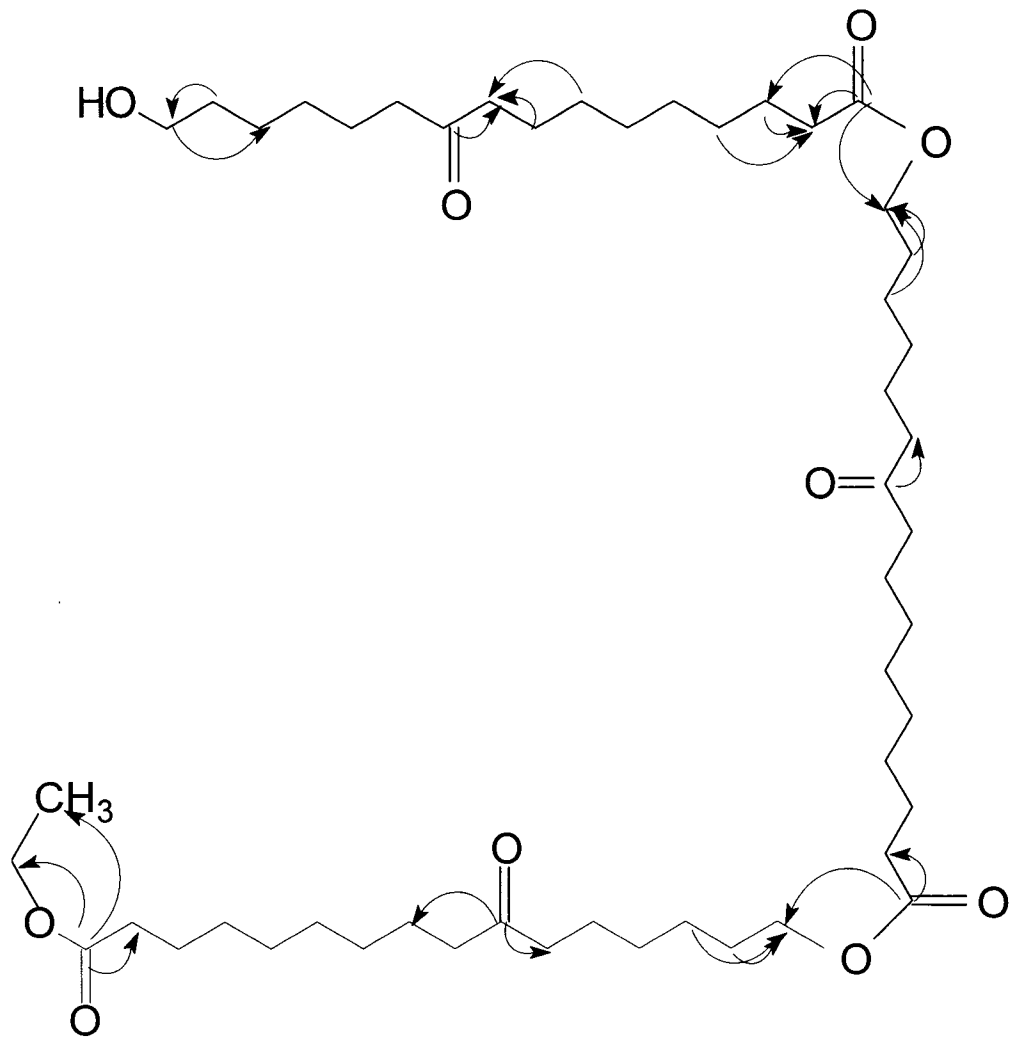

Figure 4.57. Structure of **Compound 14** and its significant gHMBC (H to C) correlations.

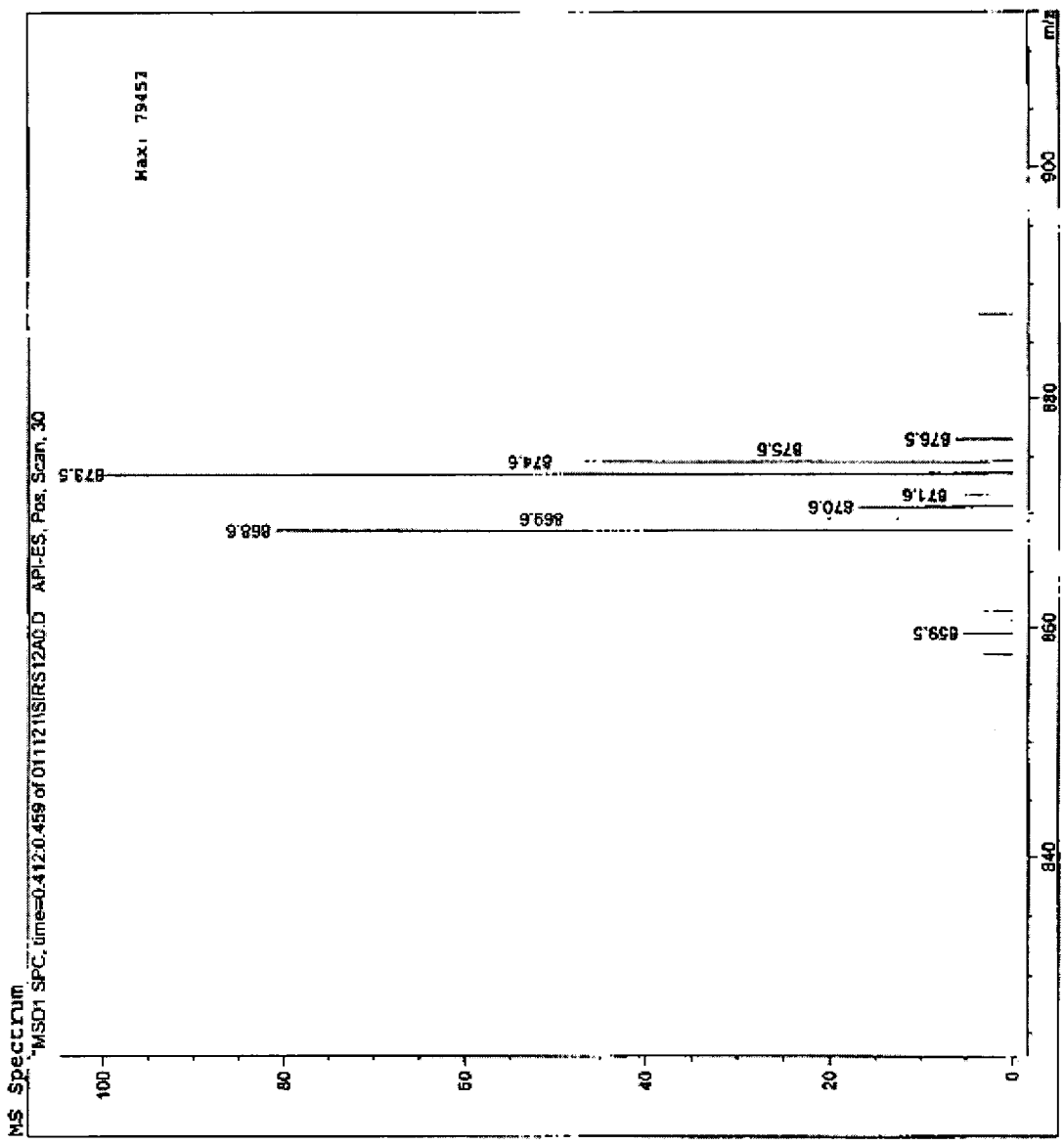

Figure. 4.58 ESI/MS spectrum of **Compound 14**, showing ion intensities and mass-to-charge ratios.

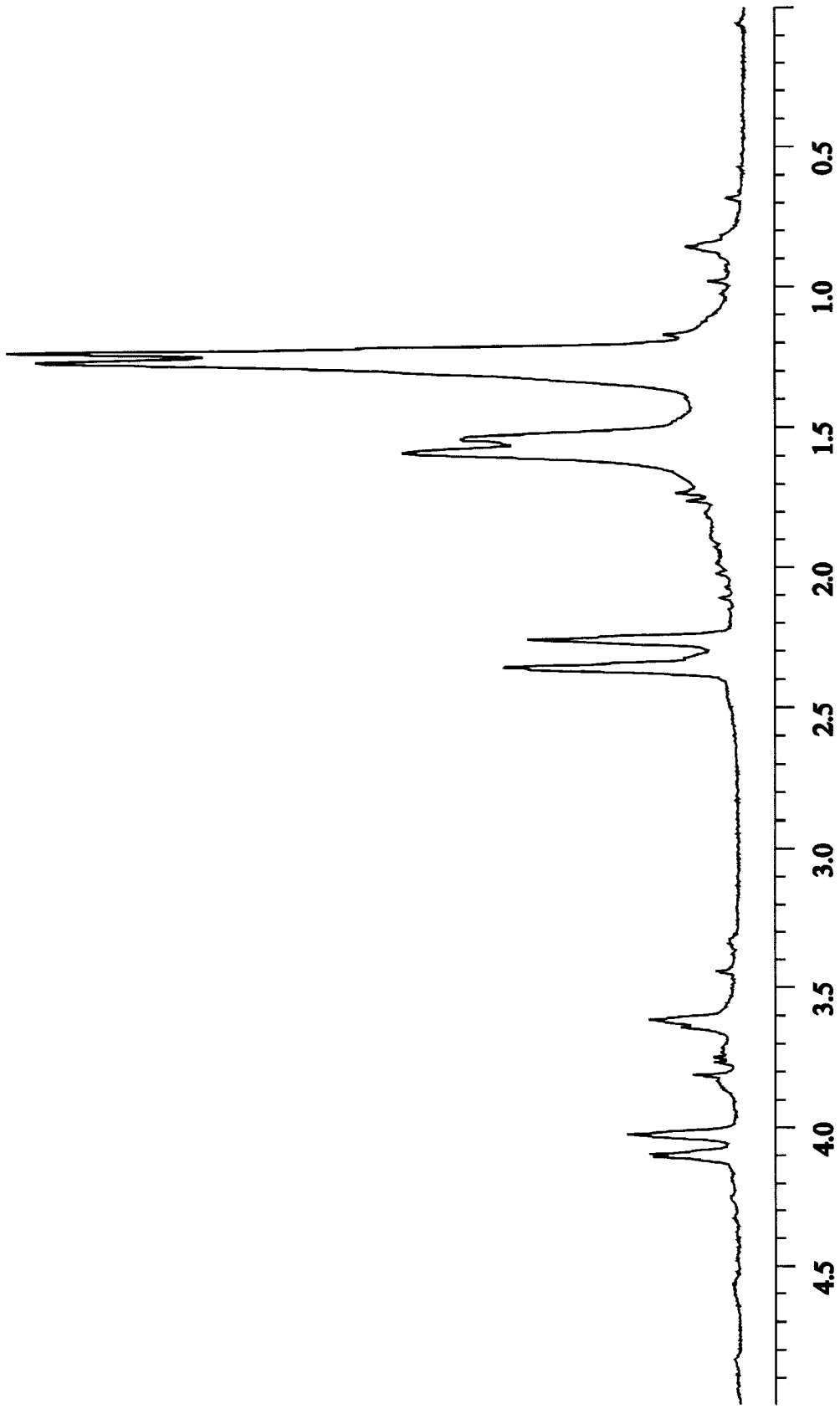

Figure 4.59. 600 MHz ^{1}H NMR spectrum of **Compound 14**.

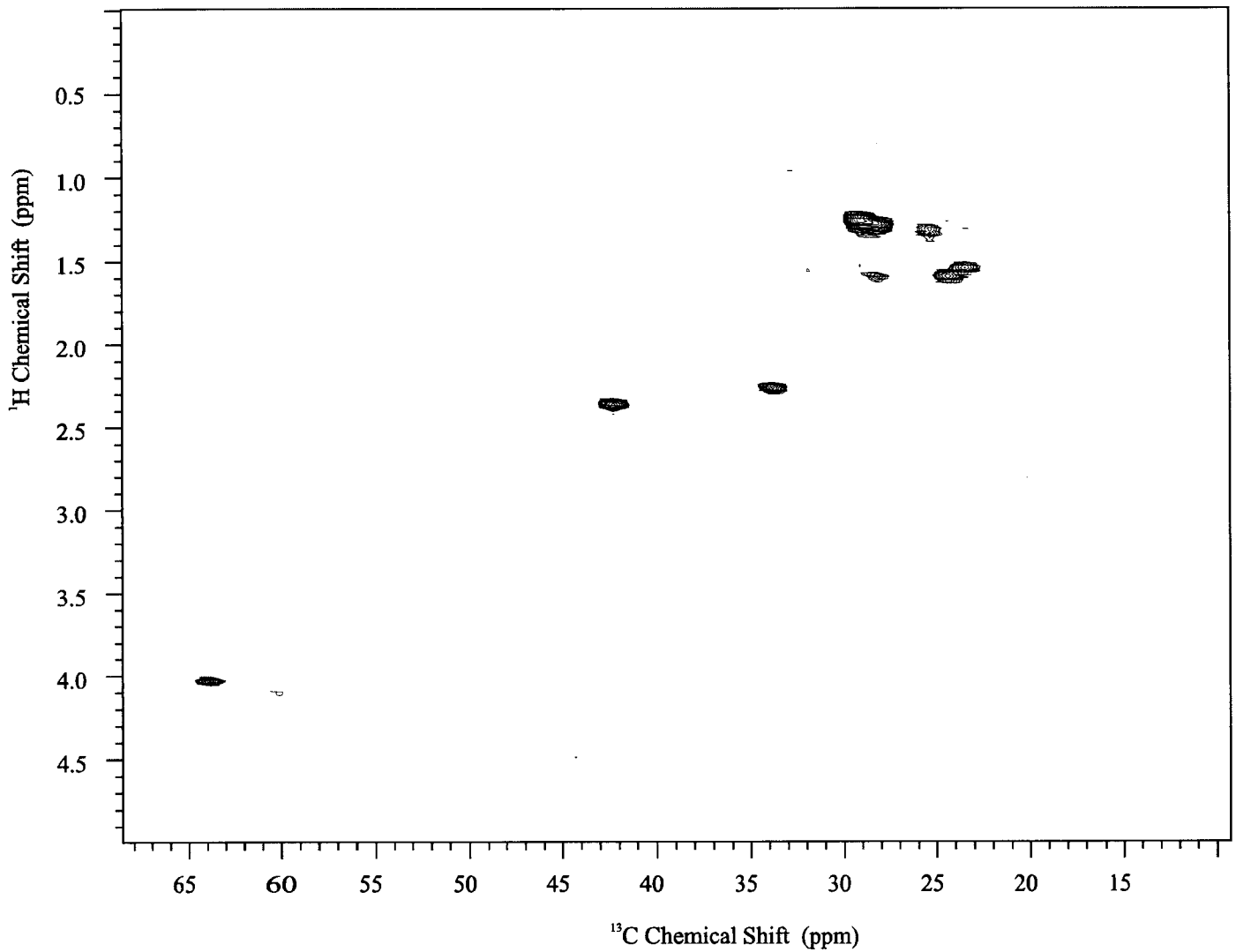

Figure 4.60. gHMQCs NMR spectrum of **Compound 14** acquired in a nanoprobe.

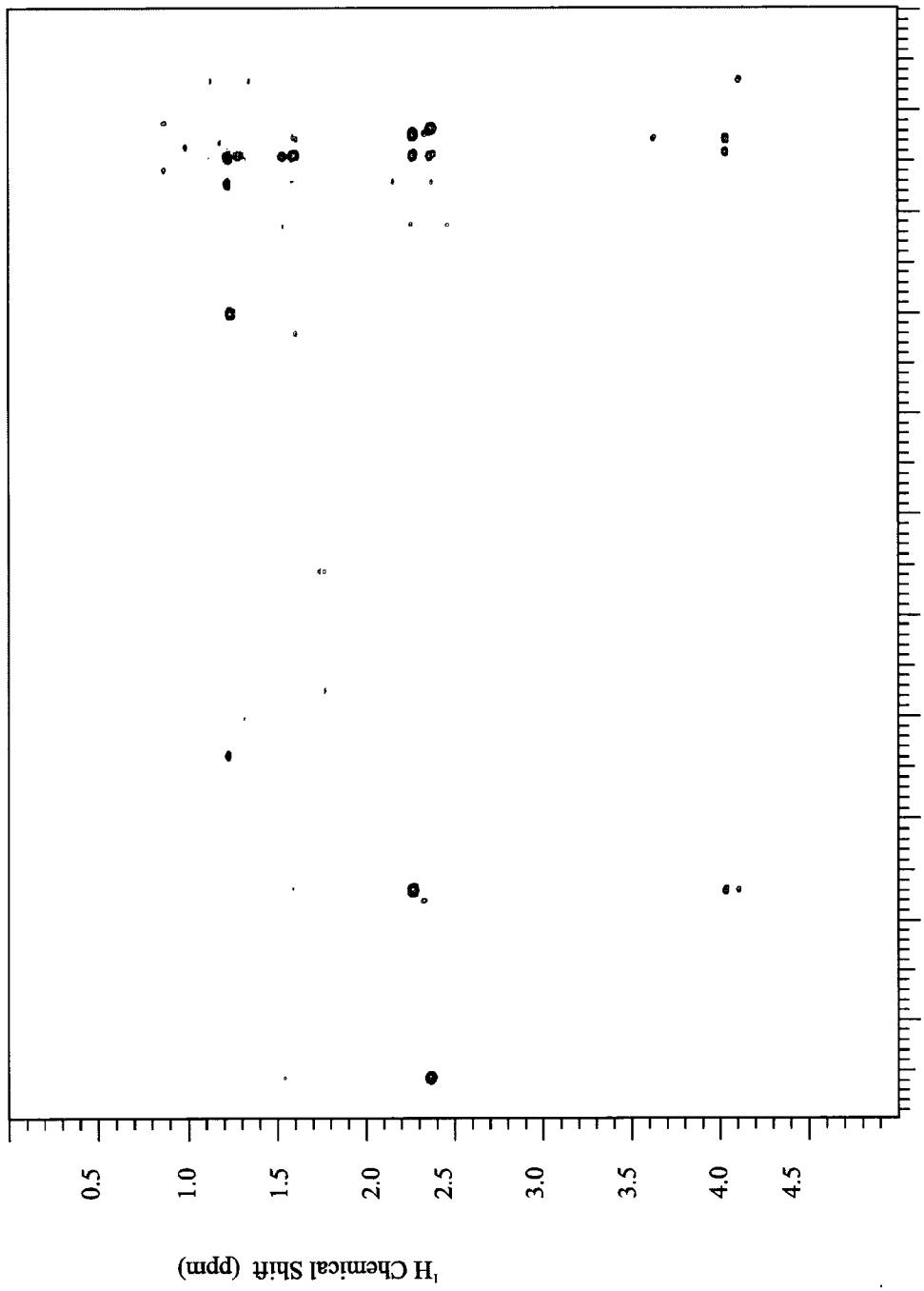

Figure 4.61. gHMBCs NMR spectrum of **Compound 14** acquired in a nanoprobe.

Compound 15 from KOH degradation was identified as a new trimer containing C16, C18, and C20 monomers (Figure 4.62). Molecular ions corresponding to $M+NH_4^+$ (m/e 910), $M+Na^+$ (m/e 915), and $M+H^+$ (m/e 893) were found in the ESI-MS spectrum of **Compound 15** (Figure 4.63). Because of the limited amount of sample, pure compound could not be obtained, and quantitative analysis of the NMR spectra was not possible. However, qualitative analysis of the NMR spectra is consistent with the proposed structure.

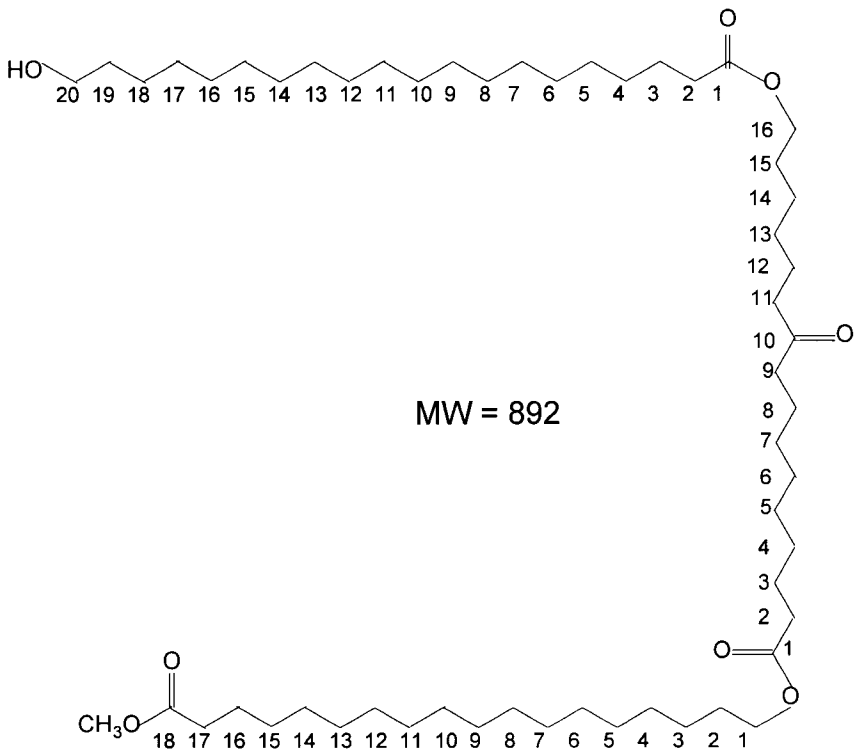

Figure 4.62. Provisional structure of **Compound 15**.

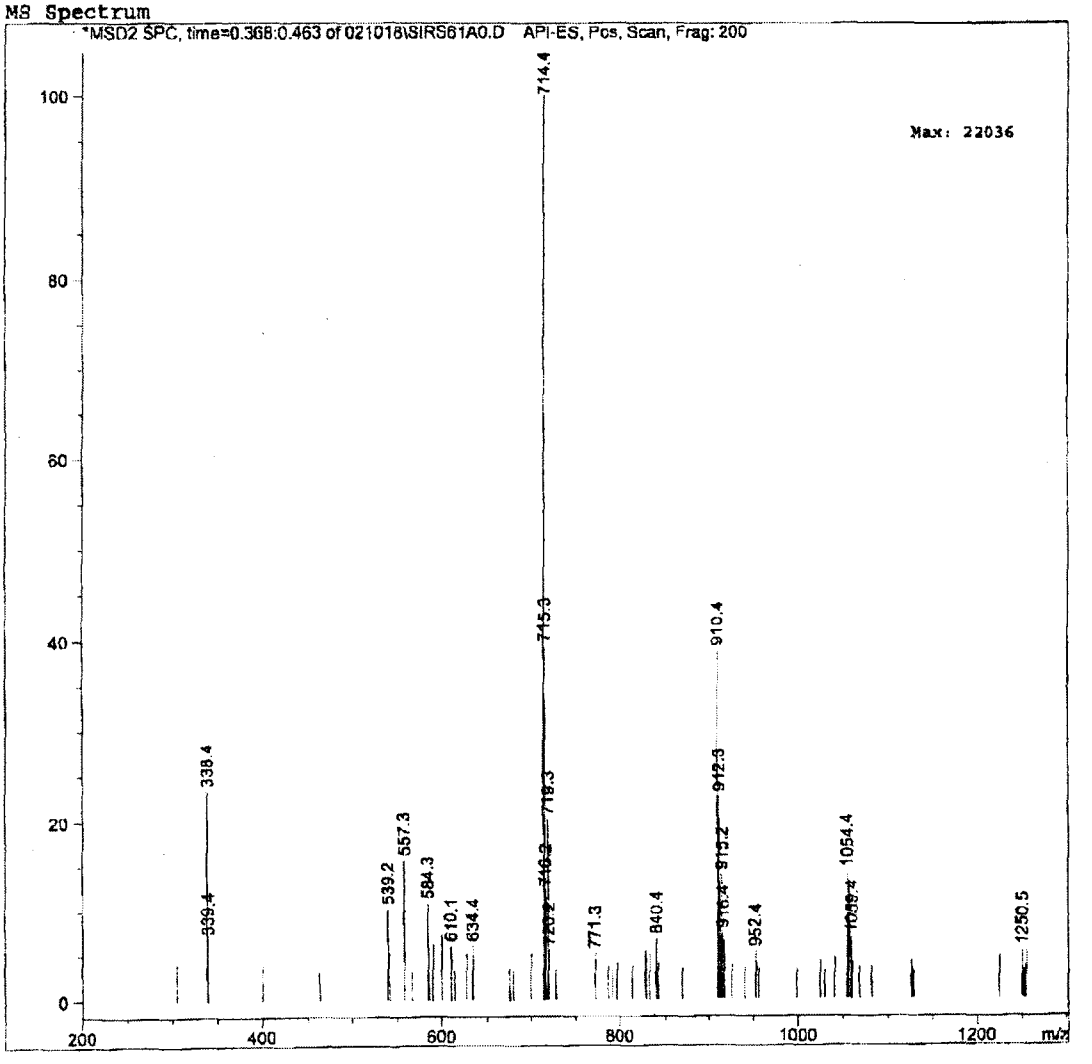

Figure 4.63. ESI/MS spectrum of **Compound 15**, showing ion intensities vs. mass-to-charge ratios.

4.1.2.4 Separation and identification of tetramers in lime cutin

Compound 16 (Figure 4.64) is a new tetramer isolated after KOH treatment of lime cutin using the modified method. It has a molecular weight of 1050 and very low polarity. Peaks corresponding to $M + NH_4^+$ (m/e 1068) and $M + Na^+$ (m/e 1073) were found in ESI-MS (Figure 4.65). The tentative structure agrees well with its molecular weight and polarity judged from HPLC. The structural elucidation of the tetramer is not yet complete, because the sample is insufficient for further analysis, such as NMR.

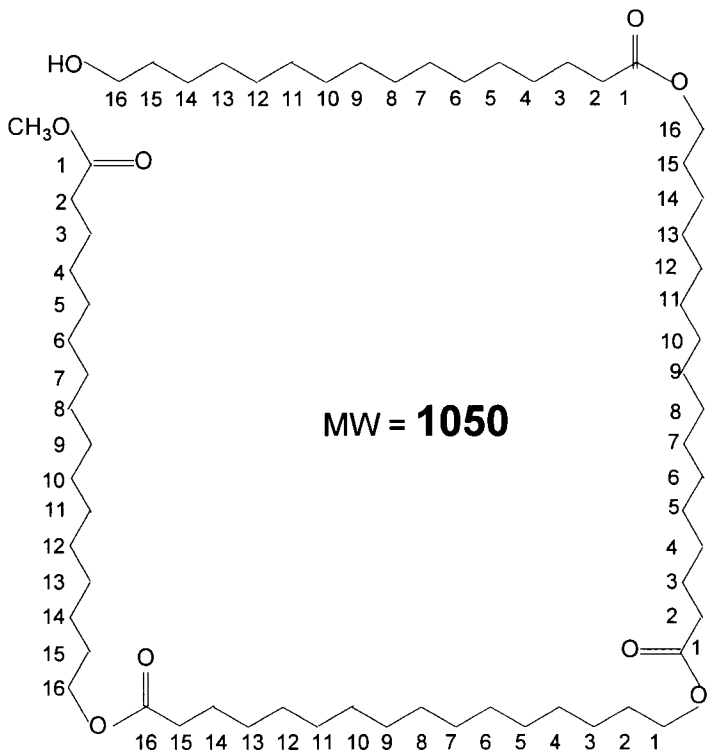

Figure 4.64. Provisional structure of **Compound 16**.

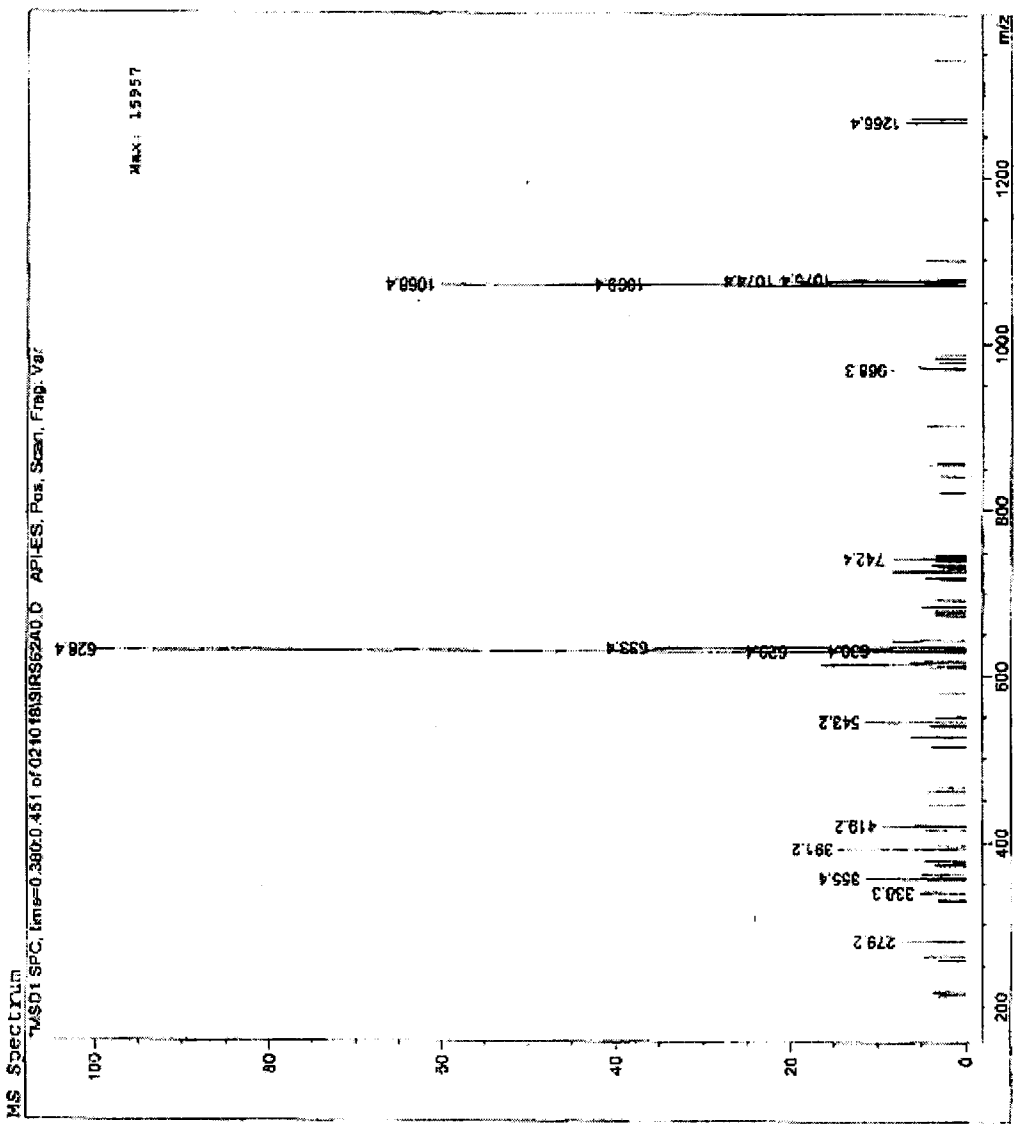

Figrue 4.65. ESI/MS spectrum of **Compound 16**, showing ion intensities vs. mass-to-charge ratios.

4.1.2.5 Monomer Connections in some known dimers

The characteristic ESI/MS fragments of **Compound 2** are the peaks at m/e 251 (100 %) and m/e 269 (30%) (Figure 4.17), where proposed cleavages that generate these fragments are marked on the structure of **Compound 2** (Figure 4.14). This characteristic fragment pattern also appeared in oligomers containing the monomer corresponding to **Compound 2**. The other monomers found in our studies are not expected to exhibit this kind of fragmentation pattern. Thus, a hydroxyl-terminated 16-hydroxy-10-oxo-hexadecanoic acid moiety can be deduced in an oligomer structure, if this diagnostic fragmentation pattern appears in the compound's ESI/MS spectrum. This reasoning was applied to deduce the connection sequence of two known dimers, **Compounds 17 and 18** (Figures 4.66 and 4.67 [33] and personal communication with X. Fang), even though the samples were not entirely pure. Both compounds have a 16-hydroxy-10-oxo-hexadecanoic acid unit at the hydroxyl end.

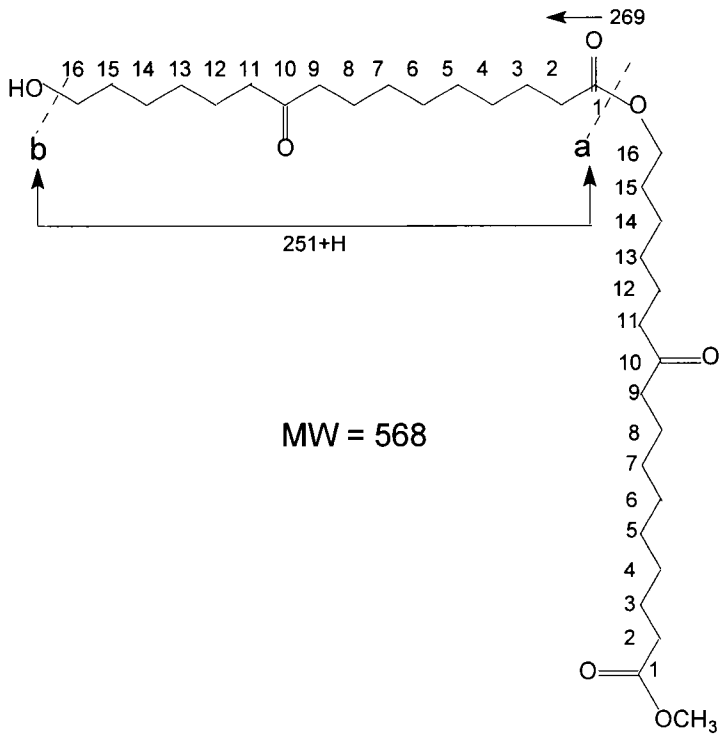

Figure 4.66. Connection sequence of **Compound 17**.

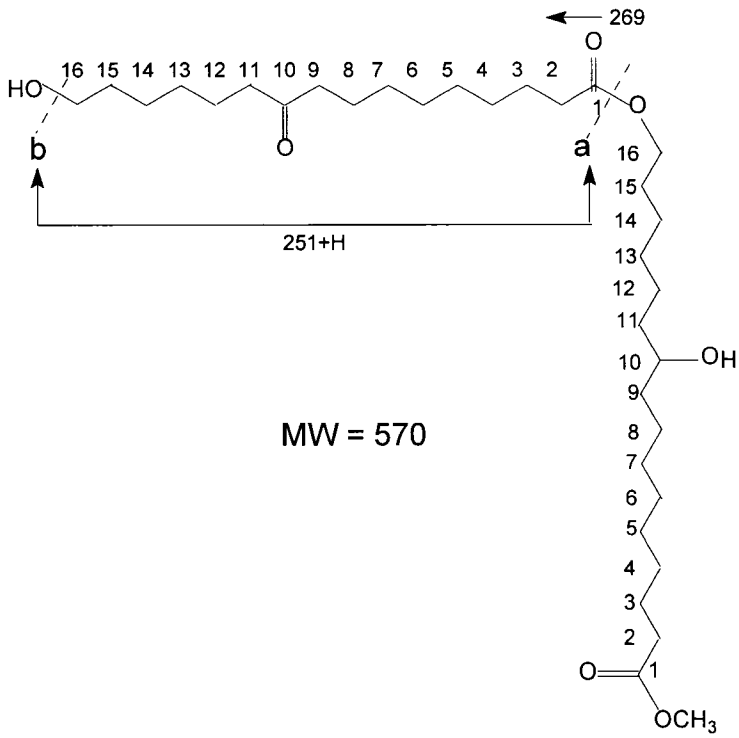

Figure 4.67. Connection sequence of **Compound 18**.

4.1.3 Conclusions (intact cutin and oligomeric fragments)

Solid-state NMR is an efficient approximate method to assess the purity of lime cutin obtained using standard preparation methods [88]. Higher magnetic field and spinning speed can improve the resolution of CPMAS the spectra of cutin, as seen by comparison of spectra in Figures 4.1 and 4.3. It remains the most direct method to establish chemical composition at the level of molecular groupings for intractable plant biopolymers.

Control of the depolymerization process is essential to generate soluble samples that retain as much architectural information as possible. Significant improvements have been achieved in generating bigger pieces of the original materials by the modified KOH depolymerization method. An HPLC separation protocol has been developed to make the separation more efficient. With the help of the protocol, many compounds have been separated from different depolymerization treatments, and more interesting compounds have been separated and tested. Recent acquisition of $(MS)_n$ instrumentation may facilitate future structure determinations without laborious separations.

Several aspects of the chemistry of cutin depolymerization are also noteworthy. The low-temperature HF treatment favors the retention of primary ester linkages to a greater degree than the KOH treatment. None of the identified oligomers from HF treatments exhibit secondary hydroxyl groups or secondary ester connectivities (previously identified products;[31] **Compounds 7 and 14**), whereas the oligomers from KOH treatment often include secondary hydroxyl groups and esters of

secondary alcohols. This trend in HF treatments contrasts with the strict selectivity of porcine pancreatic lipase for hydrolysis of esters of primary alcohols, which yielded a soluble pentamer in which only secondary ester linkages were retained. [35] KOH/MeOH depolymerizes lime cutin very rapidly at the beginning of the reaction, since 52 % of the material was depolymerized during the first 13 minutes whereas only 2 % more was depolymerized during next 15 minutes. An increase in reaction time does not enhance the yield of soluble products significantly, but longer reaction time degrades the produced oligomers and reduces the sizes and proportion of oligomers. Nonetheless, the resistance of ~ 45% of the lime cutin to degradation under conditions favor oligomers means that our conclusions regarding the biopolymer architecture are still incomplete.

The two most abundant monomers were separated and completely identified with NMR and MS data. A new dicarboxylic acid monomer was also separated and completely elucidated with NMR and MS data. Three new dimers were found, with structure determination based mainly on MS data.

Our studies and prior work[31,33,89] have isolated dimers with all possible combinations of the two most abundant monomers. Similarly, almost all possible trimers composed of the two most abundant monomers have been found, with the exception of the combination of three units of 10,16-dihydroxyhexadecanoic acid monomers. Structural isomers of trimers containing two units of 10,16-dihydroxyhexadecanoic acids and one unit of 16-hydroxy-10-oxo-hexadecanoic acid were also found. The monomer sequences within these trimers have not yet

been determined because of the lack of sufficient fragmentation information in MS, but MS-MS will be feasible with newly acquired equipment.

NMRView, a spectral processing program designed for multidimensional NMR of proteins, was used to make assignments of the lime cutin peaks and to compare spectra from various oligomers. One of the main functions of NMRView is to compare analogous NMR experiments on different products. For instance, it was possible to compare gHMBC of two monomers (**Compounds 1 and 2**) and one trimer (**Compound 11**) mentioned above (Figure 4.68). The methylene protons next to the ester bond in the carboxylic acid moiety have the same chemical shifts and correlation patterns in all of these compounds (peaks on the dashed line 1). The methylene protons next to the keto groups remain the same in both monomer and trimer (peaks on dashed line 2). The methoxyl groups in these samples were also confirmed to be the same (peaks on dashed line 3). This software tool allowed us to identify common structural elements quickly and reliably, provided added confidence in our resonance assignments, and highlighted unique spectral (structural) features of newly isolated reaction products.

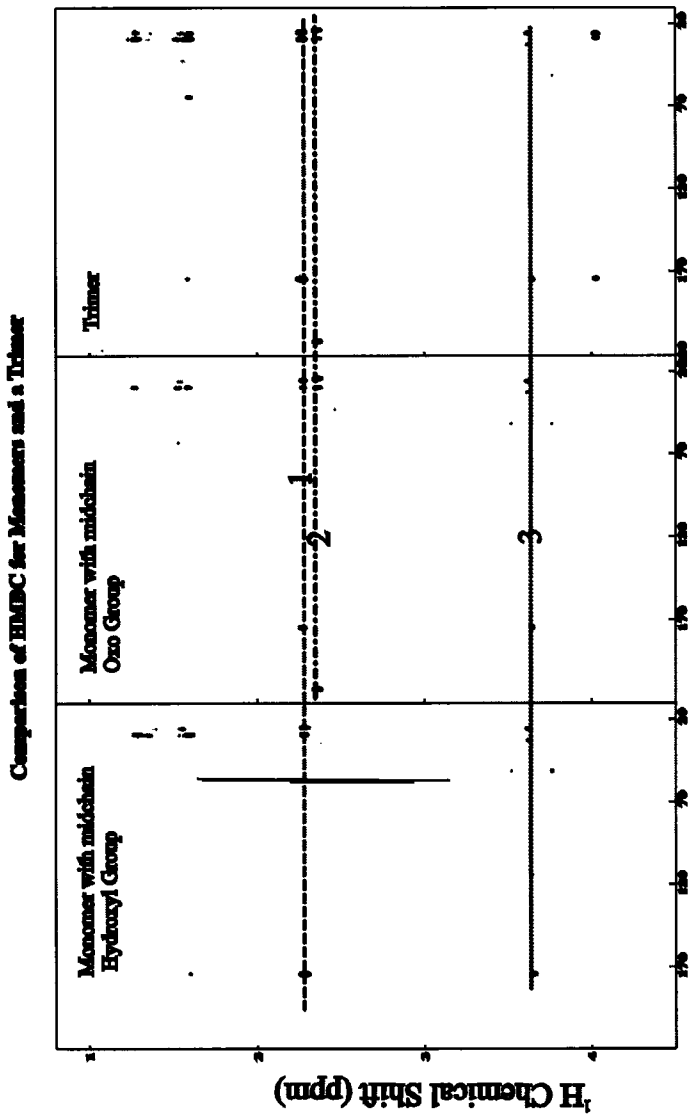

Figrue 4.68. gHMBC of two monomers (**Compounds 1 and 2**) and one trimer (**Compound 11**).

Comparison of intact materials, soluble products, and insoluble residues: In ^{1}H MAS spectra of swelled cutin and its insoluble residue from KOH treatment, box 1 highlights peaks at 3.46 ppm and 3.38 ppm in the intact material, but only the upfield peak at 3.38 ppm is retained in the residue after depolymerization (Figure 4.69). Based on the peak assignments of monomers and oligomers, the upfield peak is attributable to α-protons of secondary alcohols. Secondary alcohol groups are potential sites of cross-linking. This retention of secondary alcohols is consistent with our presumption that the depolymerization will occur mainly at sites with lower cross-link densities. The chemical shifts of bulk methylenes are similar in all of the materials (box 2 of Figure 4.69), although the better resolution of peaks from the oligomers may reflect fewer chain types as well as abundant motions in the liquid state.

As reported by Ray et al,[35] narrowing of the ^{13}C signals in the cross-polarization magic-angle spinning (CPMAS) NMR spectra of lime fruit cutin was observed after low-temperature HF treatment (Figure 4.70). The narrowing of NMR signals also occurred in the ^{1}H NMR spectra of the swelled cutin residue after HF treatment. These results indicate that the HF treatment favors the decomposition of some components and leaves the other components as dominant in the residue. Like the treatment with chemical deprotecting reagent iodotrimethylsilane, the HF treatment cleaved more ester linkages of primary alcohols, as evidenced by the diminution of ^{13}C resonances at 167 ppm ($CH_2O\mathbf{C}=O$). This interpretation was supported by the fact that none of the identified oligomers from HF treatment exhibits secondary hydroxyl group or secondary ester connectivities (**Compounds 7 and 14**), whereas

some of the oligomers from KOH treatment have secondary hydroxyl groups. Figure 4.71 compares the total correlation spectroscopy (TOCSY) for intact cutin and the unreacted residue after HF treatment. The disappearance of the cross peak between protons at 0.78 ppm ($C\mathbf{H}_3$-) and protons at 1.18 ppm (bulk methylenes) (highlighted by boxes in the upper right-hand corner of each plot) suggests that most of the methyl groups bonded to long fatty acid chains were removed from the material by the HF treatment, although no methyl-terminated fatty-acid chain has been found in any of the oligomers. There remain many fractions that have not been purified or identified, and methyl groups have been seen in NMR spectra of these fractions. The correlations among bulk methylene groups (middle boxes in each plot) in TOCSY spectra remain similar before and after the HF treatment (Figure 4.71). These trends agree well with the simplification of correlation patterns observed previously for bulk methylene groups [31]. The correlation of bulk methylene groups with methylene groups next to oxo groups (-$\mathbf{CH}_2$C(O)$\mathbf{CH}_2$-, 2.34 ppm) and methylene groups next to carbonyl groups of (-$\mathbf{CH}_2$COO-, 2.18 ppm) in TOCSY are similar before and after the treatment, but the relative intensities of the cross peaks have changed. This could be supporting evidence for the cleavage of the primary ester bonds.

Figure 4.72 displays the HMQC spectra of solvent-swelled samples of intact cutin, derivatives of the two most abundant monomers isolated from KOH treatment, and a trimer isolated from KOH treatment. A peak in box 1 is unique to the intact cutin. This peak is attributable to a methyl group and often observed in the very nonpolar fractions of the degradation products. Peaks in box 2 from bulk

methylene groups and peaks in box 3 from methylene groups next to carbonyl groups are observed in both the intact cutin and the degradation products. Peaks in box 4 from methoxyl groups are generated during the degradation process and can only be observed in the degradation products. Peaks in box 5 correspond to methylene groups of primary esters, the connection between monomers. Thus, they can only be observed in the intact cutin and oligomers from the degradation.

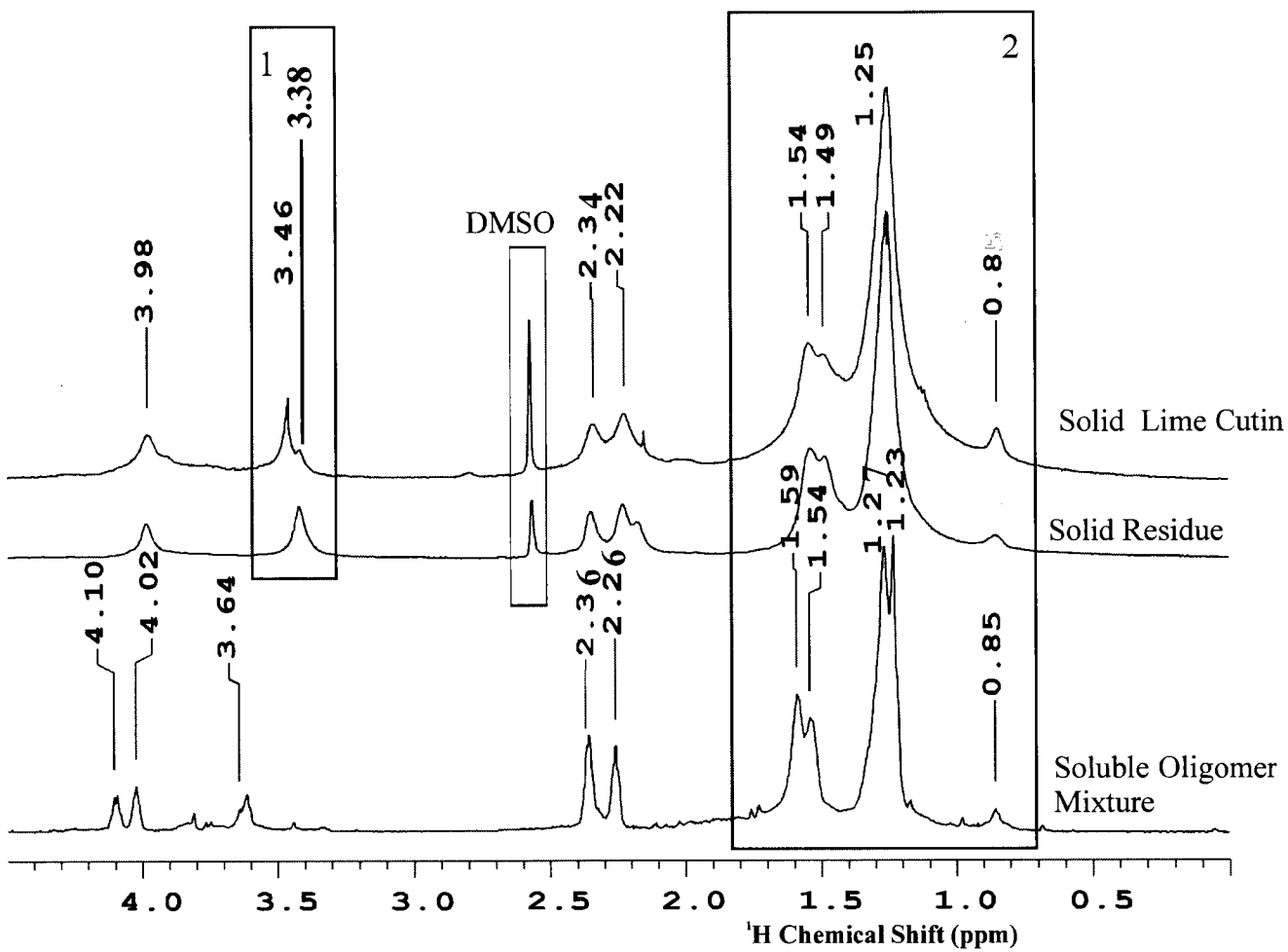

Figure 4.69. 600 MHz ^{1}H HRMAS spectra of intact materials, soluble products, and insoluble residues.

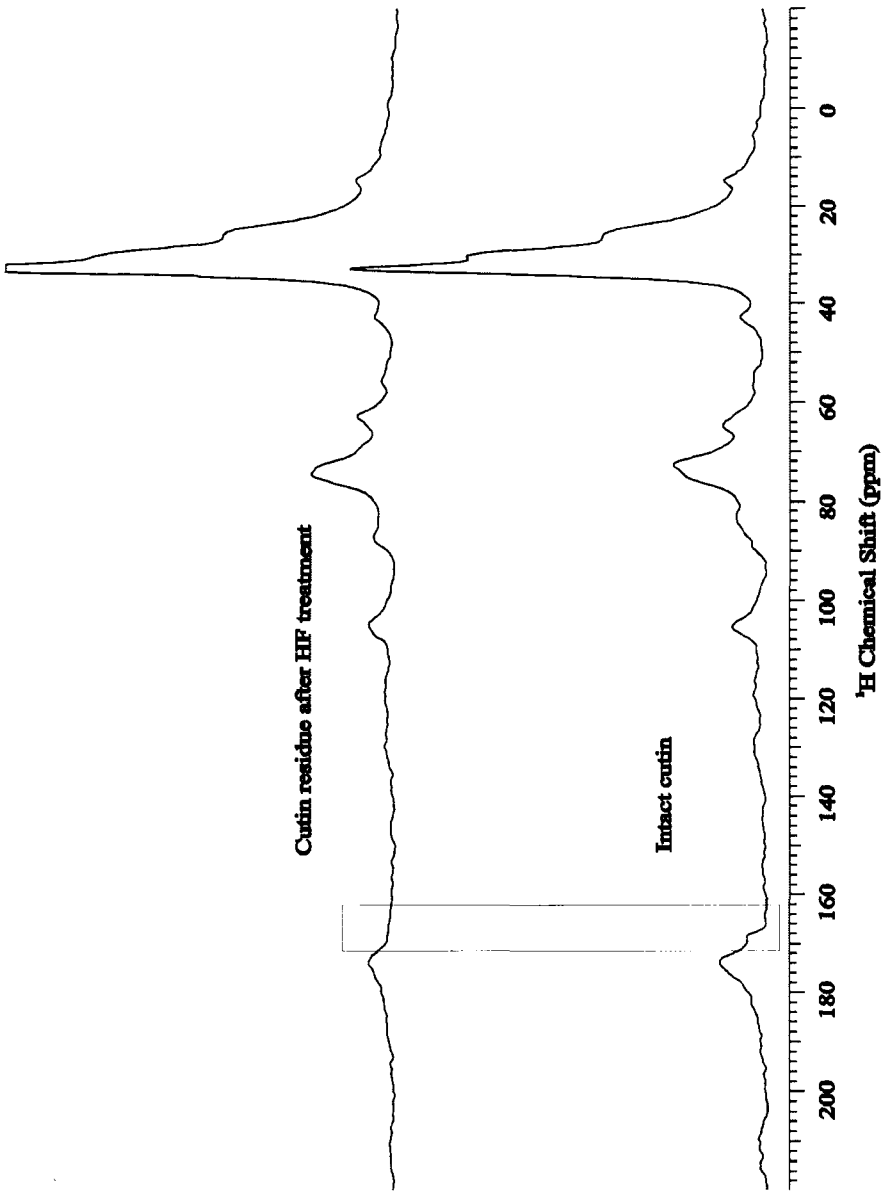

Figure 4.70. 75 MHz CPMAS ^{13}C spectra of intact materials and insoluble residues.

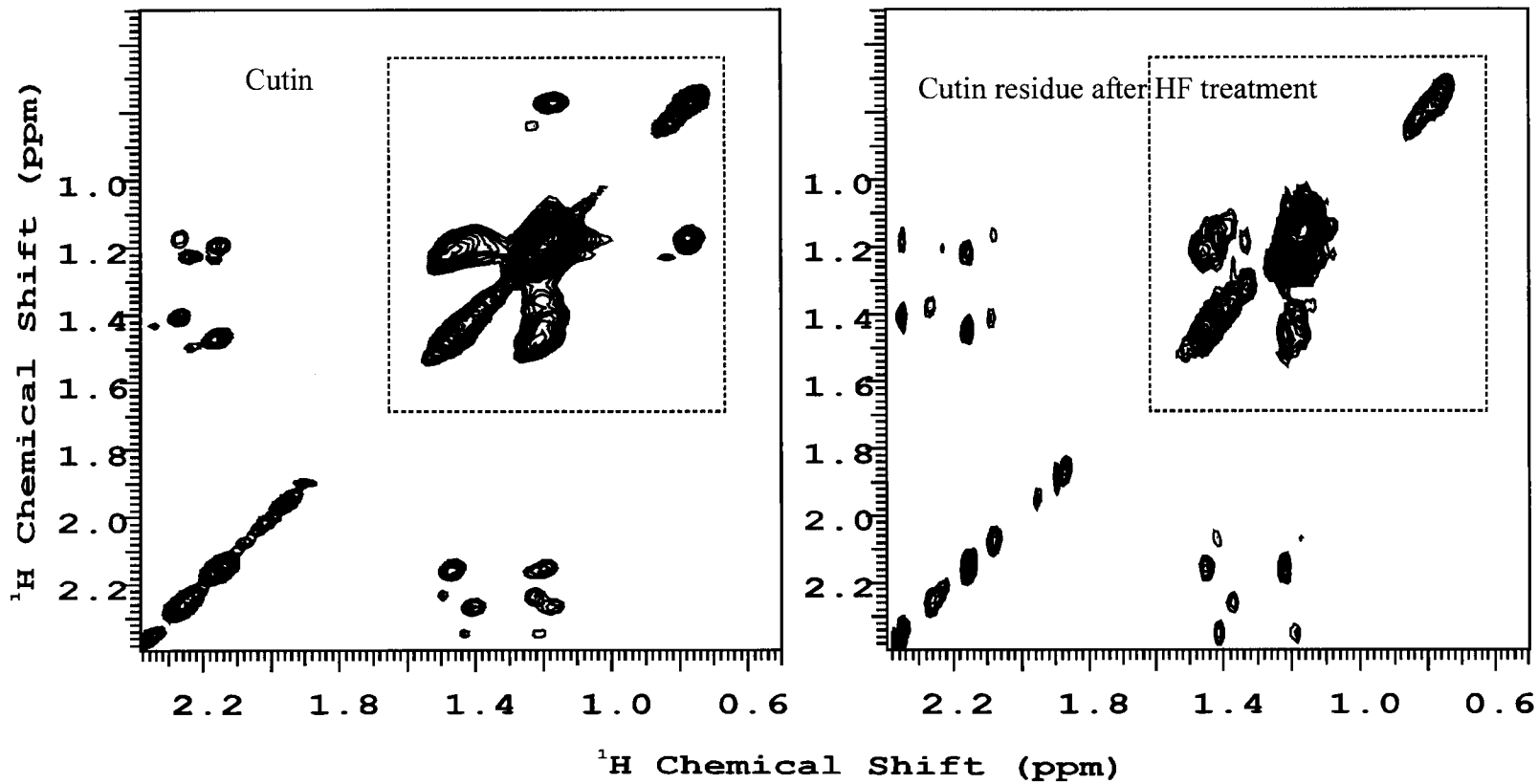

Figure 4.71. Comparison of TOCSY spectra of solvent-swelled intact materials and insoluble residues.

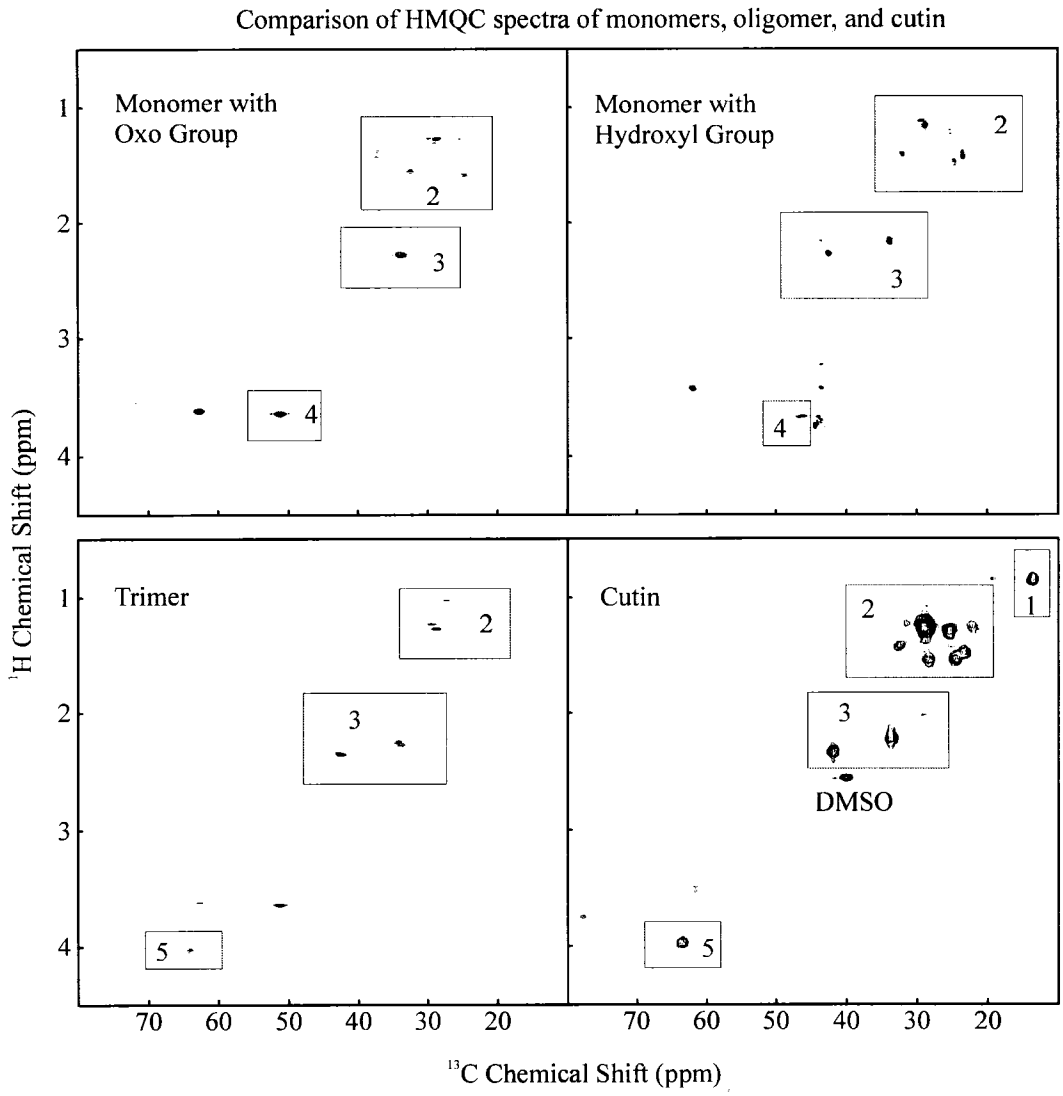

Figure 4.72. MAS HMQC spectra of monomers, trimer, and solvent-swelled intact cutin.

4.2 Results for Potato Suberin

4.2.1 MAS NMR

Effect of magic-angle spinning on the appearance of the spectra: In the solid state, the chemical shift anisotropy will cause line broadening (See Section 2.1.3). If the MAS speed exceeds the chemical shift anisotropy, the anisotropy will be averaged out and a single sharp ^{13}C NMR line will be obtained. The number of lines depends on the spinning rate. In our experiment we ran the suberin sample at 2, 4, 6 and 8 kHz and the line width was found to vary modestly (Figure 4.73). Table 4.12 demonstrates that the linewidth at 50% peak height decreases with increasing spin speed, reaching a plateau at 6 kHz. The five peaks (172, 154, 146, 130 and 115 ppm) in spectra at 6 and 8 kHz spinning speeds are not even visible in the spectrum with 2 kHz spinning speed. Peaks at 154, 146, 130, and 115 ppm in the spectrum with 4 kHz spinning speed are not distinguished as well as those in spectra obtained with 6 and 8 kHz rates.

Table 4.12. Effect of spinning speed on the line width of the 72-ppm peak in ^{13}C NMR of potato suberin.

Spin Rate	2 kHz	4 kHz	6 kHz	8 kHz
50% linewidth	600 Hz	520 Hz	500 Hz	500 Hz

The MAS NMR spectra of suberin confirm the chemical composition of this material.[90] Table 4.13 lists ^{13}C chemical shifts observed in suberin and the corresponding functional groups. Peaks between 0 and 50 ppm are attributable to

aliphatic methylene or methyl groups; peaks between 50 and 90 ppm are mainly attributable to carbons 2,3,4,5, and 6 of polysaccharide (Figure 4.74); peaks between 90 and 110 ppm correspond to carbon 1 of a polysaccharide (Figure 4.74); peaks between 110 and 160 ppm are contributable to aromatic carbons; peaks between 160 and 190 ppm are contributable to carbonyl carbons of esters, carboxylic acids or aldehydes. The peaks between 50 and 80 ppm also include contributions from the oxygenated carbons of aliphatic suberin monomers.

Table 4.13. ^{13}C chemical shifts and functional groups found in potato suberin.

Chemical Shift (ppm)	160-190	110-160	90-110	50-90	0-50
Functional Group	-C- O	aromatic	Polysaccharide (position 1)	Polysaccharide (positions 2-6)	CH_3- -CH_2-

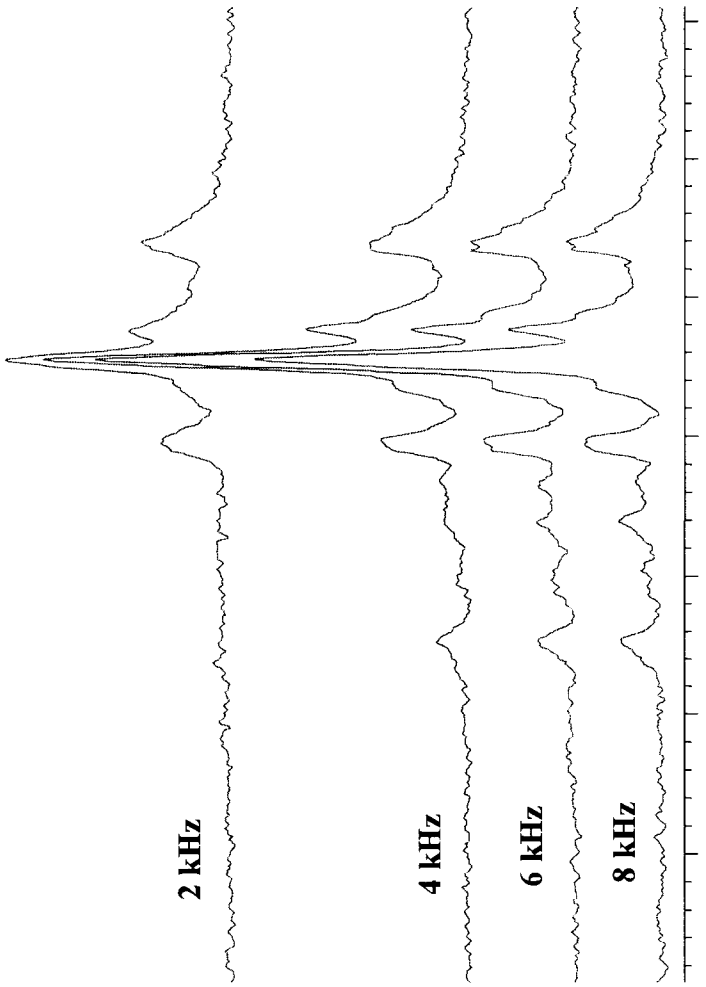

Figure 4.73. Effect of spinning speed on CPMAS ^{13}C NMR spectrum of potato suberin.

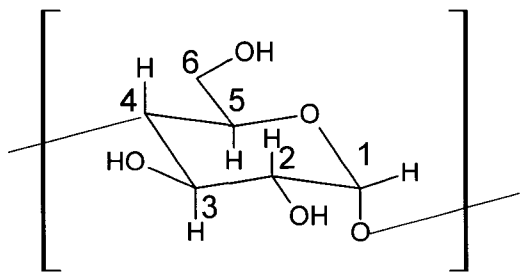

Figure 4.74. Basic structural unit of a typical polysaccharide.

4.2.2 HRMAS NMR

4.2.2.1 Natural-Abundance Potato Suberin Samples

As described in Chapter 3, we tried to remove as much polysaccharide as possible to enhance the aliphatic and aromatic portions of the potato suberin polymer. Natural-abundance potato suberin samples are those samples that meet this standard but have no isotopic ^{13}C labeling. The cutin results demonstrated that HRMAS NMR was helpful to the chemical structural studies, so the technique was also applied to suberin samples. The same functional groups found in the CPMAS ^{13}C NMR spectra of intact suberin (Figure 4.73) were also observed in the 1D proton spectrum of *swelled* intact suberin (Figure 4.75): aliphatic methylene or methyl groups (0.6 – 2 ppm); polysaccharide (3 – 4 ppm and 5 – 5.2 ppm); aromatic groups (6.6 – 7.8 ppm); esters or carboxylic acids (4 – 5 ppm and 2 – 2.4 ppm). Moreover, the relative amounts of each ^{1}H type are in rough agreement with CPMAS ^{13}C NMR of the powdered materials. The peak at 4.9 ppm was assigned to secondary ester bonds based on some known suberin monomers. The peak at 5.3 ppm is attributable to the double bond protons of some known monomers separated from suberin.

The gHMQCs spectrum of the swelled intact suberin (Figure 4.76) shows cross peaks of the protons observed in Figure 4.75 with carbons except for the aromatic groups, presumably because of their small signals. The cross peaks in box 1 of Figure 4.76 were assigned to the bulk methylene groups of aliphatic moieties of the material with ^{1}H chemical shifts between 0.5 – 1.5 ppm and ^{13}C chemical shift between 10 – 30 ppm; the cross peaks in box 2 of Figure 4.76 were assigned to

polysaccharide ^{1}H spins between 3.2 – 3.8 ppm and ^{13}C resonances between 55 – 80 ppm; the cross peak between ^{1}H 5.1 ppm and ^{13}C 100 ppm was assigned to the group at position 1 of the polysaccharide.

The gHMBCs spectrum of the swelled intact suberin (Figure 4.77) is consistent with MAS NMR, 1D ^{1}H NMR, and gHMQCs NMR. In contrast to swelled intact cutin (data not shown), suberin HMBC spectra exhibit numerous crosspeaks, suggesting better swelling and/or small particle sizes. Correlations between protons of bulk methylene groups and carbons of the bulk methylene groups which are 2 – 3 bonds apart contribute to the cross peaks in box 1 of Figure 4.77. Correlations between protons of polysaccharide and carbons of polysaccharide which are 2 – 3 bonds apart contribute to the cross peaks in box 2 of Figure 4.77. The cross peak between 3.95 ppm ^{1}H and 72.1 ppm ^{13}C is also attributable to a part of the polysaccharide moiety; this proton has another correlation with the carbon at 172.0 ppm (Figure 4.77 box 3), which must be the carbonyl carbon of an ester. The cross peak of the ^{1}H at 1.90 ppm with the carbon at 172.0 ppm (Figure 4.77 box 3) suggests that this is an ester of acetic acid. Thus, this part of the polysaccharide must be acetylated. The cross peaks in box 4 suggest an ester of an aliphatic alcohol and an aromatic carboxylic acid (based on the ^{13}C chemical shifts). The cross peak in box 5 could be a correlation between a hydroxyl-substituted benzene ring and aliphatic side chains. These observations are supported by those of the isotopically labeled suberin sample in Section 4.2.2.2 (see below), but the cross peaks of the carbon at position 1 in the polysaccharide moiety are missing in the current case. A structural fragment is proposed in Section 4.2.2.2.

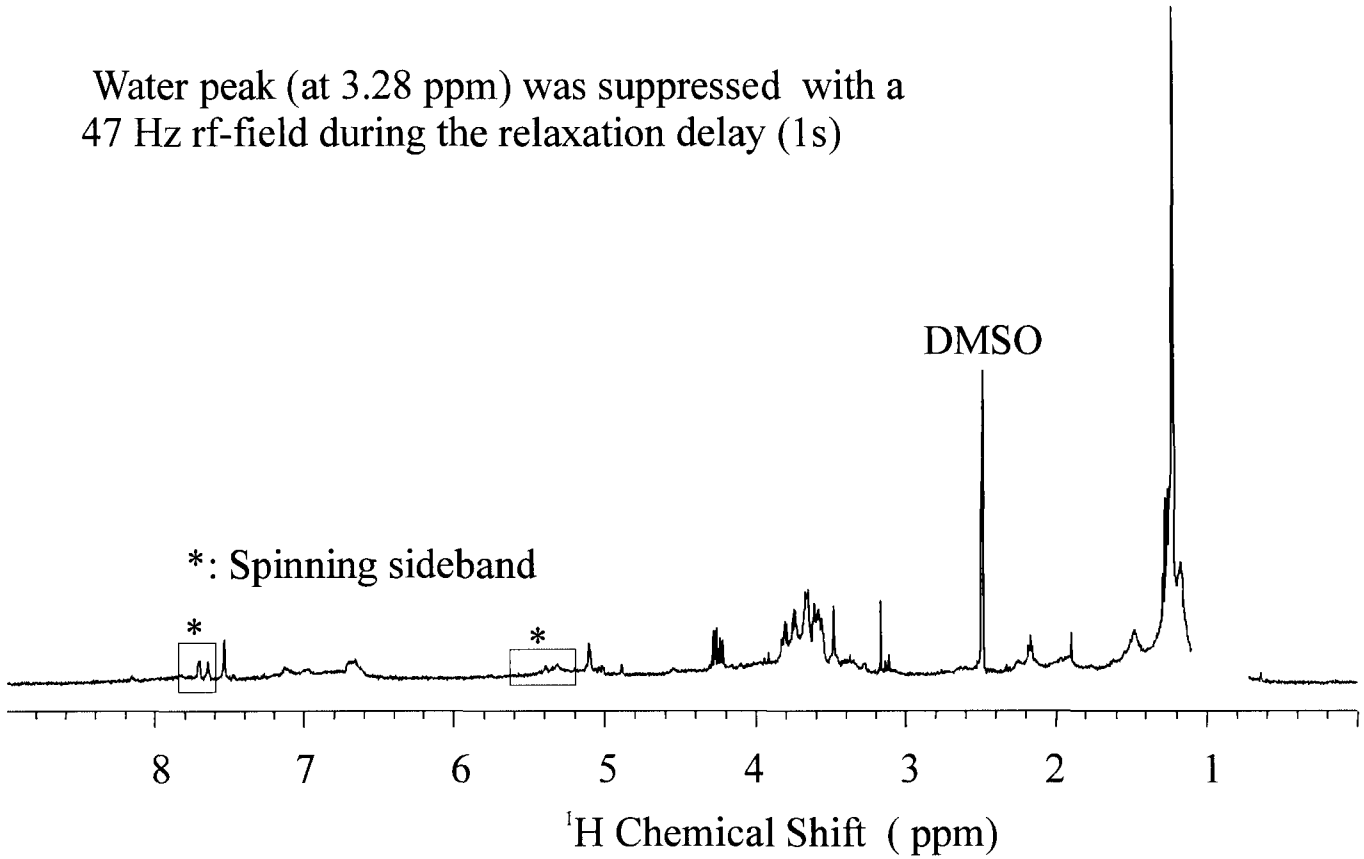

Figure 4.75. 600 MHz ^{1}H spectrum of swelled natural abundance suberin with DMSO (1 mg / 5 mg), MAS = 2.5 kHz.

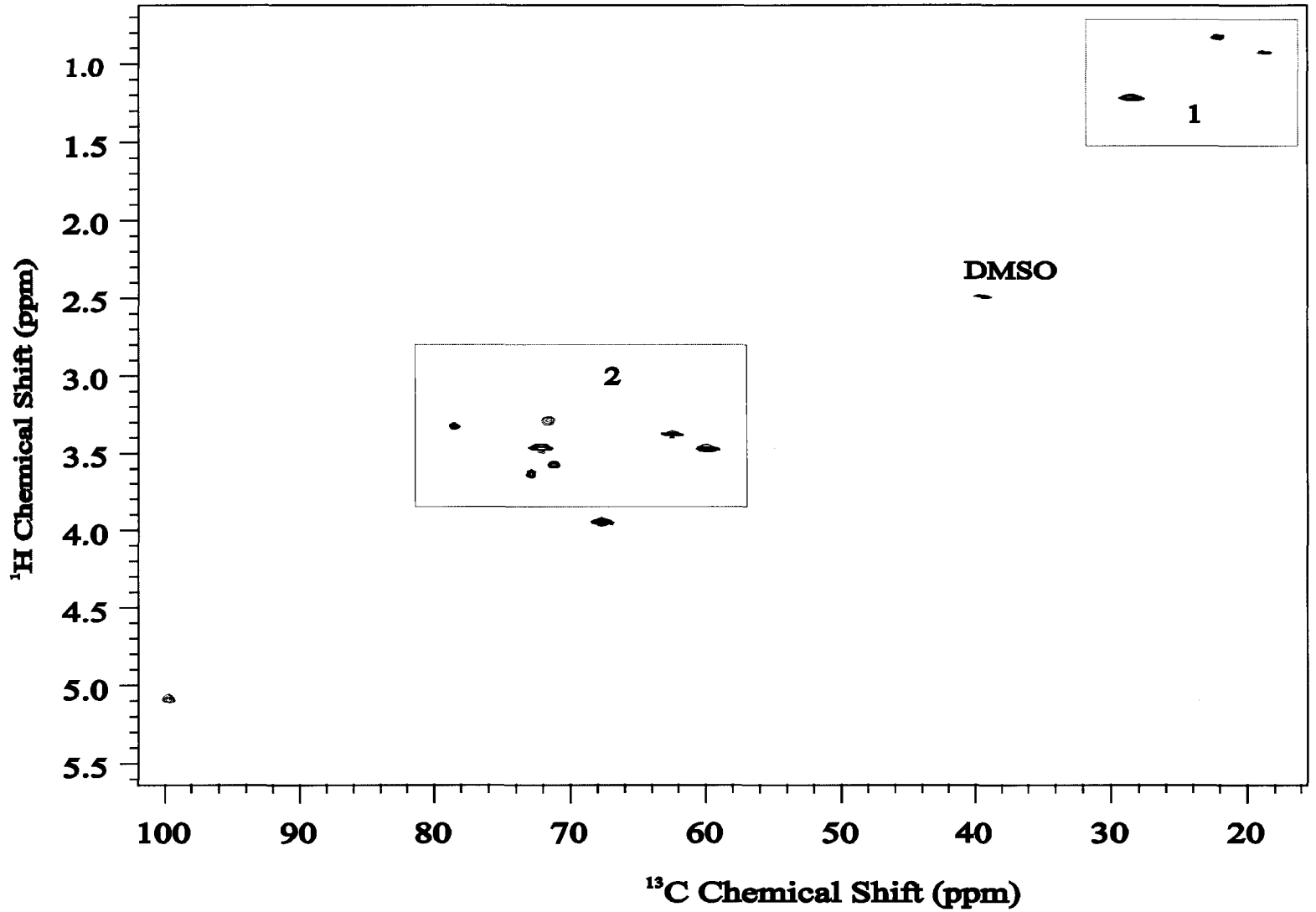

Figure 4.76. gHMQCs spectrum of swelled natural-abundance suberin with DMSO (1 mg / 5 mg), MAS = 2.5 kHz. No crosspeaks were observed to the weak resonances at 6 – 8 ppm.

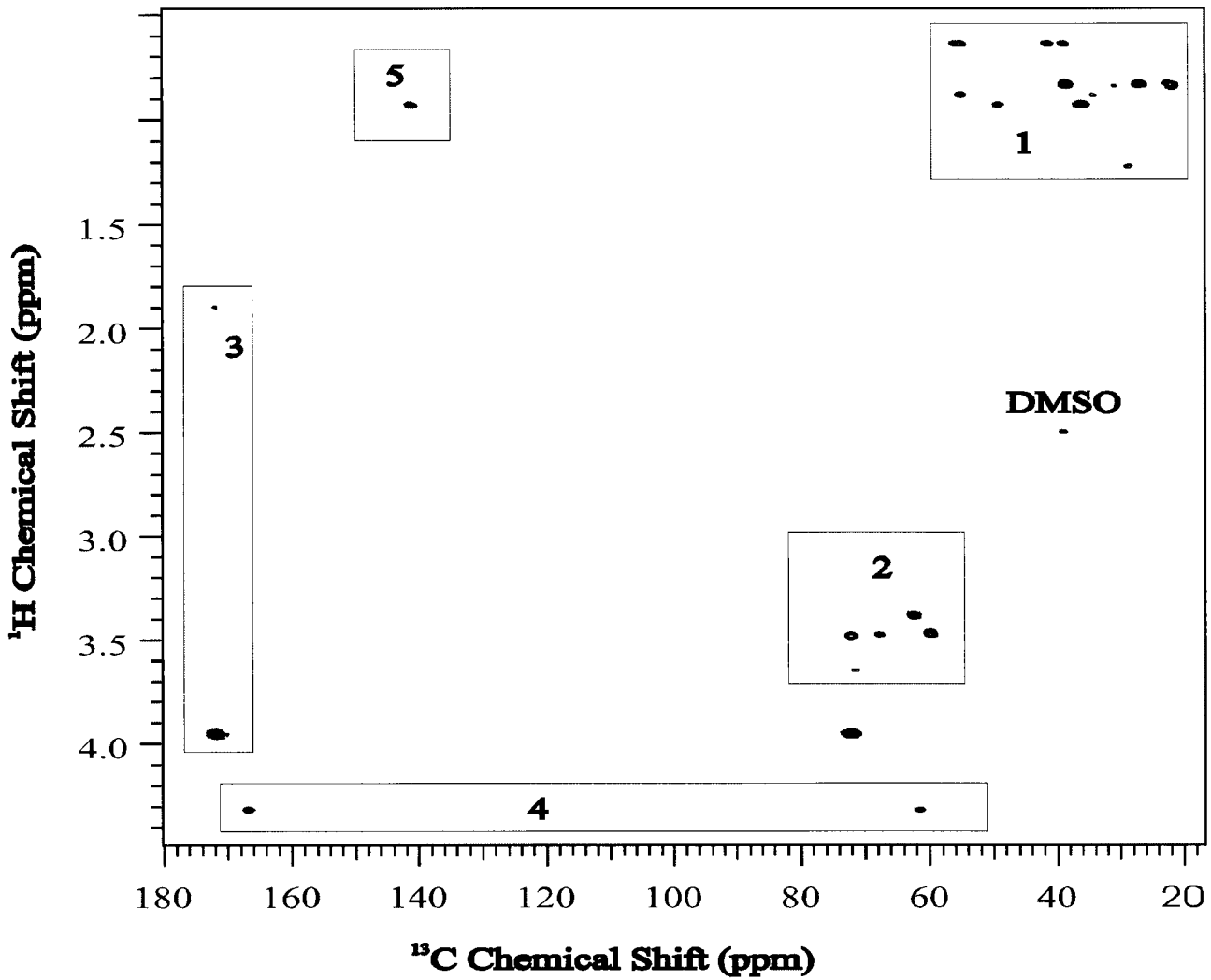

Figure 4.77. gHMBCs spectrum of swelled natural abundance suberin with DMSO (1 mg / 5 mg), MAS = 2.5 kHz. No crosspeaks were observed to the weak resonances at 6 – 8 ppm.

4.2.2.2 Isotopically Labeled Potato Suberin Samples

Isotopic labeling has been demonstrated to be a very useful technique in structural studies of potato suberin.[58] Two ^{13}C labeled precursors, 1-^{13}C-phenylalanine and sodium 1-^{13}C-acetate, were used in the preparation of potato suberin. This sample is called dual labeled potato suberin, and was prepared by Bin Yan.[58] The incorporation of the isotopically labeled precursors into the material has been demonstrated by CPMAS NMR.[58]

The proton and 2D spectra (Figures 4.80 and 4.81) of the dual labeled potato suberin sample show far fewer aliphatic peaks but extra polysaccharide features as compared with the natural-abundance potato suberin sample. The proton spectra of the two samples are expected to be the same, because the labeling is on the nonprotonated carbons. Enhancements of particular 2D signals in HMBC are expected but not observed. About 10 % of the labeled precursors are incorporated into the sample [58] and the labeling is on nonprotonated carbons. The reasons why the expected signal enhancements are not observed are under further investigation.

The dual labeled sample has stronger polysaccharide signals than the natural-abundance sample. The higher proportion of polysaccharide is evidenced by more intense signals of 3 – 4 ppm peaks in the HRMAS ^{1}H spectrum of the swelled sample (Figures 4.75 and 4.78) and more intense signals at 50 – 110 ppm in MAS ^{13}C spectrum of the dry sample (Figure 4.79, bottom). Thus the anomalously large polysaccharide contributions probably reflect incomplete cell-wall removal rather than poor swelling. 2D spectra (gHMQCs and gHMBCs) are consistent with the 1D spectra. The cross peaks in the inset of the gHMBCs spectrum of the dual labeled

sample (Figure 4.80) were not observed in the gHMBCs of the natural-abundance sample. These peaks are attributable to correlations of the ^{1}H attached to carbon 1 of the polysaccharide with other carbons of the polysaccharide. Since the relative intensities of aliphatic proportion of the dual labeled sample are so small, their cross peaks are missing in the gHMBCs of the dual labeled sample (Figure 4.77 and Figure 4.80). This observation is consistent with the anomalously large amount of polysaccharide in the dual labeled sample evidenced in HRMAS ^{1}H and CPMAS ^{13}C spectra of the swelled and dry materials, respectively.

A three-dimensional NOESY-HSQC experiment was run for dual labeled suberin on a 750 MHz spectrometer with MAS of 5 kHz at 50 °C. Two-dimensional HSQC and NOESY experiments were run under the same conditions. The HSQC acquired on a 750 MHz spectrometer has similar features to the gHMQCs acquired on a 600 MHz spectrometer with MAS of 2 kHz at 50°C (Figure 4.81). The NOESY spectrum shows correlations through space (Figure 4.82). Correlations were found among sugar protons and among aliphatic protons, but no correlations between these two moieties were observed, suggesting that they are not located proximally and may not be covalently bonded either.

The 3D NOESY-HSQC experiment was analyzed by slicing the spectrum along the ^{13}C dimension (Figure 4.83). Each slice corresponding to a specific ^{13}C chemical shift shows all of the NOESY correlations of the proton(s) attached to this type of carbon. A cross peak on the diagonal of this sliced NOESY spectrum shows the correlation of the proton(s) to itself. Thus, a diagonal cross peak in a NOESY slice should yield the same chemical structural information as a cross peak in a one-bond

heteronuclear coherence experiment, either gHMQCs or HSQC. The missing peaks for methylene groups in the HSQC spectrum were found in the 3D NOESY-HSQC data (not shown), and the results are consistent with those obtained from the natural-abundance sample which has significant aliphatic correlations in its gHMQCs. New polysaccharide and oxegenated proton-carbon pairs were found in the 3D spectrum (Table 4.14). These new proton-carbon pairs are not evident in any one-bond heteronuclear coherence spectra probably because they are buried in the adjacent strong cross peaks. The intensities of these new peaks, the correlations between these protons and other observed proton resonances, and the reasonable proton-carbon pair chemical shifts suggest that they are not artifacts. The 3D NOESY-HSQC shows more types of protons than in the NOESY spectrum, where overlap may make some types of protons with very close chemical shifts undistinguishable. These results demonstrate that 3D spectra can spread out the crowded peaks and can make more detailed structural information available from the study of swelled samples with HRMAS NMR spectroscopy.

Table 4.14. Proton-Carbon Pairs of Dual-Labeled Suberin Found Only in 3D NMR Spectra.

^{13}C Chemical Shift (ppm)	68.6	71.2	60.3	61.0	62.7	78.8	71.8	72.5
^{1}H (ppm) Attached	4.38	3.58	3.47	3.44	3.37	3.33	3.29	3.20

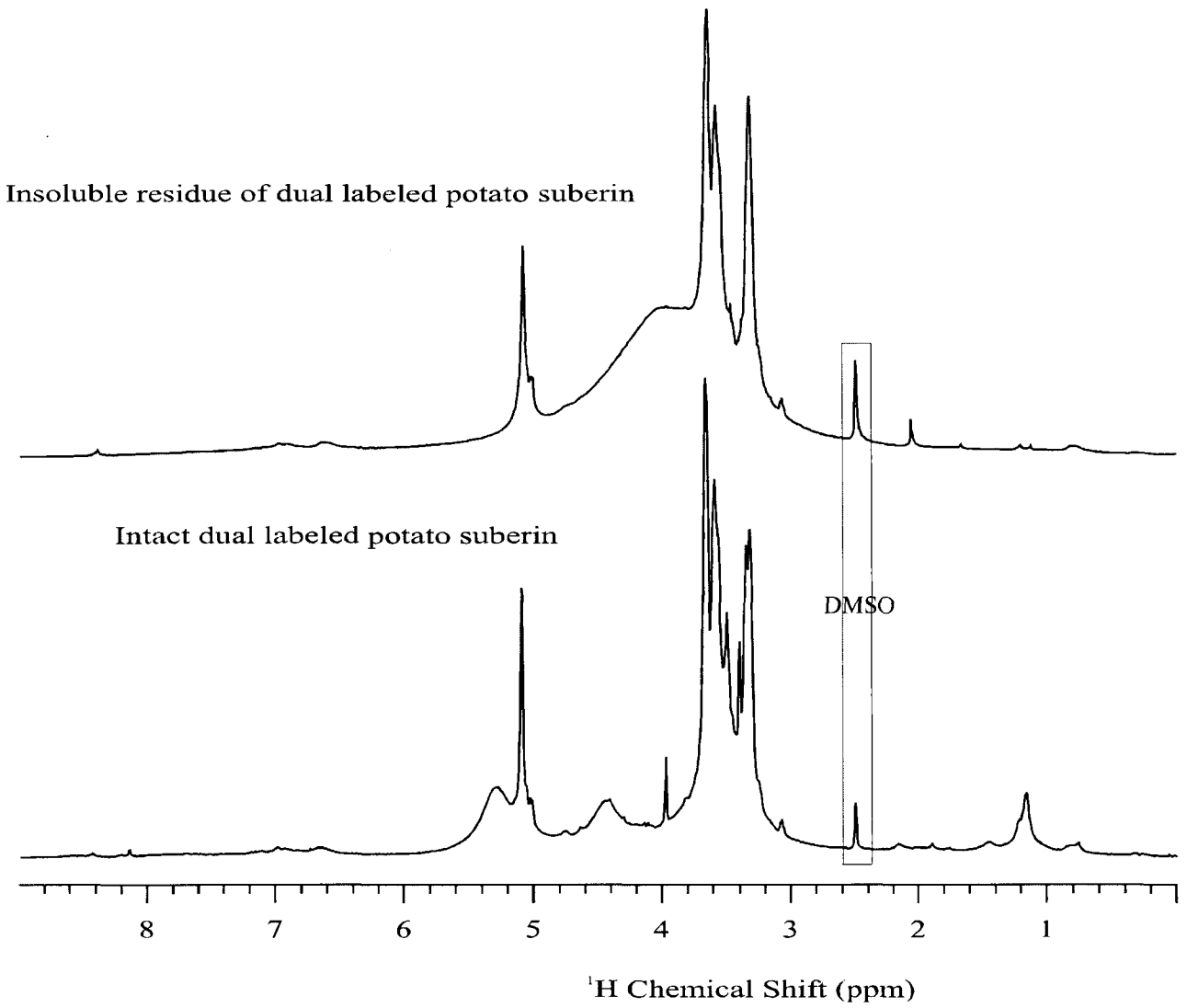

Figure 4.78. Comparison of 600 MHz ^{1}H spectra of swelled dual labeled potato suberin and its insoluble residue after KOH depolymerization, using MAS @ 2.5 kHz.

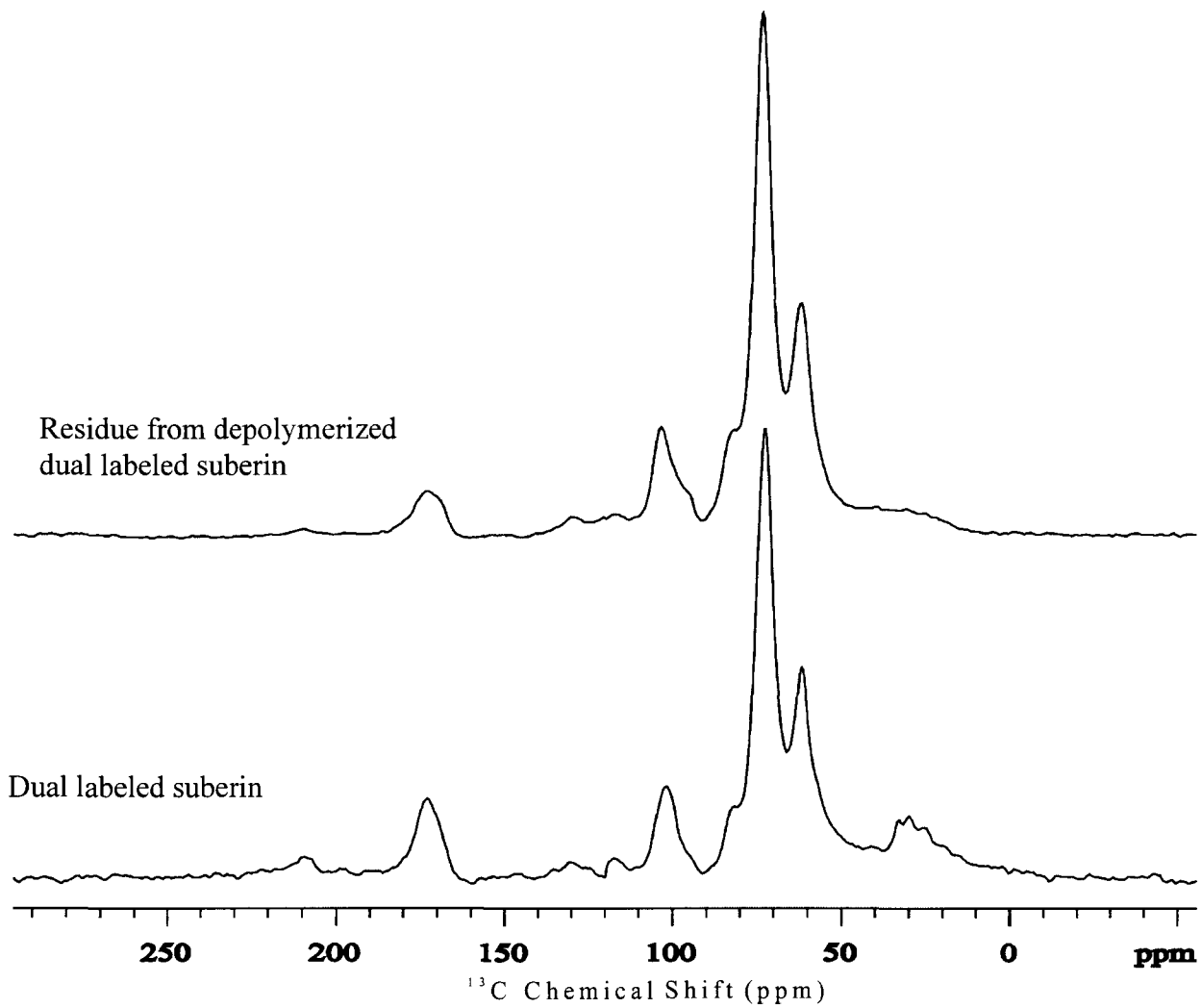

Figure 4.79. 75 MHz ^{13}C spectra of intact dual-labeled suberin and its residue after KOH depolyerization.

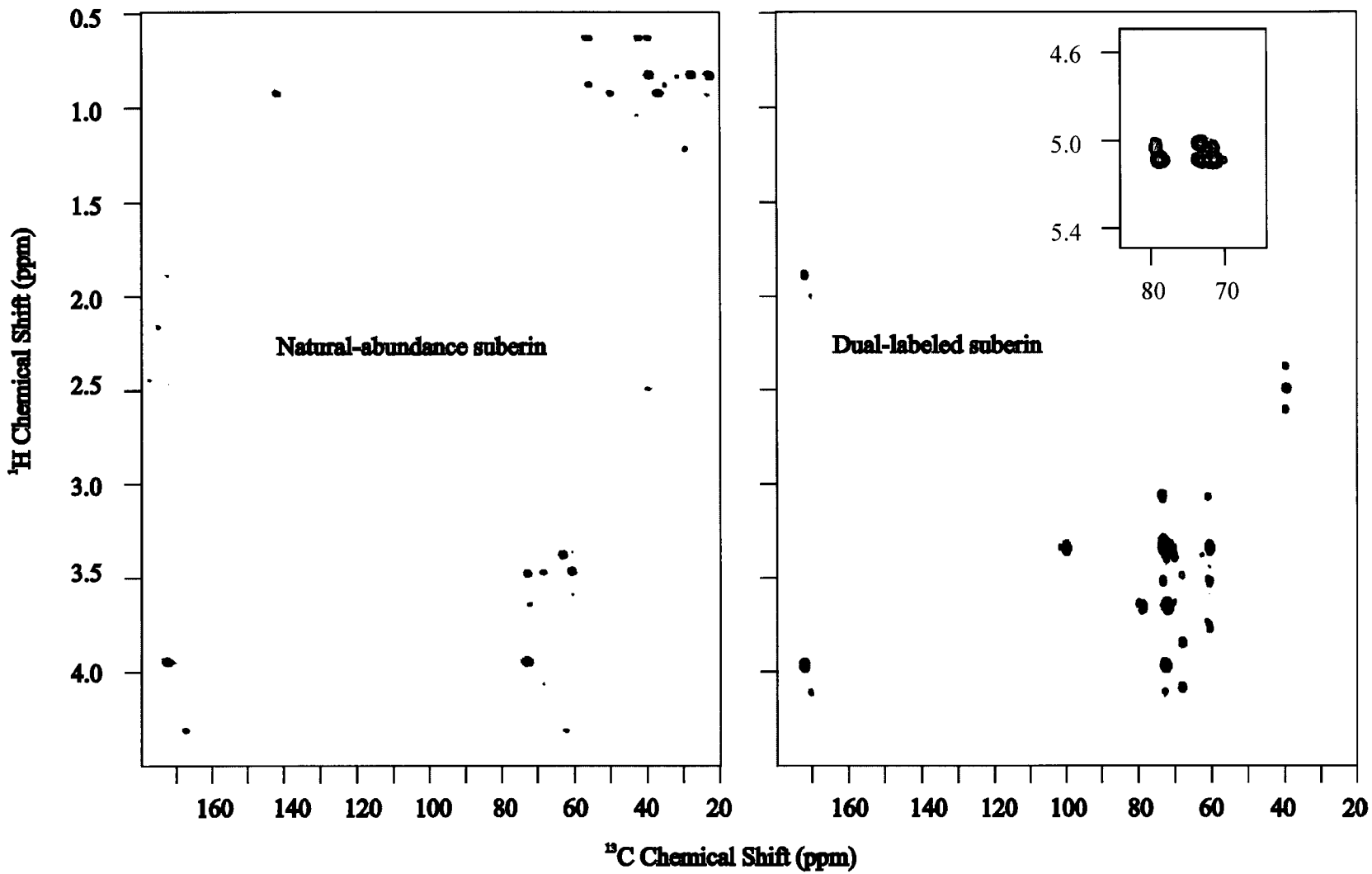

Figure 4.80. Comparison of gHMBCs spectra of swelled natural-abundcance and dual-labeled potato suberin. The inset highlights long-range correlations observed only for labeled samples.

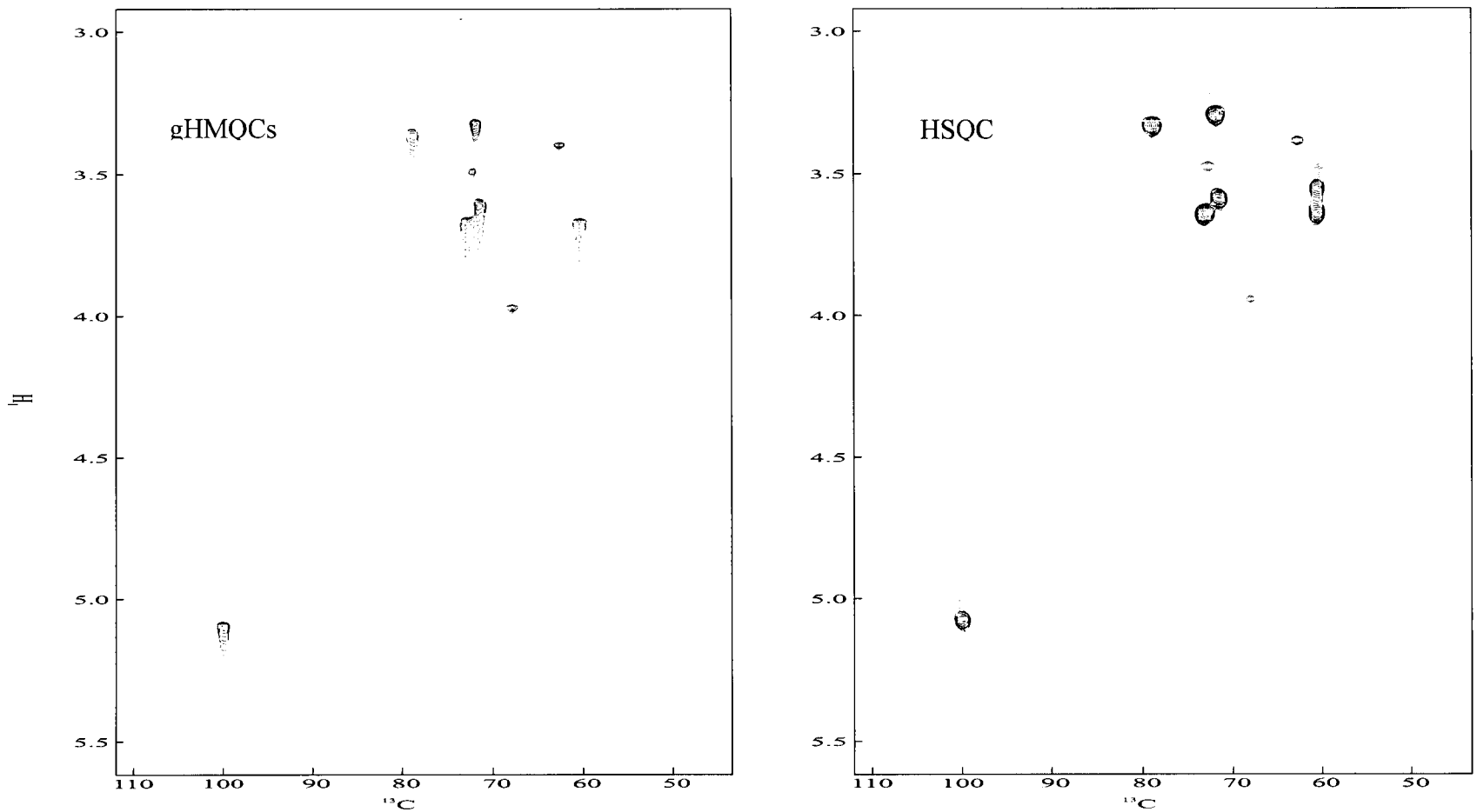

Figure 4.81. Comparison of 600 MHz gHMBCs (MAS = 2 kHz) and 750 MHz HSQC (MAS = 5 kHz) data for swelled dual-labeled potato suberin at 50 °C.

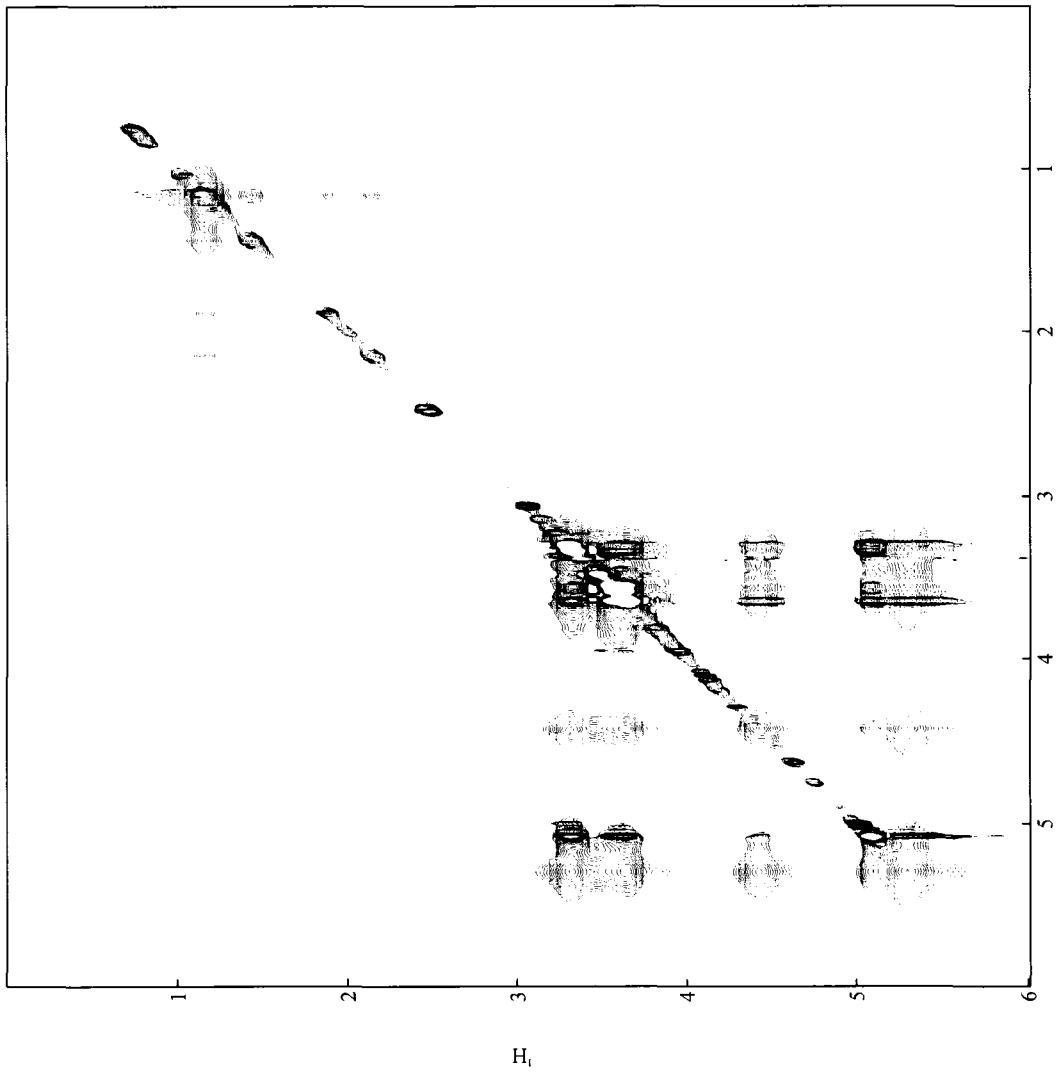

Figure 4.82. 750 MHz NOESY of dual-labeled suberin swelled in DMSO with 5 kHz MAS (mixing time is 75 ms).

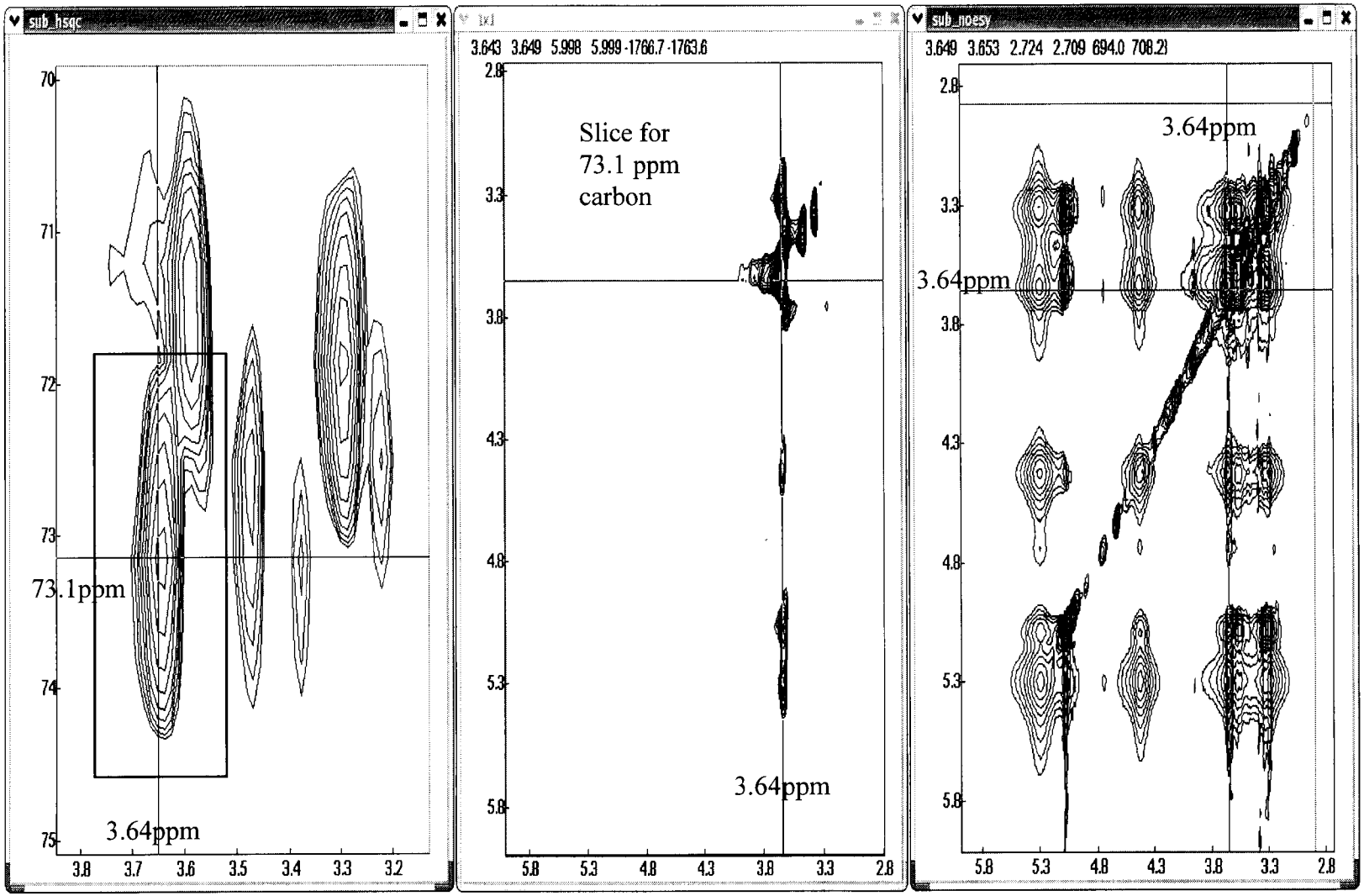

Figure 4.83. A slice of the NOESY-HSQC of dual-labeled suberin swelled in DMSO on a 750 MHz spectrometer with 5 kHz MAS (middle), 2D HSQC (left) and NOESY (right) obtained for the same sample under the same conditions are shown for comparison.

Figure 4.83 shows an example of 3D NOESY-HSQC analysis. When the 3D spectrum is sliced at 73.1 ppm carbon, a NOESY spectrum shows the through-space correlations for the proton at 3.64 ppm that is attached to this carbon. A cross peak of 3.64 ppm to 3.64 ppm on the diagonal (Figure 4.83, middle) confirms the HSQC cross peak at 3.64 ppm ^{1}H and 73.1 ppm ^{13}C (box of Figure 4.83, left). The NOESY slice of the 3D spectrum is much clearer than the 2D NOESY (right), because the slice shows only the correlations of the 3.64 ppm proton attached to the 73.1 ppm carbon. Table 4.15 shows the proton-carbon pairs found in both the 2D HSQC and the 3D NOESY-HSQC, and Table 4.16 shows the identified NOESY correlations from the 2D NOESY and the 3D NOESY-HSQC. Although some protons show diagonal NOESY cross peaks in the 3D spectrum at high field, these peaks may not represent for all ^{1}H-^{13}C pairs since the 3D experiment only covers the carbon range of 50 ppm to 110 ppm. A polysaccharide moiety was deduced from 2D gHMQCs, gHMBCs, NOESY and 3D NOESY-HSQC assignments (Figure 4.84). The observed HMBC correlations are marked on the structure with arrows in Figure 4.84. Some expected connectivites are missing probably due to the closeness of chemical shifts of some polysaccharide carbons and protons. Given the predominance of polysaccharides in this particular sample, no definite information on the polyester moieties is available.

Table 4.15. Proton-Carbon Pairs of Dual-Labeled Suberin Found in 2D and 3D NMR Spectra.

^{13}C Chemical Shift (ppm)	100.1	100.9	65.5	67.7	67.9	60.2	60.5	71.6
^{1}H (ppm) Attached	5.08	5.01	4.28	4.11	3.96	3.77	3.74	3.64
^{13}C Chemical Shift (ppm)	60.0	72.4	72.4	72.4	62.5	78.9	71.9	70.1
^{1}H (ppm) Attached	3.60	3.53	3.49	3.48	3.39	3.33	3.30	3.06

Table 4.16. NOESY Correlations of Dual Labeled Suberin Found in 2D and 3D Spectra.

Chemical Shift (ppm)	5.30	5.08	4.43	3.95	3.64	3.58	3.33	3.30	2.15	1.88	1.44	1.15	0.75
5.30		x	x		x	x	x	x					
5.08	x		x		x	x	x	x					
4.43	x	x			x	x	x	x					
3.95													
3.64	x	x	x	x			x	x					
3.58					x								
3.33					x	x		x					
3.30	x	x	x										
2.15												x	
1.88												x	
1.44												x	
1.15									x	x	x		x
0.75												x	

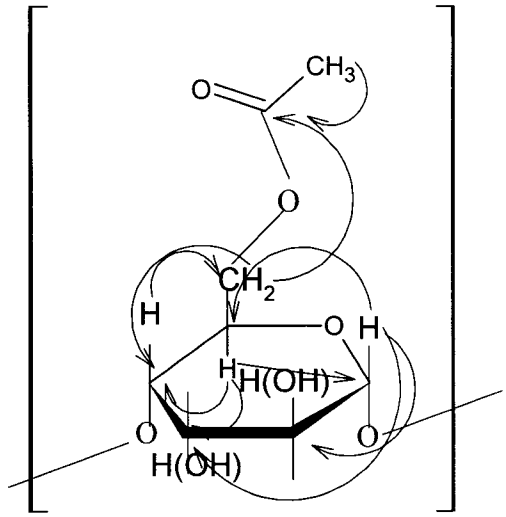

Figure 4.84. Deduced structure for part of the polysaccharide moiety, showing gHMBCs correlations.

4.2.3 Degradation and Preliminary Product Purification

Crude depolymerization products from traditional KOH treatment of potato suberin were pre-purified using silica gel column chromatography. A step gradient solvent system was used: 100% hexanes, 3:1 hexanes: acetone, 100% acetone, and 100% methanol. Each portion of the solvents was almost equal in volume. Figure 4.85 shows the ^{1}H NMR spectra of some representative fractions. From the bottom to the top the polarities of the fractions increase. At the top is the spectrum of the crude product. The peaks at 5.29 ppm are assigned to the protons of mid-chain aliphatic double bonds. These peaks show up only in the fractions with medium polarities, but not in the highly polar or highly nonpolar fractions. Peaks at 1.93 ppm correspond to the methylene groups next to the mid-chain double bonds and follow the trends for the 5.29 ppm peaks. Monomers with analogous mid-chain aliphatic double bonds are common in most monomers and oligomers from KOH depolymerization that have been separated with TLC and identified with MS and

NMR (X. Fang and W. Wang, personal communication). There are no significant peaks from these double bonds in the 1D or 2D spectra for swelled or dry suberins (Figures 4.75 – 4.83), but the peak is significant in the crude degradation products. This result could imply that the KOH treatment favors the depolymerization of monomers that contain double bonds.

Separation trends and molecular structure: Fractions from the silica gel column pre-purification reveal some structural trends with increasing polarity of the fractions. Table 4.17 lists the ^{1}H NMR peaks observed and the corresponding functional groups. Peaks between 6.5 and 7.5 ppm arise from aromatic structures in the products; the peak at 5.29 ppm from mid-chain double bonds can represent double bond monomers or their oligomers; the peak at 4.03 ppm from a primary alcohol an ester bond can represent oligomers; the peak at 3.61 ppm from a methoxyl group of an ester bond can represent a methyl ester; the peak at 2.38 ppm arising from methylene groups next to the oxo group can be derived from monomers or their oligomers; the peak at 2.28 ppm arises from the carboxylic acid side of the ester bond; peaks between 0.6 and 1.0 ppm arises from methyl groups. The nonpolar fraction eluted with 100 % hexanes (Spectrum 1 in Figure 4.85) displays no peaks at 5.29, 4.03, 3.61, 2.38, or 2.28 ppm. This suggests that there are no ester bonds or aliphatic double bonds in this fraction. Thus, this fraction has no polyester oligomers and mainly contains waxes without any functional groups. The two less polar fractions eluted with hexanes/acetone (3:1 by volume) (Spectra 2 and 3 in Figure 4.85) display no aromatic peaks; they have more intense peaks at 5.29 and weaker peaks at 2.38 than other more polar fractions and the crude product. Thus,

they mainly contain double-bond monomers and their oligomers with some amount of oxo monomers and their oligomers. It is also possible that these fractions have some oligomers containing both double-bond monomers and oxo monomers. Our subsequent HPTLC and HPLC separation and purification procedures favor the compounds falling in this polarity regime, and many of our identified monomers and oligomers contain double bond monomers (X. Fang and W. Wang, personal communication). The two polar fractions eluted with acetone (Spectra 4 and 5 in Figure 4.85) display aromatic components and a higher portion of oxo groups. These portions are more interesting because oligomers with connections between aliphatic and aromatic moieties may be found in these fractions, but their separation and purification are more challenging than the less polar fractions. Spectrum 4, which was collected at the beginning of the hexanes/acetone (3:1 v/v) elution, has a greater portion of aromatic compounds than Spectrum 5, which was collected at the end of the hexanes/acetone (3:1 v/v) elution (Figure 4.85). The very polar fraction eluted with methanol (Spectrum 6 in Figure 4.85) displays neither double bonds nor aromatic compounds, but it has a greater portion of oxo monomers or their oligomers. Further separation and purification of this fraction is also very challenging, but MS-MS could offer an alternative identification strategy.

Table 4.17. ^{1}H chemical shifts and functional groups in depolymerized products of potato suberin.

CS	6.5-7.5	5.29	4.03	3.61	2.38	2.28	0.6-1.0
FG	aromatic	-HC=CH-	$-CH_2O\overset{O}{\overset{\|}{C}}-$	$CH_3O\overset{O}{\overset{\|}{C}}-$	$-CH_2\overset{O}{\overset{\|}{C}}CH_2-$	$-CH_2CO_2-$	CH_3-

The KOH depolymerization mainly breaks down aliphatic ester bonds. The ^{13}C CPMAS NMR intensity of the peak at 175 ppm gets weaker after KOH treatment of the material (Figure 4.79). The change of the intensity of this carbonyl carbon means that some of the ester bonds have been broken down by KOH. A significant decrease of the intensities of peaks at 0 ~ 50 ppm indicates that most of the aliphatic portion of the material has also been removed from the material. A decrease in the aliphatic portion after KOH treatment is also observed in the ^{1}H NMR spectra of the insoluble residue as compared with the intact material (Figure 4.78). Relatively higher intensities for peaks at 0 ~ 2.5 ppm in the ^{1}H NMR spectrum of the soluble mixture (top, Figure 4.85) confirm that the cleaved aliphatic portion goes into the soluble part of the KOH depolymerization. The missing peak at 5.3 ppm from the ^{1}H HRMAS NMR spectrum of the insoluble residue (Figure 4.78) indicates that most of the aliphatic C-C double bonds have been depolymerized, and they are observed in the soluble mixture (top, Figure 4.85)

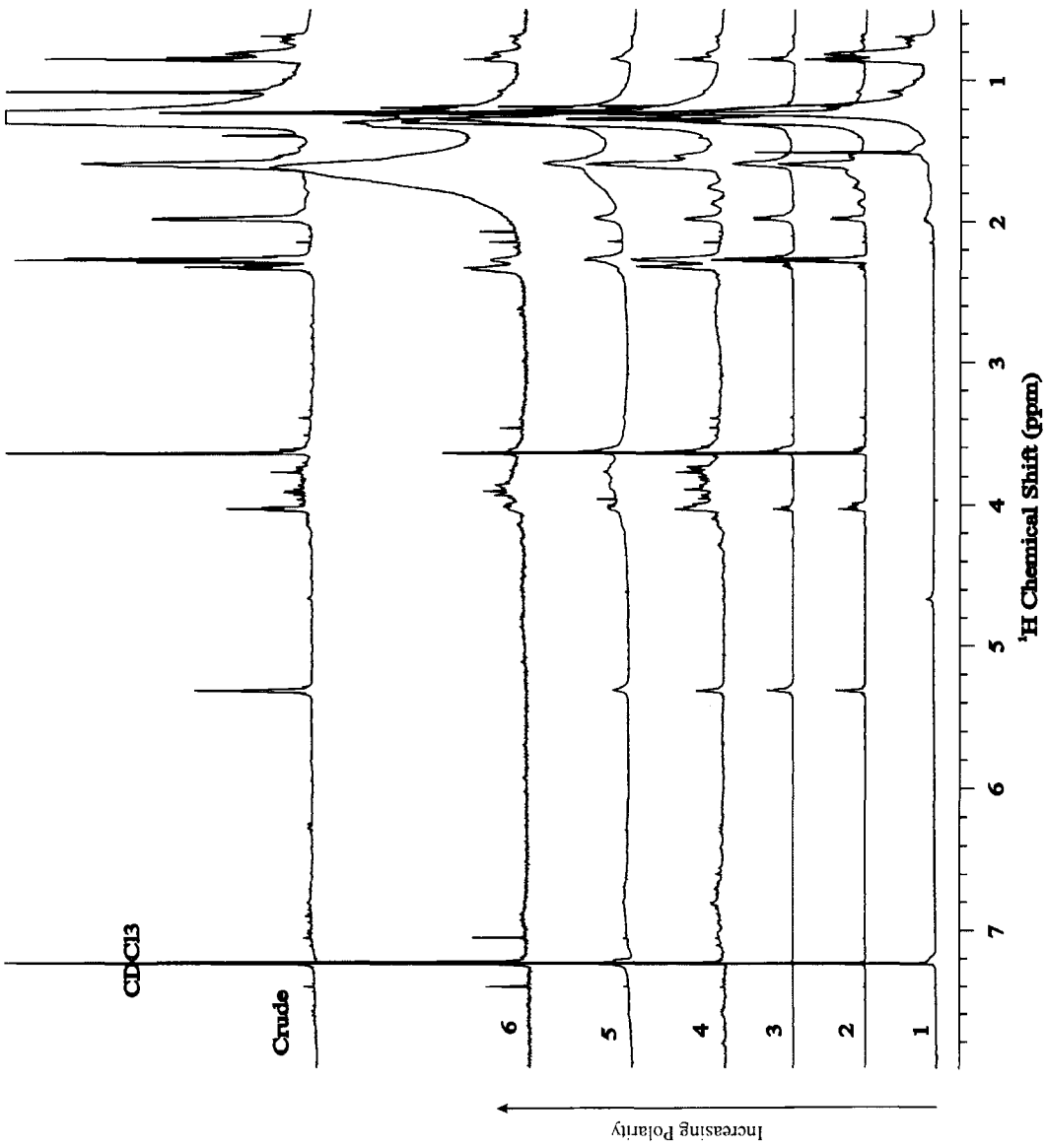

Figure 4.85. 600 MHz ^{1}H spectra of depolymerized suberin mixture and silica gel column fractions.

4.2.4 Conclusions (Intact Potato Suberin and Oligomeric Fragments)

Information on the molecular structure of suberin can be extracted from CPMAS NMR ^{13}C NMR of powdered samples, HRMAS NMR of solvent-swelled materials, depolymerization products and isotopic labeling. All strategies show that there are aliphatic, aromatic, and polysaccharide constituents in potato suberin. The absence of polysaccharides from the soluble products may result from the extraction procedure of the products, because only the organic solvent soluble products were collected in the extraction. Depolymerized polysaccharide, which should not be soluble in chloroform, may have been discarded without any study. As a complementary method, HRMAS NMR can provide more details than CPMAS NMR, but some types of chemical structures shown in CPMAS NMR do not appear in HRMAS NMR, possibly due to different swelling efficiencies of DMSO on different chemical structures. In addition to 1D and 2D experiments with HRMAS NMR, a 3D experiment was demonstrated to be applicable to the study of plant biopolymers. Isotopic labeling can enhance MAS NMR signals of some carbons related to the labeled precursors, but the corresponding signal enhancements were not observed in HRMAS NMR. The reasons for missing peaks or lack of signal enhancements of labeled samples in HRMAS NMR are under investigation.

In the depolymerization studies, we are seeking larger oligomers retaining more monomer linkage information, which is important to understand the whole molecular structure and function of the material. More efforts should be given to the polar fractions eluted with actetone, because they contain a lot of oligomers and more diverse types of chemical components (oxo, double bond aliphatic monomers

and their oligomers, aromatic compounds, and possibly oligomers containing both aliphatic and aromatic monomers). No monomer linkage information could be obtained from the nonpolar fractions since they contain no oligomers.

4.3 Results for Fungal Melanin

4.3.1 Solid-State Results

A portion of these results were published previously.[70]

In contrast to many other microorganisms, *C. neoformans* synthesizes melanin only in the presence of exogenous substrates, namely, *o*-diphenols such as L-dopa (L-3,4- dihydroxyphenylalanine) that have hydroxyl groups at positions 2 and 3 or 3 and 4 of the phenyl group. The pigment is deposited in the cell wall and can be extracted in the form of hollow particles that resemble cells (melanin "ghosts") using denaturants and hot HCl [28]. Since melanin synthesis in *C. neoformans* is completely dependent upon exogenous substrate, it is possible to obtain a biopolymer derived from a single precursor that can be labeled isotopically. Studies of melanin from labeled precursors can identify covalent linkages and close distances among different functional groups with 2D NMR. This strategy can provide much better information on chemical structure of melanin than sole reliance on chemical shift trends.

Compositional and Dynamic Profiles of Fungal Melanin from Solid-State ^{13}C NMR.[70] A comparison of CPMAS ^{13}C NMR spectra for melanins from several fungal sources is shown in Figure 4.86. In all cases, the chemical shifts were consistent with molecular structures that include open chain methylene groups (30

ppm), oxygenated aliphatic carbons (72 ppm), aromatic and/or olefinic carbons (110-160 ppm), and carboxyls (170 ppm). The peak at 72 ppm may include contributions from polysaccharides in the fungal cell wall. The signal intensities measured as a function of cross-polarization time (Table 4.18, and Figure 4.87) verify that the *C. neoformans* spectrum provides a fair compositional estimate of the rigid carbons in the melanin sample. Additional insight into the molecular architecture of this melanin was gained from MAS ^{13}C NMR spectra obtained without cross-polarization or nuclear Overhauser effects. By comparison of the integrated peak intensities with and without (6.09) high-power (DPMASSD) decoupling (17.43, DPMASDD; 6.09, DPMASSD; Figure 4.88), it was estimated that 35% ((6.09/17.43)* 100 % = 35%) of the methylene chain segments undergo sufficient motion at 75 MHz to exhibit liquid-like spectra. Significant molecular mobility of these chains is also evident from the retention of some methylene chain NMR signals under delayed decoupling conditions and the observation of 5 kHz ^{1}H CH_2 line widths in wide-line separation experiments (not shown). Although somewhat surprising in light of melanin's insolubility in organic and aqueous solvents, this finding of molecular flexibility has precedent in studies of lime fruit cutin. [37]

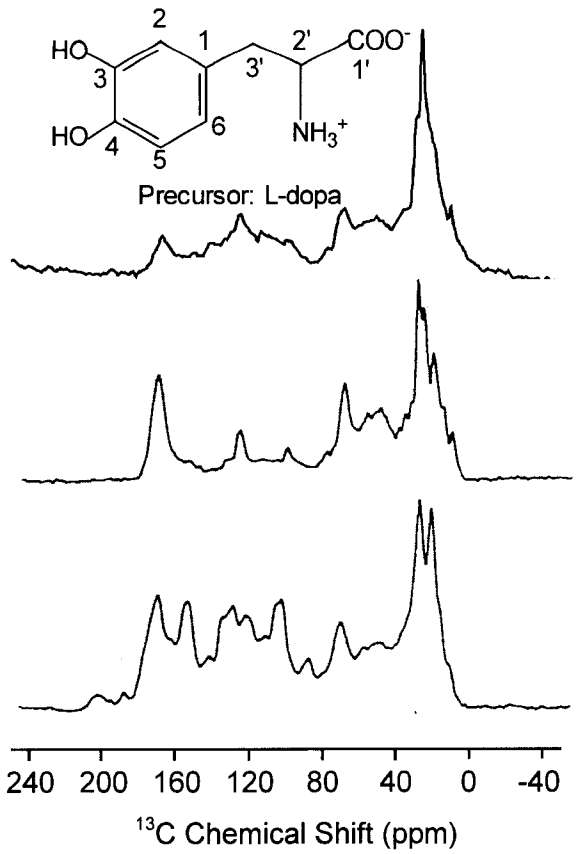

Figure 4.86. CPMAS ^{13}C NMR spectra of solid fungal melanins: 25 MHz spectrum of *Oidiodendron tenuissimum* melanin (bottom), 25 MHz pectrum of *Trichoderma harzianum* melanin (middle), and 75 MHz spectrum of *Cryptococcus neoformans* melanin, produced with a natural-abundance L-dopa precursor (shown above the spectrum) and requiring 9 h of spectral acquisition (top).

Table 4.18. Peak Intensity Changes with Contact Time for Natural Abundance Melanin

contact time (s)	30.2ppm	74.3ppm	132.4ppm	176.2ppm	207.6ppm
0.0005	144.48	71.94	63.92	42.64	30.29
0.0010	127.61	64.23	61.9	43.86	21.39
0.0015	108.83	36.94	43.56	33.08	10.74
0.0020	96.47	32.09	39.92	30.27	11.2
0.0025	85.15	27.73	33.26	23.56	4.21
Extrapolated Intensities	164.91	94.36	79.24	63.13	52.75

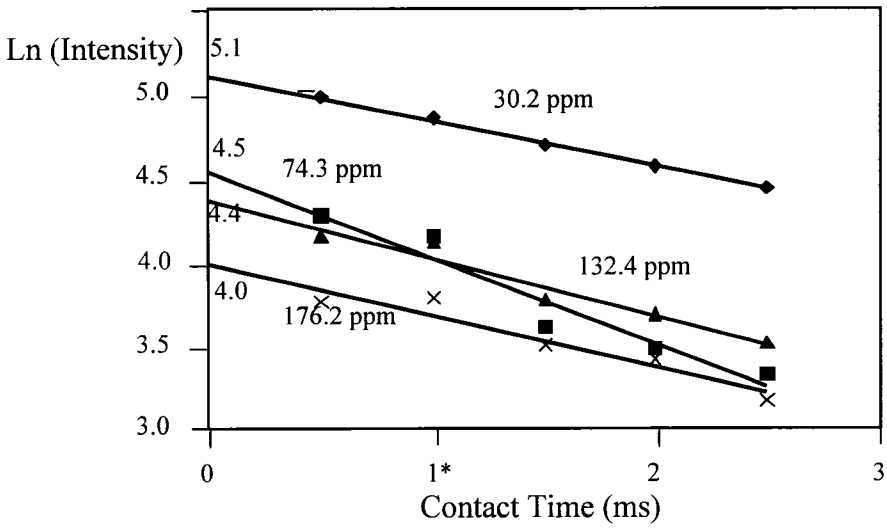

*: Contact time used to acquire data in Figure 4.87.

Figure 4.87. Variation of peak intensities with ^{1}H-^{13}C contact time for melanin carbons.

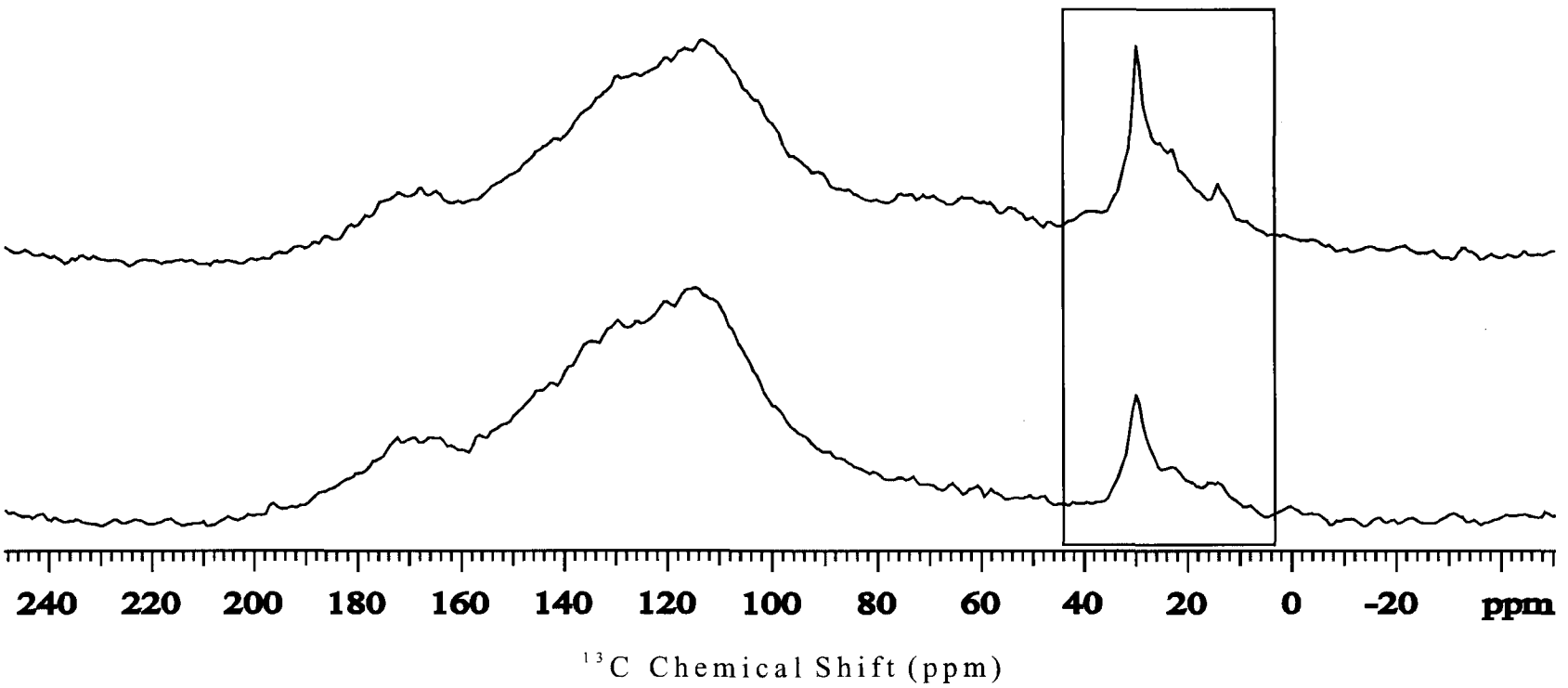

Figure 4.88. Comparison of signal intensities of methylene carbons in melanin from MAS ^{13}C NMR with (top) and without (bottom) high power decoupling during the spectral acquisition period. The broad features centered at 120 ppm are artifacts from the rotor materials.

Site-Specific Incorporation of ^{13}C Labels and Structural Information. As noted in Section 4.3.1, *C. neoformans* requires exogenous substrates to synthesize melanin. This requirement allows the investigator to choose the substrate and isotopic labeling pattern to probe particular structural elements spectroscopically and to monitor the consequences of biosynthetic incorporation into the developing polymer. Figure 4.89 shows CPMAS ^{13}C NMR results for *C. neoformans* melanin synthesized in the presence of a 2,3-$^{13}C_2$-L-dopa substrate, in which resonances corresponding to the two enriched protonated aromatic carbons are enhanced dramatically compared with the chain methylenes, but some ^{13}C incorporation may also occur for resonances at 30 and 150 ppm. If the amount of aliphatic signal in Figure 4.86 (top) is assumed provisionally to be unchanged in the spectrum of Figure 4.89, then the integrated intensity of the aromatic spectral region is found to increase 9-fold.

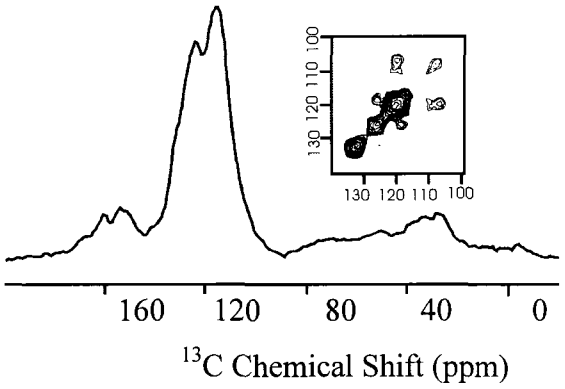

Figure 4.89. CPMAS ^{13}C NMR spectrum (75 MHz) of *C. neoformans* melanin produced with a 2,3-$^{13}C_2$-L-dopa substrate. The inset shows a contour plot from a 14 h 2D proton-driven ^{13}C-^{13}C spin diffusion experiment on the selectively ^{13}C-enriched melanin sample.

The ability to observe prominent aromatic resonances in the ^{13}C-labeled sample (Figure 4.89) suggests that the modest signal intensity evident in the natural-abundance sample can be attributed to a small proportion of this carbon type in *C. neoformans* melanin rather than a possible effect of paramagnetic broadening. Although the resonance at 124 ppm exhibits a chemical shift comparable to position 2 in the L-dopa monomer,[59] the peak at 114 ppm varies significantly from its monomer position 3 (145 ppm), suggesting that the latter site is no longer occupied by a hydroxyl group upon formation of the biopolymer.

With the incorporation of ^{13}C-enriched substrates into *C. neoformans* melanin, it also becomes possible to test hypotheses regarding the spatial proximity and covalent bonding of particular molecular sites. As an illustration, the inset of Figure 4.89 shows results from a ^{13}C-^{13}C spin diffusion experiment on this material. The observation of strong cross-peaks demonstrates the proximity of the labeled carbons, in accord with prior reports showing that these directly bound atoms in L-dopa remain covalently linked in the melanin polymer [91]. The intensities of cross peaks of a 2D ^{13}C-^{13}C spin diffusion spectrum can be estimated by integrating peaks of the 1D trace that contains the highest cross peaks in either dimension. Ratios of intensities of cross peaks can be calculated and compared with the pattern for a known labeled compound in order to deduce ^{13}C-^{13}C proximities. Figure 4.90 shows the ^{13}C-^{13}C spin diffusion spectrum of ring-labeled phenylalanine, which has 5 labeled ring carbons at higher frequency and one labeled ring carbon at lower frequency. If we set the intensity of the lower frequency ring carbon to 1, then the average intensity of the other labeled carbons (Peaks 4) is 9. By contrast, the

average ratio of the intensity of peak 1 to the intensity of peak 4 (corresponding to 1 ring carbons) of the L-dopa labeled melanin (Figure 4.91) is 1:2.1. These two experiments were run under the same conditions. Thus, almost half of the carbon pairs remain neighbors during melanin biosynthesis (calculation not shown).

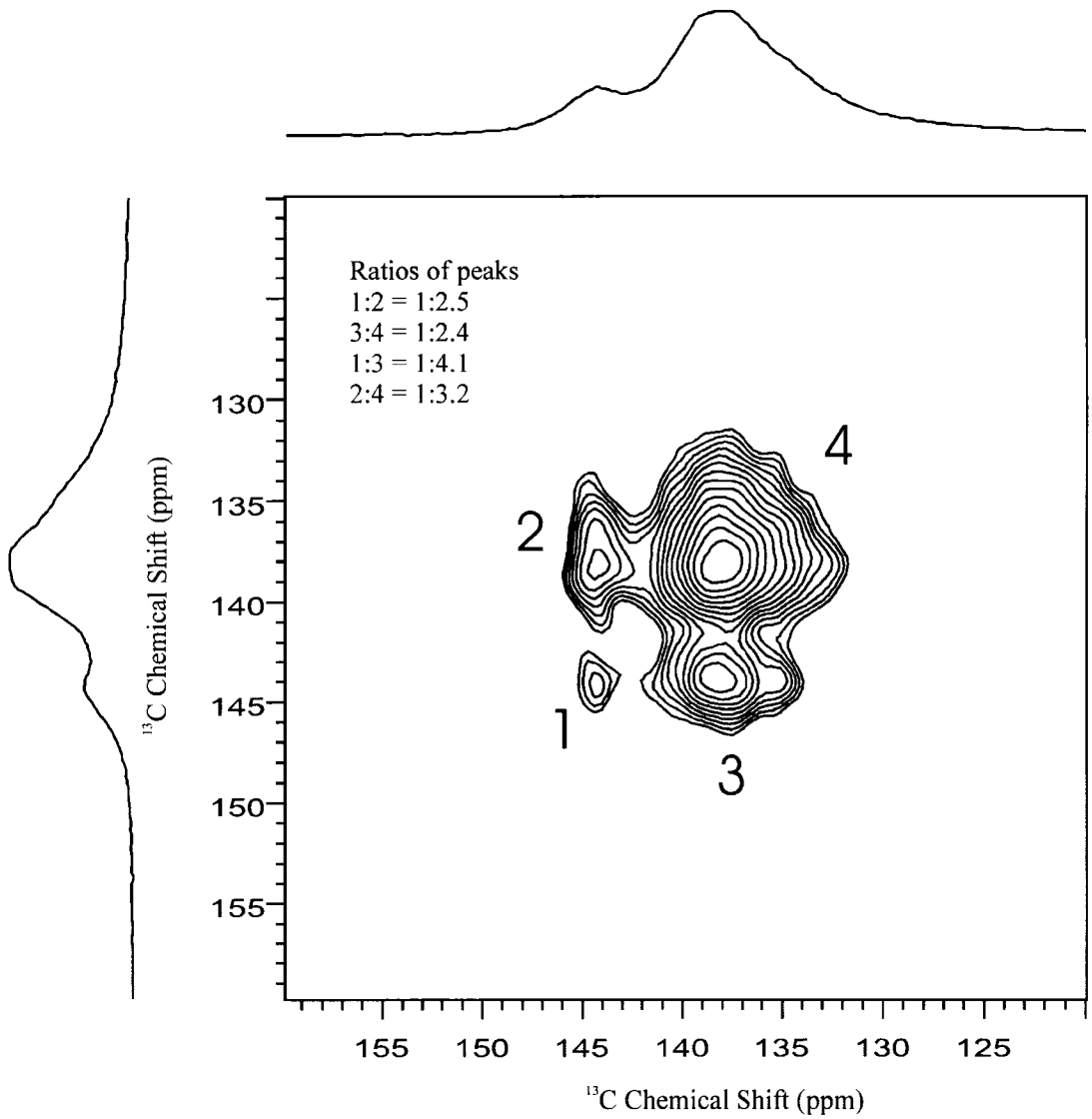

Figure 4.90. Spin diffusion experiment on ring-labeled phenylalanine.

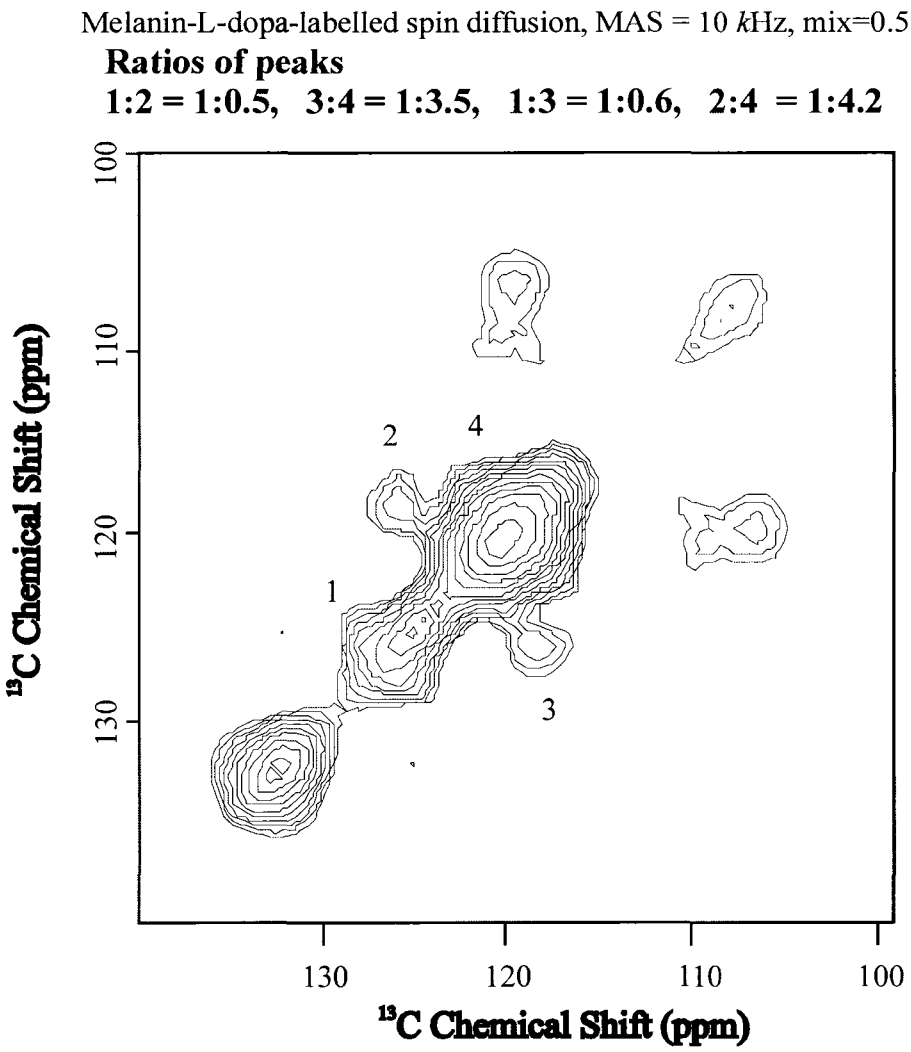

Figure 4.91. Spin diffusion experiment on L-dopa labeled melanin.

In order to demonstrate the spatial and structural relationship between cellulose in the fungal cell walls and the melanin, 1-^{13}C labeled D-mannose was used in the preparation. The results show major signal enhancement of the sugar part (Figure 4.92), suggesting that the polysaccharide is tightly associated with (or bound to) melanin, so that it is retained when the melanin ghosts are isolated.

Epinephrine has a similar structure to that of L-dopa, so it can also be used to synthesize melanin. Unexpectedly, the CPMAS ^{13}C spectrum of epinephrine melanin (Figure 4.93, bottom spectrum) acquired on a 750 MHz spectrometer at a spinning speed of 10 kHz is more similar to that of melanin from 1-^{13}C-D-mannose precursor (Figures 4.92 and 4.93) than that of the L-dopa melanins. The spectrum of epinephrine melanin has much better resolution. Although higher field and higher MAS speed undoubtedly contribute to this improvement, the presence of fewer free radicals in epinephrine melanin could play a more important role here. Figure 4.94 shows the spectral resolution improvement of 1-^{13}C-D-mannose labeled melanin caused by increasing the field by a factor of 2.5 while keeping the spinning speed constant. The improvement with increased field is not especially dramatic. Thus, the epinephrine melanin sample itself must be the primary reason for the huge resolution improvement. Other than the functional groups found in natural abundance L-dopa melanine, sugar moieties (101 ppm, 60 ppm), proteinaceous materials (C_α, ~50 ppm), and keto groups (225 ppm) were also found in epinephrine melanin. The intensity of polysaccharide peaks is comparable to that of the 1-^{13}C-D-mannose melanin. This could suggest that different precursors may result in some structural differences. The top spectrum of Figure 4.93 is the delayed decoupling

CPMAS ^{13}C spectrum of epinephrine melanin. It shows the nonprotonated and mobile methylene carbons (see Chapter 2). This finding proves that the carbons between 50 and 120 ppm are protonated carbons, and that carbons between 10 and 40 ppm are mobile methylene carbons.

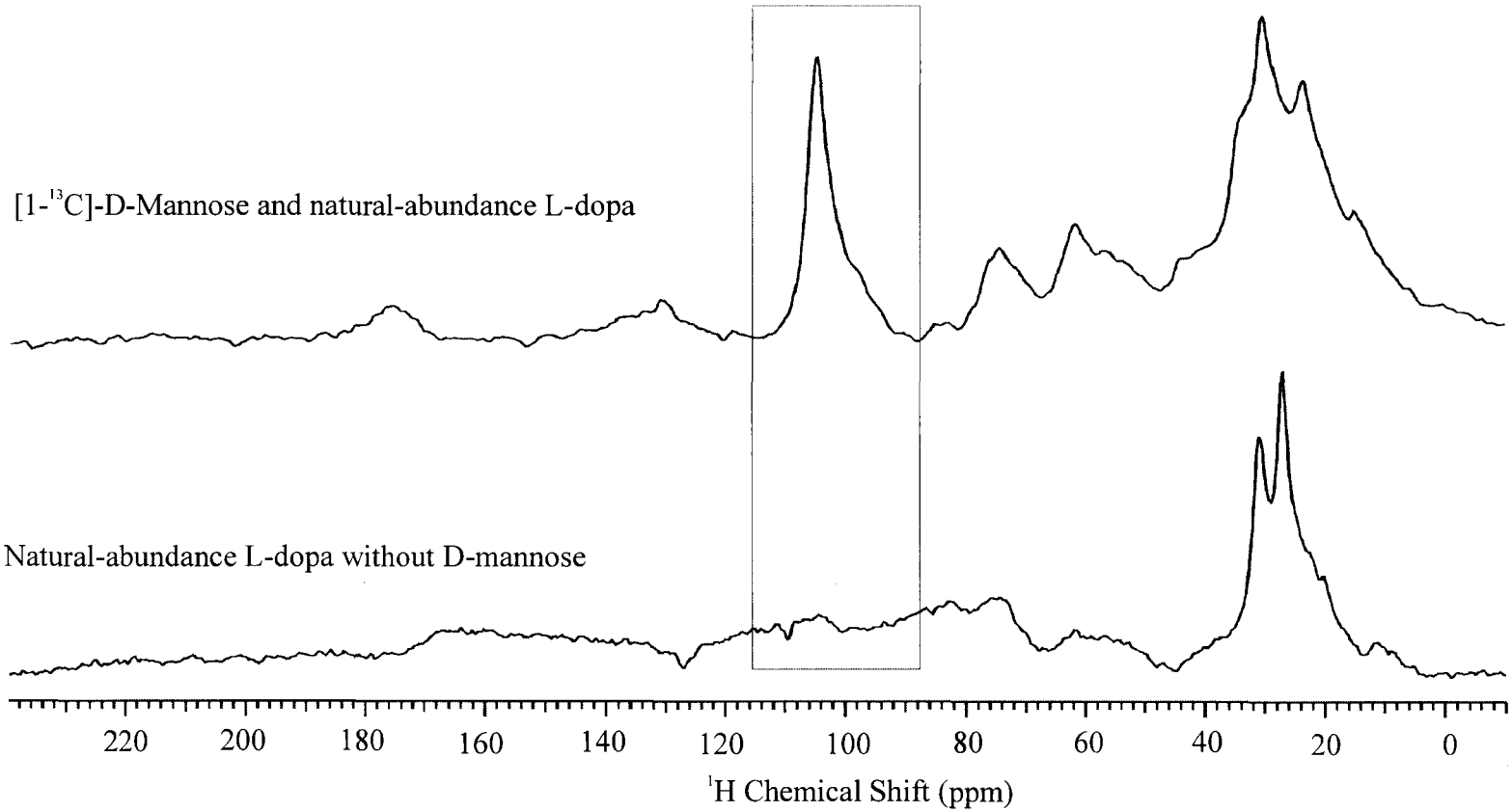

Figure 4.92. Signal enhancement of carbons from the labeled precursor confirms incorporation into the *C. neoformans* L-dopa melanin ghosts.

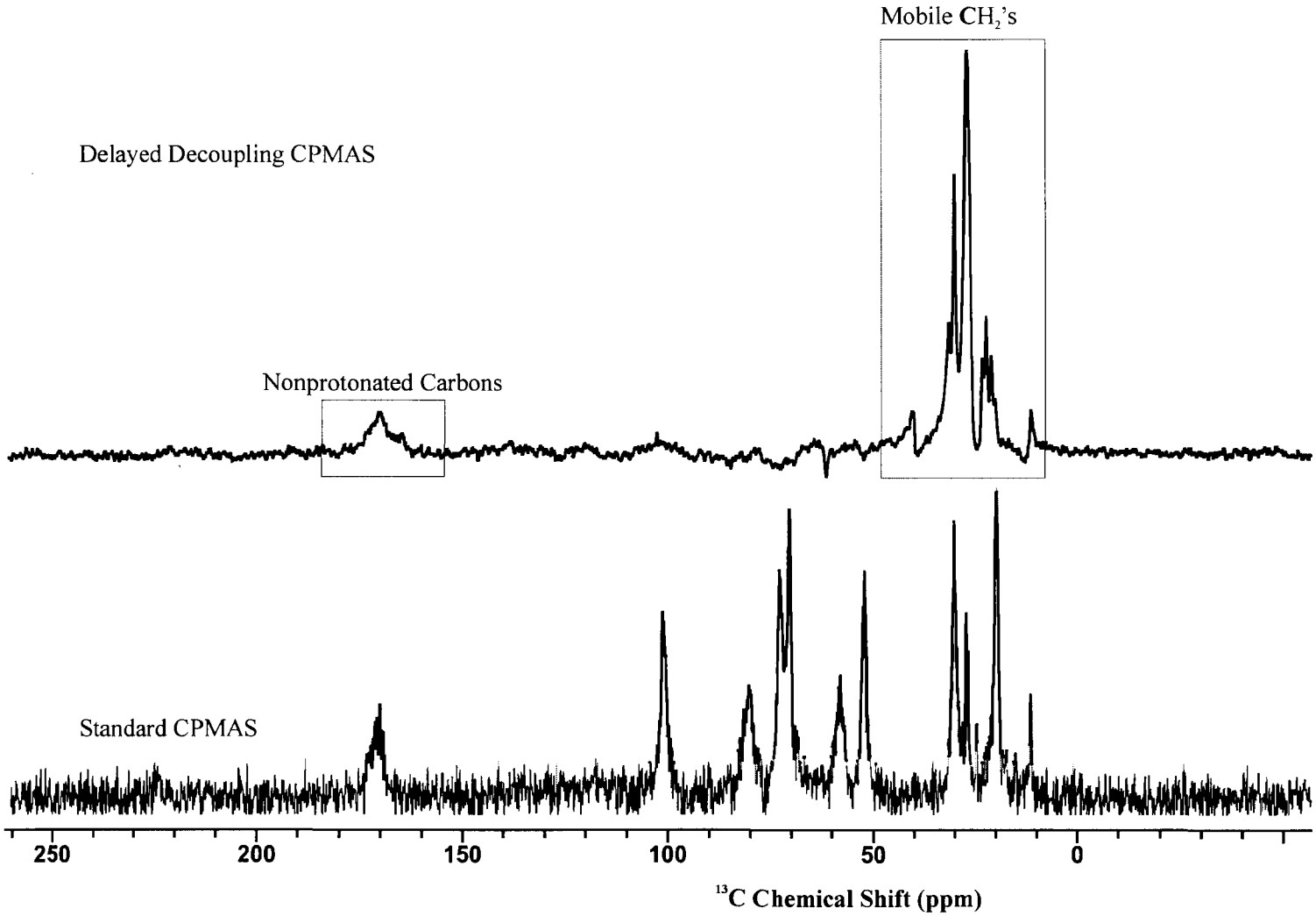

Figure 4.93. CPMAS ^{13}C NMR spectra of epinephrine melanin on a 750 MHz spectrometer.

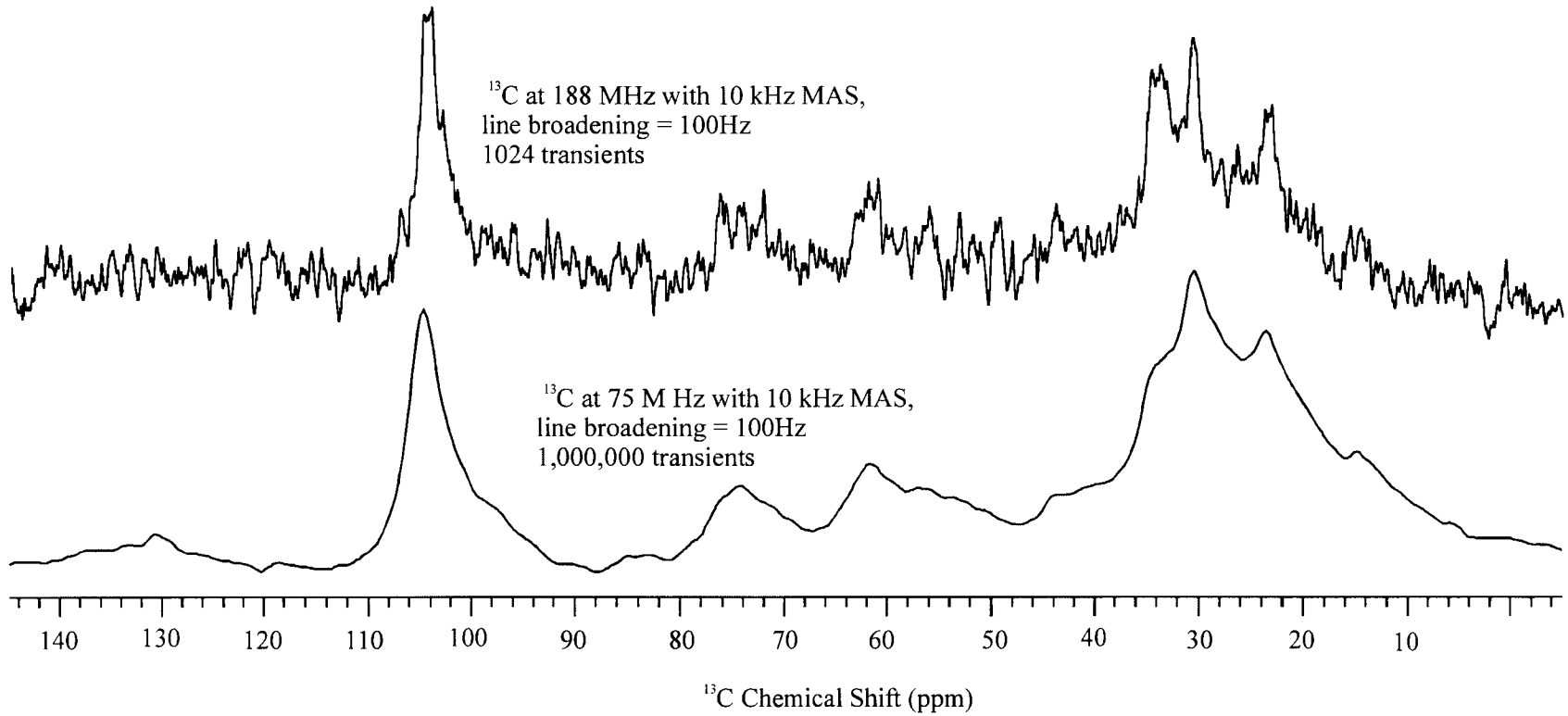

Figure 4.94. Resolution comparison of CPMAS ^{13}C spectra of 1-^{13}C-D-mannose L-dopa melanin on 300 and 750 MHz spectrometers.

4.3.2 Swelled-State Results

Molecular Structures from NMR of Swelled Melanin Samples. As noted above, MAS ^{13}C NMR indicated a surprisingly significant degree of motional averaging in unlabeled powdered melanin. In addition, the spectral narrowing evidenced for many of the resonances upon exposure to D_2O and H_2O suggested that the biopolymer could be swelled readily in common solvents (B. Yan and R. E. Stark, personal communication). These observations prompted us to collect high-resolution MAS ^1H NMR spectra under solvent-swelled conditions, as illustrated above for cutin and suberin, exploiting the fact that this protocol simultaneously enhances molecular mobility and minimizes magnetic susceptibility line broadening.[92,93] Figure 4.95 displays a typical 600 MHz NMR spectrum of *C. neoformans* melanin swelled in DMSO. Even at modest spinning speeds of 2-3 kHz, the one-dimensional (1D) spectra exhibit flat baselines and reasonably narrow lines; the 20-25 Hz line widths preclude the observation of *J* couplings but are comparable to those exhibited by neuromelanins dissolved in a strong base[69] and to those of swelled samples of plant biopolyesters.[31,94] Similar spectral features are observed at temperatures from 20 to 50 °C or if the swelling is done with D_2O. The integrated intensities of the various ^1H resonances confirmed the predominance of methylene and other aliphatic groups, as deduced independently from ^{13}C CPMAS and direct polarization MAS of dry melanin (see above). Also notable is a small resonance at 8.10 ppm, attributed provisionally to the pyrrole CH group of a carboxyl-substituted indole (ACD/CNMR Spectrum Generator (2000) Advanced Chemistry Development, Toronto, ON). Finally, a secondary alcohol peak (3.83 ppm) is visible

when the sample is swelled in D_2O, though it is partially obscured by the residual H_2O signal when the sample is swelled in DMSO. The overall concordance of compositional profiles derived from solid-state and swelled-solid NMR added a measure of confidence to the quantitative reliability of both methodologies. Nevertheless, the paucity of ^1H signals from multiply bonded moieties may indicate incomplete accessibility to solvent, and complications from paramagnetic broadening cannot be ruled out for either type of NMR data.

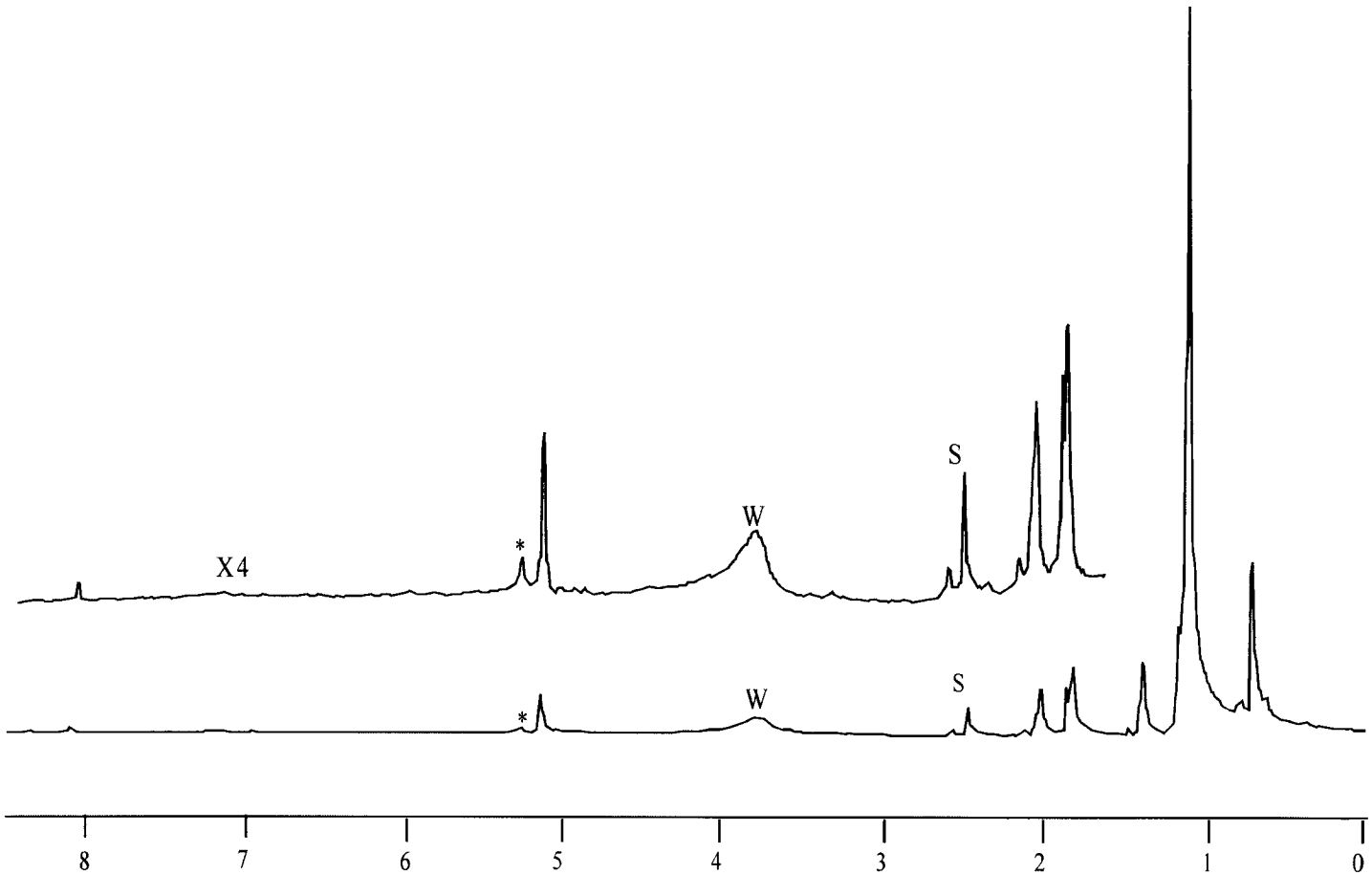

Figure 4.95. 600 MHz MAS ^{1}H NMR spectrum of *C. neoformans* L-dopa melanin, swelled at 1:5 (w/w) in DMSO-d_6 at 25 °C and spun at 2.5 kHz. Peaks from the DMSO and water are labeled s and w, respectively; a spinning sideband is marked with an asterisk. An additional peak at 3.83 ppm is visible if the sample is swelled in D_2O.

To identify functional groups definitively, the MAS-assisted NMR approach was also used to obtain two-dimensional heteronuclear correlated spectra of L-dopa fungal melanin swelled in DMSO, as shown in Figures 4.96 and 4.97. The ^{13}C HMQC spectrum (Figure 4.96) separates overlapping ^{1}H NMR signals according to the different resonance positions of their attached ^{13}C nuclei, identifies directly bonded hydrogen-carbon pairs, and serves as a fingerprint of the hydrogen- and carbon-containing functional groups present in the biopolymer [85]. With the benefit of correlated ^{1}H and ^{13}C chemical shifts, it was possible to confirm the likely presence in fungal melanin of methyl groups (**CH_3**CH_2, 0.74 and 13.8 ppm; **CH_3**COO, 2.05 and 33.7 ppm), several environmentally distinct types of long chain methylenes (e.g., 1.13 with 22.4, 29.4, and 31.8 ppm), proton-bearing carbons attached and adjacent to double bonds (**CH=CH**, 5.16 and 129.6 ppm; **CH_2**CH=CH, 1.86 and 26.9 ppm), and methylenes near carbonyls (**CH_2**COO, 1.89 and 21.1 ppm; **CH_2**C=O, 2.06 and 30.0 ppm). A cross-peak at 3.83 and 63.4 ppm, consistent with a secondary alcohol group, is also identified tentatively near the signal from residual water in the DMSO solvent (data not shown). The carbon shifts are in satisfactory agreement with the CPMAS ^{13}C data presented above; the narrow line widths of these two-dimensional (2D) spectra make it possible, moreover, to discriminate among environmentally similar protons and carbons as is done routinely for organic molecules in solution [95].

Figure 4.97 shows a HMBC spectrum for swelled fungal melanin under MAS NMR conditions. This experiment reveals long-range covalent connectivities involving nonprotonated carbons that are not reported in HMQC spectra; it also

displays cross-peaks that confirm the presence of functional groups proposed above: ketones ($C\underline{H_2}\underline{C}$=O, 2.06 and 208.7 ppm), esters ($C\underline{H_2}\underline{C}OO$, 1.89 and 173.5 ppm; $C\underline{H_3}\underline{C}OO$, 2.05 and 172.1 ppm), and olefins ($C\underline{H_2}H\underline{C}$=CH, 1.86 and 129.6 ppm). The long-range coupling shown by the cross-peak at 2.06 and 158.8 ppm may be attributed to an aromatic-linked carboxylate moiety [61]. These observations extend the structural information deduced from CPMAS, 1D, and HMQC experiments to yield definitive evidence for previously unknown fragments in the molecular structure of this fungal melanin.

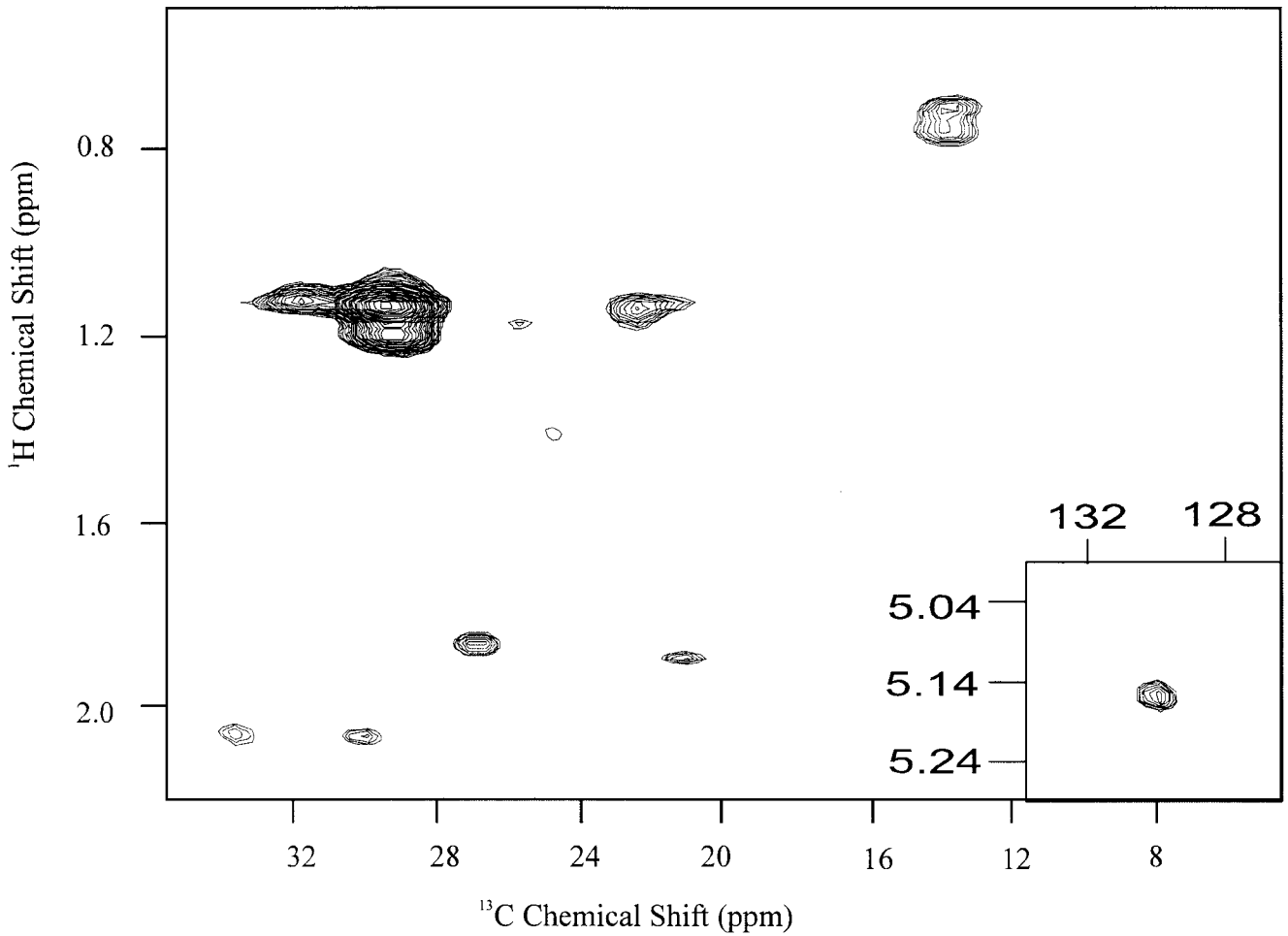

Figure 4.96. Contour plot of single-bond correlations from a gradient-assisted 2D ^{1}H-^{13}C HMQC NMR experiment on *C. neoformans* L-dopa melanin, conducted with 2.5 kHz magic-angle spinning and *z*-axis pulsed field gradients. Regions corresponding to aliphatic chain methylene, methyl, and alkene groups are shown; an additional cross-peak that can be attributed to a secondary alcohol group (3.83, 63.4 ppm) is also visible near the signal from residual water present in the DMSO solvent.

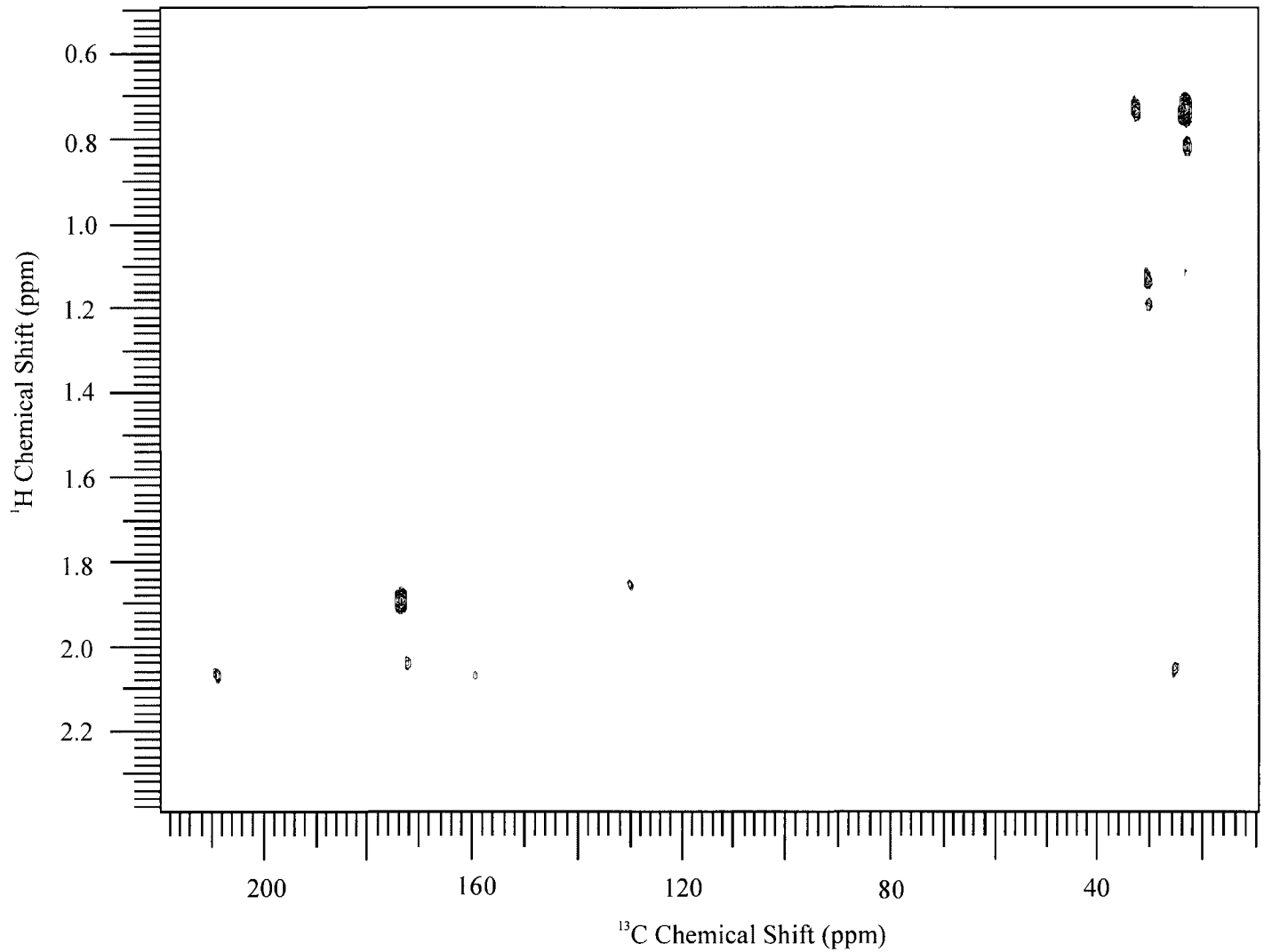

Figure 4.97. Contour plot of long-range through-bond correlations from a gradient-assisted 2D ^{1}H-^{13}C HMBC NMR experiment on *C. neoformans* L-dopa melanin, conducted as described in the legend of Figure 4.97. No other cross-peaks appeared in the spectrum.

Melanins derived from different precursors show similar aliphatic and aromatic structural features in their HRMAS NMR ^{1}H spectra (Figure 4.98). Methyl and methylene groups are the main components of all materials (peaks at 0.5 – 2.8 ppm, Figure 4.98), consistent with their CPMAS spectra (Figure 4.92), but surprising for polymeric materials that are thought to be indole-based. They all have carbon-carbon double bonds (peaks at 5.0 – 5.4 ppm, Figure 4.98). They all have protons attached to oxygenated carbons (peaks at 3.0 – 5.0 ppm, Figure 4.98). Small resonances at 8.10 ppm, attributed provisionally to the pyrrole **CH** group of a carboxyl-substituted indole (ACD/CNMR Spectrum Generator (2000) Advanced Chemistry Development, Toronto, ON), also appear in all of the spectra of Figure 4.98. The spectrum of natural-abundance L-dopa melanin was acquired at 25°C, with spin rate of 2500 Hz and water suppression, whereas the other spectra were obtained at 50 °C and spinning rate 2000 Hz. These differences in acquisition conditions may cause the difference of the chemical shift of DMSO and peaks between 3.5 ppm and 4.0 ppm. The small peaks in Box A, attributable to methyl groups, are only observed in 1-^{13}C-D-mannose melanin and norepinephrine melanin. Peaks 1, 2, and 3 in Box B are also attributable to methyl groups. They are observed in all of the samples except peak 1 is missing in methyl L-dopa melanin. The relative intensities of peaks 2 and 3 are reversed in methyl L-dopa melanin as compared with those of the other samples. The methylene peaks 1, 2, and 3 in Box C are observed in all of the samples but with different relative intensities in methyl L-dopa melanin. Peaks in Box D vary for different samples, both in types of peaks and relative intensities of peaks. Peak X is only observed in 1-^{13}C-D-mannose

melanin and norepinephrine melanin. Peaks in Box E vary for different samples. Peaks 2 and 3 in Box F are observed for all of the samples, but with different intensities. Peak 1 in Box F is only observed for norepinephrine melanin. The aromatic peaks in the inset of each spectrum were enhanced so that they are visible. The aromatic structure of 1-^{13}C-D-mannose melanin is most similar to norepinephrine melanin. The very weak aromatic peak for methyl L-dopa melanin results from the lower signal-to-noise level of that spectrum.

Two-dimensional spectra also confirmed these general similarities: cross peaks in box 2 of all of the spectra of Figures 4.99 and 4.100 are attributable to methyl and methylene groups; cross peaks in box 3 of all of the gHMQCs spectra of Figure 4.99 are attributable to carbon-carbon double bond structures, whereas only the gHMBCs spectra of 1-^{13}C-D-mannose melanin and norepinephrine melanin show cross peaks for the carbons and protons of the carbon-carbon double bond structure due to different signal to noise levels. There are no cross peaks observed for the pyrrole structure, presumably due to their very weak intensities.

The 2D spectra of Figures 4.99 and 4.100 also show some differences among different melanin precursors. Both gHMQCs and gHMBCs spectra of methyl-L-dopa melanin are more like those of L-dopa melanin than those of the other melanins. 1-^{13}C-D-mannose melanin and norepinephrine melanin have stronger 2D spectra than L-dopa melanin and methyl-L-dopa melanin, possibly due to more effective swelling. The sample of 1-^{13}C-D-mannose melanin has the strongest 2D spectra. As mentioned above, the prevalence of free radicals may contribute to the

differences in the 2D spectra. Differing amounts of samples, ratios of sample to solvent, and efficacy of solvent swelling could also play important roles.

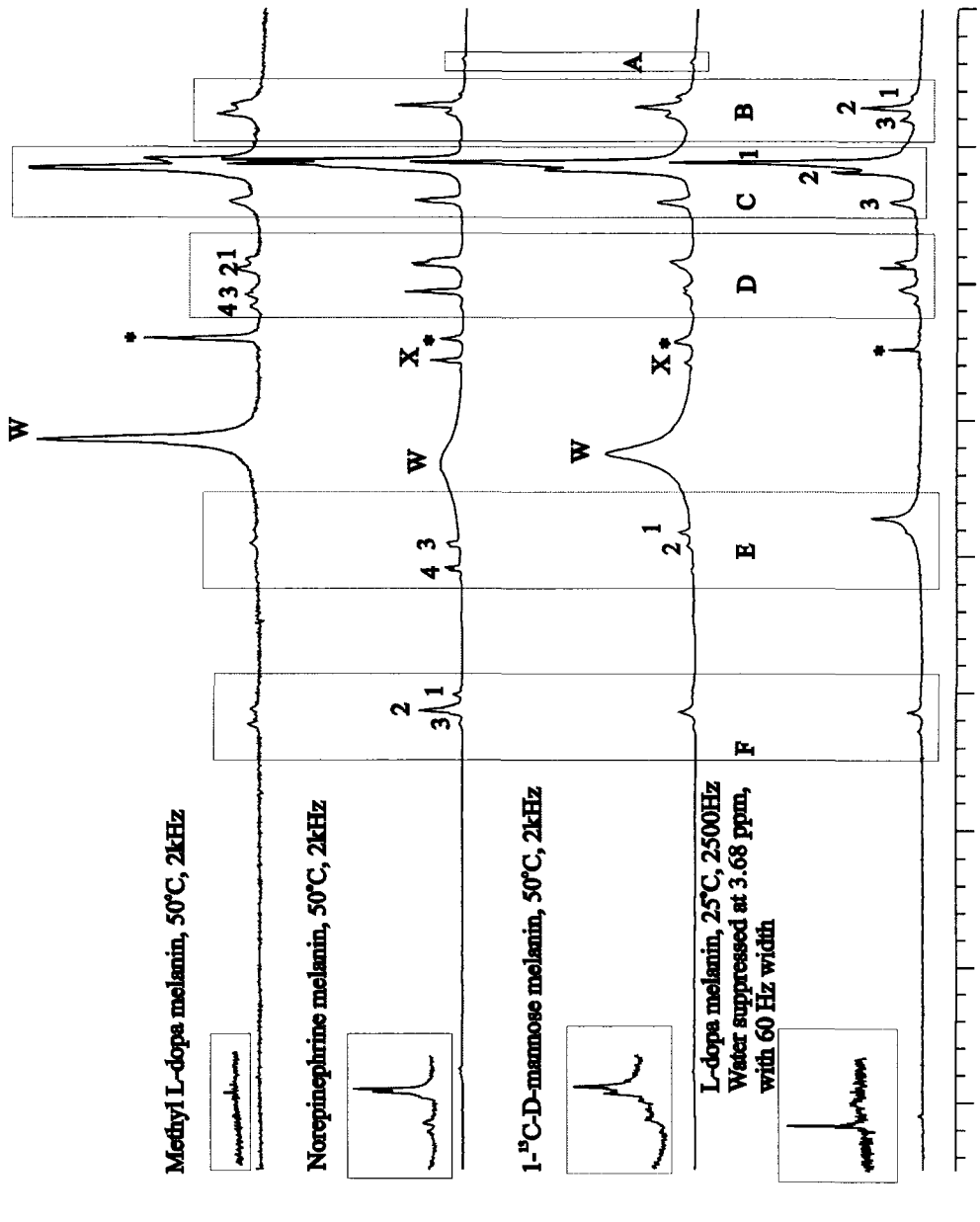

Figure 4.98. Comparison of HRMAS ^{1}H spectra of swelled melanin from different precursors. W: water peak; *: solvent peak. The top three spectra were acquired at 50 °C and with MAS of 2 *kHz*; the bottom spectrum was acquired at 25 °C with MAS of 2.5 *kHz*.

Site-Specific Incorporation of ^{13}C Labels and Structural Information HR/MAS NMR. As discussed in Chapter 2, carbons are involved in HMQC and HMBC spectra, and thus ^{13}C labeling should enhance the signals of cross peaks that involve correlations with the labeled carbons. This effect was observed in the gHMQCs data for 1-^{13}C-D-mannose melanin: box 1 of the bottom left spectrum of Figure 4.99, cross peaks (^{1}H ppm, ^{13}C ppm): 4.45, 102.2; 4.49, 102.0; 4.81, 100.8) and gHMBCs data: box 1 of bottom left spectrum of Figure 4.101, cross peaks (^{1}H ppm, ^{13}C ppm): 3.10, 102.2; 3.60, 100.8; 3.65, 102.0. Figures 4.99 and 4.100 show the signal enhancements of sugar moieties in HMQC and HMBC spectra of melanin with a 1-^{13}C mannose precursor. The chemical shifts of the enhanced carbon signals are consistent with those of the CPMAS spectra (Figures 4.92, 4.99, and 4.100). These cross peaks are not visible in the 2D spectra of natural abundance melanin. The enhanced cross peaks provide additional evidence for the incorporation of this precursor into melanin.

4.4 Conclusions

The incorporation of labeled precursors into the products is demonstrated by the NMR data, and the principal aliphatic and aromatic structures of the melanin derived from different precursors are similar. Melanins made from different precursors show some differences in their NMR spectra, attributable to differences in the sample itself (such as chemical structures and free radicals in the samples) or to differences in experimental conditions, such as sample amount, sample-solvent ratio, swelling efficiency, and parameter setup. A polysaccharide moiety was found

in 1-^{13}C-D-mannose melanin, suggesting close association or covalent binding of melanin to the fungal cell wall. Measurements at 17.5 T (^{1}H resonance frequency of 750 MHz) and MAS speeds of 10 kHz displayed both enhanced sensitivity and resolution for the CPMAS spectra, with ^{13}C chemical shifts that confirmed the functional group identifications made using CP-MAS at 7 T and HR-MAS at 14 T. Among the significant factors could be the amount of free radicals in the samples.

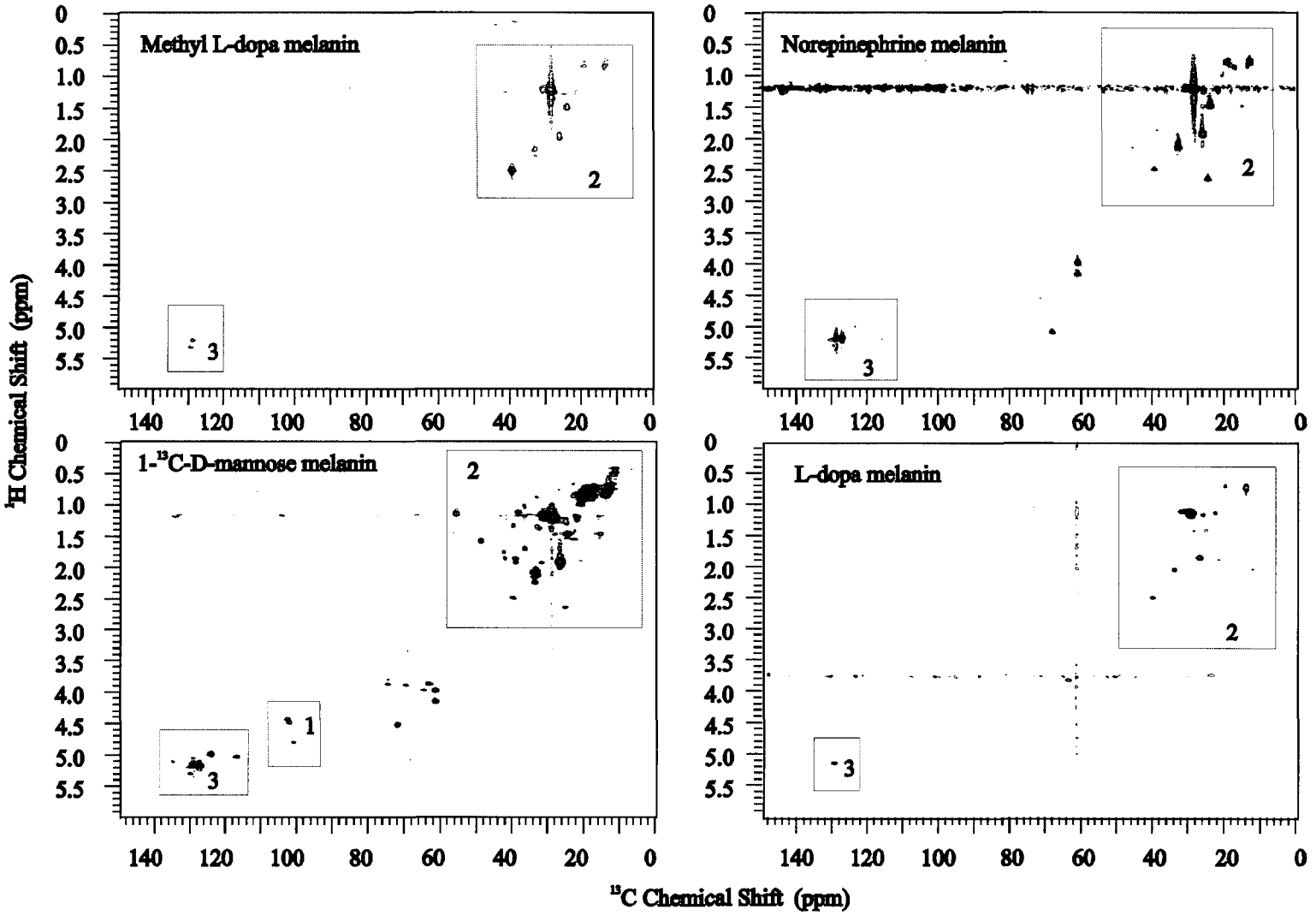

Figure 4.99. Comparison of HRMAS gHMQCs spectra of swelled melanin from different precursors, obtained on a spectrometer operating at 600 MHz.

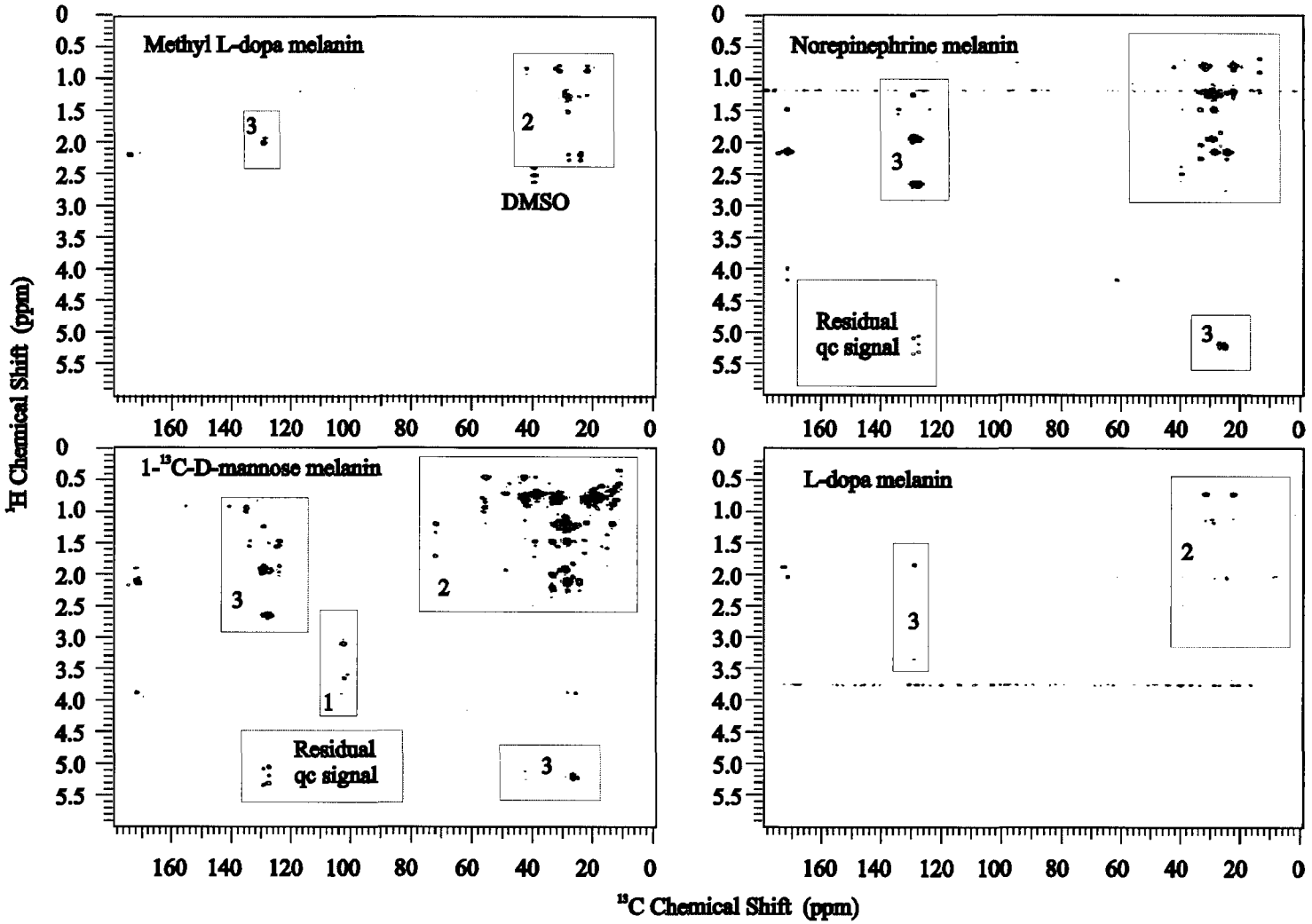

Figure 4.100. Comparison of HRMAS gHMBCs spectra of swelled melanin from different precursors, obtained on a spectrometer operating at 600 MHz.

Reference List

1. P. E. Kolattukudy, *Can. J. Bot.*, 1984, **62**, 2918-2933.
2. C. E. Jeffree, *Structure and Ontogeny of Plant Cuticles*, BIOS Scientific Publishers, Oxford, 1996,33-82.
3. T. J. Walton, *Meth. Plant Biochemistry*, 1990, **4**, 105-158.
4. P E Kolattukudy, *Biosynthetic Pathways of Cutin and Waxes, and Their Sensitivity to Enviromnmental Stresses*, BIOS Scientific Publishers, Oxford, 1996,83-108.
5. G. Kerstiens, *J.Exp.Botany*, 1996, **47**, 1813-1832.
6. M. Riederer and L. Schreiber, *Journal of Experimental Botany*, 2001, **52**, 2023-2032.
7. B. Aloni, L. Karni, I. Rylski, Y. Cohen, Y. Lee, M. Fuchs, S. Moreshet, and C. Yao, *J.Hort.Sci.Biotech.*, 1998, **73**, 743-749.
8. A. N. Round, B. Yan, S. Dang, R. Estephan, R. E. Stark, and J. D. Batteas, *BIOPHYSICAL JOURNAL*, 2000, **79**, 2761-2767.
9. P. D. Petracek and M. J. Bukovac, *Plant.Physiol.*, 1995, **109**, 675-679.
10. P. Luque and A. and Heredia, *Plant Physiol. Biochem.*, 1997, **35**, 251-256.
11. C. G. Casado and A. and Heredia, *Biochimica Et Biophysica Acta*, 2001, **1151**, 291-296.
12. C. G. Casado and A. and Heredia, *Biomacromolecules*, 2001, **2**, 407-409.
13. F. Pinot, I. Benveniste, J. P. Salaün, and and Durst F., *Plant Physiol.*, 1998, **118**, 1481-1486.
14. K. E. Espelie, R. W. Davis, and P. E. Kolattukudy, *Planta*, 1980, **149**, 498-511.
15. P. E. Kolattukudy, M. S. Crawford, C. P. Woloshuk, W. F. Ettinger, and C. L. Soliday, *The Role of Cutin, the Plant Cuticular Hydroxy Fatty Acid Polymer, in the Fungal Interaction With Plants*, American Chemical Society, 1987, Ch. 10,152-175.
16. E. C. Lulai and D. L. Corsini, *Physiol. Molec. Plant Path.*, 1998, **53**, 209-222.

17. P. E. Kolattukudy, *Ann. Rev. Plant Physiol.*, 1981, **32**, 539-567.

18. M. A. Bernards and N. G. Lewis, *Phyiochemistry*, 1998, **47**, 915-933.

19. R. E. Stark, W. Sohn, Jr. R. A. Pacchiano, M. Al-Bashir, and J. R. Garbow, *Plant Physiol*, 1994, **104**, 527-533.

20. M. H. and Bell A. A. Wheeler, *Current Topics in Medical Mycology*, 1988, **2**, 338-345.

21. J. M. Henson, M. Butler, and A. W. and Day, *Annu. Rev. Phytopathol*, 1999, **37**, 447-455.

22. H. Z. Hill, *BioEssays*, 1992, **14**, 49-56.

23. J. D. Nosanchuk, K. A. Marr, and A. and Casadevall, *J. Infect. Dis.*, 2001, **183**, 1093-1108.

24. Y. Wang and A. and A.Casadevall, *Antimicrob. Agents Chemotherap.*, 1996, **40**, 541-550.

25. Corry and Proctor P. H. McGinness, *Science*, 1974, **183**, 853-855.

26. K. Söderhäll and V. J. and Smith, *Prophenoloxidase-Activating Cascade As a Recognition and Defense System in Arthropods*, John Wiley and Sons, New York, 1986,251-285.

27. B. P. Currie and A. Casadevall, *Clin. Inf. Dis.*, 1994, **19**, 1029-1033.

28. Y. Wang, P. Aisen, and A. and Casadevall, *Infect. Immun.*, 1996, **64**, 2420-2424.

29. Y. Wang, P. Aisen, and A. and Casadevall, *Infect. Immun.*, 1995, **63**, 3131-3136.

30. K. J. Kwon-Chung, W. B. Hill, and J. E. and Bennett, *J. Clin. Microbiol.*, 1981, **13**, 383-387.

31. X. Fang, F. Qiu, B. Yan, H. Wang, A. J. Mort, and R. E. Stark, *Phytochemistry*, 2001, **57**, 1035-1042.

32. S. F. Osman, H. C. Gerard, W. F. Fett, R. A. Moreau, and R. L. Dudley, *J Agric Food Chem*, 1995, **43**, 2134-2137.

33. A. K. Ray, Z. Chen, and R. E. Stark, *Phytochemistry*, 1998, **49**, 65-70.

34. A. H. B. Deas and P. J. Holloway, *Lipids and Lipid Polymers in Higher Plants*, Springer-Verlag, Berlin, 1979,293-300.

35. A. K. Ray and R. E. Stark, *Phytochemistry*, 1998, **48**, 1313-1320.

36. T. Zlotnik-Mazori and R. E. Stark, *Macromolecules*, 1988, **21**, 2412-2417.

37. J. R. Garbow and R. E. Stark, *Macromolecules*, 1990, **23**, 2814-2819.

38. Holloway, P. J., *Cutins and Suberins,the Polymeric Plant Lipids*, CRC Press, Inc., Boca Raton, Florida,, 1984, vol. 10.

39. Luque P., Bruque S., and and Heredia A., *Arch. Biochem.and Biophys.*, 1995, **317**, 417-422.

40. F. J. Villena, Eominguez E., and and Heredia A., *J. Plant Physiol.*, 2000, **156**, 419-422.

41. A. Matas and A. and Heredia, *Zeitschrift Fur Naturforschung - Ection C Jounal of Biosciences*, 1999, **54**, 896-902.

42. P E Kolattukudy, *Advances In Biochemical Engineering/Biotechnology*, 2001, **71**, 1-49.

43. Pinot F., Salaun J.-P., Bosch H., Lesot A., Mioskowski C., and Durst F., *Biochem.Biophys.Res.Commun.*, 1992, **184**, 183-193.

44. F. Pinot, H. Bosch, J. P. Salaun, F. Durst, C. Mioskowski, and B. D. and Hammock, *Plant Physiol. Biochem.*, 1997, **35**, 103-110.

45. F Pinot, I Benveniste, J P Salaün, O Loreau, J P Noël, L Schreiber, and F Durst, *The Biochemical Journal*, 1999, **342**, 27-32.

46. A. Heredia, *Biochimica Et Biophysica Acta - General Subjects*, 2003, **1620**, 1-7.

47. R. E. Stark and J. R. Garbow, *Macromolecules*, 1992, **25**, 149-154.

48. A. M. Gil, M. Lopes, J. Rocha, and C. P. Neto, *International Journal of Biological Macromolecules*, 1997, **20**, 293-305.

49. M. H. Lopes, A. M. Gil, A. J. D. Silvestre, and C. P. Neto, *J. Agric. Food Chem*, 2000, **48**, 383-391.

50. M. H. Lopes, A. Sarychev, C. P. Neto, and A. M. and Gil, *Solid State Nuclear Magnetic Resonance*, 2000, **16**, 109-121.

51. P. J. Holloway, *Phytochemistry*, 1983, **22**, 495-502.

52. J. Graça and H. and Pereira, *Holzforschung*, 1997, **51**, 225-234.

53. O. Borg-Oliver and B. and Monties, *Phytochemistry*, 1993, **32**, 601-606.

54. O. Borg-Olivier and Monties, *C. R. Acad. Sci. Paris*, 1989, 141-147.

55. C. Lapierre, B. Pollet, and J. Negrel, *Phytochemistry*, 1996, **42**, 949-953.

56. J. Negrel, B. Pollet, and C. and Lapierre, *Phytochemistry*, 1996, **43**, 1195-1199.

57. M. A. Bernards, M. L. Lopez, J. Zajicek, and N. G. Lewis, *J. Biol. Chem.*, 1995, **270**, 7382-7386.

58. B. Yan and R. E. Stark, *J. Agric. Food Chem*, 2000, **48**, 3298-3304.

59. G. A. Duff, J. E. Roberts, and N. Foster, *Biochemistry*, 1988, **27**, 7112-7116.

60. H. Knicker, G. Almendros, F. J. Gonzalez-Vila, H.-D. Luedemann, and F. Martin, *Org. Geochem.*, 1995, **23**, 1023-1028.

61. M. Schnitzer and Y. K. and Chan, *Soil Science Soc. Am. J.*, 1983, **50**, 67-71.

62. M. Hervé, J. Hirschinger, P. Granger, A. Deflandre, and N. and Goeta, *Biochim Biophys Acta*, 1994, **1204**, 19-27.

63. S. Aime, M. Fansani, b. Bergamasco, L. Lopiano, and G. and Quattrocolo, *Adcances in Neurology*, 1996, 263-270.

64. C. C. Felix, J. S. Hyde, T. Sarna, and R. C. and Sealy, *J Am Chem Soc*, 1978, **12**, 3922-3926.

65. B. B. Adhyaru, N. G. Akhmedov, A. R. Katritzky, and C. R. and Bowers, *Mag. Res. Chem.*, 2003, **41**, 466-474.

66. F. J. Gonzalez-Vila, F. Martin, and C. and Saiz-Jimenez, *Agrochimica*, 1978, **22**, 501-505.

67. F. J. Gonzalez-Vila, C. Saiz-Jimenez, H. Lentz, and H.-D. and Ludemann, *Z. Naturforsch.*, 1978, **33c**, 291-293.

68. H. D. Ludemann and H. Nimz, *Biochemical and Biophysical Research Communications*, 1973, **52**, 1162-1169.

69. K. L. Double, *J. Neurochem*, 2000, **75**, 2583-2589.

70. S. Tian, J. Garcia-Rivera, B. Yan, A. Casadevall, and R. E. and Stark, *Biochemistry*, 2003, **42**, 8105-8109.

71. Harris, R. K., *Nuclear Magnetic Resonance Spectroscopy*, Pitman Publishing Limited, New York,, 1983, vol. 1.

72. Sanders and Hunter, *Modern NMR Spectroscopy: A Guide for Chemists*, Oxford University Press, 2nd Edn., 1993.

73. Homans, *A Dictionary of Concepts in NMR*, Oxford Science Publications, 1997.

74. O. B. Peersen, X. Wu, I. Kustanovich, and S. O. Smith, *J.Magn.Reson.A*, 1993, **104**, 334-339.

75. G. Metz, X. Wu, and S. O. Smith, *J. Magn. Reson.A*, 1994, **110**, 219-227.

76. S. J. Opella, M. H. Frey, and T. A. Cross, *J. Am. Chem. Soc.*, 1979, **101**, 5854-5857.

77. A. E. Bennett, J. H. OK, R. G. Griffin, and S. Vega, *J. Chem. Phys.*, 1992, **96**, 8624-8627.

78. Swadesh, J, *HPLC Practical and Industrial Applications*, CRC Press, New York, 1997.

79. Smith, R. M., *Understanding Mass Spectra: A Basic Approach*, John Wiley and Sons, New York, 1999.

80. Cotter, R. J. Time-of-Flight Mass Spectrometry. American Chemical Society, Washington, DC, 1997.

81. C. Griesinger, G. Otting, K. Wuthrich, and R. R. Ernst, *J.Am.Chem.Soc.*, 1988, **110**, 7870-7872.

82. L. Muller, *J. Am. Chem. Soc.*, 1979, **101**, 4481-4484.

83. A. Bax and M. F. Summers, *J. Am. Chem. Soc.*, 1986, **108**, 2093-2094.

84. A. J. Shaka, P. B Barker, and R. Freeman, *J. Magn. Res.*, 1985, **64**, 547-552.

85. R. E. Hurd and B. K. John, *J. Magn. Res.*, 1991, **91**, 648-653.

86. P. D. Murphy, *J. Magn. Reson.*, 1986, **70**, 307-309.

87. K. E. Espelie, W. Koller, and P. E. Kolattukudy, *Chemistry and Physics of Lipids*, 1983, **32**, 13-26.

88. R. A. Pacchiano, W. Sohn, V. L. Chlanda, J. R. Garbow, and R. E. Stark, *J Agric Food Chem*, 1993, **41**, 78-83.

89. A. K. Ray, Y. Y. Lin, H. C. Gerard, Z. Chen, S. F. Osman, W. F. Fett, R. A. Moreau, and R. E. Stark, *Phytochemistry*, 1995, **38**, 1361-1369.

90. R. E. Stark, T. Zlotnik-Mazori, L. M. Ferrantello, and J. R. Garbow, *ACS Symp. Ser.*, 1989, **399**, 214-229.

91. P. R. Williamson, K. Wakamatsu, and S. and Ito, *J. Bacteriol.*, 1998, **180**, 1570-1572.

92. P. A. Keifer, L. Baltusis, D. M. Rice, A. A. Tymiak, and J. N. Shoolery, *J. Magn. Reson.*, 1996, **119A**, 65-75.

93. K. Millis, W. E. Maas, S. Singer, and D. G. Cory, *Magn. Reson. Med.*, 1997, **38**, 399-403.

94. R. E. Stark, B. Yan, A. K. Ray, Z. Chen, X. Fang, and J. R. Garbow, *Solid State NMR*, 2000, **16**, 37-45.

95. G. E. Martin and A. S. and Zektzer, VCH Publishers, New York, 1988.